2010

Seismic performance of an I-girder to inverted-T bent cap bridge connection

Richard Manning Snyder
Iowa State University

Seismic performance of an I-girder to inverted-T bent cap bridge connection

by

Richard Manning Snyder

A thesis submitted to the graduate faculty

in partial fulfillment of the requirements for the degree of

MASTER OF SCIENCE

Major: Civil Engineering (Structural Engineering)

Program of Study Committee:
Sri Sritharan, Major Professor
Fouad Fanous
Lester Schmerr

Iowa State University

Ames, Iowa

2010

TABLE OF CONTENTS

LIST OF FIGURES

LIST OF TABLES

ABSTRACT

This thesis represents a portion of the research conducted as part of an investigation for the California Department of Transportation (Caltrans) regarding the seismic response and overall moment capacity of precast I-girder to inverted-T bent cap bridge connections for seismic applications. The current design practice, as outlined by Caltrans' Seismic Design Criteria, assumes that the connection between the precast I-girders and the inverted-T bent cap will degrade in a seismic event and shall therefore be designed as a pinned connection, making the precast girder option for seismic bridges inefficient. A prototype I-girder to inverted-T bent cap bridge and a 50% scale test unit was designed in order to investigate the behavior of the girder-to-cap connection region. Additionally, per the request of Caltrans, an improved girder-to-cap connection detail was developed in order to ensure a fully continuous moment connection between the I-girders and inverted-T bent cap.

A finite element grillage model was developed using SAP2000 and was used to predict the global and local responses of various aspects of the test unit. The test unit was constructed and tested in two phases of quasi-static cyclic testing. The first phase was a horizontal load test phase, which simulated the effects of gravity and seismic loads on the entire test unit. The second phase was a vertical load test phase, which specifically focused on the positive and negative moment capacity of the connection. Both the results of the finite element grillage model and the testing were used to make conclusions regarding the performance of I-girder to inverted-T bent cap bridges.

It was concluded that the current I-girder to inverted-T bent cap bridge connection is capable of acting as a fully continuous connection for both positive and negative moments during both gravity and seismic loading, contrary to the design assumptions stated in Caltrans' Seismic Design Criteria. The improved connection detail demonstrated the ability to ensure a fully continuous moment connection between the I-girders and inverted-T bent cap. Both connection details also exhibited a significant moment resistance beyond what was expected, during the vertical load test.

Chapter 1. INTRODUCTION

1.1 General

The state of California has experienced a significant number of earthquakes over the past few decades, quite a few of which resulted in significant structural damage to both bridges and buildings in the surrounding areas. As a direct result, a considerable amount of time, money, and more importantly, human life was lost by the state of California. The 1994 Northridge earthquake alone resulted in 57 fatalities and property damage estimated to be in excess of $20 billion dollars in 1994 (PEER, 2005). However, each earthquake exposed design deficiencies and provided the engineering community with another opportunity to gain more information regarding the design of structures in earthquake-prone regions. This was particularly evident after the 1989 Loma Prieta Earthquake.

The Loma Prieta earthquake resulted in significant damage to a number of bridges and highway structures near the San Francisco and Oakland areas, including the San Francisco-Oakland Bay Bridge and the Cypress Street Viaduct. Damage to the Bay Bridge resulted in significant time and economic losses as it had to be closed for a month. The damage to the Cypress Street Viaduct was even more catastrophic as 48 of the 83 bents supporting the roadway collapsed, resulting in 41 human fatalities (Housner & Thiel, 1990). Based on the observations made from the Loma Prieta earthquake, as well as other significant earthquakes that had occurred within the past decades, the Governor of California appointed a Board of Inquiry to investigate the Loma Prieta earthquake in order to address the apparent design and regulation inadequacies with respect to the seismic performance of structures. In 1990, the Governor of California signed Executive Order 86-90, which set a policy stating that, "All state owned and operated structures are to be seismically safe and that important structures are to maintain their function after earthquakes," (Housner & Thiel, 1990). Additionally, one of the significant findings and recommendations that the Board of Inquiry made was that the California Department of Transportation (Caltrans), "Fund a continuing program of basic and

problem-focused research on earthquake engineering issues pertinent to Caltrans responsibilities," (Housner & Thiel, 1990).

Many of the bridges that are currently in place in California were designed in the 1950's and 1960's. Since little was known about the seismic behavior of structures, the practice at that time was to overdesign structures with the intention that they would remain elastic during an earthquake. However, observations of bridges that were designed to remain elastic and were severely damaged during earthquakes, in addition to experimental research, indicated that the design methods that were employed during that time period were inadequate. It was determined that the earthquake design forces were grossly underestimated, which resulted in an underestimation of deflections and an inability for the structure to develop a stable inelastic response mechanism. Fortunately, the elastic design philosophy was able to somewhat cope with the underestimated forces, as the working stress was often greater than what was assumed in the design. However, the main deficiency with the elastic design philosophy was that there was no plan to accommodate the higher than expected forces, meaning a stable inelastic response hierarchy was not built into the structural system. As a result, the following inadequacies often developed in response to a seismic event: Brittle failure mechanisms; incorrect quantities, placement, and termination of reinforcement; unseating of the girders; structural pounding; shear, confinement, anchorage, and lap-splice failure; joint failure; and buckling of longitudinal reinforcement (Priestley, Seible, & Calvi, 1996). Figures 1.1 and 1.2 illustrate a number of the aforementioned inadequacies that were observed during both the 1971 San Fernando and 1989 Loma Prieta earthquakes. Therefore, as a direct result of California's Board of Inquiry, in order to improve the seismic performance and ensure that the structure behaved in a more predictable manner, the capacity design philosophy was adopted (Housner & Thiel, 1990).

Figure 1.1: Example of 1971 San Fernando Earthquake Damage

Figure 1.2: Example of 1989 Loma Prieta Earthquake Damage

The goal of the capacity design philosophy was to allow the structure to behave in an inelastic manner through flexural yielding, but detail it such that a strength hierarchy was formed so that a stable response mechanism could occur. The locations of inelastic flexural yielding, referred to as plastic hinges, were preselected and detailed in order to achieve a specified level of ductility, without allowing the rest of the structure to experience any of the aforementioned failure mechanisms in the event of an earthquake. Plastic hinges are typically placed within the columns of a bridge structure to prevent any catastrophic damage from occurring in the superstructure, while maintaining the ability of the structure to support its self-weight in addition to carrying any dead or live load. Bridges typically have less redundancy than buildings. Therefore, in order to prevent the entire bridge from failing, it is of crucial importance that the column does not fail. This is typically achieved by designating the sections of the structure that are meant to remain elastic and designing them to be protected under the capacity design philosophy, which is often referred to as capacity protected design. This is accomplished through the use of overstrength factors in order to ensure that the members are designed with enough capacity that they remain elastic even under the highest expected magnitude of force to be experienced by the structure. While it is likely that the bridge will need significant maintenance, and in some cases complete replacement after an earthquake, the potential for catastrophic damage and loss of life is dramatically reduced through the use of the capacity design philosophy.

Following the 1994 Northridge Earthquake, it was shown that the bridge retrofits that were developed under the more modern design philosophy performed very well compared to those that were not retrofitted and were designed prior to the advances made as a result of the Loma Prieta Earthquake (Priestley, Seible, & Uang, 1994). Though the new design procedure and the research that was performed as a result of the Loma Prieta earthquake inspire a greater sense of confidence in structures that are built today, extensive research is still required in order to ensure that the structures that were designed previously, as well as those designed in the future, will behave sufficiently in a seismic event. Additionally, although a significant amount of research was aggressively carried out on the majority of the transportation structures within California immediately after the Loma Prieta earthquake, some structural details have yet to be investigated. More specifically, further research into

the connection details between the superstructure and substructure is required. As the infrastructure in the United States continues to age, the 24,000 bridges throughout the state of California (California Department of Transportation, 2007) will be in need of replacement and/or repair and the seismic performance of both the new and old structures will be pushed to the forefront. Furthermore, the ability to build quality structures at an accelerated and efficient pace, through the use of precast components, will be preferred over the traditional methods of cast-in-place components.

1.2 Inverted-T Bent Cap Connections

One such connection, which requires further investigation, is the inverted-T bent cap-to-girder connection. The detail has been used in a number of bridges, primarily in county bridges or overpasses, throughout the state of California. However, its moment capacity and thus its influence on the behavior of the rest of the bridge during a seismic event are still unknown. Therefore, before Caltrans incorporates this detail in any of their future designs, extensive research into its behavior must be conducted. Additionally, depending on the capacity of the connection, a retrofit or revisions to other aspects of the bridge may need to be made. Currently, no research regarding this topic has been performed and presented to Caltrans for review.

The inverted-T bent cap system can be used for single or multi-column bent configurations and consists of a cap beam, placed on top of the columns, in the shape of an upside-down letter "T". Precast girders, typically with dapped ends, are then placed with ease in the field on the ledge of the inverted-T, as shown in Figure 1.3. The structure is made continuous for live load by pouring the concrete deck over the length and width of the structure, in addition to pouring a diaphragm around the girders and cap. Hooked reinforcement is typically placed between the cap and diaphragm to establish a connection between the diaphragm and inverted-t bent cap. Additionally, dowel bars are often placed within the girders, which extend into the diaphragm in order to further establish a connection between the embedded ends of the girders and the diaphragm.

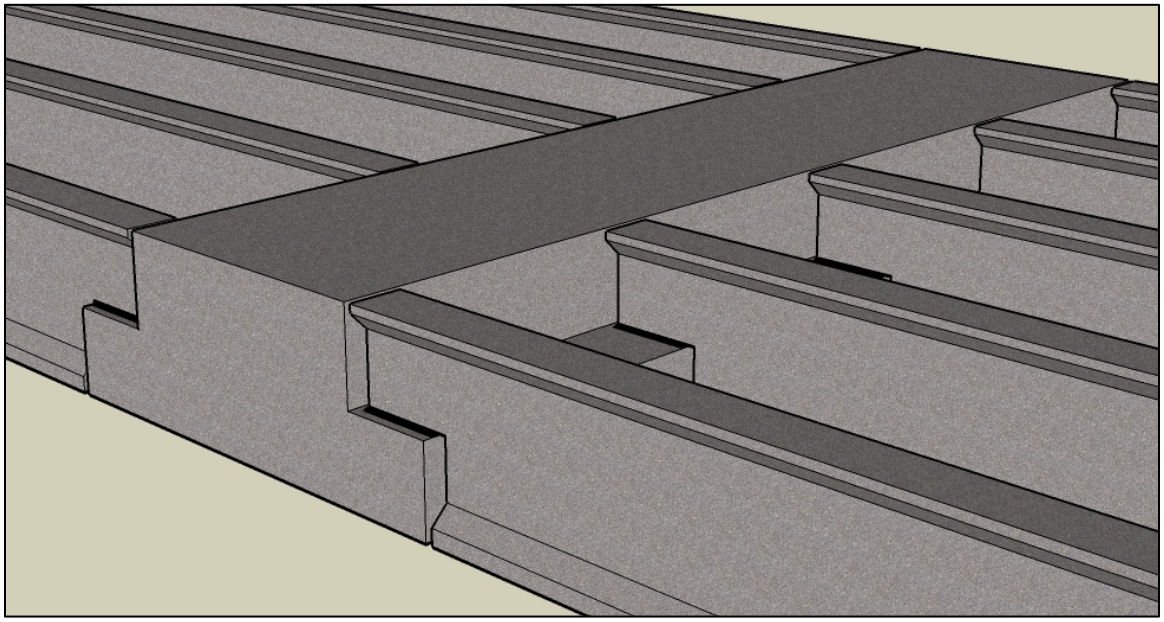

Figure 1.3: Inverted-T Bent Cap

Use of the inverted-T bent cap system has a number of significant advantages, when compared to traditional cast-in-place systems, as well as other precast methods including spliced girders made continuous. First, inverted-T bent caps allow for the use of precast girders, which can be cast in a controlled environment off site and shipped to the site for placement. Not only does this result in a higher quality girder than would be produced in the field, but it also allows for substantial economic savings as it lends itself to accelerated bridge construction practices. Construction time is typically reduced when precast components are employed as they may be cast ahead of schedule. Additionally, once they arrive at the job site, they are typically easier and quicker to place; this reduces the amount of congestion created due to stopping or delaying traffic during construction. Also, environmental benefits may be observed, such as a reduction in noise and air pollution. Second, the use of the inverted-T system decreases the required depth of the superstructure when compared to more traditional types of bent caps; this is especially noticed when using girders with dapped ends. Finally, compared to the method of spliced girders made continuous, the inverted-T system requires less supporting falsework, as it would only be required when casting the inverted-t bent cap. The girders may then be placed directly on the

bent cap without any direct support from falsework. This advantage will also result in economic, time, and environmental savings.

Unfortunately, the use of precast components is still not frequently used for bridges in areas of seismic activity. This is mainly due to a lack of a definite design methodology and research regarding the connection details between the precast members. However, if a design methodology were developed and proven to be reliable, it is very likely that the use of precast construction would become widely accepted in seismic areas. The advantages would be numerable, as previously discussed, and the use of precast components would contribute significantly to the use of accelerated bridge construction practices, which has become a significant interest in today's industry due to the significant time and cost savings that it provides. Furthermore, if the connection between the precast I-girders and the inverted-T bent cap were improved and tested successfully, the system could be used in future bridges as a very viable precast system, which would easily lend itself to accelerate bridge construction.

Currently, when designing bridges incorporating the inverted-T bent cap detail, Caltrans design engineers assume that the connection has no positive or negative moment resistance. In other words, the top of the column is assumed to be a pinned connection for any transverse or longitudinal loading conditions. This is done in accordance with California DOT's Seismic Design Criteria, which assumes, based on the previous seismic behavior of precast girders, that the moment connection between the girders and cap beam would likely degrade to a pinned connection (Caltrans, 2006). Therefore, the columns are designed with only one plastic hinge, located at the base of the column. However, it is likely that a significant amount of negative moment resistance would be provided given the reinforcement in the deck over the bent cap. Furthermore, given the reinforcement extending from the cap and into the diaphragm, as well as the dowel bars extending from the girders into the diaphragm, it is possible that the connection could support enough moment to develop a hinge at the top of the column as well. If that were the case, it would be possible to reduce the size of both the columns and the footings, as each hinge would experience a reduced moment demand. As a result, significant cost savings could be achieved. Additionally, the use of two plastic hinges provides additional redundancy to the system, reduces the displacement at the top of the column and therefore the likelihood of unseating of the girders,

and allows for the use of a pinned-base if desired. Conversely, if the connection does have a significant moment capacity, then the inverted-T bridges that are currently in place must be inspected as the connection could potentially pose serious consequences in the event of an earthquake. It is possible that the existing connection would not have been detailed with an adequate shear or moment capacity or an inappropriate amount of anchorage of the reinforcement that is entering column. More importantly, an unstable mechanism of inelastic response could occur at the top of the column, possibly resulting in a failure of the column. Damage to various parts of the structure, including the column and the superstructure, may also be likely if they were not designed under the capacity protection design philosophy, which ensures a suitable strength margin in order to prevent undesirable inelastic action from occurring in areas outside the specified plastic hinge regions. Finally, it has been identified that, given the potential for large rotations between the superstructure and the cap, the potential for damage of the girders and surrounding superstructure exists. This damage could be further compounded by the fact that a relatively small contact area between the girders and inverted-T cap is available to transfer shear forces into the joint, which could potentially further damage the concrete within the joint area. Therefore, it is likely that simply fixing the column to avoid failure would not solve all of the potential problems that could be encountered by the structure. These consequences must be addressed, as a serious possibility for large economic and human losses would exist.

1.3 Research Objective

The objective of the following research was to quantify the behavior and moment resistance of the inverted-T bent cap-to-girder connection in order to gain better understanding of its performance under seismic conditions. Additionally, modifications to the previous inverted-T details were proposed in order to achieve a connection that would provide a substantial resistance to positive moment as well as a more predictable seismic response.

A prototype bridge was developed based on the current Caltrans procedures used for bridges incorporating inverted-T bent caps. Unlike the inverted-T bridges that were designed previously, the prototype bridge was detailed with a plastic hinge in both the top and bottom of the column. This was done based on the initial hypothesis that the connection would be

able to develop enough moment to activate the hinge. Also, the decision to use I-girders, over bulb-tee or bathtub girders, was made by Caltrans as the majority of the bridges using inverted-T bent caps that are currently in place within the state of California were built using I-girders.

The test unit structure was then developed based on a 50% scale of the prototype bridge. The test unit, shown in Figure 1.4, consisted of a single column; an inverted-T bent cap; and a half span of five girders on each side of the bent cap. The current inverted-T connection details were used on one side of the bent cap, while the proposed modifications were employed on the other. This was done in order to make efficient use of the test unit specimen, as it was possible to test both connection types independently based on the side of the bent cap experiencing a positive moment demand. The test unit was constructed, heavily instrumented, and subjected to two phases of testing at the Powell Laboratory of the University of California San Diego (UCSD). The first phase involved pushing the superstructure horizontally in the longitudinal direction in order to simulate the monotonic response of the entire bridge during an earthquake. The second phase focused more on the behavior of the connection and involved pushing the superstructure vertically. This was done on both sides of the bent cap separately, in order to test both connection details. More about the test unit and test phases will be discussed in the subsequent text.

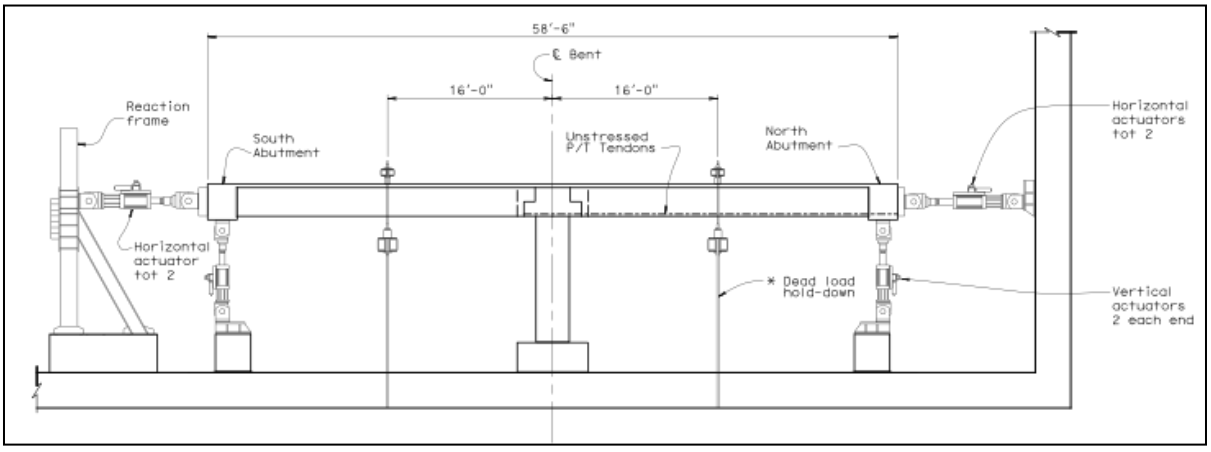

Figure 1.4: Proposed Test Unit Structure

This thesis represents only a portion of the overall scope of the research project. However, as such, the focus of the thesis and its contribution to the project consisted primarily of the development of a finite element grillage model of the test unit and the construction and testing of the 50% scale test unit. The majority of the information contained in this thesis, as well as the other portions of the research that are not found here, were included in the final report that was submitted to Caltrans.

A finite element grillage model of the test unit was produced, using SAP2000, based on the plan set provided by PBS&J and on recommendations from Zach Thiemann's finite element analysis described in his thesis, "3-D finite element analysis of the girder-to-cap beam connection of an inverted-t cap beam designed for seismic loadings" (Thiemann, 2009). The grillage model was used in order to predict the results of the physical testing and highlight any areas of the structure that needed special consideration during the testing phases. Additionally, the grillage model was used in connection with the physical testing in order to validate any results and conclusions.

Finally, a set of recommendations and conclusions regarding both the current and future performance of the inverted-T bent cap were submitted to Caltrans for their review. Additionally, a grillage model of the prototype, along with grillage modeling recommendations, were included in the report and submitted to Caltrans. All of the results and conclusions will be discussed in further detail within this thesis.

1.4 Thesis Layout

Following the introduction presented in Chapter 1, a literature review regarding previous research of positive moment connections as well as the use of grillage finite element modeling is provided in Chapter 2. Chapter 3 is an overview of the test unit and explores both the construction and testing of the test specimen. Chapter 4 provides a thorough explanation of the development of the grillage model, which flows into the validation of the grillage model and a series of predictions based on its results, as presented in Chapter 5. Chapter 6 discusses the results of both phases of testing. Finally, Chapter 7 provides a series of conclusions and recommendations for future work to be presented to Caltrans.

Chapter 2. LITERATURE REVIEW

2.1 Introduction

In order to better understand the seismic performance of an I-Girder to inverted-T bent cap connection, as well as the various finite element models and details required to complete the project, an in-depth literature review was performed. It was found that little research has been performed on precast girder-to-cap connections under seismic loading. The previous research mainly focused on the use of integrally cast cap beams, some with the use of precast girders, both steel and concrete, while no research was discovered relating to the use of inverted-T cap beams or a complete precast system for seismic regions.

It is now widely known that the use of precast components offers a substantial amount of benefits to both contractors and designers. For example, construction time is reduced, less falsework is required, the construction requires less of an impact on the surrounding environment, and the components are constructed in a more controlled environment, which results in a higher quality of craftsmanship. However, it could be argued that the use of spliced girders with an integral cap beam could be a disadvantage in terms of constructability, when compared to an inverted-T cap. If an adequate moment resisting connection can be developed and practically implemented in the field in order to achieve continuity with an inverted-T system, then this type of system may be used more frequently than it is currently. Since the girders would not need to be supported by falsework while constructing the integral cap beam for an inverted-T concept, a smaller environmental impact, less labor intensive construction procedures, and improved cost savings could be achieved with this system compared to those described in the studies presented above.

As these precast systems become more common, the need for experimental studies to predict their behavior during seismic events becomes an increasing priority. Specifically, the connection behavior between the precast girders and cap system is of interest, as it will govern the placement and possibly the formation of the column plastic hinges as well as the generalized behavior. Previous experimental studies, which will be discussed in more detail

below, have indicated that the negative moment resistance provided by these connections can most often be developed by the reinforcement placed within the deck slab. However, more information is still desired regarding the formation of any positive moment resistance within the connection.

The use of lab testing, of any scale, is of common use in engineering research. A search of bridge research proves that a high percentage of the research projects include lab testing, either exclusively or for validation. This method can effectively predict the true response of a bridge as long as any scaling has been done properly. The use of lab testing to validate other analytical models has been a common practice in the past. Superstructure to cap beam connection testing by (Almer & Sanders, 2007) has shown that a scaled test unit can be used to validate the analytical work done using more simplified means. The research focused on precast girder to cast-in-place bent caps and they were able to investigate the performance of the superstructure to cap beam connection, for both positive and negative moment, when subjected to a seismic application. They have tested two test units at the time of the paper publishing and will design the next two to improve upon the response of the first tests. The information gathered from testing in the lab for research is valuable and, as long as the setup is correct, is the best indicator of true response of a system. However, lab testing is not always the most efficient way to gather the response of a system. The cost of a few bridge test units can become very costly when considering the labor, materials, lab space, etc. The ability to secure funding to test multiple designs is challenging, now that other more cost effective means have been found to analytically predict the same response.

The following literature review begins with a brief background on the experimental research that has been conducted on the seismic performance of bridges made continuous for positive moment at the girder-to-cap connection. Information regarding positive moment connection and then the use of finite element analysis techniques to predict and understand the behavior of various aspects of the bridge, such as the rotation, strains and displacements, will be presented. Finally, the need, benefits, and means for establishing positive moment connections between girders and bent cap systems, as well as related previous experimental studies, are discussed.

2.2 Positive Moment Connection

2.2.1 Background

The use of precast girders has become a common place in bridge design, as it allows for the construction time to be greatly reduced. However, careful consideration has to be given to the area over the cap beams to ensure that sufficient continuity is provided through the girder-to-cap connection. For negative moment resistance, reinforcing bars are typically placed in the deck over the cap beam to provide the necessary moment resistance (Miller, Castrodale, Mirmiran, & Hastak, 2004). Mechanical splices, provided directly between the girder top flanges and the cap beam, have also been used in order to develop negative moment resistance. Testing of the connection from the superstructure to cap beam has been conducted by Portland Cement Association, and discussed in the NCHRP 519 report (Miller, Castrodale, Mirmiran, & Hastak, 2004), that showed that using the reinforcing in the deck for negative moment was adequate in design. During the aforementioned testing, cracking was observed in the diaphragms and the cause was believed to be from positive moment. The positive moment was caused from time-dependent effects on the girders. Therefore, a recommendation was made that a connection from the bottom of the diaphragm, next to the girder, to the girder should be provided. Multiple positive moment connections, which are discussed later, were then constructed and tested. During the testing, it was observed that the formation of cracks in the slab was the first sign of failure of the positive moment connection. Once the connection failed, the slab acted as a hinge during further loading (Miller, Castrodale, Mirmiran, & Hastak, 2004).

Many states currently use precast, prestressed girders for continuous highway bridges(Freyermuth, 1969). A survey of 150 agencies in Japan, Canada and the United States was performed regarding the use of positive moment connections. One-third of the surveys were returned and about half of the respondents said they had designed less than 200 continuous precast girder bridges while seven-percent responded indicating that they had designed more than 1,000 (Hastak, Mirmiran, Miller, Shah, & Castrodale, 2003). The main application of continuous, precast bridges was on interstates and high volume urban highways. Another observation from the survey was that over 60 percent of the respondents reported that they considered positive moment continuity for live load and superimposed

dead load during their design process. For seismic regions, most of the respondents preferred positive moment continuity to be provided in all multi-span bridges. The connections were used with girders primarily of the AASHTO Type III and IV size. Other girder sizes that have been used were the PCI-BT, Quad-T, NEBT, U-Beams and Texas shapes. Finally, for the design of the cap beam to superstructure connections, half the respondents replied that a standard detail was used regardless of the application while the majority of the remaining responses used the PCA Method developed by Freyermuth, which is briefly discussed below. It was reported that some found the PCA Method to be conservative in design.

One of the first research projects undertaken to provide details for moment connections was performed to develop what is known as the PCA method, which provided details for designing connection between the superstructure and cap beam to resist creep, shrinkage and live load moments at the cap beam (Freyermuth, 1969). Testing was conducted on the connection that was considered most practical, shown in Figure 2.1, was performed both in a static manner and a fatigue test with a stress range of 20,000 psi. Based on the results, some design recommendations were presented. During the design of the structure, it is recommended that the stress on the bottom face of the girder be limited to 80 percent of the modulus of rupture. A similar recommendation was stated to limit the stress in the connection reinforcing bars to 0.6 times the yield stress. The limit was developed to keep the diaphragm concrete from cracking under positive moments. Also, multiple connections were tested and it was found that most of the bars failed at 670,000 applications of the load. The failure was of the brittle manner at knee of the hooks. As a result, in order to avoid this mode of failure, a recommendation was made that the maximum stress where the bar bends begin should be limited to 50 percent of the fatigue strength (Freyermuth, 1969). Also, it was recommended that, due to the amount of design calculations, standard details should be used for each common girder types in all loading scenarios.

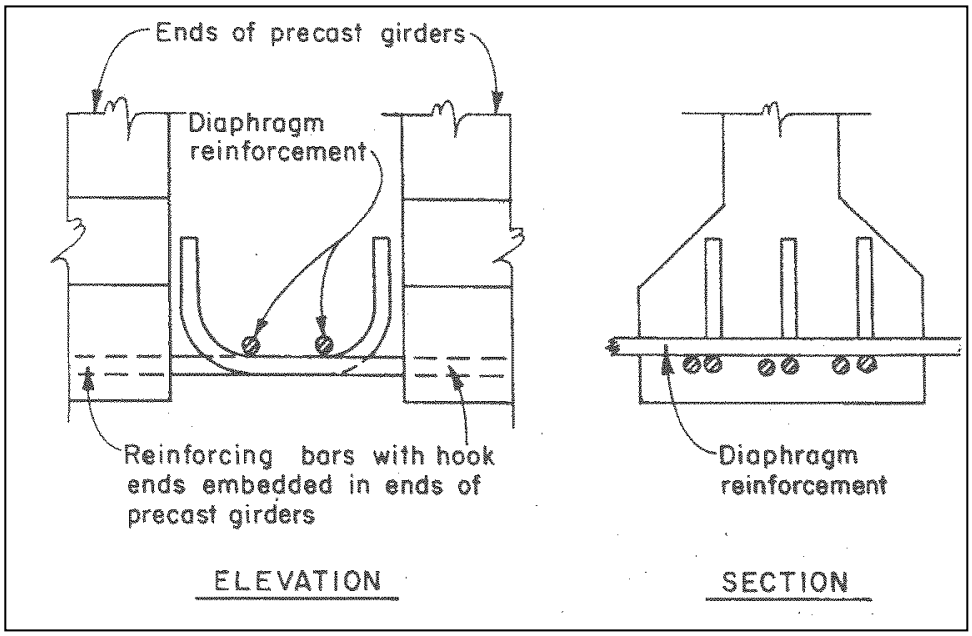

Figure 2.1. Connection Selected for Testing by Freyermuth (1969)

2.2.2 Causes of Positive Moment at Connections

The cause of positive moment comes from multiple effects, while each could appear minor, they can have large effects on the behavior of the structure. A few common causes of positive moment are creep, shrinkage and temperature strain in the decks and girders (Miller, Castrodale, Mirmiran, & Hastak, 2004). In the testing performed for the NCRHP 519 Report, creep, shrinkage and temperature strains were assumed to produce a positive moment equivalent to the nominal cracking moment at the beam-diaphragm interface (Miller, Castrodale, Mirmiran, & Hastak, 2004). The combined creep, shrinkage and thermal effects may cause the girder to camber up resulting in end rotations of the girders. When this occurs, a positive moment develops at the diaphragm next to the girder and may be large enough to crack the diaphragms as seen in Figure 2.2 (Hastak, Mirmiran, Miller, Shah, & Castrodale, 2003). However, it was found that the creep effects are partially counteracted by the differential shrinkage between the precast girders and the cast-in-place deck (Freyermuth, 1969).

In some cases the shrinkage did not appear to cause any negative moment, the reactions actually showed that additional positive moment was forming (Miller, Castrodale, Mirmiran, & Hastak, 2004). The thermal effects were found to be significant as it caused a daily moment change of over one-half the cracking moment capacity of the diaphragm

(Miller, Castrodale, Mirmiran, & Hastak, 2004). Finally, once the spans are made continuous, the effects in one span will cause positive moment in remote spans leading to additional positive moment demands. In addition to those investigations, seismic excitation of a structure was also found to produce positive moments in the connection regions (Priestley, Seible, & Calvi, 1996). As the superstructure displaces laterally from the seismic excitation, one side of the cap beam will experience positive moment while the other will undergo negative moment.

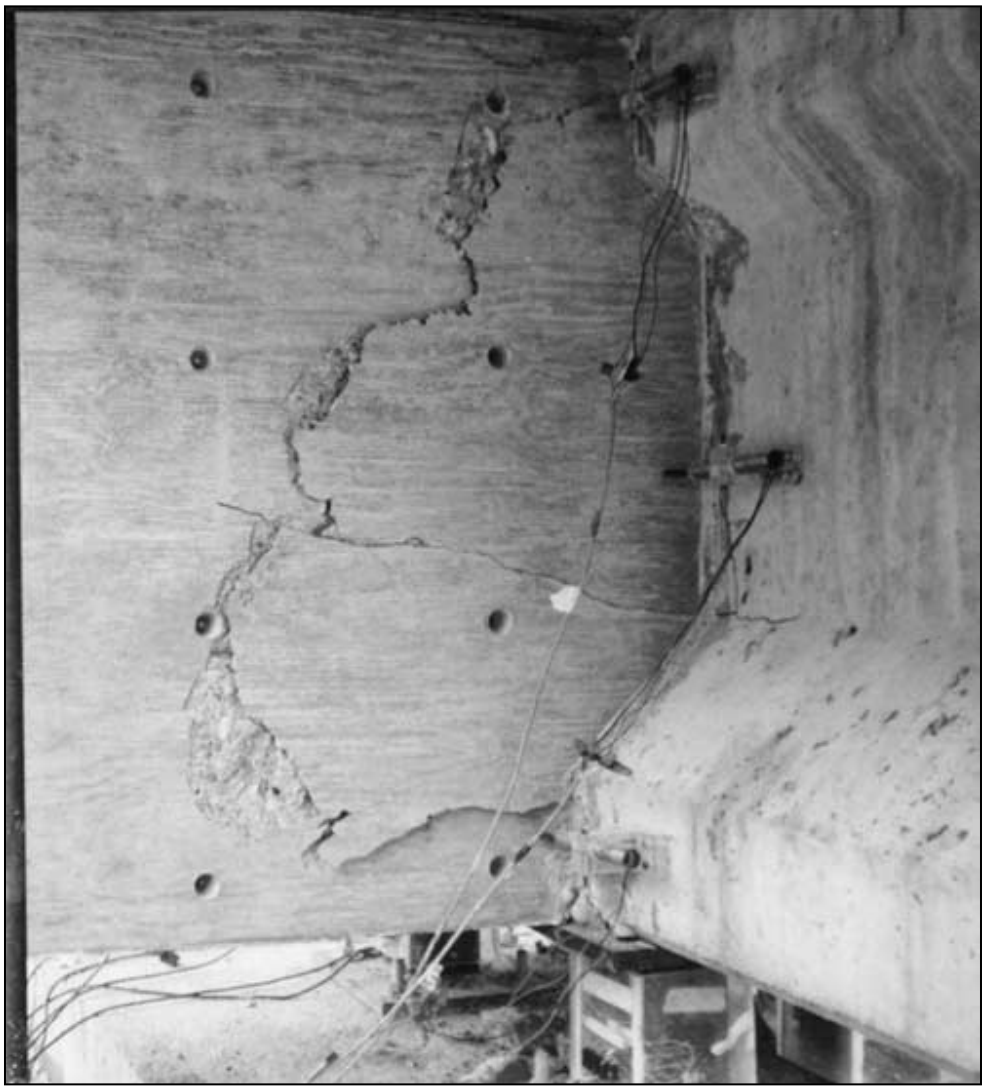

Figure 2.2. Diaphragm Cracking from Positive Moment

2.2.3 Benefits of Positive Moment Connections

A general goal for many state DOT's is to make bridges continuous-for-live-load using prestressed, precast concrete components. The obvious reasons for this goal are to counteract the aforementioned causes of positive moment in order to prevent cracking of the diaphragm, deck and girders. A structure with a sufficient positive moment connection will exhibit an enhanced seismic resistance (Tadros, Ficence, Einea, & Holdsworth, 1993). In addition, superior structural integrity and lower deflection levels can result when a positive moment connection between the superstructure and cap beam is active. Also, providing positive moment continuity between the girders and cap beam via integral bents, or connecting the girder ends across the depth of the cap beam, allows for the combined depth of the cap beam and girders to be reduced (Sritharan, Vander Werff, Abendroth, Wassef, & Greimann, 2005). Providing integral connections also eliminates girder bearings, which, in turn, reduce future maintenance costs. In general, the benefits of a continuous bridge are the improved durability, elimination of bridge deck joints and reduced maintenance costs (Hastak, Mirmiran, Miller, Shah, & Castrodale, 2003).

Several additional advantages of a positive moment connection directly benefit the seismic performance of the bridge (Priestley, Seible, & Calvi, 1996). The redundancy in the bridge structure is increased, which allows for additional plastic hinges to be formed. With additional plastic hinges forming, the potential for energy dissipation increases. When the response of the bridge in the longitudinal direction is concerned, the columns will be under double bending when the plastic hinges are formed at the top and bottom of the column. This allows for greater shear resistance of a given section size and reinforcement content of the columns. Additionally, a double bending behavior of multi-column bents is preferred because the stiffness in the longitudinal and transverse direction is equal, which is the optimum condition for seismic design. Also, by allowing a moment transfer at the top of the column, a pin connection can be designed at the column base; this will significantly lower the cost of the substructure. Furthermore, a pinned base is preferred for bridge columns in areas of low soil stiffness and a positive moment connection will allow for that to occur. Finally, under small seismic displacements, the connection is insensitive to the seismic displacement.

2.2.4 Types of Connections

A number of systems have been developed in order to establish a positive moment connection between the superstructure and cap beam. Most of these systems require a connection mechanism to be developed between the girder and the diaphragm, in order to resist moment at the connection due to the applied loading. The following are examples of systems that have been incorporated into a bridge structure in order to establish the desired positive moment connection: bent bars and untensioned prestressing strands, straight bars, welded bars, reinforcement placed through the web of the girders and into the diaphragms, additional stirrups placed in the diaphragms, mechanical strand connectors, a partial diaphragm to pre-compress the section, and embedding the ends of the girders into the diaphragms at the cap. However, the use of bent bars and bent strands extending into the diaphragm is the most commonly used system for the superstructure to cap beam connection, both of which are used equally as frequent (Hastak, Mirmiran, Miller, Shah, & Castrodale, 2003). Therefore, the advantages, limitations, and applications of these two systems will be of focus in the following text. The research has mainly been performed for non-seismic applications, to resist creep, shrinkage and vehicular live loads; however, some experimental research has been performed and will be discussed in the next section.

2.2.4.1 Bent Bars

According to (Freyermuth, 1969), the most practical positive restraining moment connection was the hooked bar connection. This type of connection was further tested, under monotonic and cyclic loading, and the results were published in NCHRP 519 (Miller, Castrodale, Mirmiran, & Hastak, 2004). The 90-degree hooks used in the testing were designed using the AASHTO Standard Specifications regarding hooked bars (Miller, Castrodale, Mirmiran, & Hastak, 2004). It should also be noted, according to (Freyermuth, 1969), that the maximum bar size used for this connection, if the bars are bent in the field, should be limited to No. 6 (diameter = 0.75 in.). The full-scale test specimen used in the NCHRP report consisted of two I-girders, which were connected using eight hooked No. 5 bars (diameter = 0.625 in.). The girders were placed 10 in. away from each other and a diaphragm and deck was poured around the girders in order to establish the connection, shown in Figure 2.3. Though some cracking occurred at the connection during the testing,

the end reactions and strains within the section demonstrated that continuity was achieved and that the connection detail was effective for the dead and live loading cases (Miller, Castrodale, Mirmiran, & Hastak, 2004). This test focused on the use of bars hooked at a 90-degree angle; however, it was also noted in this report that the use of a 180-degree bend might also be a viable option.

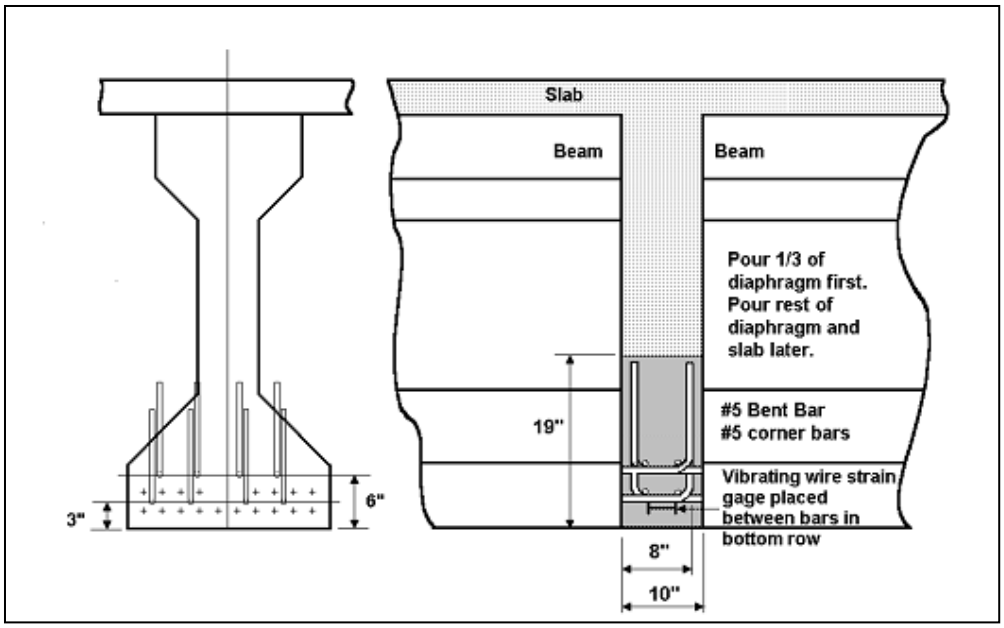

Figure 2.3. NCHRP Bent Bar Specimen

2.2.4.2 Bent Strands

The aforementioned NCHRP report also performed a positive moment connection test, under monotonic and cyclic loading, on a similar full scale test specimen incorporating bent strands as the connection mechanism, as shown in Figure 2.4. Scaled pullout tests were also conducted on specimens using 90 degree bent, straight, and frayed strands. The results of the full-scale test demonstrated that bent strands are able to effectively establish positive moment continuity in the system, even if cracking occurs at the joint. Continuity was only lost when the slab and diaphragm cracked and the connection was near failure. The scaled tests also showed that the bent strands resulted in the optimum anchorage when compared to the straight or frayed strands, which slipped twice as much as the bent strands. Additionally, these tests found that systems involving bent strands and girder ends that were not embedded

in a diaphragm, had a tendency for the girders to separate from the face of the diaphragm. However, this separation from the diaphragm did not result in any damage. Finally, the results of the testing did show that, though the specimens did provide continuity, the bent strands also had a tendency to slip under cyclic loading. As a result, it may be concluded the bent strand detail would not be preferred for seismic applications.

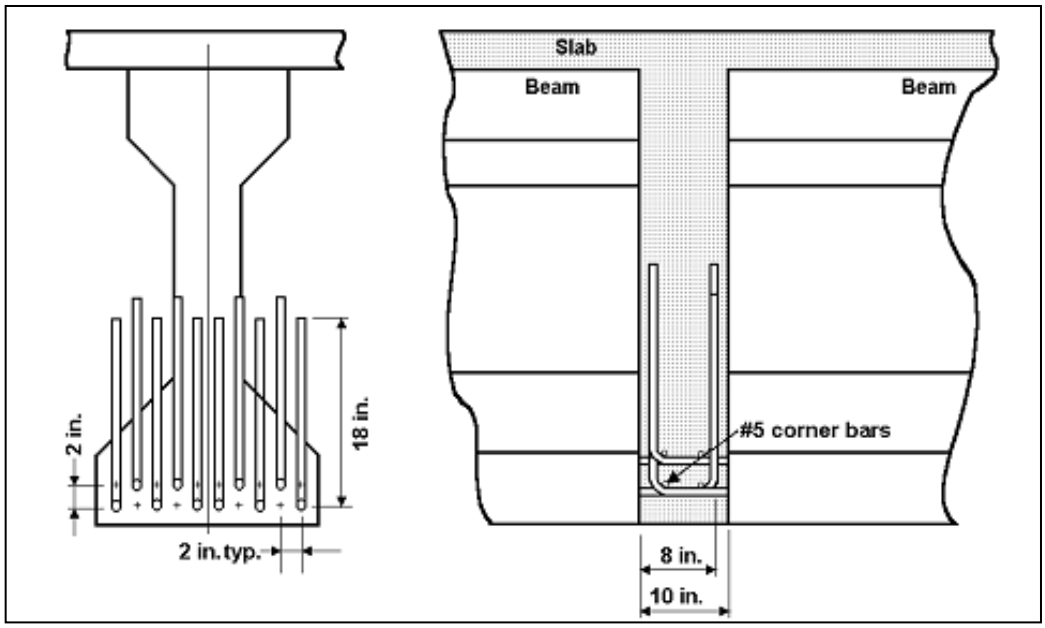

Figure 2.4. NCHRP Bent Strand Specimen

The behavior of untensioned prestressing strands, for use in positive moment connection details, was also investigated by Salmons and McCrate (Salmons & McCrate, 1977). Their findings showed that the helical orientation of the strands tended to unscrew the strand from the surrounding concrete. Additionally, under high stress levels, local crushing at the strand-concrete interface was observed, which contributed to both creep and slipping effects on the strand. However, under cyclic loading, additional creep was not experienced until the load returned to its previous maximum. Similar to the findings presented in the NCHRP report, Salmons and McCrate concluded that bent strands provided a higher strength and stiffness when compared to straight and frayed strand configurations. Salmons and McCrate went further to investigate which characteristic of the section had an influence on the slip behavior experienced by the untensioned strands. First, it was concluded that the

relationship between stress within the strand and slip were independent of the embedment length of the strand. Second, varying the concrete between 3750 and 6900 psi did not have a significant effect on the bond characteristics of the strand before slipping occurred. Finally, the diameter of the strand also did not have a significant effect on the stress-slip behavior of the steel strands. Based on these findings, Salmons and McCrate were able to develop and present a series of equations pertaining to the embedment length of the untensioned strands to establish a superstructure to cap beam moment connection.

2.2.4.3 Embedded Girder Ends

The aforementioned NCHRP report also investigated the effect that embedding the ends of the girders into the diaphragm had on establishing a positive moment connection. In general, it was determined that embedding the ends of the girders 5 in. into the diaphragm reduced the stresses in the connection and allowed for a higher number of cycles to be reached before failure of the positive moment connection. Girders that were connected using bent strands and embedded ends failed at a number of cycles that was three times greater than that required for the same detail without embedded ends as the strains in the embedded details were lower than those in the non-embedded. As a result, it appeared as though embedding the ends of the girders for sections connected with bent strands was beneficial. However, the general effects of the embedded were hard to quantify, specifically for the bent bar details, and as a result, it was recommended that the effects of embedment be ignored in the design process.

2.2.4.4 Additional Stirrups

A few other connection components were also examined as a part of the NCHRP report, one of which was the placement of additional stirrups within diaphragm in the joint region. During testing, it was noted that the additional stirrups helped to control diagonal cracking and increase ductility after the main bars fractured. However, in general, the stirrups had little effect on the overall strength of the connection. Finally, the report suggested that the ends of the girders should be embedded in order for the stirrups to provide the additional ductility.

2.2.4.5 Through Web Reinforcement

Another NCHRP connection component was the use of reinforcement placed through the webs of the girders and into the diaphragm. It was found that, though the web reinforcement improved the performance of the connection, the bars caused cracks to develop in the webs of the girders, which is undesirable.

2.2.4.6 Partial Diaphragm

The final connection component that was investigated as a part of NCHRP 519 was the use of a partial diaphragm to improve the connection performance. It was initially assumed that the partial diaphragm would place the bottom of the diaphragm in compression, which would reduce the tension in the section caused by the positive moments within the joint and increase the capacity of the connection. However, it was found that though the concept worked, it was not by the originally assumed mechanism and that it did not provide continuity. Based on the results of the testing, it was implied that more research regarding the use of partial diaphragms should be performed in order to better understand this mechanism.

2.2.5 Concerns Regarding Positive Moment Connections

Though methods for establishing a positive moment connections and their respective behaviors have been established, there are still a number of concerns and issues associated with positive moment connections. This primarily includes fabrication issues, the lack of a well-defined design procedure, and the age at which the connection is established.

2.2.5.1 Fabrication Issues

In general, the additional reinforcement that is required in order to achieve continuity in the connection often results in congestion within the section, which causes difficulties related to construction in the field. However, it was found that, though the diaphragm may be congested, the connection should still have adequate strength. Additionally, the bent connection bars are difficult to construct, labor intensive, and are often asymmetrical, which can lead to uneven stresses and failure in the section (Miller, Castrodale, Mirmiran, & Hastak, 2004). The asymmetry is due to the fact that the bent connection bars must be installed straight and then be bent in the field. Also, it is not uncommon for the extended

bars or strands to be damaged or fractured during fabrication and transport. In the event of a fractured piece of reinforcement, holes must be drilled into the girder ends in which the new reinforcement is embedded in epoxy. Finally, it has been observed that strands that are detensioned have a tendency to experience a "bird cage" effect, where the wires unravel, which renders the section ineffective.

2.2.5.2 Lack of a Well-defined Design Procedure

Though NCHRP 519 makes design recommendations based on the results of their extensive testing of positive moment connections, a design method for determining the amount and spacing of reinforcement for the connection has not yet been accepted. As a result, there are often concerns associated with placing too many reinforcing bars in one area without an adequate spacing within the diaphragm. It is typically assumed that cracking will occur at the interface of the beam-to-diaphragm connection region, but the failure will not occur within the diaphragm. However, it is unclear as to whether or not this cracking will affect the continuity of the system. Furthermore, it has been found that the cracking did not affect the negative moment capacity, but it did reduce the negative cracking moment. Therefore, in order to help ensure an adequate capacity, designers recommend that the positive moment connection at the diaphragm have a capacity no greater than 1.2 times the cracking moment of the section. This limit is imposed in order to prevent the section from being overdesigned, as additional reinforcement in the section will only increase congestion, while providing little impact on the overall behavior of the connection.

2.2.5.3 Age at which the Connection is Established

Based on the results of the NCHRP testing, it was found that the age of the girders at the time at which continuity was established was the "single most important factor in the behavior" of the section. If the girder is relatively young, creep can produce significant positive moments within the connection. Conversely, if the girders are older, the differential shrinkage that will be experienced between the girder and the deck can produce significant negative moments within the connection. Therefore, it was decided that it would be unnecessary to limit the age of the girder, but rather a minimum advisable limit for the age is

advisable in order to limit the formation of large positive moments, which might be generated during aging.

2.3 Experimental Research

One example of previous research regarding the use of precast components in a bridge structure made continuous was a report and research completed by Holombo (Holombo, Priestley, & Seible, 1998) regarding the use of precast sliced-girder bridges. In his report, an investigation on the seismic behavior of bridges using precast girder segments, which were spliced together using prestressing strands and made continuous for seismic loading as well as any live load or self-weight, was presented. The benefits of using spliced precast girders over a more conventional, cast-in-place or simply supported precast girder system are that longer spans may be achieved and that the design moment may be reduced, resulting in a reduced superstructure depth, smaller foundation, and ultimately a reduction in cost.

The results of the testing by Holombo showed that spliced precast girders, both the bulb-tee and bathtub, could be used effectively in areas of high seismic activity with a high degree of performance. Both of the test units used in this research achieved a level of ductility (μ_Δ= 8 for the bulb-tee unit and μ_Δ= 6 for the bathtub unit) that was significantly greater than that of the design value (μ_Δ=4), while only minor cracking in the superstructure was observed.

Another example is the experimental research performed in order to develop design guidelines for integrally constructed cap beam to steel girder joint regions (Patty, Seible, & Uang, 2002). Four specimens were tested with combinations of cap reinforcement, either post-tensioning or conventional reinforcement, and girder stiffeners, with or without. The study focused on the torsional behavior of the cap beam with the different concepts, as shown in Figure 2.5.

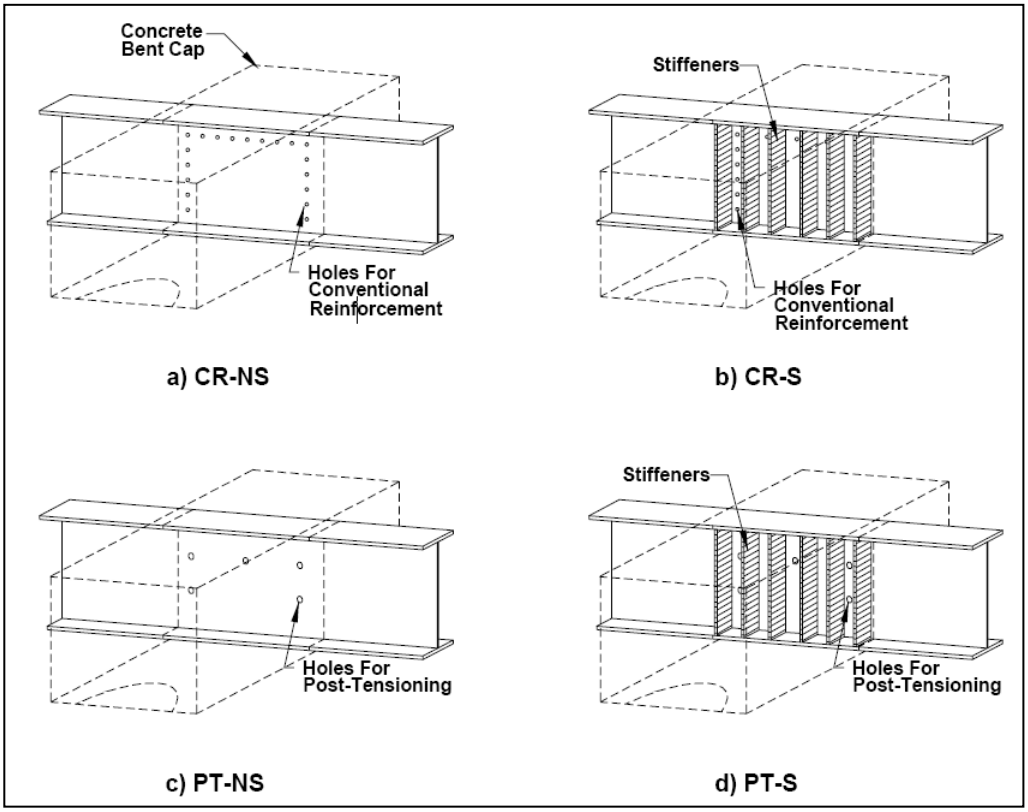

Figure 2.5. Test Concepts for Torsional Behavior of Integral Cap Beam

After testing the four concepts, the results showed that the torsional moment capacity of the component with stiffeners increased by 25%. The strain gauges recorded higher strains on the outer stiffeners than the inner stiffeners, indicating the outer stiffeners are more effective in transferring the flexural moment of the girders to the cap beam, resulting in a torsional moment. The stiffeners also contributed in reduced dilation of the bent cap by approximately 33% compared to the specimens without stiffeners. Next, the effect of the post-tensioning from the concept testing was discussed. Bent caps with post-tensioning experienced almost zero dilation and significantly less cracking up to maximum moment. Also, the bent caps with post-tensioning instead of conventional reinforcement are easier to construct.

Additional research was conducted at Iowa State University into the behavior of concrete cap beam and steel girders constructed integrally (Sritharan, Vander Werff, Abendroth, Wassef, & Greimann, 2005). A connection was used that made the girders continuous across the cap beam by using flange and web plate connections. The girders were

welded to steel splice plates that were in line with the flanges and girder web. After the testing of two test units was completed, it was noted that the superstructure, girder-to-cap-beam connection and the column-to-cap beam connection all remained essentially elastic. Minor spalling in the deck was observed, which was attributed to the punching column longitudinal bars through the bridge deck. The failure of the test units was measured to occur at a displacement ductility of 4; however, modification to the shear connectors that extended from outside of the cap beam into the column would have allowed for greater ductility.

2.4 Grillage Finite Element Analysis

2.4.1 Introduction

The use of finite element analysis in structural engineering has become commonplace in today's industry. Complex structures, that were once thought to be unapproachable, can now be analyzed to an approximate solution in a cost effective manner involving minimal engineering time. However, engineers are constantly searching for innovative methods to make the use of a finite element analysis more user-friendly, time-efficient, and overall simpler for use on a regular basis. As a result, it is often more convenient for an engineer to employ the use of the simpler finite element model, known as a grillage model, in order to gain a basic understanding of the forces, stresses, strains, and displacements of a structure due to various load cases.

2.4.2 Background

A grillage model consists of a network, or grid, of longitudinal and transverse beam elements, used to model specific aspects of the structure. In a bridge application, the longitudinal members typically represent the girders and a portion of the slab for which they support (Jaeger & Bakht, 1982). The transverse members typically model members that act across the structure, for example: cap beams, diaphragms, and effective portions of the bridge deck. Simplifying the model in this manner, when compared to a more complex finite element model, often reduces the likelihood of introducing errors or uncertainties associated with using unfamiliar elements in the analysis (Kostem & Ragazzo, 1993). Also, simplifying the model often allows the engineer to more easily visualize and organize the model, thus reducing the time spent to produce the model and making it easier to understand and verify

its results (Srinivas, Ramanjaneyulu, Sukhesh, Sasmal, & Gopalakrishnan, 2004), (Jaeger & Bakht, 1982). According to the article entitled, "Grillage Analogy for Multigirder Bridges," (Kostem & Ragazzo, 1993), "The effort required for a grillage model is about 10% of the effort required for a true finite element model."

Grillage analysis has been used to model a wide variety of structural engineering applications. Though it is most commonly used to model bridge structures, it has also been used to model slabs, buildings, and other structures. Complicated bridge features, a variety of bridge decks, prestressed girders, I-, T-, and bathtub girders, and other unique bridge components have also been accurately modeled using the grillage analogy. As a result of its wide range of flexibility, ease-of-use, and time saving potential, the grillage analysis is commonly used tool for analysis.

2.4.3 Analysis Limitations

Though the use of a grillage analysis offers a lot of appealing benefits over a complicated finite element analysis, it is not without its own limitations. First, it is important to note that all finite element analyses offer an approximate solution rather than an exact solution. The accuracy of any finite element model depends on the knowledge and assumptions made by the user, the elements used in the model, the enforced boundary conditions, etc. (Kostem & Ragazzo, 1993). Grillage analyses typically result in an equilibrium solution that may often be used as lower bound solution (Gordon & May, 2004). In other words, the results are often used to obtain more of a general feel for how the structure will behave given specific loading conditions (Jaeger & Bakht, 1982). However, this is not to say that the results could not, or should not, be used for design purposes.

Comparisons to more accurate finite element models, as well as actual test results, have shown that, while certain characteristics of the models agreed very well, other aspects showed a gross disagreement (Kostem & Ragazzo, 1993). For example, it has also been shown that the accuracy of mid-span moment predictions may vary with the length of the girders being modeled (Kostem & Ragazzo, 1993). Short-to-medium span bridges can predict moment values with roughly 10% error, while the accuracy decreases as the span length increases. However, long span bridges do tend to provide an acceptable degree of accuracy when predicting mid-span moments (Kostem & Ragazzo, 1993). The same study

also showed that the grillage analysis provides better results when used to model simple span bridges with prestressed concrete girders, than bridges with reinforced concrete decks and steel girders (Kostem & Ragazzo, 1993). These types of errors, often associated with over simplification of the model, have led some researchers to conclude that the use of a grillage analysis should be avoided when a more accurate finite element analysis is feasible (Gordon & May, 2004).

2.4.4 Model Construction

As stated earlier, a grillage analysis consists of network of longitudinal and transverse beam elements. The structural components that those elements represent depend upon the structure being modeled. A typical bridge grillage model consists of members representing the column, cap, girders, diaphragms, and the bridge deck. In order to accurately capture the behavior of the structure, it is crucial that the properties of these elements be accurately modeled within the analysis software.

Typically the various member properties, cross-sectional area, moment of inertia, etc. should be computed and input into the program using typical mechanics of materials equations. In order to reflect the nonlinear behavior and plastic hinging of the column, it is recommended that plastic hinges, or springs elements, be placed at the top and bottom of the column. More information regarding the modeling of this nonlinear behavior will be presented below.

When modeling a bridge, the girders are a very important component of the grillage analysis. Typically the longitudinal beam elements within the grillage analysis are used to model the girders. In order to accurately model the girders and their contribution to the system, the beam elements are usually located at the centroid of the girder that it represents (Keogh & O'Brien, 1996), (Jaeger & Bakht, 1982). Also, if a deck is present above the girders and composite action between the girders and the deck is considered, a portion of the deck should be included when calculating the various section properties for the member in order to reflect the composite section (Jaeger & Bakht, 1982). The effective flange width of the deck above the girder should be calculated per AASHTO guidelines (Staudt, 2002). Also, a common means to approximate the effective stiffness of the girders after cracking is to reduce the gross stiffness by 75% (Holombo, Priestley, & Seible, 1998).

Since the majority of lateral load is transferred to the column and supports by the diaphragm action of the deck, it is important to accurately model the deck within the grillage analysis (Kostem & Ragazzo, 1993). The majority of the transverse beam elements in the grillage model are used to capture the behavior of the deck. The primary concern when modeling the deck is the spacing of the transverse beam elements. Though some researchers have argued that a coarse mesh is sufficient for design and that the spacing is somewhat arbitrary, if the mesh is too coarse, the deck will not deflect in a smooth manner and could generate inaccurate forces on surrounding members (Hambly, 1990). As a result, it is recommended that the members be spaced at approximately one quarter to one eighth of the effective span as a guideline. It is also convenient to maintain a uniform spacing, when possible, of the transverse members. The section properties of the grillage elements should then be calculated based on the tributary area of the deck for which they represent. Other grillage analyses have also suggested that half the gross section properties of the deck be used to reflect the cracked properties of the deck when bending about its transverse, while zero stiffness should be considered for bending about the axis perpendicular to the surface of the deck (Holombo, Priestley, & Seible, 1998). When diaphragms are present in a structure, it is also important to model them with a transverse beam element. The properties of the diaphragm should be calculated considering the contribution of the deck as an effective flange width acting with the diaphragm (Hambly, 1990).

Finally, once all of the members are placed within the grillage model, it is important to mesh or link them together so that they may act as a unified network. Though there are many options that can be considered when joining elements (rigid end links, springs, etc.), it has been shown that extending the elastic member properties to the centerline of their respective joints typically provides more accurate results when compared other options, specifically rigid end links (Holombo, Priestley, & Seible, 1998).

Another crucial aspect of the grillage model is accurately capturing the boundary conditions. This becomes a greater concern when only a portion of the actual is being modeled; this is likely due to symmetry. Typically, for a symmetric structure, only half of the structure need be modeled as it may be split down a longitudinal centerline. In this case, it is important to accurately capture the effects of the other half by applying boundary

conditions along the "line of cut." In such a case, it is usually recommended that the centerline be restrained against a translation perpendicular to the centerline as well as rotation about the centerline (Holombo, Priestley, & Seible, 1998). These boundary conditions are used, as the structure (a bridge for example) would not likely translate horizontally due to the displacements being applied in the longitudinal direction for a typical push-over analysis. However, if it were not for the applied boundary conditions, the model might have a tendency to do so as it is would be asymmetric. Also, the model should not allowed to rotate about its longitudinal axis as the presence of its other half would result in zero rotational displacement along the centerline.

2.4.5 Nonlinear Behavior

Nonlinear behavior is a very important aspect that must be captured within a model, especially if the structure is located within a seismic region. Bridges in seismic regions are typically designed to develop plastic hinges in their columns during a seismic event in order to preserve its superstructure and prevent catastrophic damage. Therefore, these nonlinear characteristics should also be present within a grillage model. The modeling of nonlinearity has been accomplished primarily through two methods: event scaling analysis and the use of nonlinear springs or hinges.

An event scaling analysis, also commonly referred to as a collapse mechanism analysis, is a sort of roundabout method of performing a nonlinear analysis. Essentially, the method requires a linear elastic grillage model and knowledge of the behavior of the structure at each significant nonlinear event, i.e. the formation of a plastic hinge, reinforcement yielding, cracking, etc. A series of linear analyses are performed using the linear elastic grillage model until the forces within the model reach the first specified nonlinear event; at which point, adjustments are made to the model to reflect the occurrence of the nonlinear event, which is typically done by changing the stiffness of specific members surrounding the nonlinear event. Another linear analysis is then performed using the updated member properties and the process is continued until the final nonlinear event, or a failure mechanism, is reached. Though the method can be performed through hand calculations, the structures being analyzed are typically too complicated and require the use of automated software (Priestley, Seible, & Calvi, 1996). However, this analysis technique is somewhat

outdated and is significantly more time consuming when compared to more current techniques. As a result, this method is not typically preferred over other nonlinear analysis techniques such as the use of nonlinear springs or hinges.

Briefly, another method is based on the "Linear elastic stiffness matrix approach" (Deng, Ghosn, Znidaric, & Casas, 2001). This method of analysis includes the effects due to nonlinear behavior of the structural members by adjusting the stiffness matrix at the end of each load increment in order to reflect the softening of a given member.

Currently, the standard method used to perform a nonlinear grillage analysis is through the use of nonlinear spring, hinge, or link elements. In order to accurately employ this method, the location of potential plastic hinges must be known (Deng, Ghosn, Znidaric, & Casas, 2001). In the case of a bridge structure located in a seismic region, the current design practice is to design the structure such that plastic hinges will form within the columns. Therefore, the springs should be placed at their respective locations within their respective column. Typically, the behavior of the nonlinear springs is based on a moment-rotation, or moment-curvature, relationship that is input by the user into the analysis software (Deng, Ghosn, Znidaric, & Casas, 2001). As a result, it will often be necessary to perform a moment-curvature analysis on the portions of the structure that will develop the plastic hinges. The moment-curvature relationship can then be converted into a moment-rotation analysis and input into the spring parameters within the analysis software. Once the nonlinear springs are in place, the analysis can be run as a nonlinear analysis and the structure will undergo normal elastic deformation before undergoing plastic deformation per the moment-rotation properties of the given spring. This method is much more efficient and accurate compared to the former methods, and thus, is often the preferred method for a nonlinear grillage analysis.

2.4.6 Hysteretic Behavior

The nonlinear behavior in a bridge is usually forced into specific plastic hinge locations, which are defined by a nonlinear plastic spring or hinge, as mentioned previously. Seismic loading on a structure occurs in a cyclic manner and, as a result, the nonlinear spring will be forced to load in a given direction, unload, and reload in the opposite direction. However, once the hinge region has reached a given amount of nonlinearity, the effective

stiffness of the column will be reduced. Hence, the manner in which the spring unloads and reloads will change with loading and will not simply follow the original curve as it must reflect the energy that is dissipated due to hysteretic damping as plastic behavior is developed. Therefore, it is important to accurately reflect these changes in behavior by incorporating some form of a plastic hinge hysteretic model. Currently, there are two main hysteretic models that are widely used and accepted: The Takeda Model and the Pivot Model.

2.4.6.1 Takeda Model

Toshikazu Takeda developed the Takeda Model in 1970 with a focus on modeling the hysteretic behavior of reinforced concrete (Takeda, Sozen, & Nielsen, 1970). This model defines an initial "Primary curve" to define the initial loading of the hinge. This primary curve is tri-linear and defined by the load and displacement at first cracking as well as the load and displacement at yield, as depicted by curve (a) of Figure 2. The slope of the final segment of the tri-linear curve is defined by the strain-hardening properties of the reinforcement, as the section has previously cracked and the reinforcement has yielded. The curve then follows a series of case-specific rules for unloading and reloading, which are governed by the amount of load or displacement that has been reached within the hinge. Unfortunately, the rules are a bit too complex and lengthy to list in their entirety; for a more in-depth description refer to (Takeda, Sozen, & Nielsen, 1970). Curves (b) and (c) in Figure 2.6 display an example of how a given hinge might load and unload based on the aforementioned set of rules provided in (Takeda, Sozen, & Nielsen, 1970). As part of the development of the model, Takeda performed dynamic excitation tests on a reinforced concrete test specimen. The results of these tests were then compared to the results of the calculated dynamic response based on the Takeda Model. A comparison of the results obtained via the testing provided satisfactory agreement and the model has since been widely accepted as a valid hysteresis model. A modified version of the Takeda Model has also been developed, which updates the rules of the original simplified model in order to provide more accurate results. One main difference from the original model is that the initial stiffness of the member is based on the cracked section properties rather than the pre-cracked properties (Dowell, Seible, & Wilson, 1998).

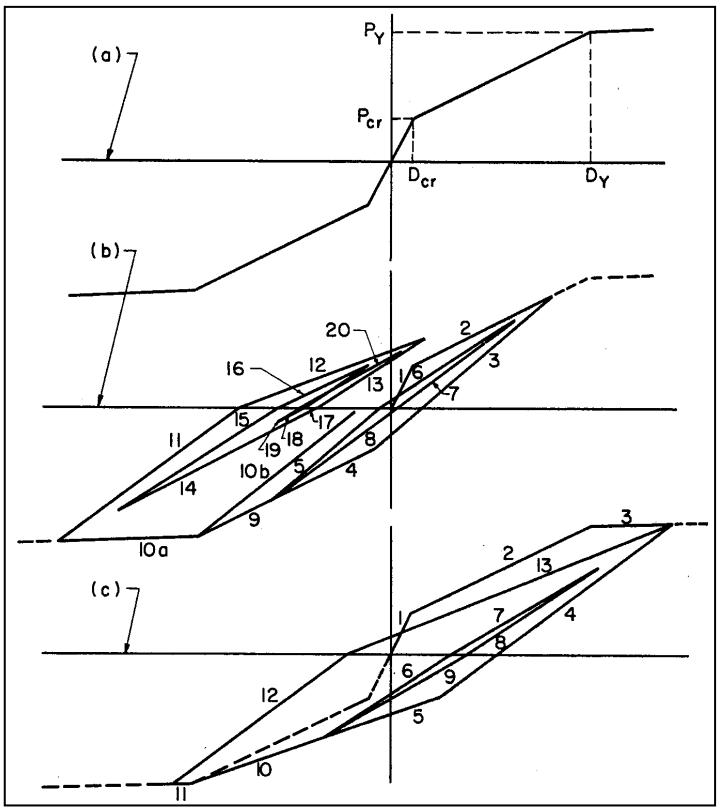

Figure 2.6: Takeda Model

2.4.6.2 Pivot Model

Another commonly used model is the Pivot Model, which was recently developed by Dowell et al. in 1998 (Dowell, Seible, & Wilson, 1998). Similar to the Takeda Model, the Pivot Model was also developed for plastic hinges in reinforced concrete members. The Pivot Model has the ability to account for cyclic axial loads, asymmetric sections, and strength degradation. However, compared to the Takeda Model, it is much simpler as the response can be predicted by three rules based on the geometry of the member. By observing the force-displacement hysteresis results from reinforced concrete members subjected to cyclic forces, Dowell was able to make the following conclusions (Dowell, Seible, & Wilson, 1998): First, the unloading stiffness decreases as ductility increases. Second, once the load is reversed after a nonlinear event, the hysteresis plot crosses the initial stiffness line before reaching the corresponding idealized force. When unloading to a condition of no load, from any point on the plot, it usually follows a path that points towards a single point along the

initial stiffness line. This point is referred to by Dowell as the, "Primary pivot point." Finally, during loading, it was observed that the plot tended to cross the elastic loading lines shown in Figure 2.7 at the same point, known as the "Pinching pivot point." All of these observations form the backbone of the Pivot Model. The elastic loading lines mentioned earlier are also used to divide the plot into four quadrants, as shown in Figure 2.8. These quadrants are used to determine which set of rules will apply to the hysteresis plot given the force and displacement condition at which the load or unloading is applied. Unless a reversal in displacement direction occurs, the hysteresis will follow a given strength envelope; one envelope is used prior to yielding of the section and another envelope is used after the section has yielded. Figure 2.9 shows a typical post-yield strength envelope that a section may be expected to follow. In order to incorporate strength degradation under cyclic loading, the pinching pivot points are allowed to move towards the origin and the plot is adjusted to intersect at these new points. Also, after a nonlinear event, the initial stiffness will often soften. As a result, the model allows the elastic loading lines to rotate in order to reflect these changes in stiffness. Comparisons of the Pivot Model to both the Takeda Model and test results from the dynamic loading of a reinforced concrete member led to the conclusion that the Pivot model generally behaved as well as, if not better than, the Takeda Model. However, the Pivot model currently does not account for the strength degradation experienced under cyclic loading to the same amount of displacement, strength degradation in one direction due to a sudden strength loss in the opposite direction, or biaxial bending effects (Dowell, Seible, & Wilson, 1998).

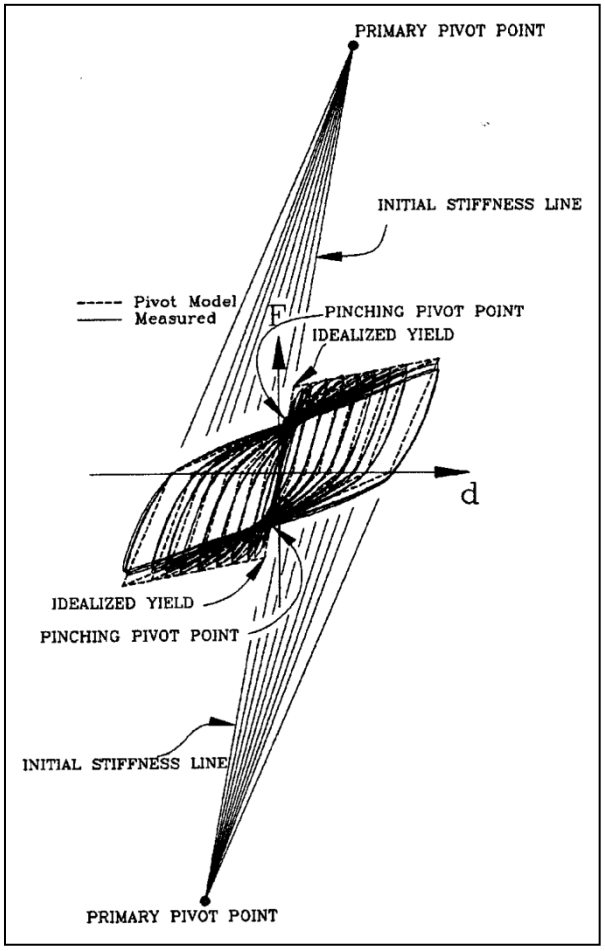

Figure 2.7: Pivot Model Observations

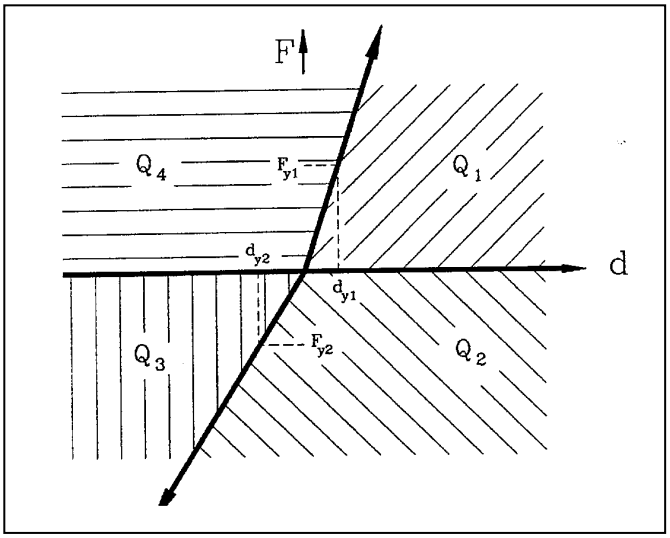

Figure 2.8: Elastic Loading Line Quadrant Division

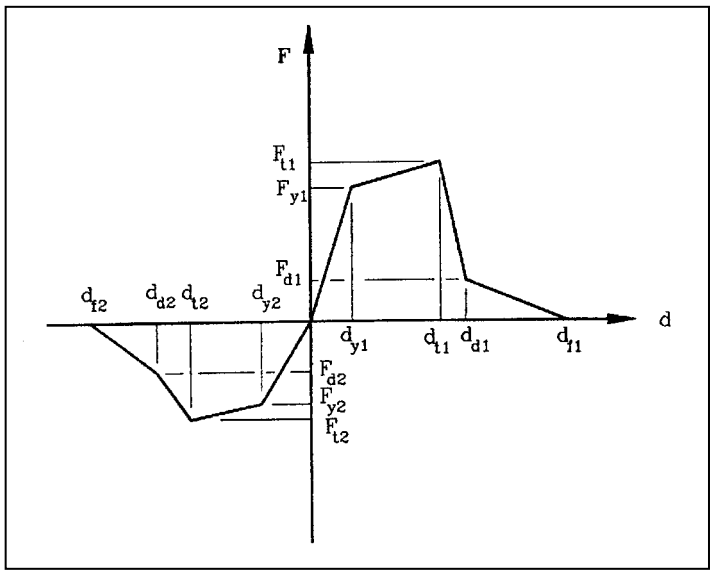

Figure 2.9: Typical Strength Envelope

2.4.7 Torsional Behavior of Concrete

The torsional behavior of reinforced concrete is still a relatively new field of study. As a result, compared to other areas of focus within structural engineering, little information exists and much of the predictions made regarding this topic are based on a series of assumptions. However, in order to develop a more accurate finite element model, or make any sort of prediction, many of these assumptions must be adopted.

It is known, however, that an applied torsion will generate shear stresses along the perimeter of a given cross-section. Therefore, the inner core of the given cross-section is typically neglected in regard to the contribution of torsional resistance. This assumption has also been validated through experimental testing (Rahal K. N., 2000). Instead, a hollow tube analogy, which considers only the outer portion of the section for torsional resistance, is often used when analyzing the torsional behavior of the cross-section, as shown in Figure 2.10 (Collins & Mitchell, 1991), (Rahal K. N., 2000). The following equation, Equation 2.1, which was presented by Rahal and Collins and validated through experimental results, may then be used to predict the cracking torque for a given section. The variables A_c and p_c represent the cross-sectional area and the perimeter of the section, respectively.

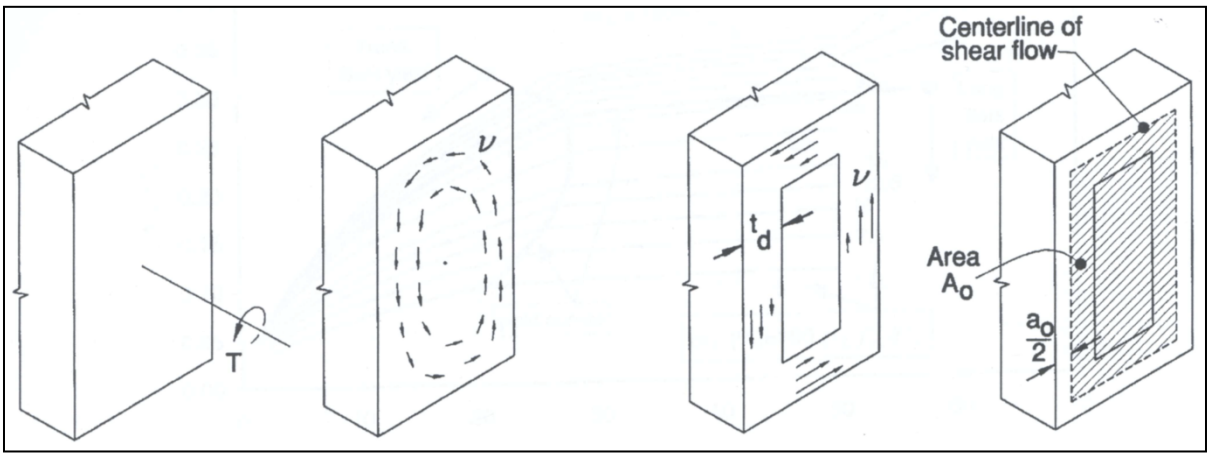

Figure 2.10: Torsion Hollow Tube Analogy

$$T_{cr} = \frac{A_c^{\,2}}{p_c} 4\sqrt{f_c'}\sqrt{1+\frac{f_{pc}}{4\sqrt{f_c'}}}(psi) \qquad (2.1)$$

Collins and Mitchell also present an approach to calculating the ultimate torque for a section, post-cracking. After torsional cracking occurs along a section, the torsion is typically resisted by the diagonal compressive stresses in the concrete that wrap around the beam at an angle of θ, as shown in Figure2.11. However, due to the applied torsion, the outer surface of the section will no longer be plan and result in a non-uniform diagonal stress distribution along its surface. Eventually, at a certain depth below the surface, the stresses become tensile rather than diagonal, leaving the remainder of the section ineffective in resisting the applied torsion. Additionally, as the section continues to deform, the cover concrete will spall and fall away from the section. Therefore, a version of the hollow tube analogy may continue to be used when analyzing the section post-cracking, shown in Figure 2.12. As a result, the following equations may be used together in an iterative manner, as outlined by Collins and Mitchell, to converge on the torque and angle of twist at the ultimate limit state for the section (Collins & Mitchell, 1991).

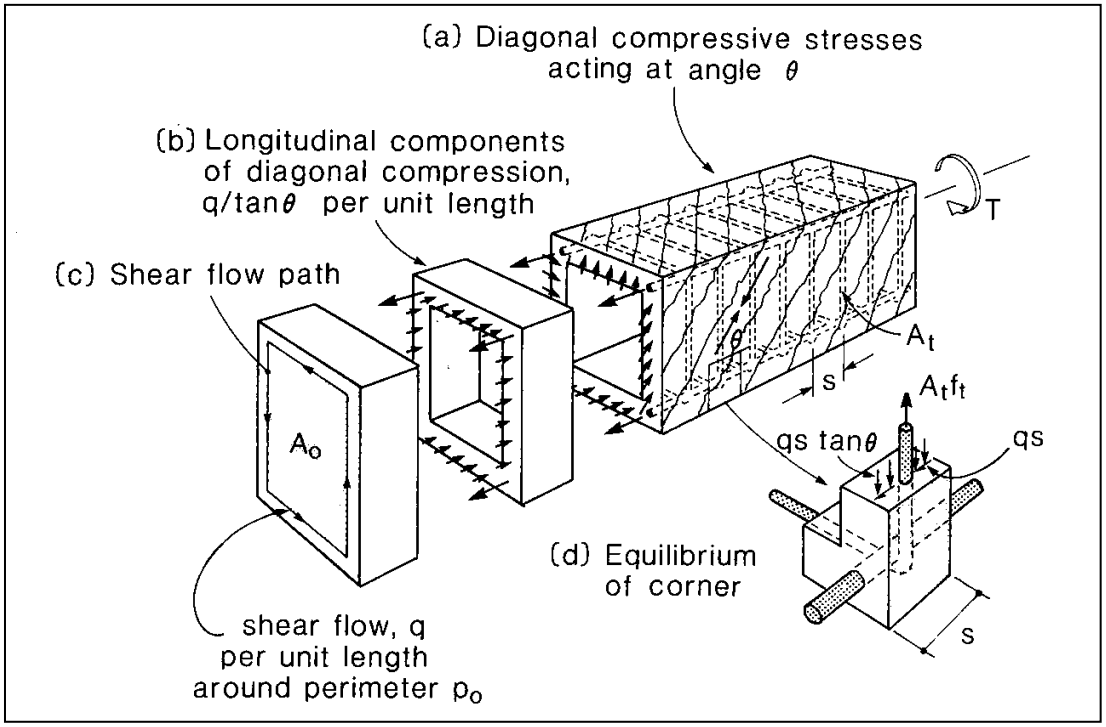

Figure 2.11: Torsional Behavior Post-Cracking

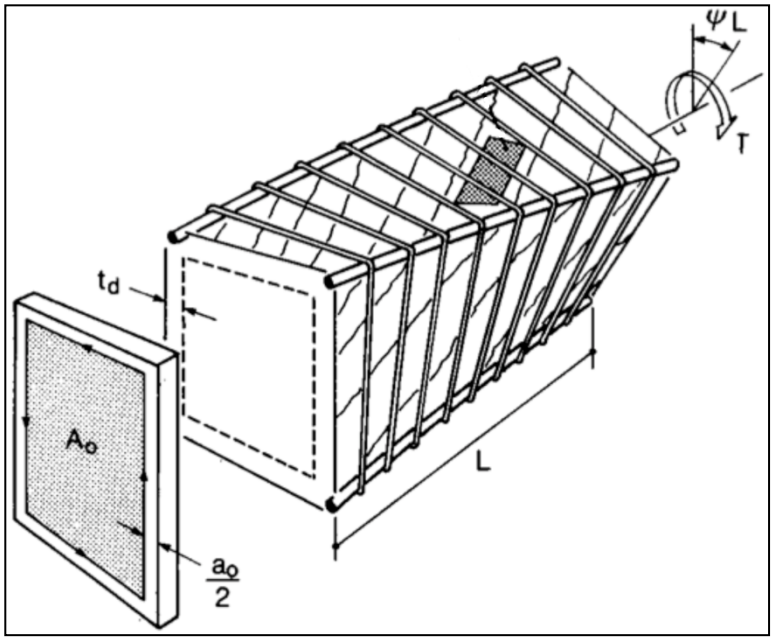

Figure 2.12: Post-Cracking Hollow Tube Analogy

$$T = 2A_o \frac{A_t f_t}{s} \cot\theta \qquad (2.2)$$

In the above equation, Equation 2.2, A_o represents the area surrounding by the shear flow path as shown in Figure 2.12.A_t and f_t represent the area and tensile stress in the hoop reinforcement surrounding the section, respectively, while s represents the spacing of the hoop reinforcement.

$$a_o = \frac{A_{oh}}{p_h}\left[1 - \sqrt{1 - \frac{Tp_h}{\alpha_1 f_c' A_{oh}^2}(\tan\theta + \cot\theta)}\right] \quad (2.3)$$

Equation 2.3 is used to solve for the thickness around the section that is used in resisting the applied torsion, a_o. A_{oh} represents the area enclosed by the centerline of the hoop reinforcement, while p_h represents the perimeter of the centerline of the hoop reinforcement. The value for α_1 is typically assumed to be 0.70.

$$N_v = \frac{Tp_o \cot\theta}{2A_o} \quad (2.4)$$

Equation 2.4 is used to calculate the tensile force, N_v, in the longitudinal reinforcement. The variable p_o represents the perimeter of the shear flow path.

$$\varepsilon_x = \frac{N_v}{A_l E_s} \quad (2.5)$$

Equation 2.5 determines the longitudinal strain in the reinforcement and has been simplified by removing the terms accounting for prestressing. A_l and E_S represent the area and modulus of elasticity of the longitudinal steel, respectively.

$$f_2 = \frac{Tp_h}{A_{oh}^2}(\tan\theta + \cot\theta) \quad (2.6)$$

Equation 2.6 is used to quantify the principal compressive stress in the concrete, f_2, and is used to check whether or not the concrete has experienced any diagonal crushing.

$$\varepsilon_1 = \varepsilon_x + \frac{\varepsilon_x - \varepsilon_2}{\tan^2\theta} \quad (2.7)$$

Equation 2.7 is used to calculate the principal tensile strain in the concrete, ε_1. The value for ε_2 is typically estimated to be -0.0015.

$$f_{2\max} = \frac{f_c'}{0.8 + 170\varepsilon_1} \quad (2.8)$$

Equation 2.8 is used to determine the limiting compressive stress, f_{2max}, in the concrete, for which the compressive stress is not allowed to exceed.

$$\varepsilon_t = \varepsilon_1 - \varepsilon_x - 1.5x10^{-3} \quad (2.9)$$

Equation 2.9 is used to calculate the tensile strains in the stirrups to confirm that they are yielding at failure.

$$\gamma_{xy} = 2(\varepsilon_x - \varepsilon_2)\cot\theta \qquad (2.10)$$

Equation 2.10 determines the shear strain n the section at failure.

$$\psi = \frac{\gamma_{xy} p_o}{2A_o} \qquad (2.11)$$

Equation 2.11 may then be used to predict the angle of twist in the section at failure.

One commonly used method for determining the torsional capacity of a section is the torsion shear-friction model shown below in Figure 2.13. The model assumes a constant shear friction stress over the section and that it is subjected to horizontal and vertical shear forces V_V and V_L, torque T, and a clamping force acting normal to the section P. The clamping force P is defined in Equation 2.12, where F is the prestressing force on the section, V_T is an axial force acting on the section produced by any transverse shear, and A_{st} is the total area of the reinforcement in the section. The constant term in the equation, 0.0006, corresponds to the assumed maximum dilation strain in the steel, due to doweling action of the reinforcement, at the point of torsional failure.

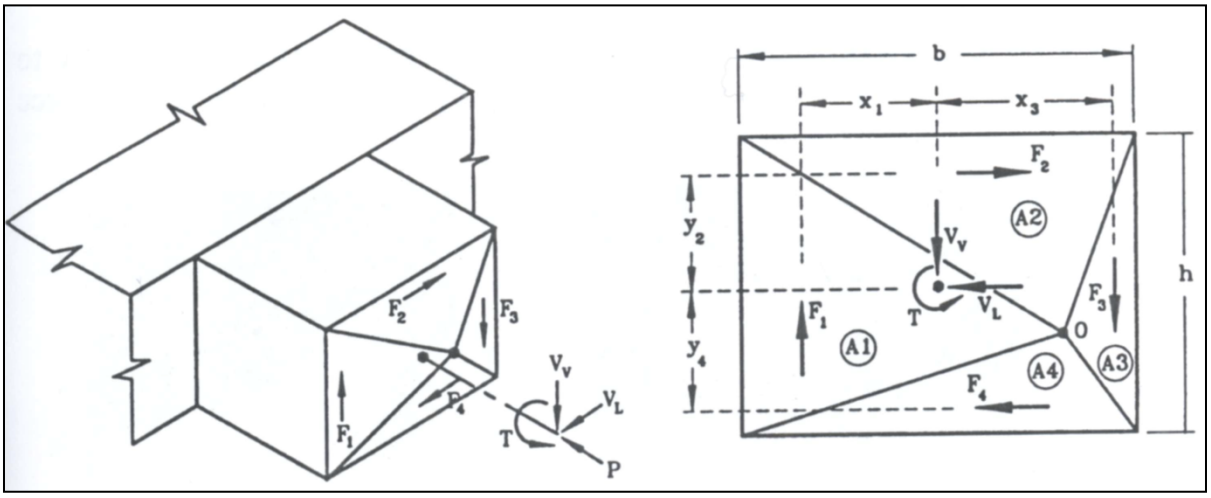

Figure 2.13: Torsion Shear-Friction Model

$$P = F + V_T + 0.0006 E_s A_{st} \qquad (2.12)$$

The section may be divided into four unequal quadrants, each of which contributes a shear friction resistance to the applied torque T. The shear friction of each quadrant is defined by a

force, F, acting parallel to the outer edge of the quadrant, where $F = \tau A$ and $\tau = \mu P/A$; A is the cross-sectional area of the section and μ is the coefficient of friction over the interface. Therefore, the resisting shear forces to V_V and V_L may be defined and used to determine the resulting torsional capacity of the section via the following equations:

$$V_V = F_1 - F_3 \tag{2.13}$$

$$V_L = F_2 - F_4 \tag{2.14}$$

$$T = F_1 x_1 + F_2 y_2 + F_3 x_3 + F_4 y_4 \tag{2.15}$$

The variables x1, y2, x3, and y4, in Equation 2.15,represent the distance between the shear friction force, F, which acts through the centroid of its respective quadrant and the centroid of the entire section (Priestley, Seible, & Calvi, 1996).

2.4.8 Strain Penetration

It is often critical that the effects of strain penetration be included in a nonlinear analysis of a structure in order to achieve an accurate behavioral prediction. Strain penetration is a slip experienced by the reinforcement, typically at the end of a member, and is caused by the localized crushing of the concrete surrounding the reinforcement as the strain in the concrete increases. The effects due to strain penetration, such as increased displacements and rotations due to slip, are particularly noticeable in the joint regions during seismic-type loading conditions. Therefore, the following equation, Equation 2.16, may be used to calculate the amount of slip experienced at the yield condition, s_y (Zhao & Sritharan, 2007).

$$s_y(mm) = 2.54\left(\frac{d_b(mm)}{8437}\frac{f_y(MPa)}{\sqrt{f_c'(MPa)}}(2\alpha+1)\right)^{1/\alpha} + 0.34 \tag{2.16}$$

The value for α is taken as 0.4 in the above equation per (Zhao & Sritharan, 2007), while the variable d_b represents the bar diameter and f_y is the yield strength of the reinforcement that is experiencing slip; f_c' is the compressive strength of the surrounding concrete.

2.4.9 Bond-Slip Behavior of Strands in Concrete

Bond slip is another critical effect that must be included for an accurate analysis. The effect occurs along the length of reinforcement that is embedded in either concrete or grout

and is caused by strain penetration along its length. As the stresses and strains on a given bar increase, the surrounding concrete crushes and allows for the bar to slip relative to the concrete. Eventually, this will penetrate to the end of the specimen, resulting in an entire slip of the bar relative to the concrete, otherwise known as a bond failure of the bar (Raynor, Lehman, & Stanton, 2002). Though experimental tests have been performed on specific bar and strand sizes, not all of the data is immediately applicable to any size and configuration. Also, the tests are typically performed on short specimens, which can be inaccurate when applied to a global response, as the results are more indicative of the localized behavior of an embedded strand. However, the results of the test have been used to develop empirical equations that may be used to predict the behavior of a given diameter strand. Raynor presented the following equation, Equation 2.17, in order to predict the average debonded length of a given prestressing strand diameter, which may be multiplied by the strain in the strand to determine the amount of overall bond-slip experienced by the strand:

$$l_{ua} = \frac{2.1\left(\sigma_u - \sigma_y\right)}{\left(f_g'\right)^{1.5}} d_b \qquad (2.17)$$

The values σ_u and σ_y represent the ultimate and yield stress of the strand, respectively, and are expressed in terms of MPa. The value f_g' represents the compressive strength of the grout surrounding the strand and d_b represents the strand diameter. The following figure, Figure 2.14, depicts the effects of bond-slip and what is meant by the term debonded length of the strand (Raynor, Lehman, & Stanton, 2002).

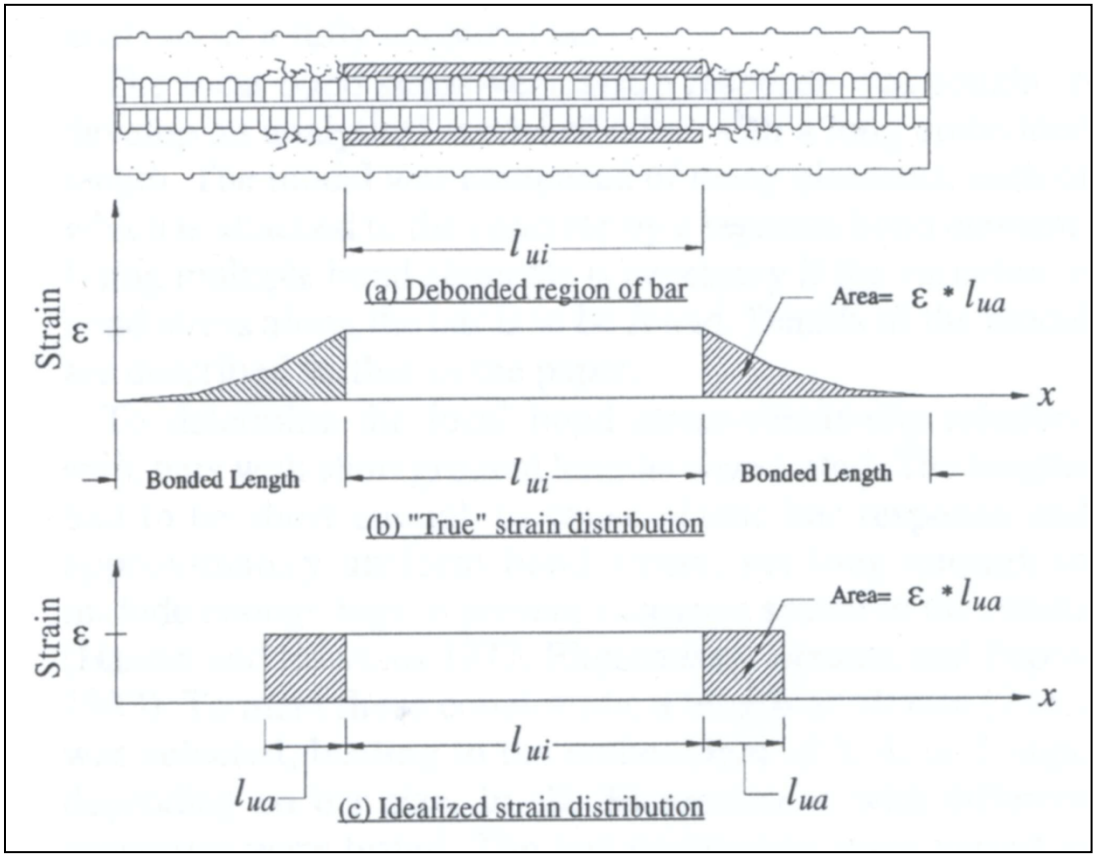

Figure 2.14: Bond-Slip Unbonded Length

Chapter 3. TEST UNIT

3.1 General Description

The test unit was developed based on a 50% dimensional scale of the prototype structure, which represented a typical inverted-T bridge. The specifics regarding the design of both the prototype and the test unit are outlined in (Thiemann, 2009). Since the behavior of the connection between the girders and the inverted-T cap beam was the main focus of this study, only one column with half of a span on each side was constructed and tested. Therefore, the test unit consisted of a single column with an inverted-T cap beam and a superstructure of five I-girders overlaid with a deck on each side. In order to test both the "as-built connection" as well as the proposed "improved connection" without building two test units, one side of the inverted-T cap beam was constructed using the as-built details while the other was constructed using the improved connection details for the girder-to-cap region. This was possible as the majority of the negative moment contribution was provided through the deck (Hastak, Mirmiran, Miller, Shah, & Castrodale, 2003), which meant that regardless of the type of positive moment connection incorporated, both sides would behave identically when subjected to a negative moment. As a result, based on whether the superstructure of the test unit was pushed or pulled horizontally, it was possible to isolate the effects of the behavior of only one of the connection types. Given the orientation of the test unit within the lab at UCSD, the South side represented the as-built condition while the North represented the behavior of the improved connection, as shown in Figure 3.1.

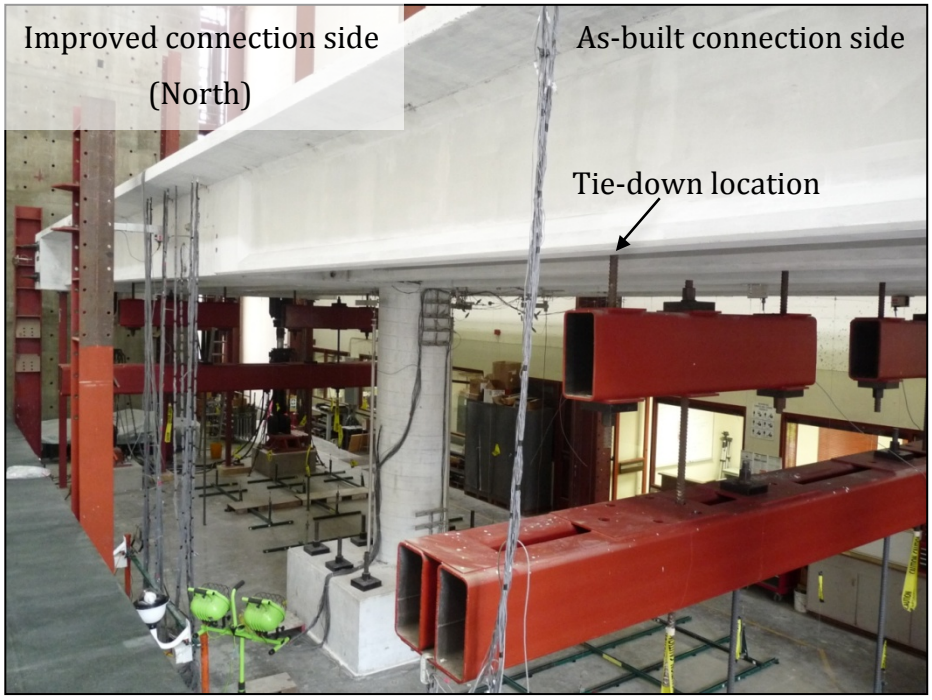

Figure 3.1: Test Unit Orientation

It was decided that two phases of testing would be necessary in order to fully capture the behavior of each connection detail and their influence on the overall behavior of the test unit. The first phase of testing, referred to as Phase 1, was a horizontal push/pull of the superstructure. Using two horizontally mounted actuators on each end of the abutment, the superstructure was cyclically pushed and pulled through the following series of increasing system displacement ductility levels, μ_Δ, until the specimen reached a maximum displacement ductility of 10. The nature of the test was quasi-static, which meant that the cycles were performed over a very long duration relative to that of a real earthquake. However, cycling the structure at various displacement levels ensured that the same amount of energy was input into the system, as one might expect during an actual earthquake. The second phase of testing, referred to as Phase 2, isolated the local performance of each connection region. Vertical actuators were used to simultaneously cycle each span of the superstructure up and down. This allowed the individual local response of each connection detail to be captured at various displacement levels until the ultimate condition was reached.

3.2 Test Unit Plan Details

The prototype bridge and test unit were designed by PBS&J and independently checked and discussed in detail by Thiemann (Thiemann, 2009). The design drawings developed for the test unit by PBS&J are reproduced in Figures 3.2 to 3.8.

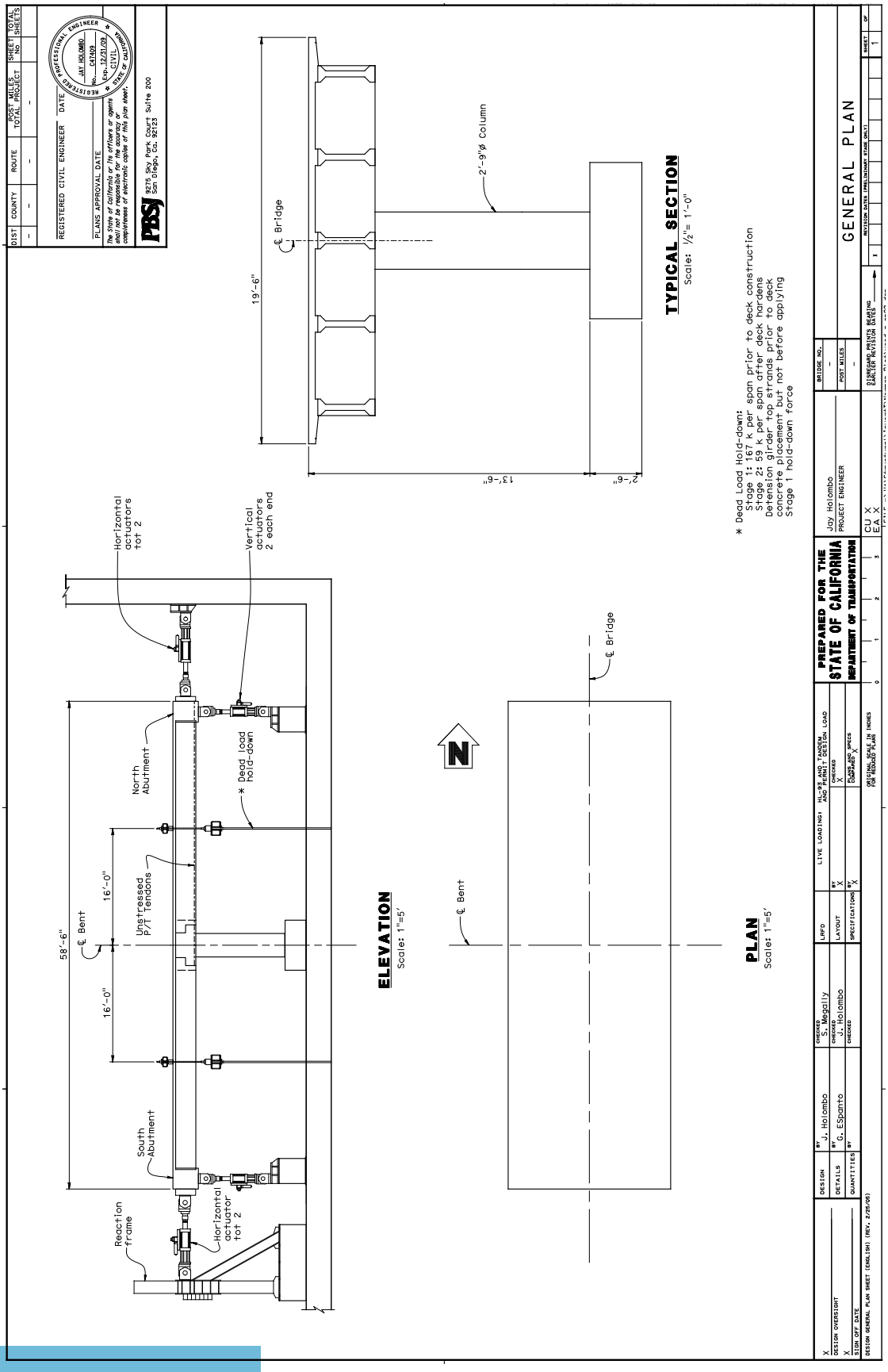

Figure 3.2: General Plan

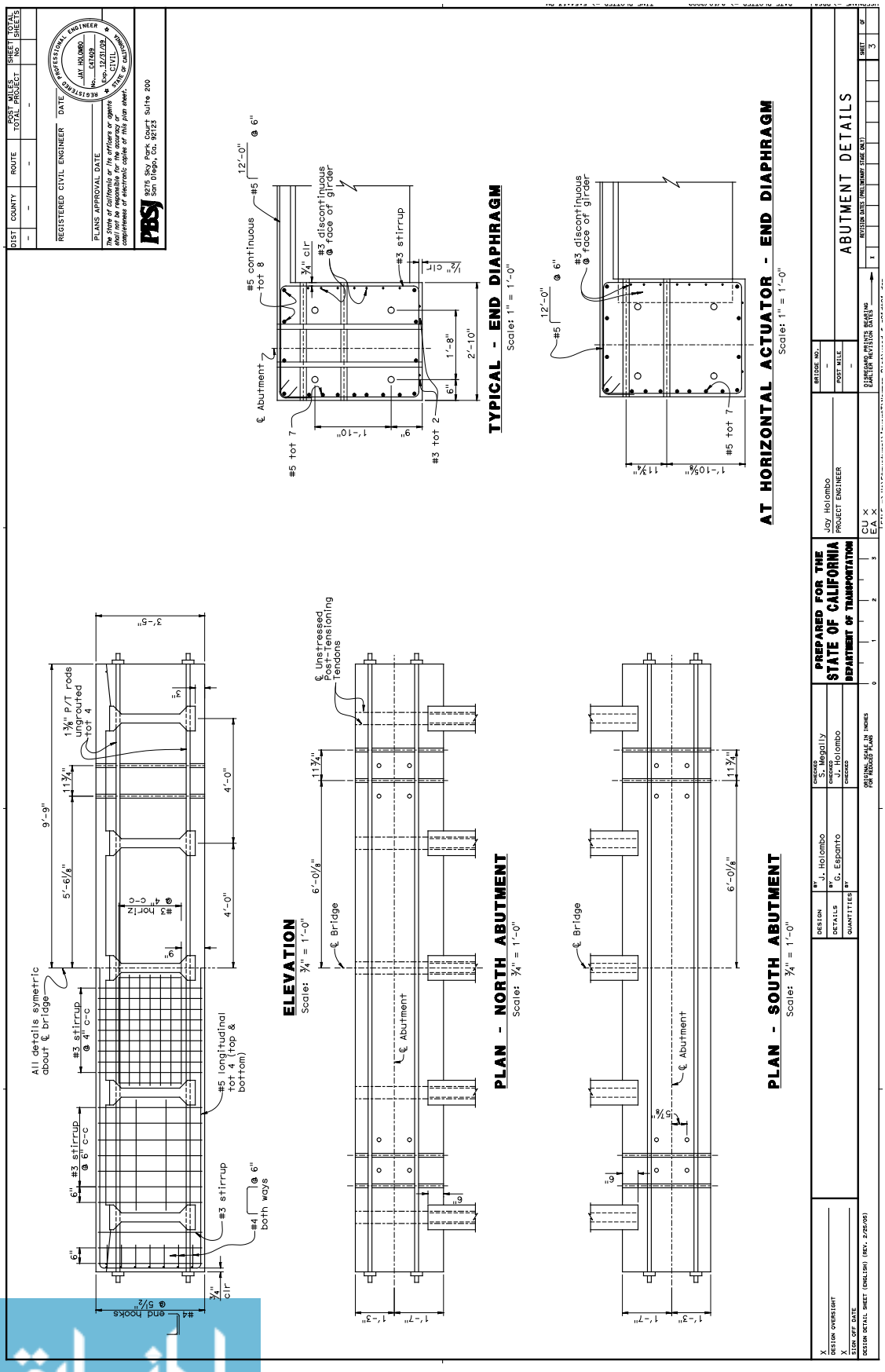

Figure 3.3: Abutment Details

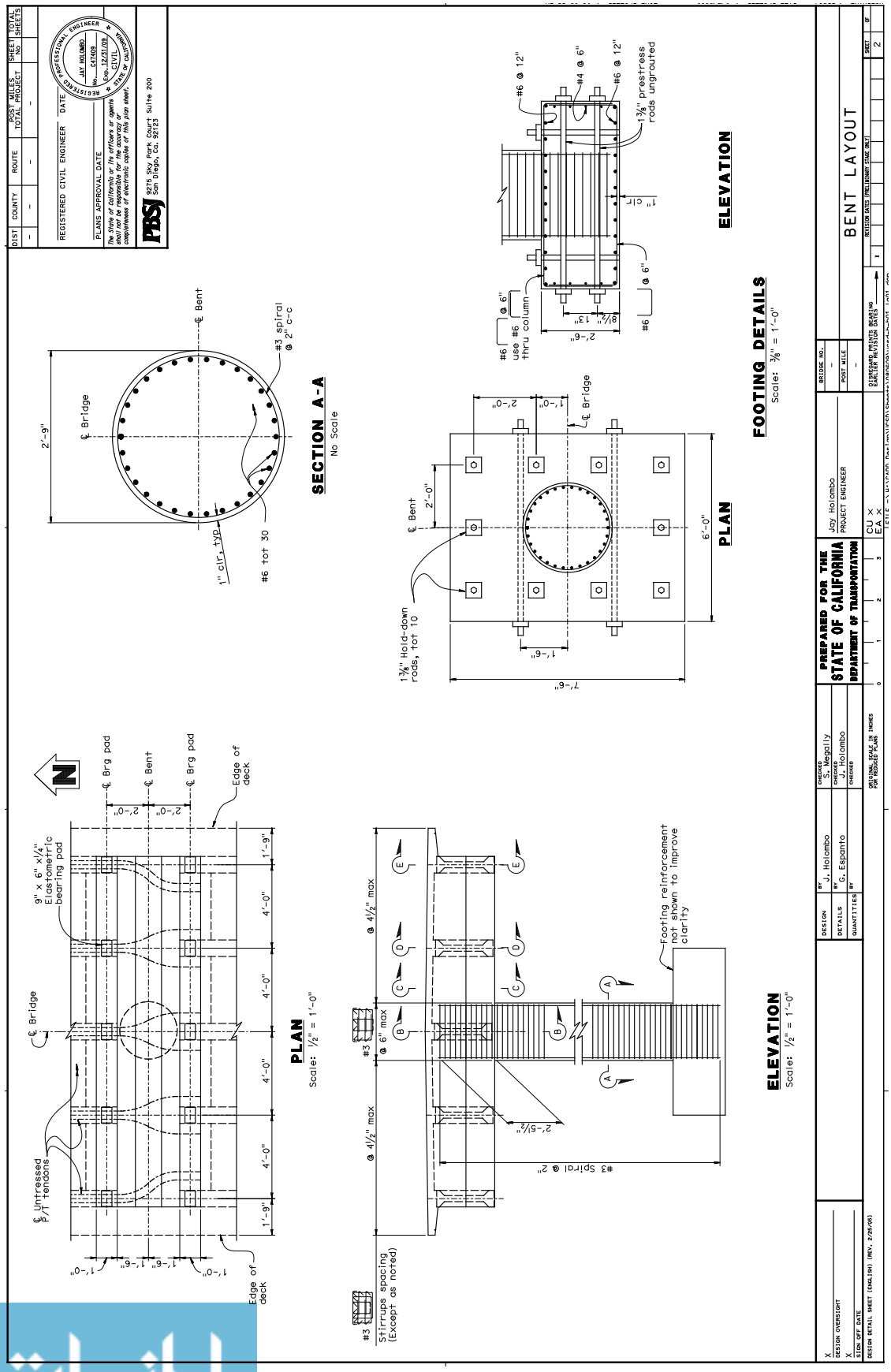

Figure 3.4: Bent Layout

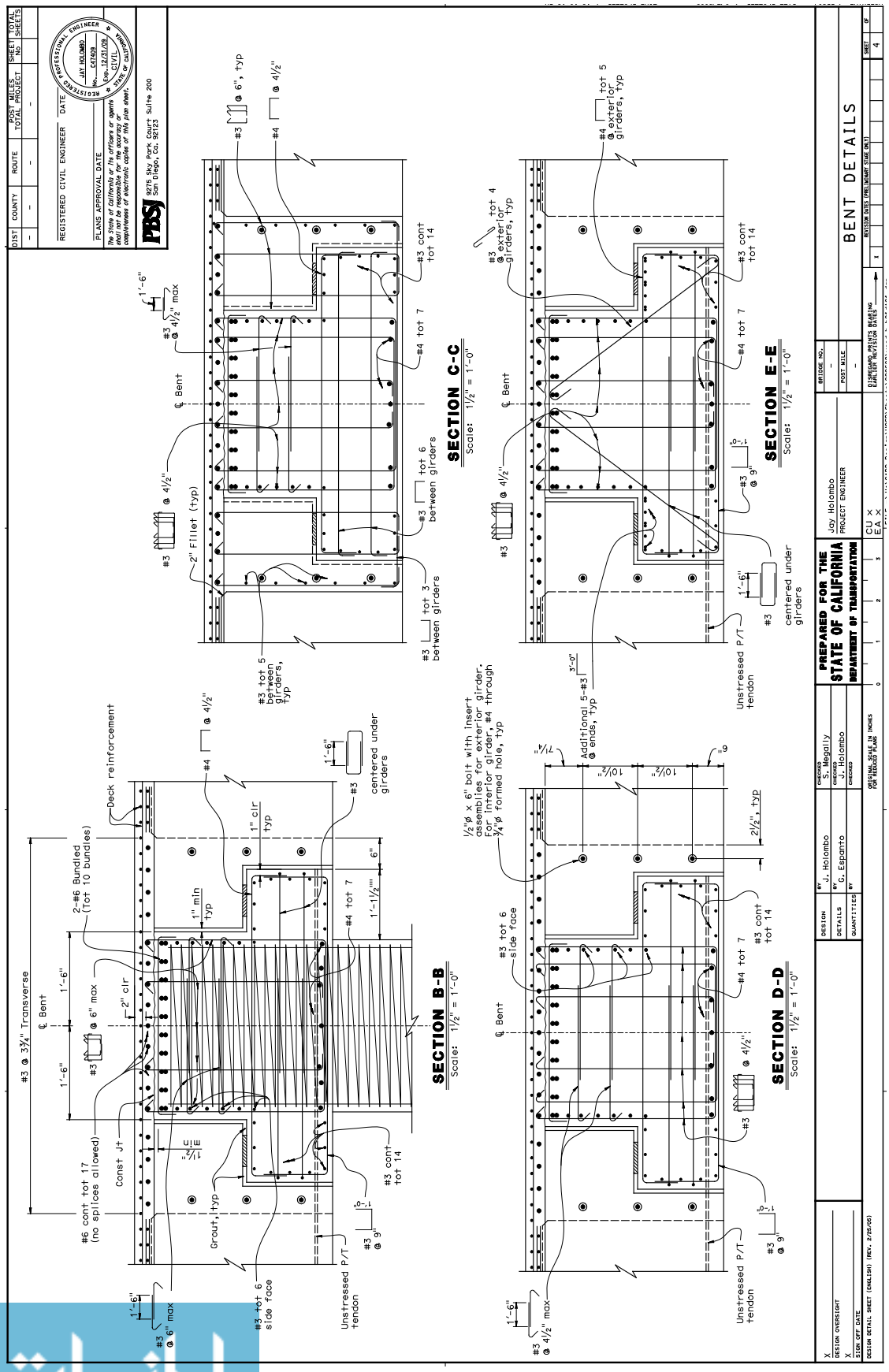

Figure 3.5: Bent Details

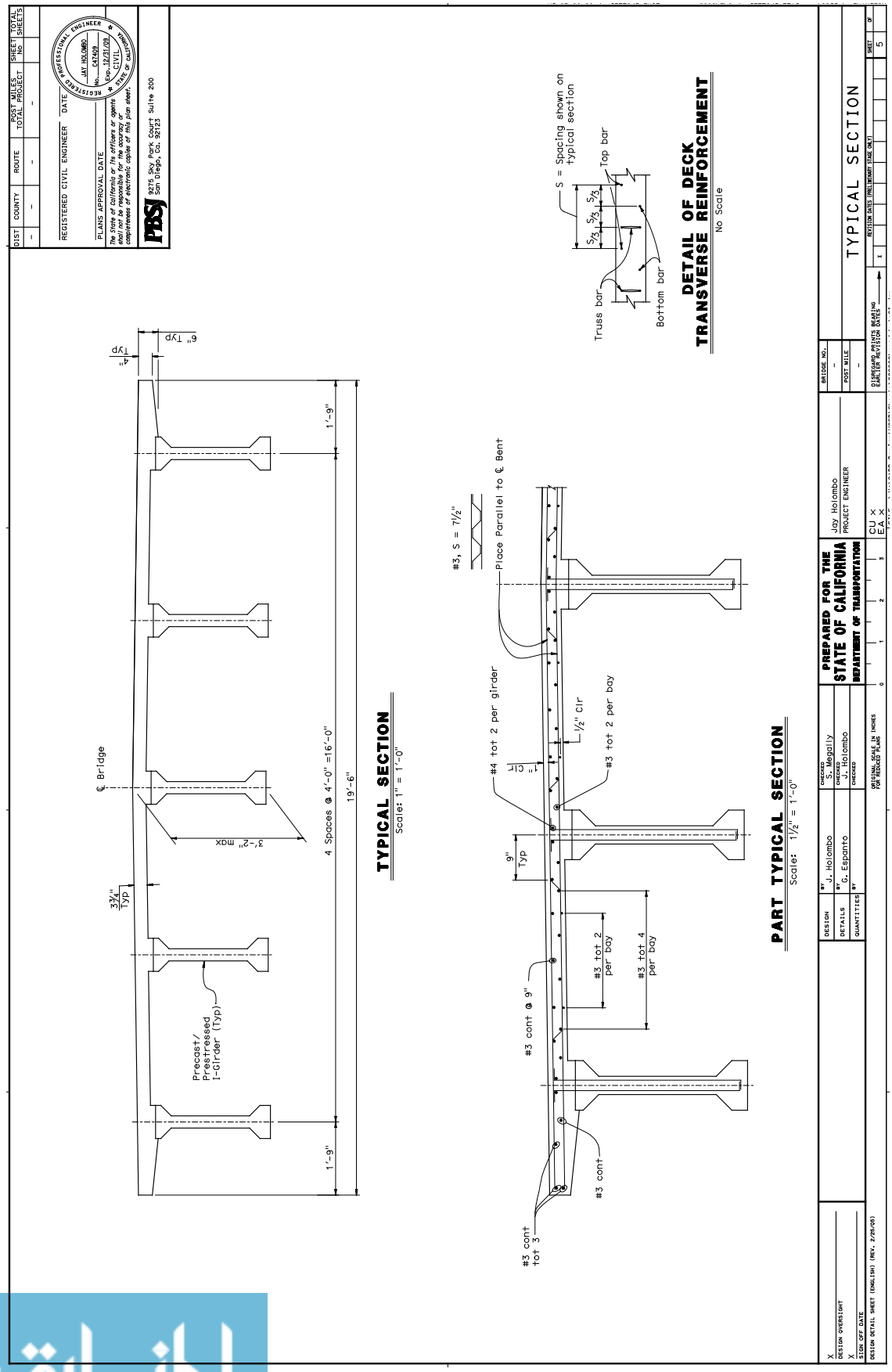

Figure 3.6: Typical Section

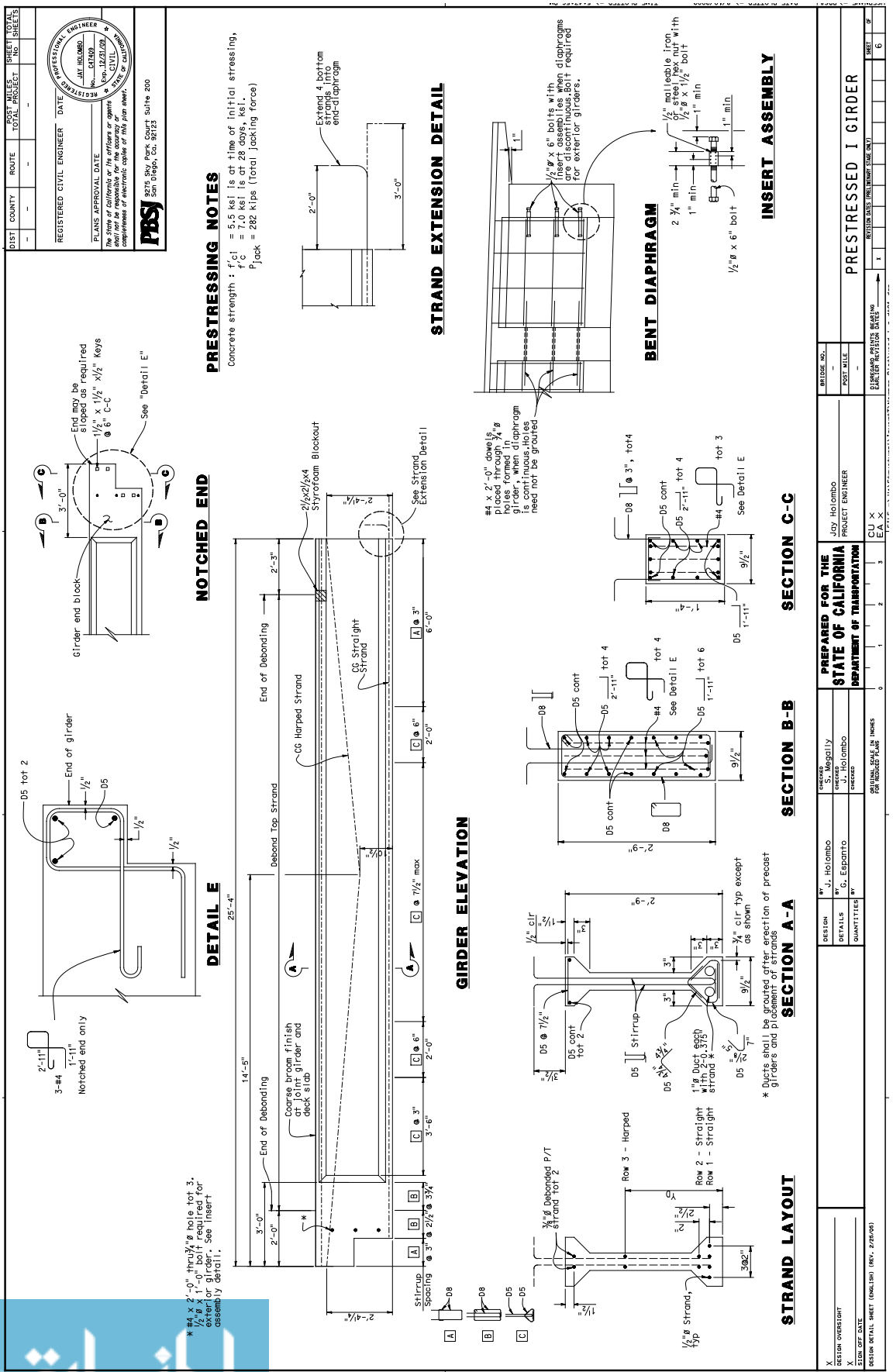

Figure 3.7: Prestressed I-girder

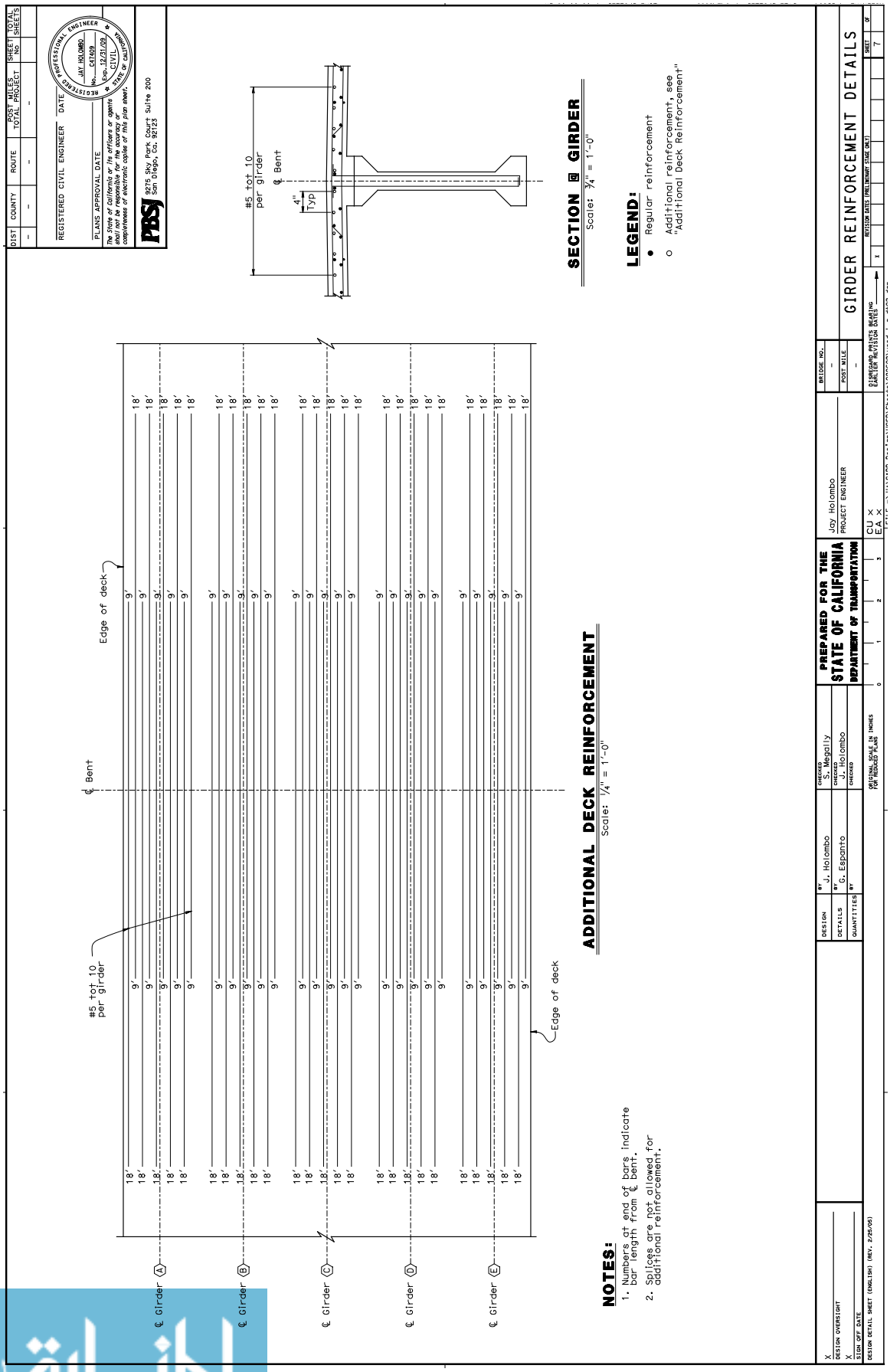

Figure 3.8: Girder Reinforcement Details

3.3 Improved Connection Detail

After considering several alternative connection details that could be used to establish a fully positive moment resisting connection, it was decided that placing untensioned, bonded prestressing strands through the connection was the preferred alternative. As shown in Section B-B of Figure 3.5, four 1-3/8 in. diameter strands were placed along the length each girder and were continued through the cap beam. The strands were then grouted in place, however they remained untensioned. This method was selected because it was relatively simple and economical to install. Additionally, since prestressing strands can develop much higher stress levels at relatively low strains, compared to Grade 60 steel, it was determined that the addition of the untensioned strands would provide enough additional tension force resistance to make the connection behave with the desired positive moment resistance. Furthermore, a finite element analysis of the connection demonstrated that adding the untensioned strands should develop a more than adequate moment capacity in order to develop a plastic hinge at the top of the column in the test unit (Thiemann, 2009).

When used in the prototype structure, these strands would run continuously along the length of each girder and through the cap from one end of the structure to the other. This, however, was not the case for the test unit. As stated previously, the test unit was detailed such that both the as-built connection and the newly proposed connection could be tested using the same test unit. In order to make that possible, the untensioned strands were terminated at the edge of the corbel on the as-built connection side; that way the untensioned strands would not alter the performance of the as-built connection.

3.4 Construction Sequence

3.4.1 General Sequence

In order to make the test unit as close to a real world inverted-T bridge as possible, typical construction practices and techniques that are used in the field were employed in the construction of the test unit in laboratory at UCSD. The basic construction sequence is shown in Figure 3.9.

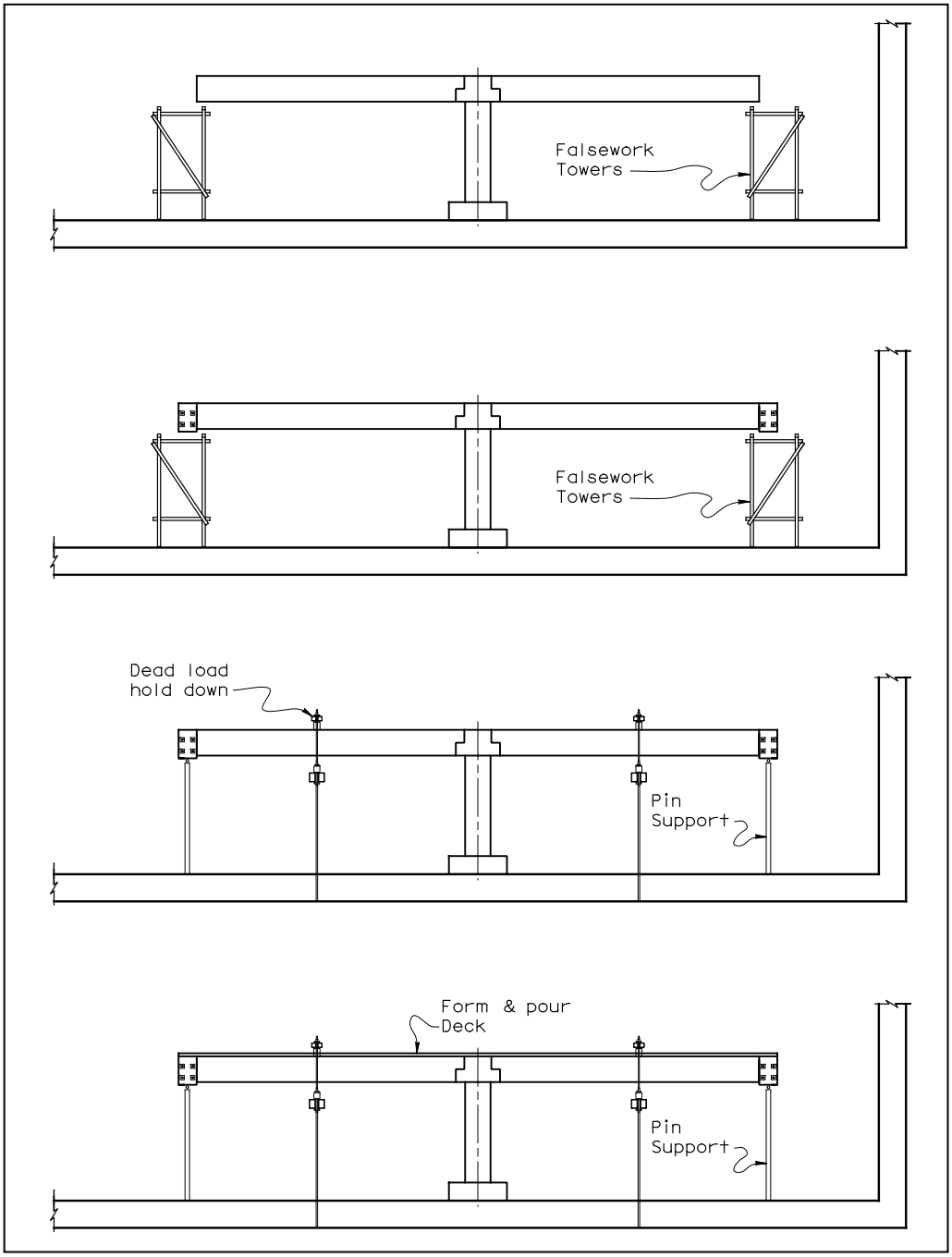

Figure 3.9: Schematic of Construction Sequence Used for Building the Test Unit

However, the availability of space within the laboratory and the concerns associated with the stability of the test unit during certain phases of the construction also dictated portions of the construction sequence as noted. The construction of the test unit proceeded as follows:

1. The footing was first constructed within an available portion of the lab space. The column cage and formwork was then constructed on top of the footing (Figure 3.10).

Figure 3.10: Completed Column and Footing Cage

2. As space within the lab opened, the footing and column cage were moved and placed in the space designated for testing (Figure 3.11). Hydrostone was then poured underneath the footing to ensure an even bearing surface. Once this was complete, the concrete was poured for the column. The pour for the column was terminated at the height of the base of the inverted-T cap beam.

Figure 3.11: Replacing the Column and Footing

3. Temporary shoring was erected around the column to support the construction of the inverted-T bent cap. The bent cap was constructed and poured so that it would be even with the top flanges of the girders, rather than pouring it to its full height (Figure 3.12).

Figure 3.12: Completed Bent Cap Construction on Top of Column

4. Temporary shoring was also installed on both the North and South ends of the bridge to support the girders as well as to aid the construction of the abutments. However, this set of shoring was installed at a height that was 3 in. lower than that which was used for the cap beam in order to compensate for the increased depth of the abutment that was specified in the plans in order to adequately embed the girder ends.
5. The girders were lifted into their respective places on both the North and South sides of the bent cap, with the South side being placed first due to the unavailability of space on the North side of the laboratory at that point in time (Figure 3.13).

Figure 3.13: Installation of Southern Girders

6. The abutment cage was then constructed on the ground, lifted into place, and the concrete was partially poured to a height corresponding to the underside of the deck (Figure 3.14). The South side was again constructed first and was followed by the North side.

Figure 3.14: Casting of the North Abutment

7. Prior to removing the falsework under the abutment and placing it on the pinned support system, a partial pour of the diaphragm was completed, adjacent to the cap on both sides, in order to provide added stability to the system. Only the 6 in. wide portion next to the corbel of the inverted-T cap was poured, up to the full height of the corbel.
8. Four support columns were placed beneath each abutment. Half-rounds were welded to the top of each column, which were used to create a pinned condition at the abutments (Figure 3.15). The falsework under both the abutments and the column was removed and the loads at the abutments were subsequently transferred to the support columns.

Figure 3.15: Temporary Support System Used Under Each Abutment

9. The Stage 1 hold-down force of 167 kips was then applied to each span and the ducts within the girders, containing the untensioned strands, were grouted.
10. The deck, along with the remaining portion of the diaphragm, abutment, and the haunch above each girder, was then cast in one large pour.

11. Once the deck hardened, two horizontal and two vertical actuators were mounted to each abutment, as shown in Figure 3.3, and the Stage 2 hold-down force of 59 kips was applied to each span. The specimen was then ready to begin testing.

3.4.2 Construction Challenges

The following are challenges that were encountered during the construction of the test unit and are presented in order to aid with future construction of this bridge type in the field.

3.4.2.1 Pouring the Bent Cap

Forming and pouring the inverted-T bent cap proved to be somewhat challenging due to the geometry of the bent cap. Prior to pouring the bent cap, the concern was raised that the pressure head of the concrete at the top of the inverted-T would likely be enough to force the concrete in the corbel portion of the bent cap to overflow its formwork. Therefore, in order to remedy this concern, the bent cap was poured in lifts, which necessitated the use of a construction joint. The first lift was poured to the top of the corbel portion and was allowed to set for around 20 minutes. The remainder of the bent cap was then poured in the second lift (Figure 3.16). Though some of the concrete in the corbel still rose slightly above the formwork, pouring the bent cap in lifts seemed to solve the overflow problem. An alternate solution that could be used for bridges of this type in future would be the use of a precast bent cap, instead of cast-in-place. The use of a precast bent cap would also significantly reduce the amount of construction time for the project and result in cost savings.

Figure 3.16: Casting of the Bent Cap

3.4.2.2 Installing the Ducts through the Cap Beam

Installing the ducts for the untensioned prestressing strand that was placed through the cap and the Northern girders proved to be a fairly significant challenge. First, since the strand did not extend straight through the cap beam and into the Southern girders, the ducts had to be bent as they passed through the cap so that they would terminate at the edge of the corbel and straddle each girder. Therefore, it was decided that the standard corrugated duct used for prestressing applications would be too stiff to accommodate such bends. As a result, a flexible, corrugated, low-grade steel electrical conduit was used instead. This alternative proved to be very effective as it was easily routed within the cap beam (Figure 3.17). It should be noted, however, that this problem is somewhat specific to the test unit and would likely not be encountered in the prototype structure, as the ducts would continue straight into

the Southern girders, thereby eliminating the need to bend them. However, the rebar in the bent cap should be spaced such that it allows for the accommodation of the duct.

Figure 3.17: Routing of Bent Cap Ducts

Second, it was decided that it would be prudent to make the duct in the cap beam larger than the ducts that were inside the girders. This was done in order to increase the tolerance in the alignment of each section of duct, making it easier to place the ducts in the cap in line with the ducts in the girders to accommodate and grout the strand. Therefore, a 1-½ in. electrical conduit was selected, while 1 in. diameter sheathing was used in the girders.

Third, the bent cap was highly congested with reinforcement, especially in the vicinity of the column, which made it difficult to place ducts large enough to accommodate the strands (Figure 3.18). This was also true given the fact that a slightly larger diameter conduit was selected within the cap beam. This challenge was solved by routing the ducts around the column instead of passing through it. This problem is not expected if four girders are used instead of five, as a girder would not have had to pass directly through the center of the column.

Figure 3.18: Placement of Ducts in the Bent Cap around the Column

3.4.2.3 Inserting the Strands through the Ducts in the Cap Beam

Running the strands through the ducts also proved to be difficult, given the bends in the ducts, as there was little clearance within the duct for both strands. Furthermore, grout tubes were mounted on each duct and ran through to the top of the cap to ensure proper grouting. However, in order to mount the grout tubes, a condulet in the shape of a box was placed at the center of the cap beam with a series of connectors that were used to splice on the main duct sections as well as the grout tube. This was a significant obstacle when placing the strands as they had a tendency to get caught in the corners of the conduit, making it difficult to force the strand out and to the other end of the cap beam. This problem would likely not be encountered in the prototype structure as the ducts would not be bent, nor would they likely enter a similar box section. However, in order to remedy the situation, a series of increasingly larger diameter and stiffer objects were fished back and forth across the cap beam. Once a stiff enough wire was pulled through the cap beam, it was attached to one of the strands and was used to pull it through. The first strand was then used to pull the second

strand through the cap beam. The strands were then fed down the length of the girder. Though the process was rather time consuming, it proved to be the most effective.

Figure 3.19: Pushing the Strands through the Girder

3.4.2.4 Partial Pour of the Diaphragm

Safety concerns were raised regarding the stability of the superstructure while transferring the abutments from the falsework to the pinned support system. Initially, the girders were independent of one another at the cap end as they were supported on the corbel of the inverted-T cap beam. This was done to replicate the simply supported condition that the girders would experience as they were placed in the prototype bridge during construction. However, concerns were raised that the girders might fall out of place during the transfer of the abutment support conditions. Therefore, in order to improve the lateral and rotation stability, and hence safety, of the superstructure, it was decided that a partial pour of the diaphragm would be completed. Only the portion of the diaphragm next to the corbel was poured to the full height of the corbel within each bay between girders, as it would provide lateral stability for the girders while still allowing them remain in simply supported condition at the bent cap, as required in order to produce a realistic moment profile along the length of the girder. This would not have been possible had the entire diaphragm been poured.

However, this did introduce a construction joint in the diaphragm along the top of the corbel of the bent cap, as shown in Figure 3.20.

Figure 3.20: Partial Diaphragm Pour between Girders

3.4.2.5 Termination of Untensioned Strands

Unfortunately, due to a miscommunication in the lab as well as the field decision to make a partial pour of the diaphragm, the untensioned strands were not terminated at the face of the inverted-T bent cap on the as-built connection side, as specified. Instead, the strands were extended and grouted all the way to the outside face of the diaphragm. Since the presence of the strands within the effective as-built connection region could have falsely improved the performance of the connection, it was necessary to render the strands ineffective within the as-built connection. Therefore, the grout within the duct on the as-built side of the bent cap was drilled out over the length of the diaphragm, in order to debond the strands, as shown in Figure 3.21. Additionally, as much of the duct was removed as possible, which was somewhat feasible as the electrical conduit that was used could be easily

unraveled and fractured over the first couple of inches. It was assumed that any remaining duct would be easily fractured or unraveled as the girder pulled away from the cap.

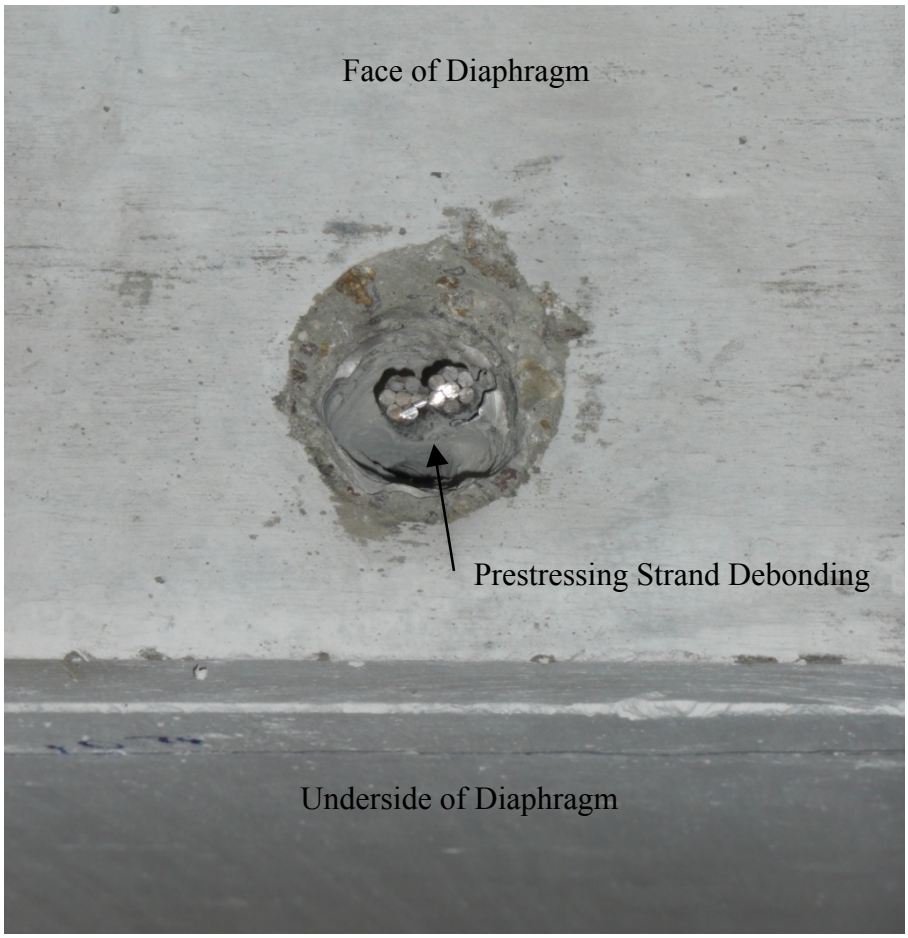

Figure 3.21: Untensiond Strand Debonding

3.5 Instrumentation

Given the magnitude of the test specimen, a significant number of both internal strain gauges and external devices were used to capture the response of the structure in its critical regions. A total of 282 strain gauges were used internally, while a combination of 51 string potentiometers, 67 linear potentiometers, and 11 rotation devices were used externally. The following presents the instrumentation plan that was used for both the internal and external instrumentation.

3.5.1 Strain Gauges

3.5.1.1 Column-to-Cap beam Connection

Two spirals within the column-to-cap beam connection were instrumented with four strain gauges each, in the configuration shown in Figures 3.22 and 3.23. Note that a red "X" in the figures indicated the strain gauges. The instrumented spirals were located near the middle of the connection, at approximately 7 and 10 spirals from the point of anchorage at the bottom of the column respectively, and a full un-instrumented spiral was placed in between them, as the spacing was rather tight, as shown in Figure 3.24.

The longitudinal reinforcement within the joint was instrumented with a higher number of gauges placed on the extreme tension and compression bars. Some of the reinforcement in the configuration was only instrumented with two strain gauges, while the extreme tension and compression bars were instrumented with four gauges along their length as shown in Figure 3.25. Starting at the column-to-joint interface, the configuration was evenly spaced along the longitudinal reinforcement at approximately 9.5 in. on center. The sections receiving only two gauges followed the same spacing, but were discontinued along the remainder of the length as shown in Figure 3.26.

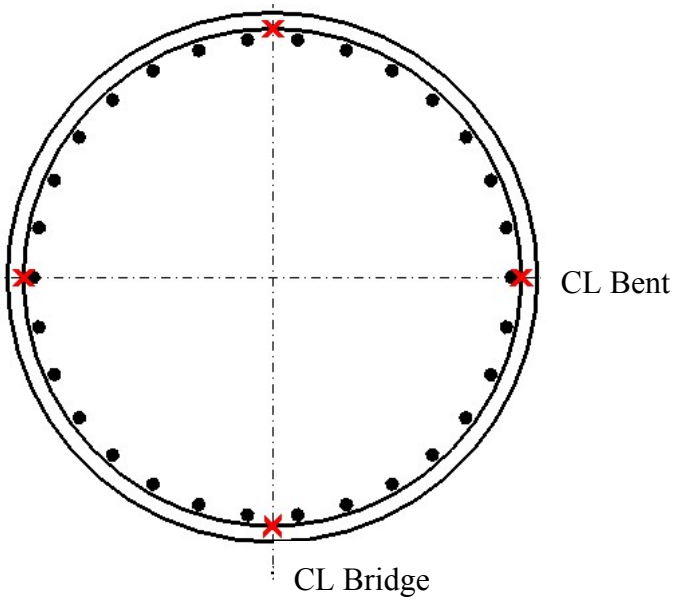

Figure 3.22: Column-to-Cap Beam Spiral Strain Gauge Location within Cap Joint Region

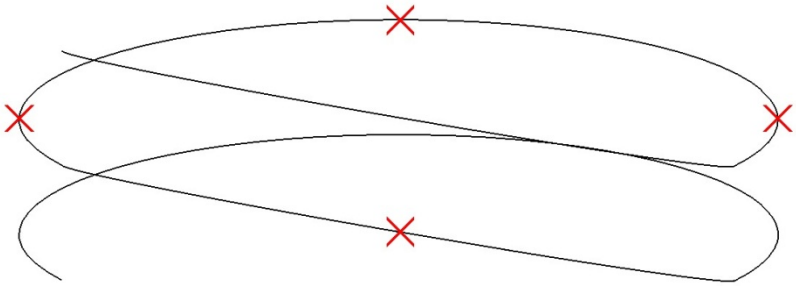

Figure 3.23: Column-to-Cap Beam Typical Spiral Instrumentation Profile

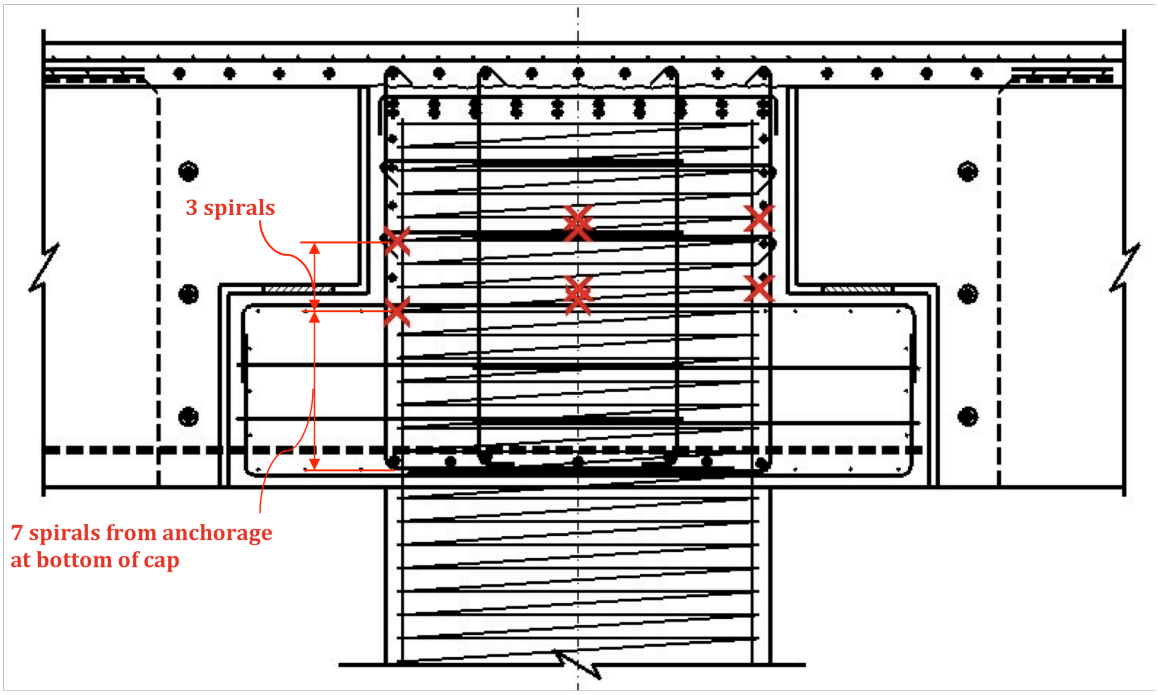

Figure 3.24: Column-to-Cap Beam Spiral Instrumentation within the Joint

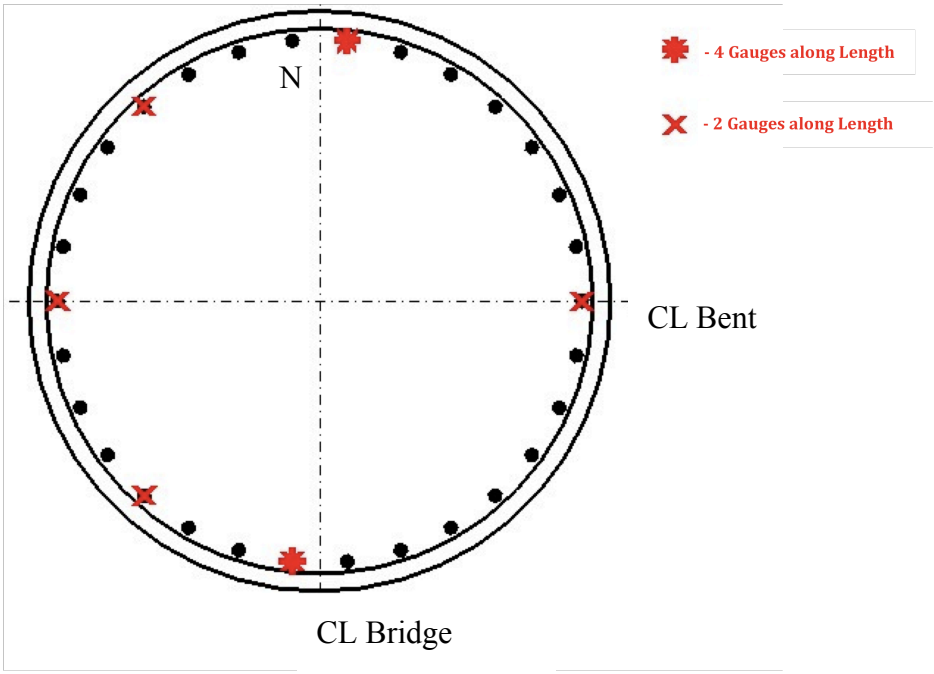

Figure 3.25: Location of Gauged Longitudinal Column Reinforcement

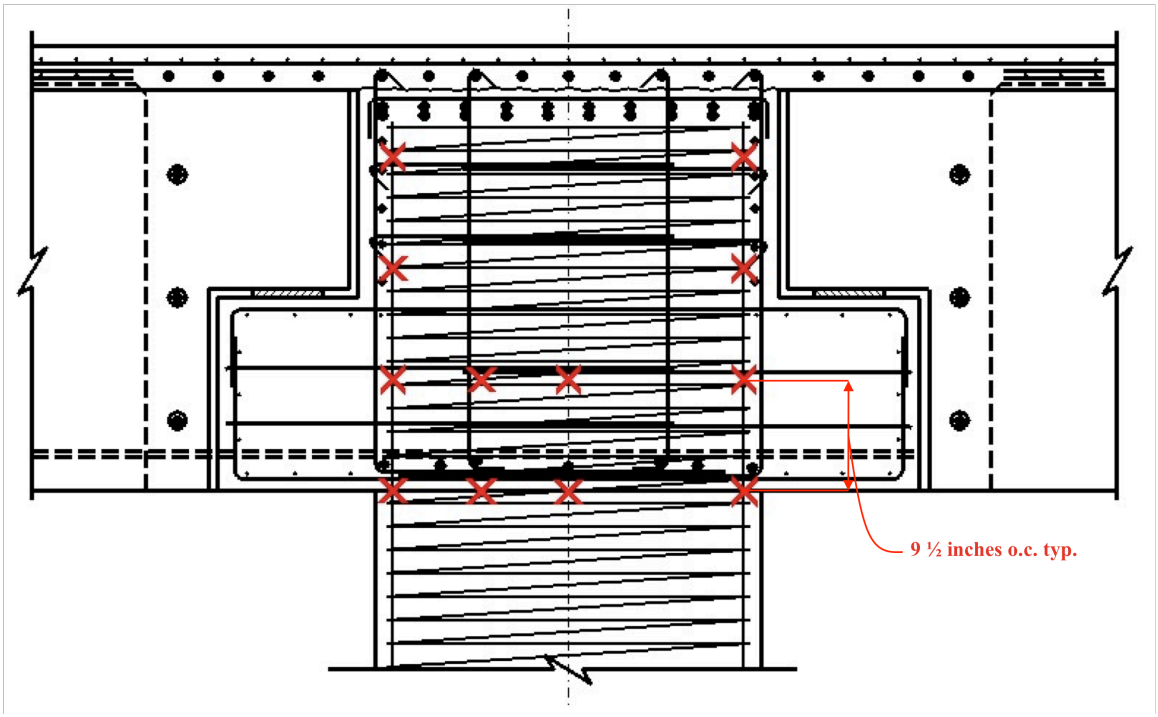

Figure 3.26: Profile of Gauged Longitudinal Column Reinforcement within the Joint

3.5.1.2 Column

The performance of the column was not of critical concern; as a result a significantly smaller number of gauges were used within the column. Gauges were placed on the spirals in the configuration as shown in Figure3.27 in order to capture the behavior of the confinement within the column. One spiral was instrumented within the hinge at both the top and bottom of the column as shown in Figure 3.28.

The longitudinal bars at the base of the column were also be minimally gauged. Each bar received only one gauge at approximately 1 in. from the top of the footing, as shown in Figure 3.29.

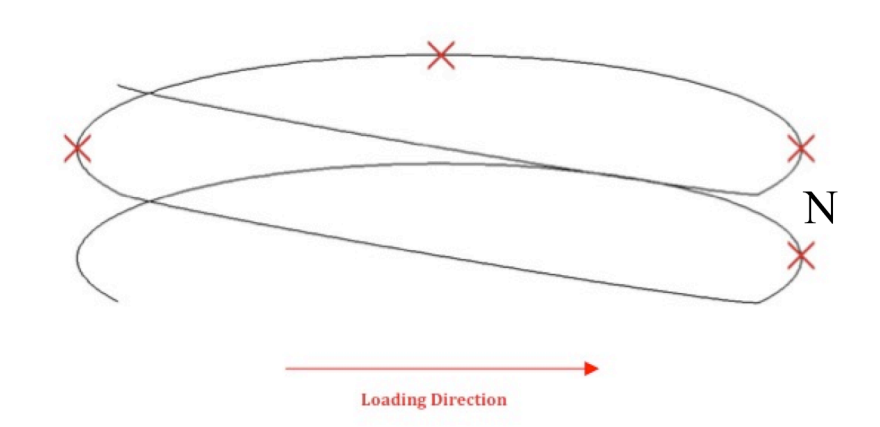

Figure 3.27: Typical Column Spiral Gauge Location

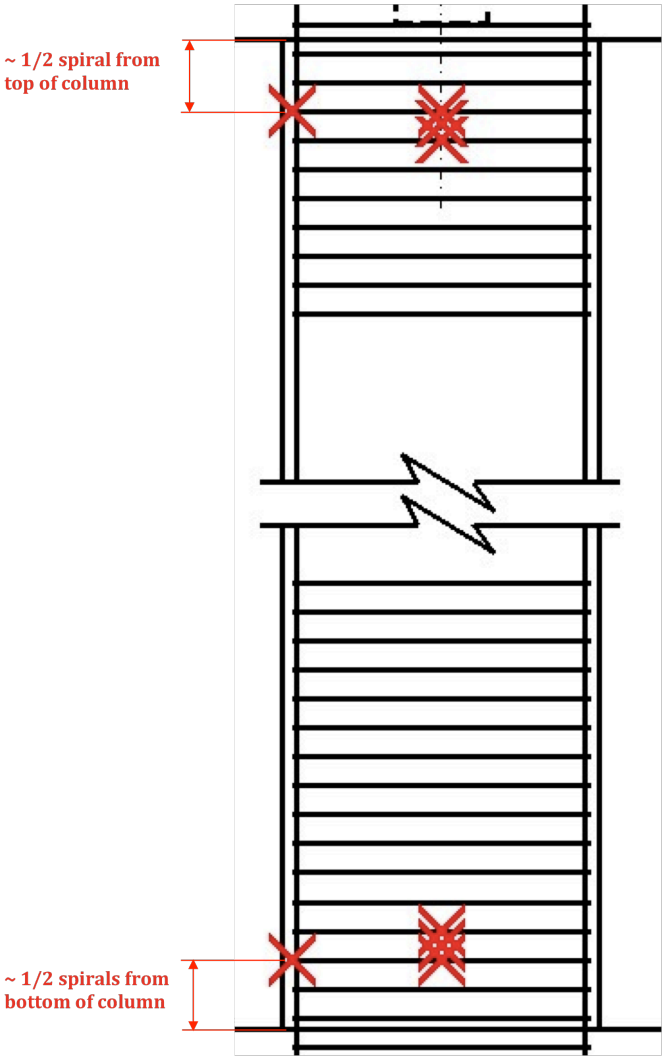

Figure 3.28: Spiral Gauge Location in the Column

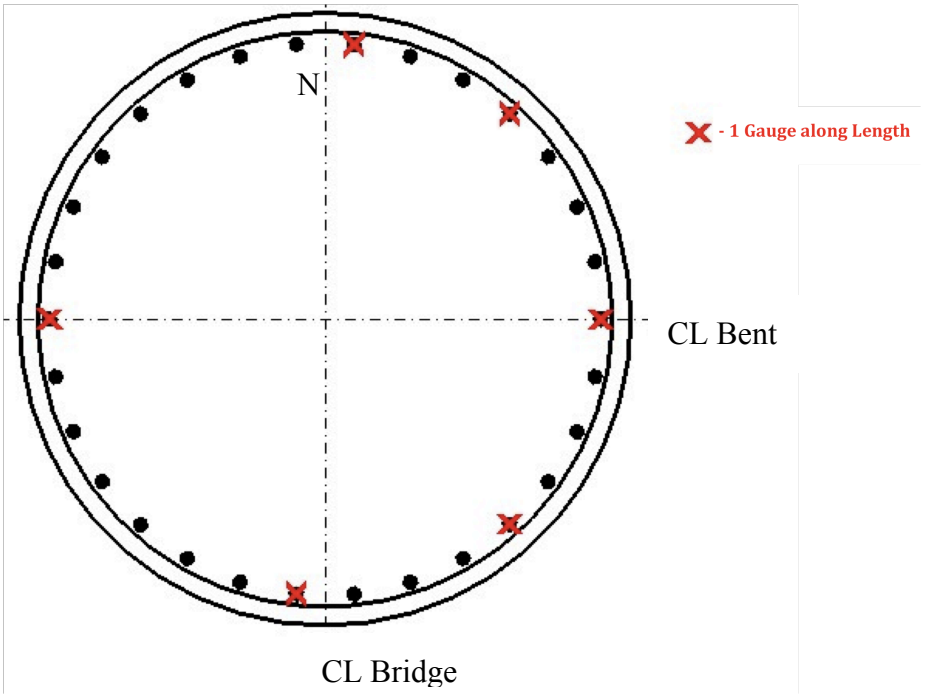

Figure 3.29: Bottom of Column Longitudinal Reinforcement Gauges

3.5.1.3 Footing

Since the footing in the test unit did not accurately represent true field conditions, it was not instrumented with any strain gauges.

3.5.1.4 Cap-to-Diaphragm Interface

The hooked reinforcement, which spanned the interface between girders, was instrumented in order to monitor the performance of the cap-to-diaphragm connection. Figures 3.30 and 3.31 depict the gauge layout for this section of the test unit. On one side of the column, each bar received one strain gauge, placed at the interface. The bar located closest to the column was instrumented with two additional strain gauges located approximately 5 in. from the interface on each side, as shown, in order to capture the slip behavior of the bar. On the opposite side of the column, only the bars in the center of each set of three were gauged. Each of these bars received one strain gauge, placed at the interface. Also, one gauge was placed at the mid-point of the hooked diaphragm reinforcement. However, rather than instrument each stirrup in the set of three between girders, the center stirrup in each set was excluded. All of the stirrups along the length of the

cap were instrumented in this manner in order to further capture the performance of the joint, as shown in Figure 3.31.

Additionally, the stirrups between the girders in this region, shown in Figures 3.32, 3.33, 3.34, and 3.35, were each instrumented with one gauge at the mid-point of each vertical leg. This configuration was applied to a larger number of the stirrup sets on West side of the column than the East side.

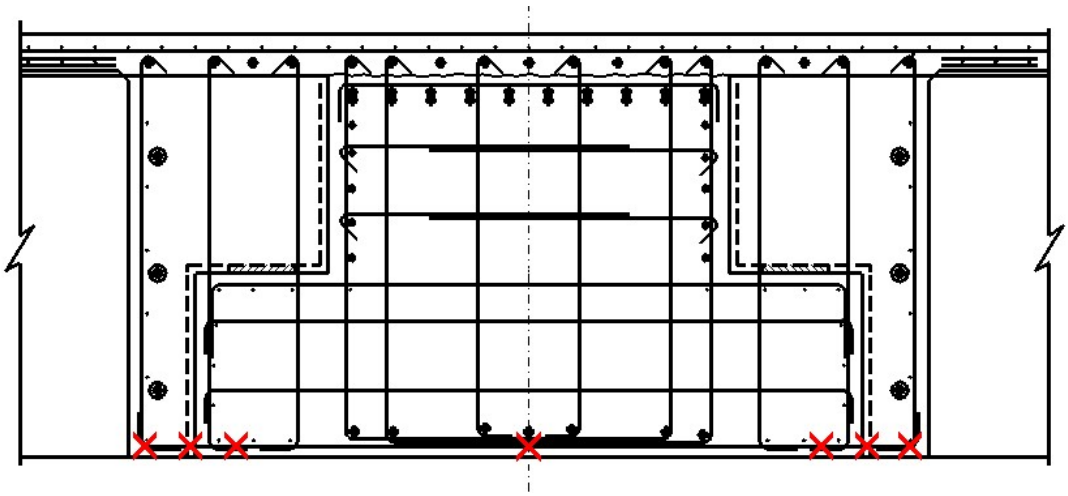

Figure 3.30: Cap-to-Diaphragm Hooked Reinforcement Strain Gauge Layout

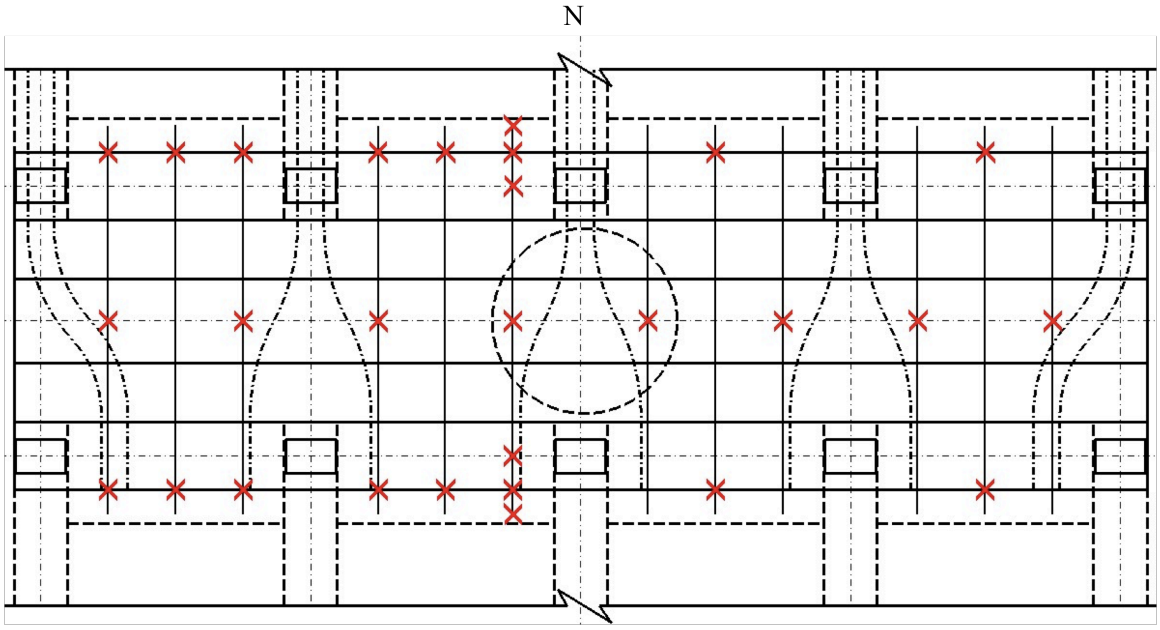

Figure 3.31: Cap-to-Diaphragm Hooked Reinforcement Strain Gauge Layout

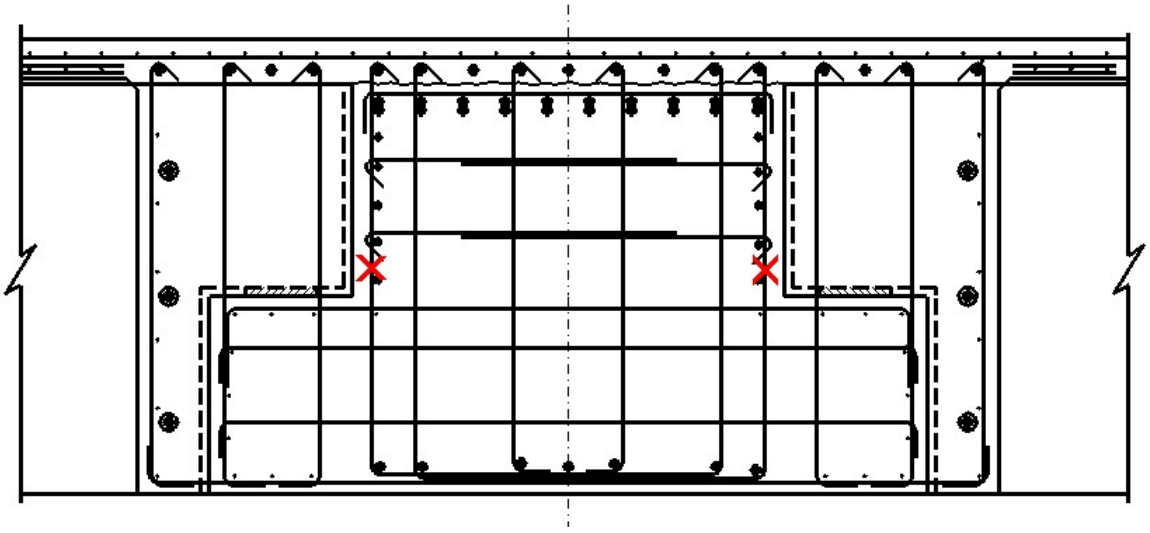

Figure 3.32: Cap Beam Inner Stirrup Strain Gauge Locations

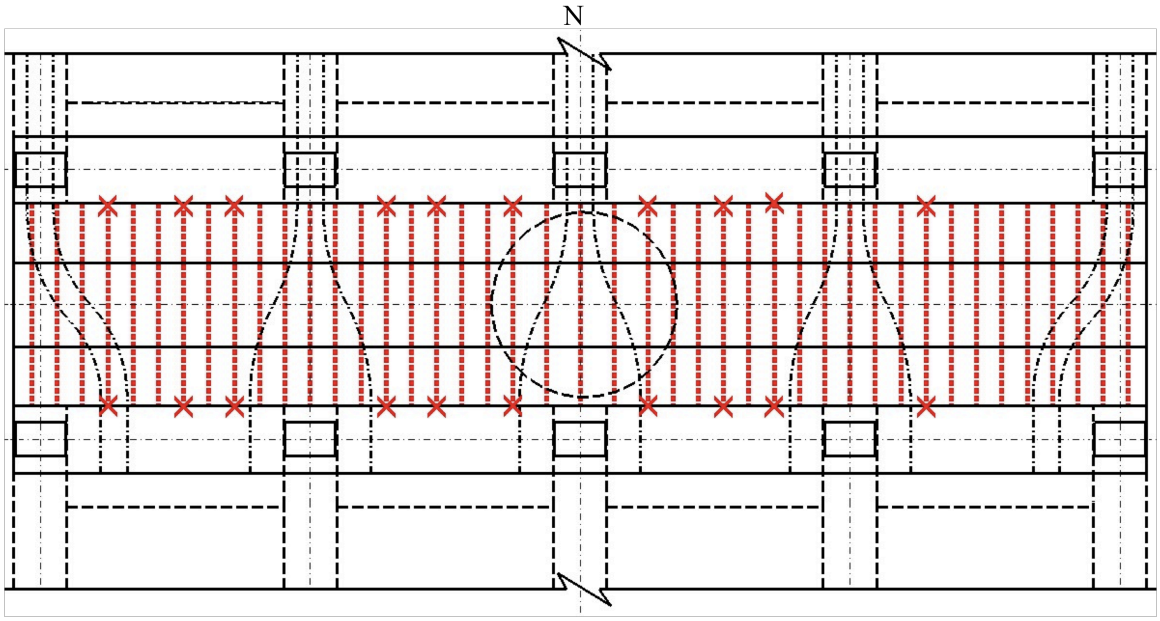

Figure 3.33: Cap Beam Inner Stirrup Strain Gauge Layout

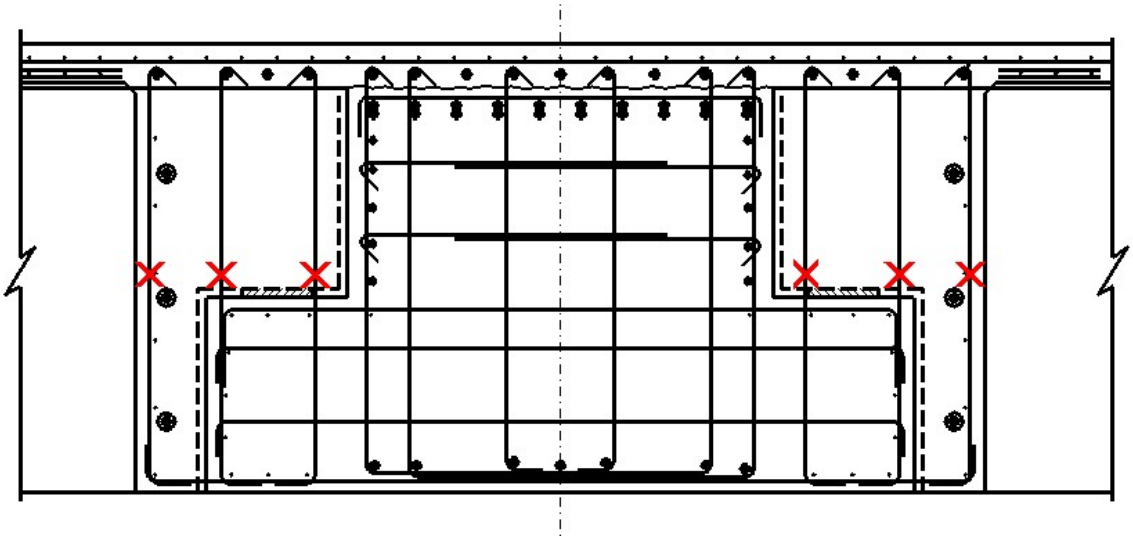

Figure 3.34: Cap Beam Outer Stirrup Strain Gauge Locations

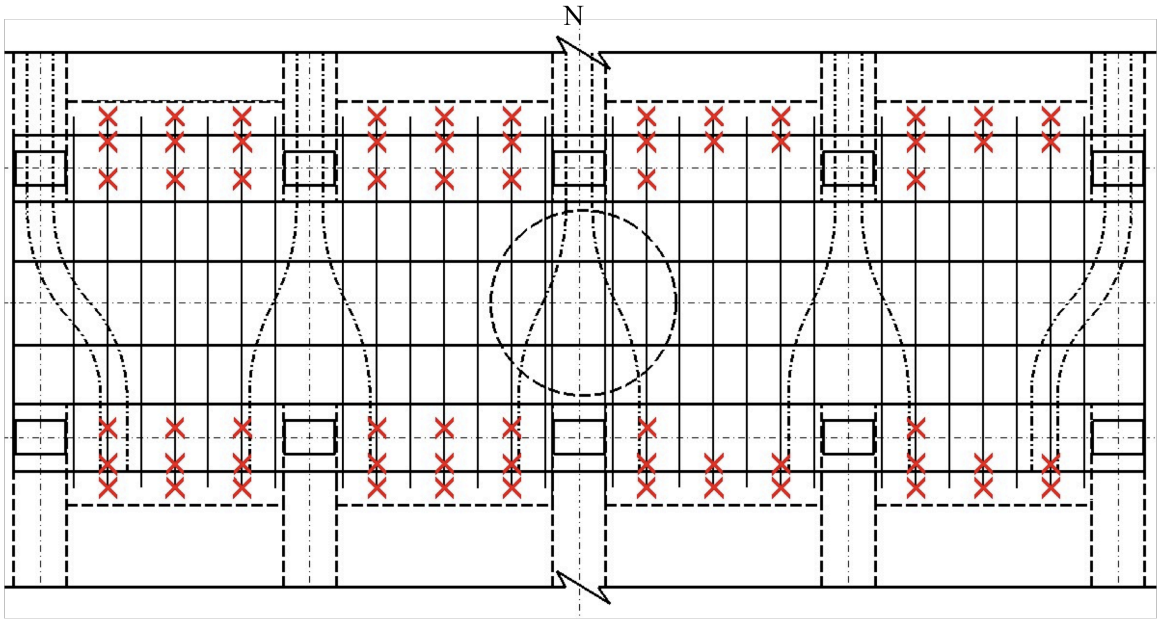

Figure 3.35: Cap Beam Outer Stirrup Strain Gauge Layout

3.5.1.5 Girders

The girders were minimally instrumented with strain gauges. The center girders, along with one intermediate and one exterior girder on the as-built side were instrumented.

The stirrups within the girders were instrumented in order to capture the shear demand in the girders. Both vertical legs were instrumented at their mid-point as shown in

Figure 3.36. The last stirrup in the blocked-out region at the dapped end of the girder, and the first three beyond this portion, were instrumented as shown in Figure 3.37. One of the stirrups within the dapped end detail of the aforementioned girders was also instrumented as shown in Figure 3.38.

The prestressed strands on one of the center, intermediate, and exterior girders on the as-built side were also instrumented. Each harped strand was instrumented with one gauge at a distance of the transfer length (taken as 40 in.) from the dapped end, as shown in Figure 3.37. The horizontal strand at the bottom of the section, and closest to the center, as shown in Figure 3.36, was also instrumented with two strain gauges: one at the mid-span of the strand and one at a distance of the transfer length (again taken as 40 in.) from the dapped end. Additionally, the horizontal strand at the outside of the bottom layer, as shown in Figure 3.36, was instrumented with one strain gauge at the mid-span of the strand.

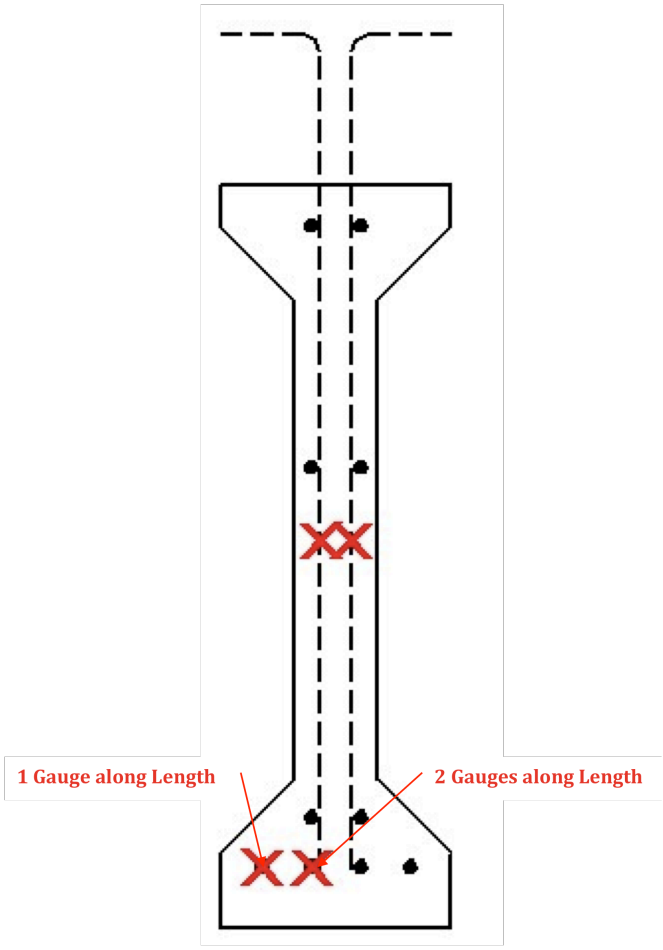

Figure 3.36: Girder Cross-Section Strain Gauge Locations

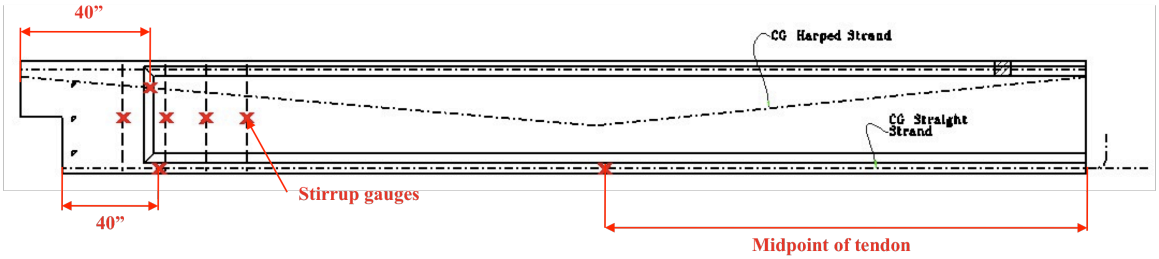

Figure 3.37: Girder Strain Gauge Layout

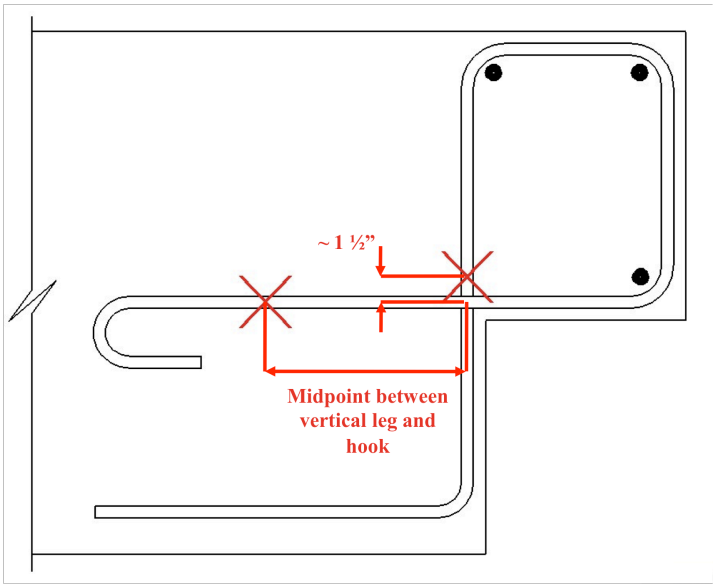

Figure 3.38: Girder Dapped End Detail Strain Gauge Locations

3.5.1.6 Girder-to-Diaphragm Connections

The girder-to-diaphragm connections were one of the most critical regions of the test unit. Therefore, these connections were heavily instrumented.

The dowel bars connecting the girders to the diaphragm, on both the as-built and retrofit side, were instrumented as shown in Figure 3.39. It was decided that the bottom dowel on each girder would be the critical bar as it would be the first to see the effect of a positive moment. Therefore, these bars received additional strain gauges as shown in Figure 3.39. The gauge on the bottom dowel that is placed away from the face of the girder was located at the mid-point of the dowel on which it was placed. It should also be noted that Figure 3.39 was always taken to be looking in the North direction when applying instrumentation to both the as-built and improved connection sides of the cap beam.

Strain gauges were also placed on the unstressed strands within the improved connection detail. As shown in Figure 3.40, one strand per girder, on the improved connection side, was instrumented with four gauges each. One gauge was placed at the interface between the bottom of the cap and the girder. An additional gauge was placed along the strand within the girder, approximately 10 in. from the gauge at the interface. One more gauge was placed on the portion of strand within the cap beam, spaced at approximately 10 in. from the previous gauge.

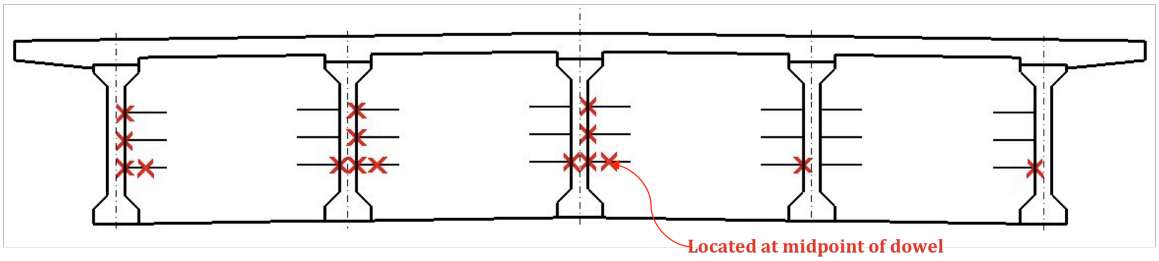

Figure 3.39: Girder-to-Diaphragm Dowel Strain Gauge Locations

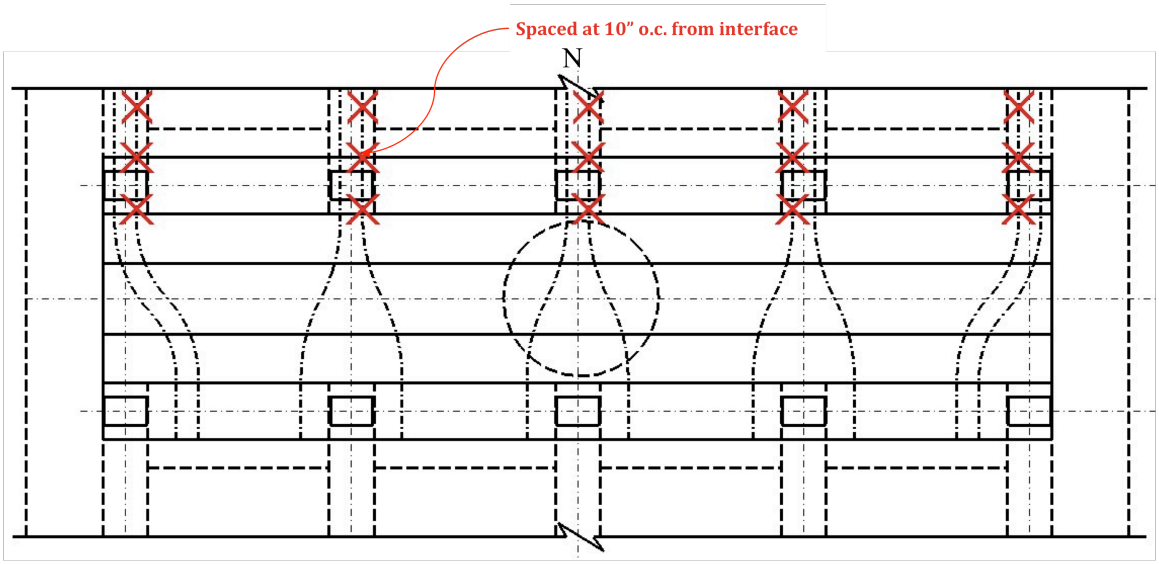

Figure 3.40: Improved Connection Strand Strain Gauge Locations

3.5.1.7 Deck

The deck reinforcement was mounted with strain gauges as shown in Figures3.41 and 3.42, with gauges located both above the girders and at the mid-point between girders. The

first set of gauges was placed on the longitudinal reinforcement directly above the gap between the girder and the top portion of the cap. The second set was placed on the longitudinal reinforcement directly above the end of the diaphragm. Both of these sets, as shown in Figure 3.41, were used to monitor the contribution of the deck in the moment resistance of the connection. The final set was placed at a distance of 1.5 ft from the second set of gauges, on each side of the column, as shown in Figure 3.42. These gauges were used to capture the general behavior of the deck away from the connection.

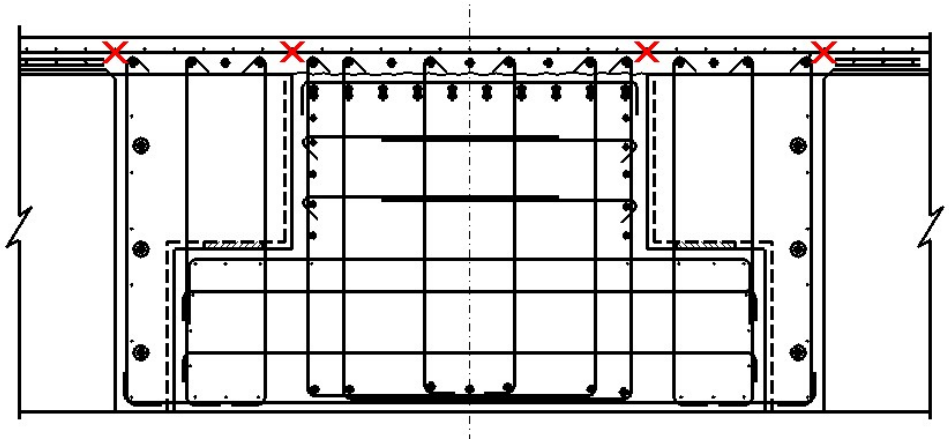

Figure 3.41: Deck Reinforcement Strain Gauge Locations

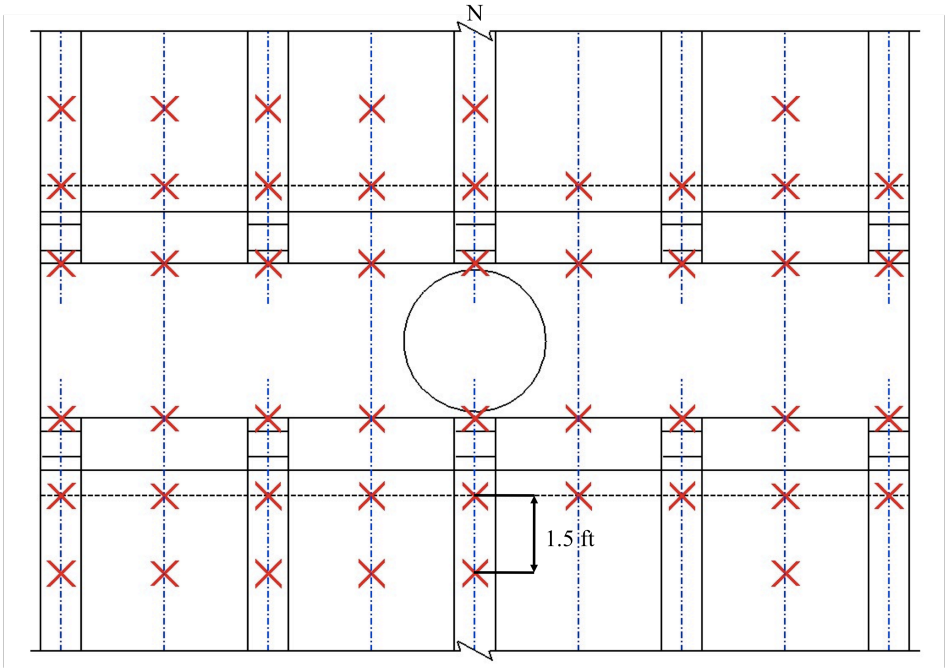

Figure 3.42: Deck Reinforcement Strain Gauge Layout

3.5.2 External Instrumentation

3.5.2.1 Horizontal Displacement of Cap and Superstructure

Each end of the bridge deck was mounted with a string potentiometer along its centerline in order to validate the displacement readings provided by the horizontal actuators as shown in Figure 3.43. On the reaction frame side of the test unit, an extra string potentiometer was added to the side of the deck in order to obtain an additional displacement and deck rotation reading. Additionally, each end of the cap beam was instrumented with string potentiometers in order to provide both the horizontal displacement of the cap in the longitudinal direction of the bridge and to indicate any twisting of the superstructure as shown in Figure 3.44.

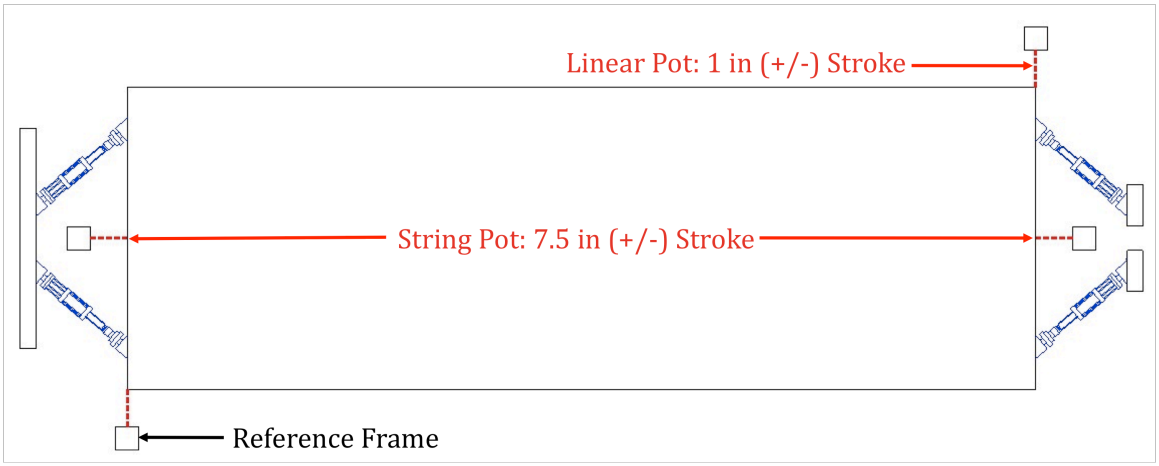

Figure 3.43: Location of Deck Displacement Devices

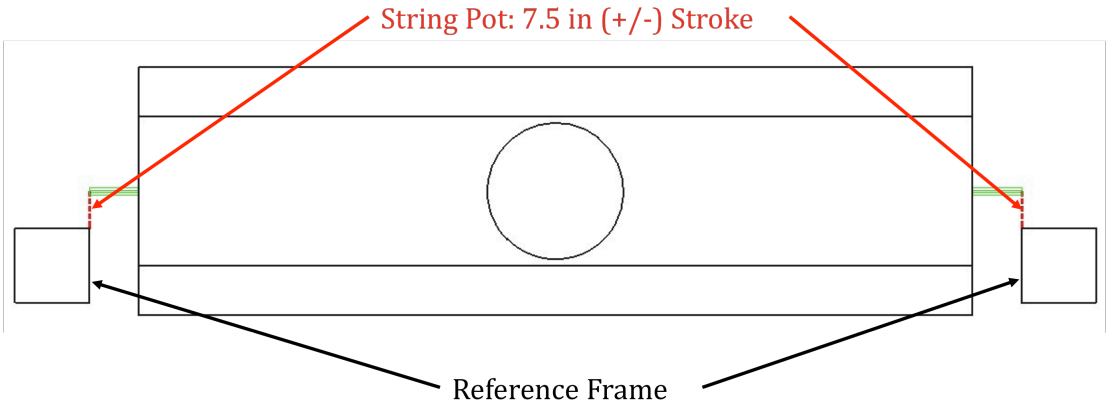

Figure 3.44: Plan View of Horizontal Cap Beam Displacement Devices

3.5.2.2 Vertical Displacement of Girders/Superstructure

1.1.1.1.1 Phase 1

It was important to obtain a relative vertical displacement profile for the superstructure and girders in order to investigate the force path along the deck and the moment distribution between the girders. Therefore, string potentiometers were mounted between the bottom side of the flanges of the designated girders and the strong floor, as shown in Figure 3.45. Only half of the bridge was instrumented as shown in Figure 3.46. A string potentiometer was placed next to each actuator, located between the floor and the abutment, in order to verify the displacement readings provided by the actuator.

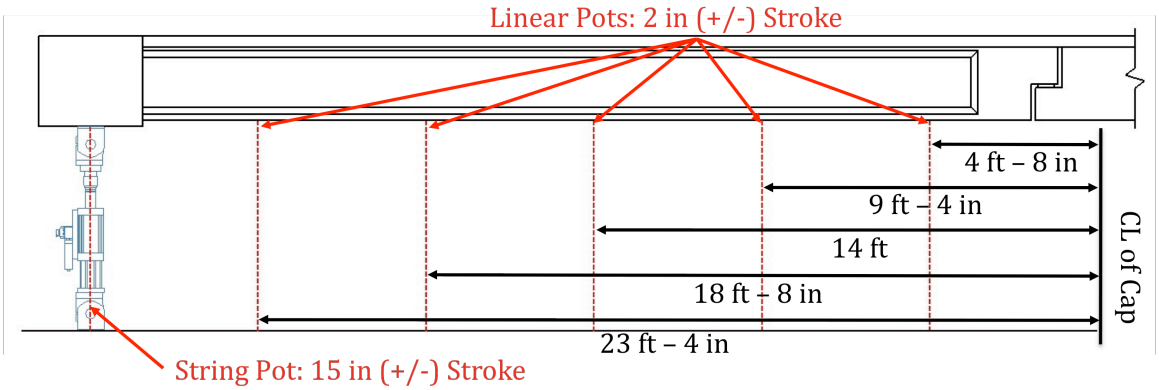

Figure 3.45: Phase 1 Vertical Girder Displacement Device Locations

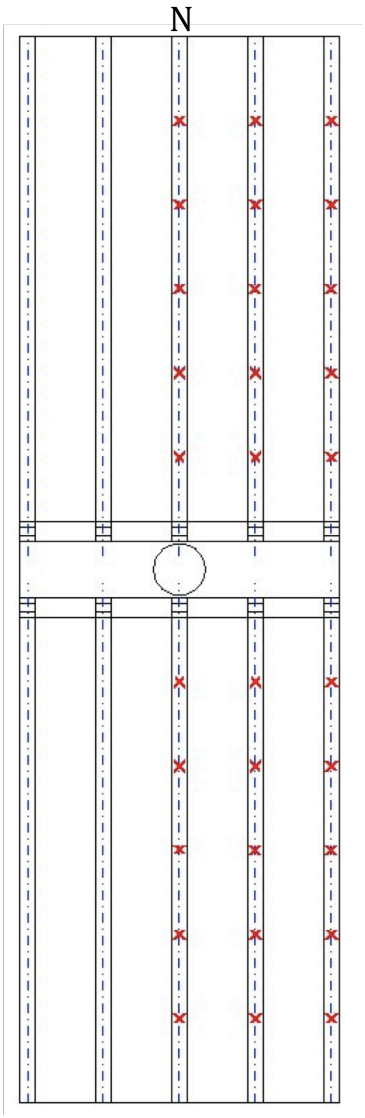

Figure 3.46: Locations of Vertical Displacement Devices along the Girder Length During Phase 1 of Testing

1.1.1.1.2 Phase 2

The vertical displacements of the girders were also measured during Phase 2 of the testing. However, since the expected displacements were larger than those for Phase 1, a combination of string and linear potentiometers with a larger stroke, as shown in Figure 3.47, replaced many of the potentiometers that were specified for Phase 1. It should be noted that, in order to reduce the setup time, the locations of the potentiometers were the same and one

set of potentiometers was removed. Additionally, the same girders that were instrumented for Phase 1 were instrumented for Phase 2.

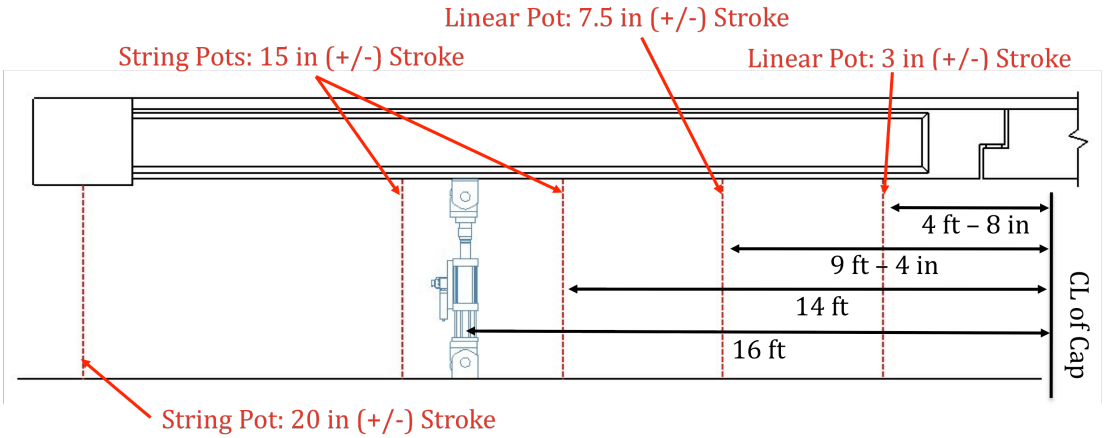

Figure 3.47: Phase 2 Vertical Girder Displacement Device Locations

3.5.2.3 Column Curvature and Growth

The curvature of the column, mostly within the plastic hinge regions, was recorded by placing a series of four linear potentiometers, spaced at 6 in. on center, along the extreme tension and compression fibers of the column, as shown in Figure 3.48. An additional linear potentiometer was mounted along the length of the column on both its East and West sides in order to measure any longitudinal column growth.

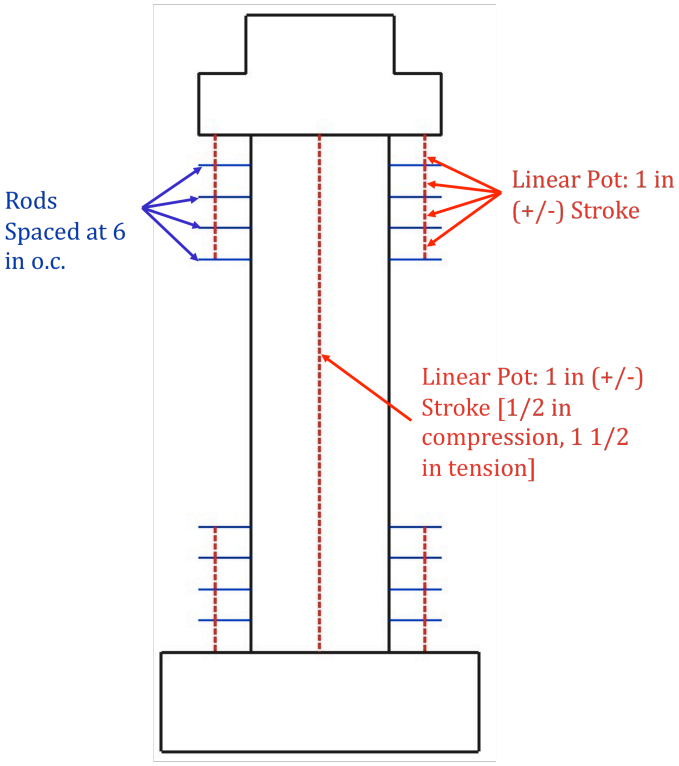

Figure 3.48: Column Curvature and Growth Device Locations

3.5.2.4 Cap Beam Twist and Dilation

The angle of rotation due to torque acting along the length of the column, between girders, was measured via rotation devices placed at the midpoint between girders and along the centerline at the bottom of the cap beam, as shown in Figures 3.49 and 3.50. The sensitivity of these devices needed to be high, as the expected rotations are relatively small. Linear potentiometers were also placed between the rods, to which the rotation devices were mounted, in order to measure the dilation of the cap along its longitudinal axis. Since the column interfered with the linear potentiometers running along the length of the cap beam, the rods and linear potentiometers in the vicinity of the column were placed on the top of the cap beam as shown in Figure 3.49. Only half of the cap beam was instrumented in this manner, again due to symmetry. Additionally, a rotation device was mounted to the rod directly above the column in order to measure the rotation of the cap beam. Finally, a rotation device was placed on each end of the cap beam in order to further measure any twist.

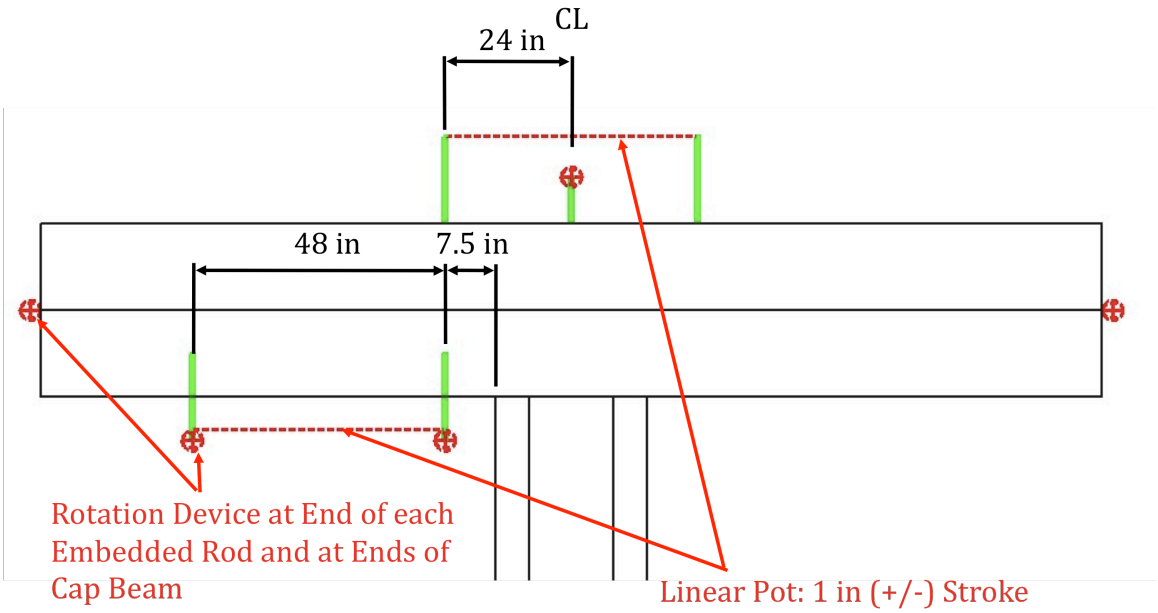

Figure 3.49: Profile View of Cap Beam Twist and Dilation Instrumentation Scheme

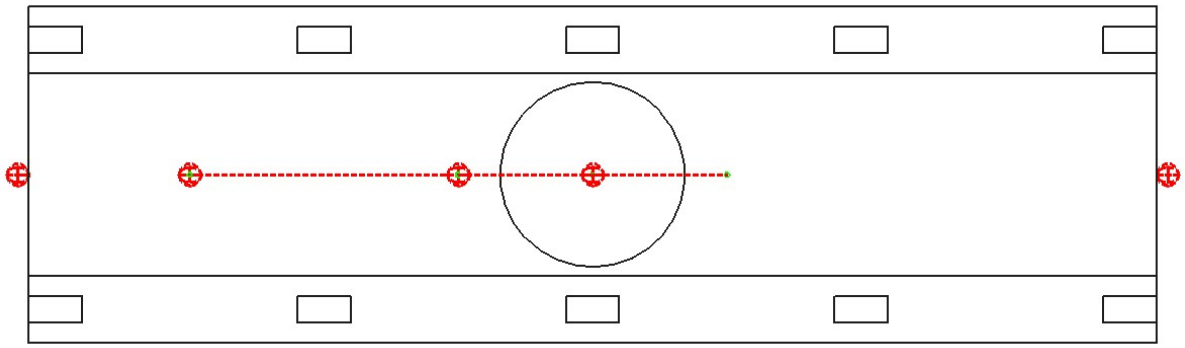

Figure 3.50: Plan View of Cap Beat Twist and Dilation Instrumentation Scheme

3.5.2.5 Connection Rotation and Neutral Axis Depth

Similar to the strain gauge plan, the instrumentation within the connection region was critical. A linear potentiometer was mounted on the underside of the superstructure spanning the connection between the girder and the cap, as shown in Figure 3.51. A rotation device was also mounted on the rod that was embedded in the girder and used in mounting the aforementioned linear potentiometer. Together, the linear potentiometer and the rotation device were used to determine the neutral axis and rotation of the connection at each girder.

One center, intermediate, and exterior girder on each side of the cap was instrumented in this manner.

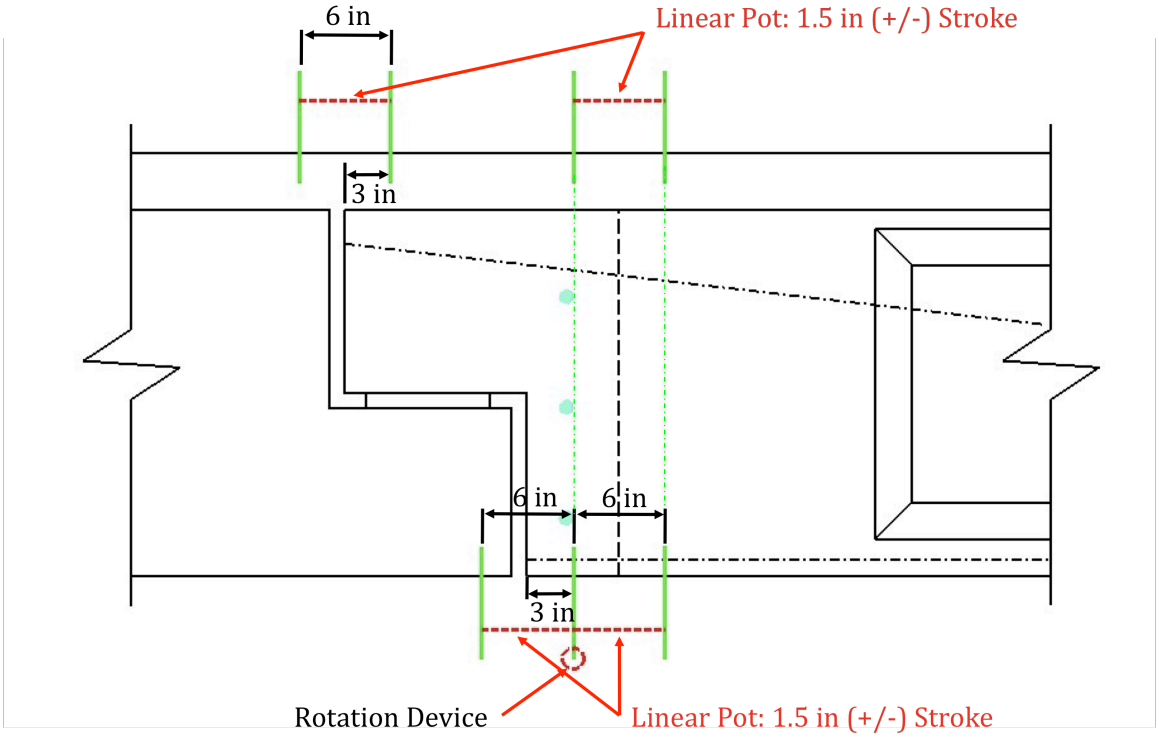

Figure 3.51: Girder-to-Cap Beam Connection Instrumentation Scheme

3.5.2.6 Girder Curvature

The linear potentiometers at the bottom of the girders, as detailed in the previous section, were also used to determine the curvature of the girders near the connection region. An additional linear potentiometer was placed along the bottom of the girder away from the connection. A second linear potentiometer was placed at the top of the girder, directly above the additional pod that was added to the bottom. A third linear potentiometer was placed above the girder and spanned the interface between the girder and cap beam. These details are shown in Figure 3.51. One center, intermediate, and exterior girder on each side of the cap received this instrumentation.

3.5.2.7 Lateral Displacement Measurement Between Girders

Since some lateral displacement between the girders was observed during the preliminary finite element analysis of the superstructure, string potentiometers were placed between girders at a distance of 16 ft from the center of the cap beam, as shown in Figure 3.52. Both the center and one of the interior girders as well as one of the interior and exterior girders received this configuration. The lateral displacement between girders was only measured on the as-built side of the connection.

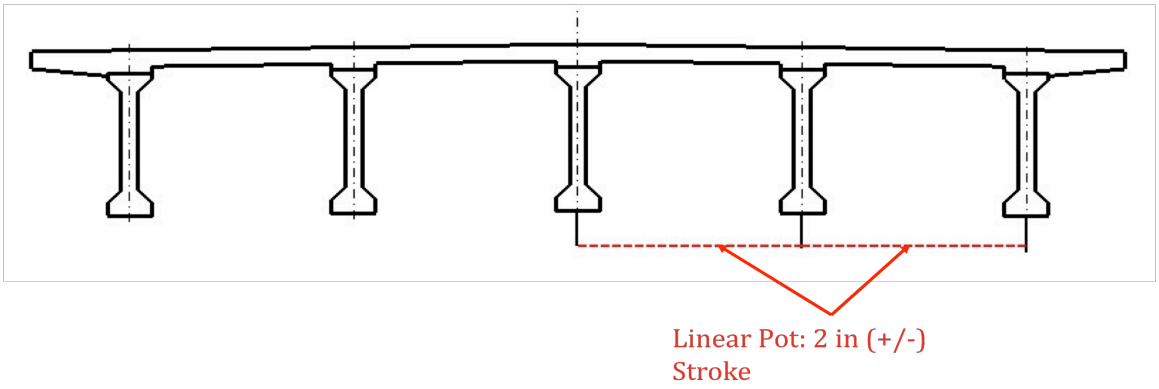

Figure 3.52: Lateral Displacement between Girders Device Locations

3.5.2.8 Improved Connection Strand Slip

As noted previously, the untensioned strands that were used in the improved connection detail were incorrectly terminated at the face of the diaphragm on the as-built connection side of the bent cap. However, this did have one benefit, in that it allowed any slip of the strands to be measured. One strand directly East of the center girder and one strand directly East of the West intermediate girder were therefore mounted with a linear potentiometer in order to measure any strand slip. The potentiometers were mounted to the strand via a circular clamp around the strand, which then measured any displacement relative to the face of the diaphragm, as shown in Figure 3.53.

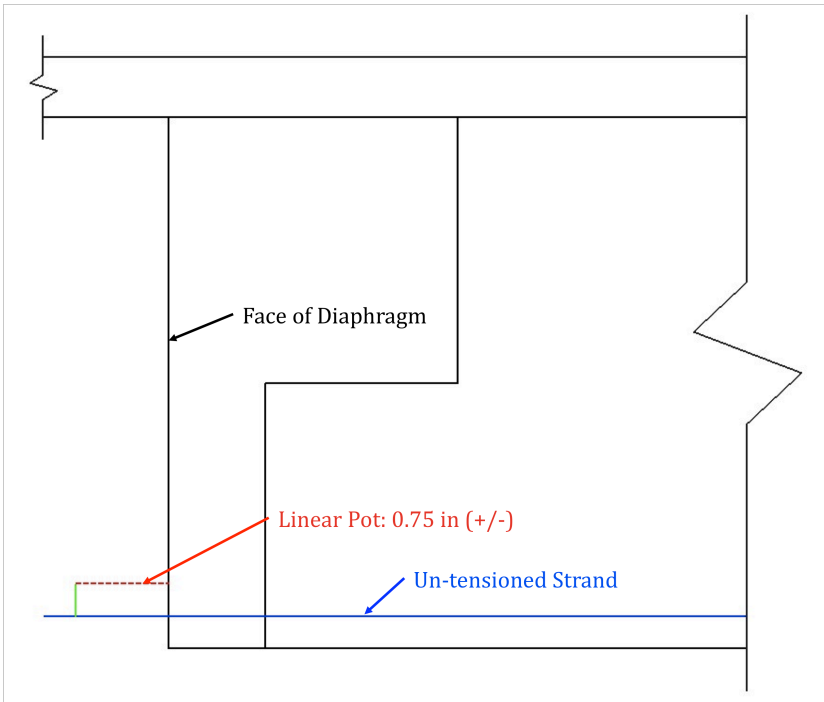

Figure 3.53: Strand Slip Device Location

3.5.2.9 Footing Movement

In order to ensure that the footing did not experience any displacement during the testing, one linear potentiometer was placed between the footing and the floor in the push direction. An additional linear potentiometer was placed perpendicular to the loading direction on each side of the footing. These linear potentiometers were placed diagonally from each other in order to detect any torsion in the footing as well, as shown in Figure 3.54.

The uplift of the footing was also monitored by placing a linear potentiometer on the North and South side of the footing, which was mounted to the floor as a point of reference, as shown in Figure 3.55.

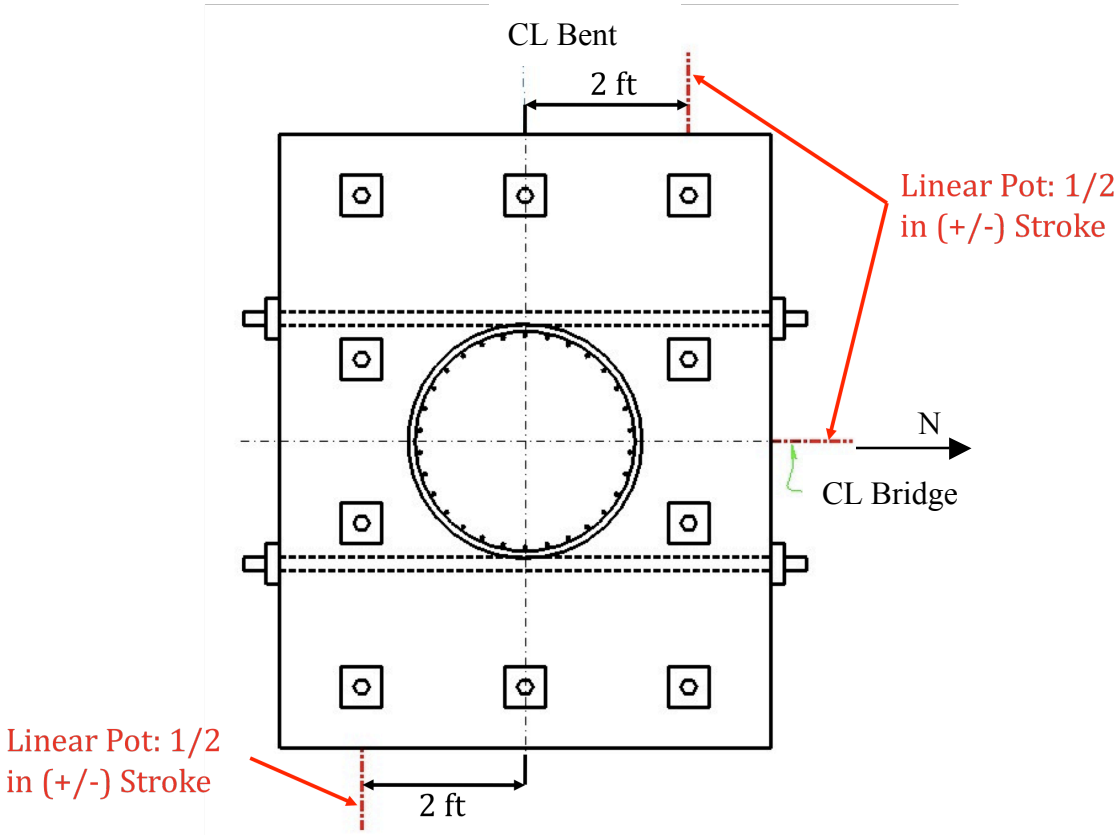

Figure 3.54: Footing Displacement Device Locations

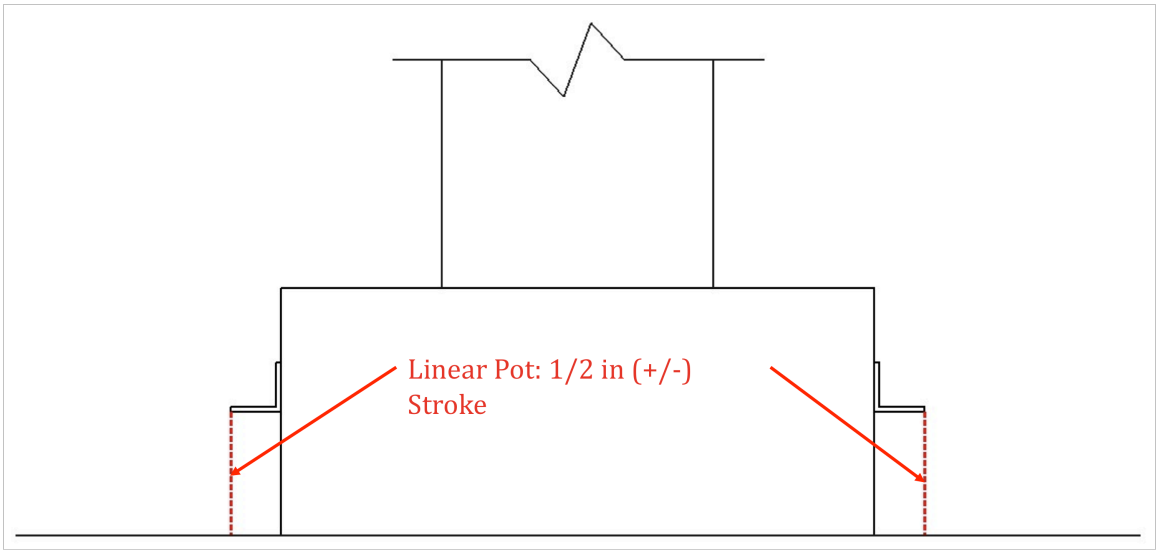

Figure 3.55: Footing Uplift Device Locations

3.6 Material Testing

During each concrete pour, unconfined test cylinders were cast in order to establish the compressive strength of the concrete. The compressive strength was determined for each pour at the age of 7, 14, 21, and 28 days, as well as on the day of testing. The average strength of three cylinders was taken as the compressive strength in each case and is represented in the Table 3.1.

Table 3.1: Measured Unconfined Concrete Strengths

Member	f'_c (ksi)					
	7 Day	14 Day	21 Day	28 Day	Day of Testing (Phase 1)	Day of Testing (Phase 2)
Footing	3.94	4.36	4.73	4.89	6.70	6.68
Column	3.91	4.36	4.80	5.04	6.81	7.07
Bent Cap	4.27	4.78	5.06	5.27	7.60	7.39
Girders (Average)	6.00	7.36	8.08	8.94	11.36	11.13
North Abutment	-	-	5.31	5.49	7.75	7.89
South Abutment	-	-	5.48	5.59	8.03	7.98
Partial Diaphragm	4.27	4.67	5.28	5.45	6.86	7.31
Deck, Haunch, and Remainder of Diaphragm	4.06	4.79	4.88	5.28	5.67	5.91

Three samples for each batch and bar size of the steel reinforcement were also collected and tested, under a uniaxial tension, in order to obtain the stress-strain response and thus the average yield and ultimate strength and strain parameters for each bar size. Due to the fact the samples for the spirals within the column were previously bent in the shape of a spiral, and had therefore already experienced yielding, they did not have a well defined yield point or plateau. As a result, the yield stress was approximated at strain of 0.5% in accordance with ASTM A370 specifications (Collins & Mitchell, 1991). The obtained yield stress was then divided by the modulus of Elasticity, E_s, in order to obtain a theoretical yield strain. The results of the reinforcement testing are summarized in Table 3.2. It should be noted that σ_y and σ_u represent yield and ultimate stress, or strength, and ε_y and ε_u represent yield and ultimate strain, respectively. Additionally, a welded wire mesh was used for the

girder #3 stirrup reinforcement, which explains the different yield and ultimate stress-strain behavior.

Table 3.2: Reinforcement Material Properties

Specimen		f_y (ksi)	ε_y (in./in.)	f_u (ksi)	ε_u (in./in.)
Abutment	#3	64.7	0.00232	104.5	0.109
	#4	64.7	0.00230	91.9	0.125
	#5	64.2	0.00255	92.2	0.119
	#6	61.7	0.00239	89.5	0.123
Bent Cap	#3	64.6	0.00206	104.5	0.113
	#4	65.4	0.00236	92.5	0.128
	#6	62.6	0.00221	92.2	0.122
Column	#3	59.7	0.00206	97.0	0.121
	#6	62.3	0.00238	92.4	0.115
Deck	#3	62.4	0.00216	101.2	0.111
	#4	61.3	0.00208	89.1	0.127
	#5	63.6	0.00232	91.0	0.130
Footing	#4	64.1	0.00198	91.4	0.124
Girders	#3	71.4	0.00246	76.7	0.0161
	#4	71.3	0.00246	94.4	0.0963

Chapter 4. GRILLAGE MODEL DEVELOPMENT

4.1 Introduction

In order to obtain a better understanding of the generalized behavior of the test unit, a grillage finite element model was developed using SAP2000. Compared to other forms of finite element modeling, a grillage model is typically viewed as being simpler to construct and, as a result, its output is generally simpler to interpret and its use in design offices is relatively frequent. However, in order to produce meaningful results, it is crucial that all elements within the model are defined as accurately as possible, in regard to both their material and behavioral properties and boundary conditions. For example, since the test unit was symmetrical about its longitudinal axis, it was determined that only half the structure needed to be modeled. However, in order to obtain accurate results, special consideration was applied to the boundary conditions along the axis of symmetry, as detailed below. Furthermore, one limitation of a grillage model is that nonlinear behavior cannot be easily included in the analysis, unless the behavior is defined and added to the model via specific nonlinear link elements at any location expected to potentially undergo a nonlinear response. Therefore, some assumptions regarding aspects of the localized behavior of the structure must be made prior to performing the analysis. Greater details regarding all of these concerns will be presented and discussed in the following sections.

4.2 Element Properties

A grillage model is a network of frame elements, which are placed at the center of gravity of the various components of the bridge for which they represent, as shown in Figure 4.1. Therefore, the definition of the properties of each frame element was of crucial importance when developing the model and ensuring its validity. Hence, the development of each set of frame elements and any special considerations given to the development of these elements are discussed below.

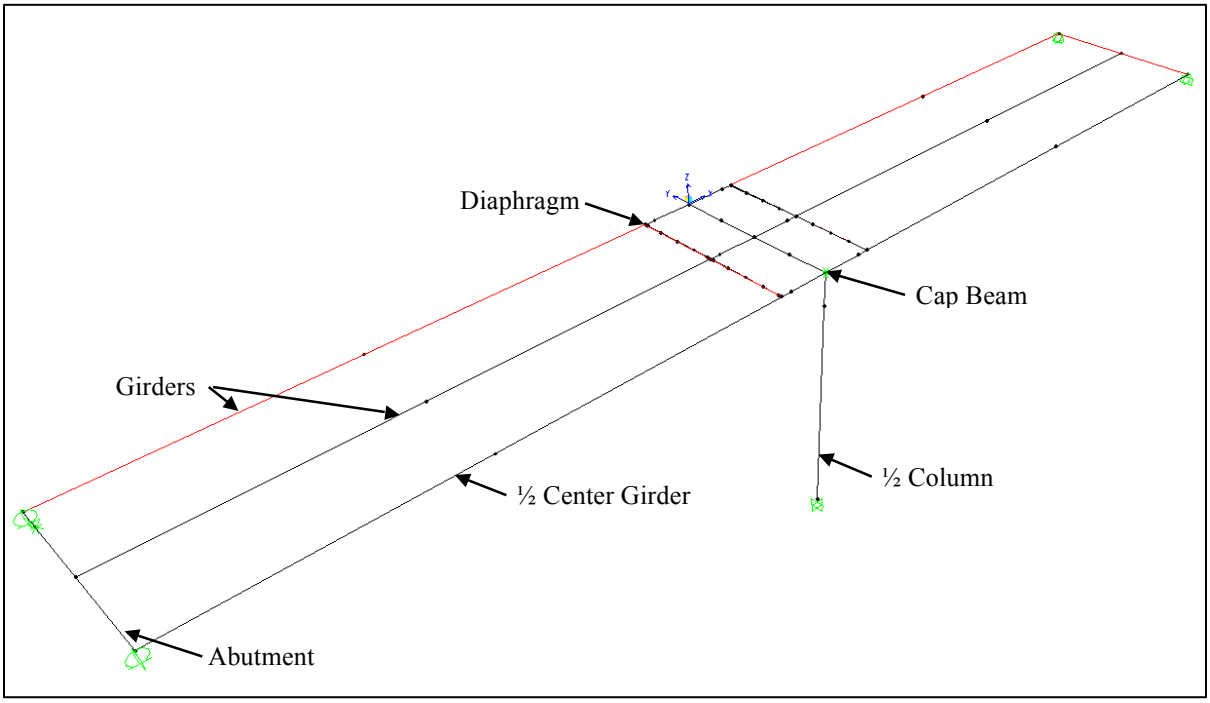

Figure 4.1: Test Unit Grillage Model

Additionally, the method of connecting each frame element to any surrounding frame elements was an important consideration. Previous experimental research involving grillage models have investigated the use of rigidly connecting the elements, using offsets, and connecting the elements directly via their respective elastic properties (Holombo, Priestley, & Seible, 1998). Based on the recommendations, it was decided that connecting the elements directly, based on their effective elastic properties, would lead to a satisfactory result. Therefore, unless otherwise noted, the frame elements were connected in that manner.

Since each member had a specific concrete strength, an isotropic concrete material model was defined using an unconfined Manders stress-strain curve within SAP for each element. The values for f'_c, modulus of elasticity, and Poisson's ratio were all required in order to define the concrete model within SAP. Since the value for f'_c was known, Equation 4.1 was used to calculate the modulus of elasticity, E_c (Priestley, Seible, & Calvi, 1996). Poisson's ratio was conservatively assumed to be 0.2 (Wight & MacGregor, 2008).

$$E_c = 57000\sqrt{f'_c\,(psi)} \qquad (4.1)$$

Finally, some of the elements required property modifiers to be manually input into SAP. The modifiers were necessary when an element met the following circumstances:

Scaling was required to reduce the member from the prototype level to the test unit level, the element was modeled as a composite section and needed material transformation, minor cracking of the member was expected, or only a portion of a section was modeled due to symmetry. As noted, these properties were determined prior to the analysis and were input via the appropriate element scale factors within SAP.

4.2.1 Column

The column was relatively simple to model. The cross-sectional properties of the test unit were directly input into SAP and were scaled by an appropriate 50% scaling factor in order to take into account that only half of the column was modeled due to symmetry. However, based on the moment curvature analysis that was performed on the column, an effective value was determined for the flexural moment of inertia, using Equation 4.2. As a result, an effective scale factor was derived to convert the gross moment of inertia to the effective value and was manually input into SAP. These scale factors may be found below in Table 4.1.

$$I_{eff} = \frac{M_y'}{\phi_y' E} \tag{4.2}$$

Table 4.1: Column Element Properties Used in the Grillage Model

Column Element Properties	
Diameter (in)	33
Material Properties	
f_c' (ksi)	5.042
E (ksi)	4047
Sap Property Modifiers	
Cross-section (Axial) Area	0.5
Shear Area in 2 Direction (Vertical Local Axis)	0.5
Shear Area in 3 Direction (Transverse Local Axis)	0.5
Torsional Constant	0.5
Moment of Inertia about 2 Axis (Vertical Local Axis)	0.1895
Moment of Inertia about 3 Axis (Transverse Local Axis)	0.1895
Mass	0.5
Weight	0.5

The height of the column was 10 ft.-4 in., however it needed to extend to the centerline of the inverted-T cap beam. Therefore, an additional frame element, that was 19 in. in length, was added to the top of the column and connected to the centerline of the cap beam. However, an end offset was applied over its entire length so that its mass and stiffness would not be counted twice within the overlap of the cap beam.

4.2.2 Girders

Since SAP has built-in definitions for standard Caltrans girder shapes, only limited information needed to be input for the girder frame elements as well. The 1676 mm I-girder shape was selected and its cross-sectional dimensions were all scaled from the prototype dimension level and manually altered in SAP to match the test unit dimension level. Since the girders were modeled as a composite section, which included the haunch directly above the top flange of the girder, it was necessary to further modify the section properties in order to account for the transformed composite section. As mentioned previously, this was accomplished by altering the scale factors within SAP. The thickness of the haunch was also included in the alteration of the overall height dimension of the girder. This was required in order to achieve the proper neutral axis height for the composite behavior between the girder and deck element, which is discussed later.

Additionally, based on similar experimental research that was conducted in the past, it was assumed that the superstructure would likely experience some degree of cracking (Holombo, Priestley, & Seible, 1998). As a result, the stiffness of the girders was reduced in order to take into account the weakening in stiffness that would likely be expected due to the cracking. An effective, cracked girder stiffness was determined based on a moment curvature analysis, which was performed for the composite girder and deck section. Two effective stiffness values were obtained based on whether the section was subjected to a positive or negative moment. The appropriate stiffness factor, given the corresponding loading direction, was then input into the model, as indicated in Tables 4.2 and 4.3. It should be noted that this sequence had to be performed separately for both the North and South superstructure spans, as the reinforcement details were different, due to the presence of the untensioned strands used in the improved connection, which ran along the length of the

girders on the North side of the bent cap. Furthermore, positive bending was defined as the case in which the bottom flange of the girder was in tension. Through a simplified model of a single cantilevered girder, it was discovered that the same forces would be achieved regardless of whether a gross effective stiffness or a series of decreasing stiffness values were applied along the length of the beam. Therefore, the gross reduction in effective stiffness was applied over the entire length of the girder.

Table 4.2: Grillage Model Girder Properties

Girder Properties	
Material Properties	
f'_c (ksi)	8.94
E (ksi)	5389
SAP Property Modifiers	
Cross-section Area	0.980
Shear Area in 2 Direction (Vertical Local Axis)	0.980
Shear Area in 3 Direction (Transverse Local Axis)	0.980
Torsional Constant	1
Moment of Inertia about Axis 2 (Vertical Local Axis)	0.958
Moment of Inertia about Axis 3(Transverse Local Axis) [Gross]	0.953
Moment of Inertia about Axis 3 (Transverse Local Axis) [+ Moment North Girder]	0.285
Moment of Inertia about Axis 3(Transverse Local Axis) [- Moment North Girder]	0.643
Moment of Inertia about Axis 3 (Transverse Local Axis) [+ Moment South Girder]	0.25
Moment of Inertia about Axis 3(Transverse Local Axis) [- Moment South Girder]	0.636
Mass*	1.003
Weight**	1.003
* Between the cap and diaphragm, a modifier of 0.0001 was used in order to prevent the mass from being accounted twice within the cap region	
** Between the cap and diaphragm, a modifier of 0 was used in order to prevent the weight from being accounted twice within the cap region	

Table 4.3: Grillage Model Center Girder Properties

Center Girder Properties	
Material Properties	
f'_c (ksi)	8.94
E (ksi)	5389
SAP Property Modifiers	
Cross-section Area	0.490
Shear Area in 2 Direction (Vertical Local Axis)	0.490
Shear Area in 3 Direction (Transverse Local Axis)	0.490
Torsional Constant	0.5
Moment of Inertia about Axis 2 (Vertical Local Axis)	0.479
Moment of Inertia about Axis 3(Transverse Local Axis) [Gross]	0.477
Moment of Inertia about Axis 3(Transverse Local Axis) [+ Bending North Girder]	0.1425
Moment of Inertia about Axis 3 (Transverse Local Axis) [- Bending North Girder]	0.322
Moment of Inertia about Axis 3(Transverse Local Axis) [+ Bending South Girder]	0.125
Moment of Inertia about Axis 3 (Transverse Local Axis) [- Bending South Girder]	0.318
Mass*	0.501
Weight**	0.501
* Between the cap and diaphragm, a modifier of 0.0001 was used in order to prevent the weight from being accounted twice within the cap region	
** Between the cap and diaphragm, a modifier of 0 was used in order to prevent the weight from being accounted twice within the cap region	

Since the girders extended from the centerline of the cap to the centerline of the abutment, end offsets were applied to both ends in order to prevent the overlapping stiffness and mass from being accounted for twice within the analysis. Additionally, since half the structure was modeled about its centerline, only half of the center girder was modeled, as

reflected by its SAP property modifiers being defined as half of what was used for the other girders.

4.2.3 Cap Beam

The cap beam was modeled as a composite rectangular section that included the inverted-T as well as the deck and portions of the diaphragms within the cross-sectional span of the inverted-T, as shown in Figure 4.2.Therefore, it was necessary to transform the section, so that all sections had the same effective f'_c as the bent cap, which was 5.27, when calculating the effective cross-sectional properties. Additionally, since the girders extended to the centerline of the cap, and the cap was modeled as a solid rectangular section, it was necessary to apply end offsets to the ends of the girders in order to prevent their stiffness from being included twice within the model.

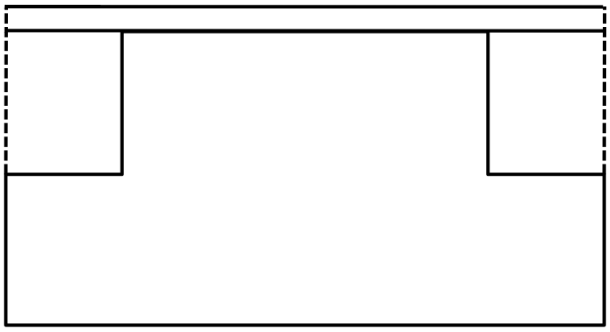

Figure 4.2: Cap Beam Composite Cross Section

It was determined that the cap beam would likely experience some torsional cracking during testing, which will be discussed in the nonlinear element section of the following text. As a result, it was necessary to include nonlinear link elements along the length of the cap beam in order to capture the axial rotations associated with the torsional cracking. However, in order to prevent the elastic rotation of the cap from artificially increasing the rotation that was specified within the nonlinear link elements that were placed along the length of the cap beam, a modifier was input into SAP to make the cap torsionally rigid, as shown in Table 4.4

Table 4.4: Grillage Model Cap Beam Properties

Cap Element Properties	
Depth (in.)	38
Width (in.)	60
Material Properties	
f'_c (ksi)	5.27
E_c (ksi)	4138
SAP Property Modifiers	
Cross-section Area	1
Shear Area in 2 Direction (Vertical Local Axis)	1
Shear Area in 3 Direction (Transverse Local Axis)	1
Torsional Constant	1.0E+10
Moment of Inertia about Axis 2 (Vertical Local Axis)	1.002
Moment of Inertia about Axis 3 (Transverse Local Axis)	0.994
Mass	1
Weight	1

4.2.4 Diaphragm

Even though the cap beam and diaphragms would normally be treated and modeled as a monolithic section, it was necessary to create separate elements for the vertical portion of the diaphragm in order to provide a transverse member at the location of the cap-to-diaphragm reinforcement; the transverse member was used to accommodate the nonlinear link elements that were used to model the slip behavior of the hooked reinforcement between the cap and the diaphragm. However, since two elements were required and each were used to model the diaphragm, it was necessary to reduce the properties of each element by 50%, in order to prevent the effects of the diaphragm from being doubled within the model. Furthermore, since a partial pour of the diaphragm was completed prior to the final pour of the deck and diaphragm, it was necessary to transform the section properties to a uniform concrete strength. The two elements were each modeled with a rectangular cross-section, which represented only the vertical portion of the diaphragm located beyond the corbel of the inverted-T cap beam, as well as the portion of the deck directly above this section of the diaphragm. Each element was placed as close to one another as possible within the model

and the two were connected by the nonlinear link elements representing the diaphragm reinforcement, to be discussed later. Finally, since any elastic effects of their behavior were captured within the nonlinear link elements representing both the diaphragm reinforcement and the girder-to-diaphragm connection, it was necessary to make each diaphragm element torsionally rigid. The properties used for each diaphragm element are listed below, in Table 4.5.

Table 4.5: Grillage Model Cap Diaphragm Element Properties

Cap Diaphragm Properties	
Depth (in.)	38
Width (in.)	6
Material Properties	
f'_c (ksi)	5.36
E_c (ksi)	4208
SAP Property Modifiers	
Cross-section Area	0.488
Shear Area in 2 Direction (Vertical Local Axis)	0.488
Shear Area in 3 Direction (Transverse Local Axis)	0.488
Torsional Constant	1.0E+10
Moment of Inertia about Axis 2 (Vertical Local Axis)	0.488
Moment of Inertia about Axis 3 (Transverse Local Axis)	0.489
Mass	0.5
Weight	0.5

4.2.5 Deck

Initially, the deck was modeled using a series of transverse frame elements. The deck was divided into sections and each element represented its respective section. In this configuration, the girders were also modeled as a composite section, based on an effective width as specified in AASHTO.

However, based on the results of the analyses of the superstructure that were performed in ABAQUS (Thiemann, 2009), it was determined that the aforementioned method was not adequately including the membrane or strut action of the deck. Therefore, the slab was modeled using an area element, as shown in Figure 4.3, and the girders were

modeled as a non-composite section as described above. The area deck element improved the results, as it was able to more accurately incorporate the membrane and diaphragm action of the deck. Additionally, it was simpler to model, and relied on fewer assumptions, than the initial method. Using the area deck also provided better output data as it made it possible to obtain and visualize stress and strain data within the deck.

As mentioned in the section regarding the properties used to model the girders, the stiffness of the superstructure was reduced in order to reflect expected cracking. Based on the moment curvature analysis of the composite girder and deck section, it was determined that the deck would crack completely at the condition for which the effective stiffness of the superstructure was calculated, during the case of negative bending. Therefore, the axial stiffness and dominant membrane stiffness were both removed from the area element, as noted in Table 4.6. The deck remained effective for the case of positive bending, and thus, the aforementioned factors were not removed for that case.

Table 4.6: Grillage Model Deck Area Element Properties

Deck Area Properties	
Membrane Thickness (in.)	3.75
Bending Thickness (in.)	3.75
Material Properties	
f'_c (ksi)	5.28
E_c (ksi)	3605
SAP Property Modifiers	
Membrane f11 (Stiffness about Longitudinal Local Axis) [- Bending]	0
Bending m22 (Stiffness about Longitudinal Local Axis) [- Bending]	0

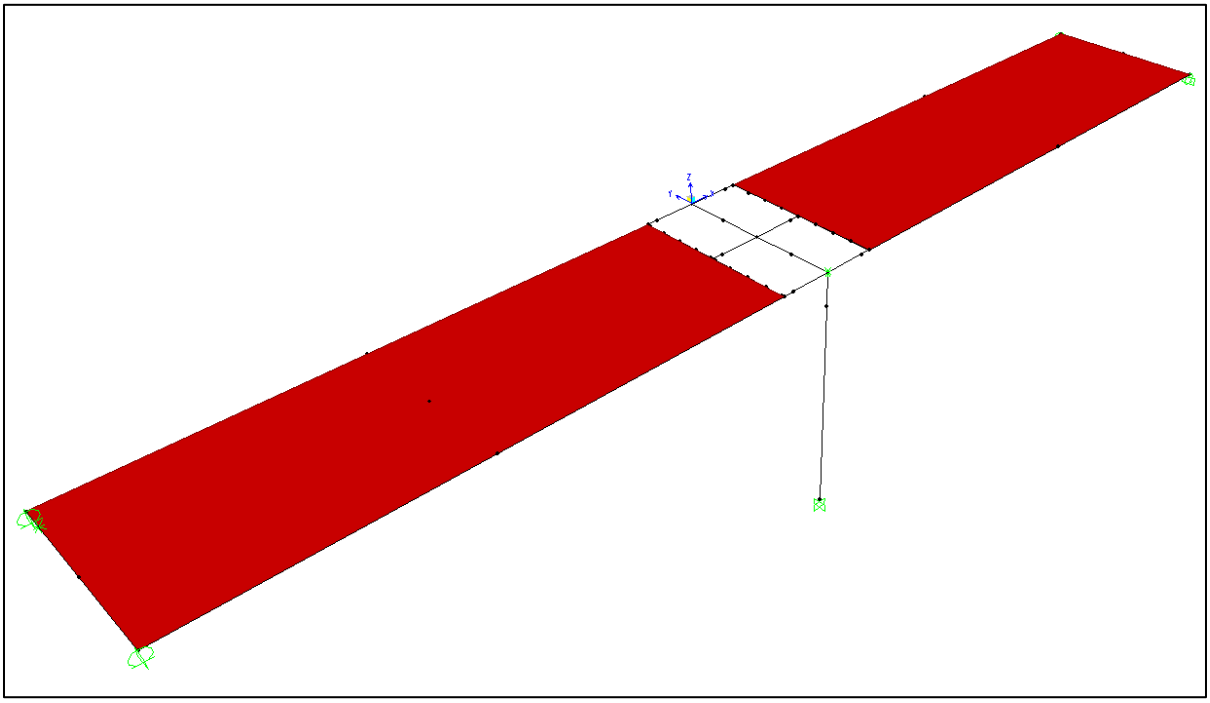

Figure 4.3: Grillage Model After Adding the Deck Area Elements

The properties in Table 4.6 were input into SAP when defining the area deck element. A thick shell element was specified for the area element as it included the desired membrane and bending action and had a tendency to be more accurate, and was thus recommended over the other types of area elements within SAP (Computers and Structures, Inc., 2008). Since the definition of all of the nonlinear link elements within the cap beam and the connection region included the stiffness contribution from the deck, in order to prevent the stiffness of the deck element from being accounted twice within the analysis, the deck was not allowed to span over the nonlinear link elements. Therefore, two area elements were used to model the deck. One element was used on each side of the cap that extended from the centerline of the abutment to the centerline of the section of diaphragm that was furthest from the cap. In order to still ensure an adequate diaphragm action of the deck within the cap beam region, where the discontinuity of the area element occurred, the cap beam was modeled as a composite cap beam consisting of the dapped ends of the girders, deck, and bent cap. The overhang portion of the deck was also not included in the modeling of the deck. Instead, the dead load of the overhang was calculated and equally distributed between each girder. A representative dead load was then applied to each girder in order to account for the dead load

effects of the overhang portion of the deck. The grillage model was constructed in that manner as it more accurately represented what was done during the design of the test unit structure and would thus provide a means to validate the model. Furthermore, it was assumed that the overhang had little effect on any slab action or the overall behavior of the structure.

Finally, though the deck elements were placed at the centerline of the girder elements, they had to be offset in order to capture the composite action between the girders and the deck. Therefore, the nodes at each corner of the deck elements were offset from the center of the deck by a distance of 19 in., which corresponded to the distance required to make the bottom side of the deck come into contact with the top of the haunch above the girder element, as shown in Figure 4.4.

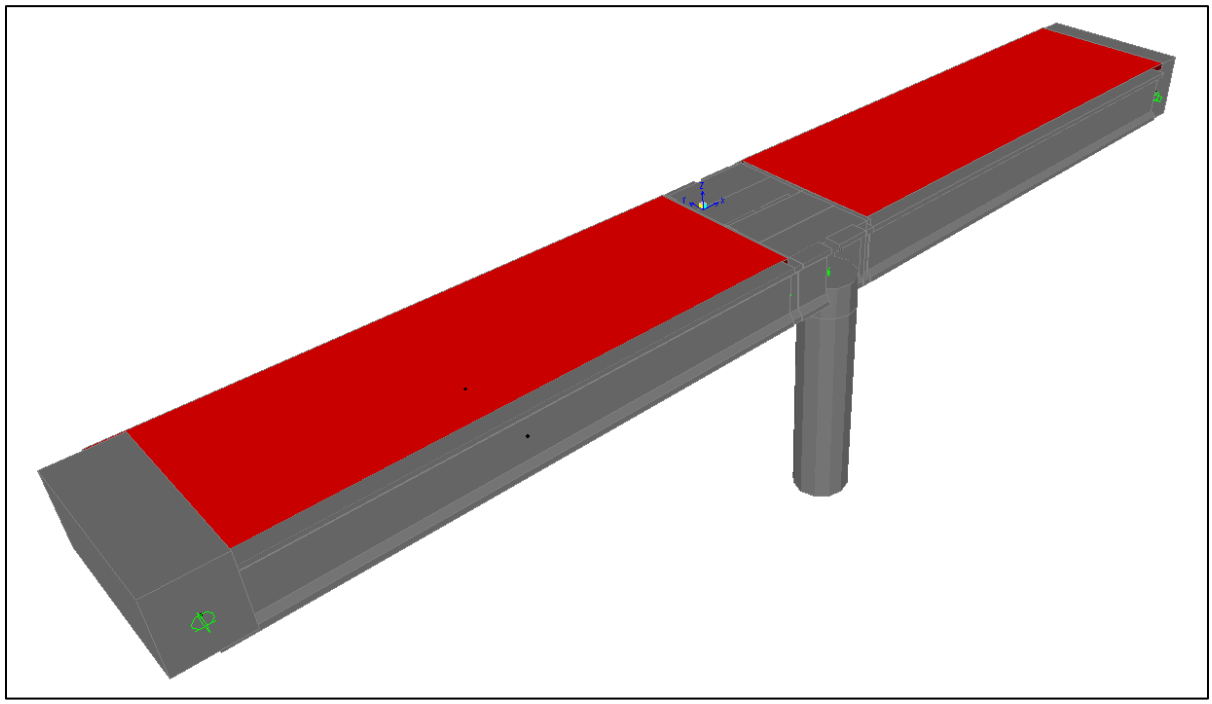

Figure 4.4: Extruded Grillage Model Deck Offset

4.2.6 Abutments

The abutments were modeled as a simple rectangular cross-section on each end of the span, which included the abutment as well as the composite portion of the deck. As

mentioned, end offsets were used on the portion of the girder within the abutment in order to prevent its mass and stiffness from being accounted twice within the abutment region.

Table 4.7: Grillage Model Abutment Element Properties

Abutment Properties	
Depth (in.)	41
Width (in.)	34
Material Properties	
f'_c (ksi) North End	5.49
E_c (ksi) North End	4223
f'_c (ksi) South End	5.59
E_c (ksi) South End	4262

4.3 Boundary Conditions

All of the degrees of freedom at the base of the column were restrained as it was designed and performed during testing as a fixed base. The ends of the girders at the abutment were placed on rollers as the superstructure was allowed to translate only in the longitudinal direction. Finally, since only half of the structure was modeled about the longitudinal axis, it was necessary to restrain any transverse displacement as well as any rotation about both the longitudinal, X, and vertical, Z, axes of the superstructure.

4.4 Nonlinear Elements

The frame elements used in SAP2000, which represented the components of the test unit discussed in Section 4.2, were designed to experience only elastic deformation. Therefore, in order to perform a nonlinear analysis for a structure that was modeled with frame elements, the locations of nonlinearity needed to be determined prior to the analysis and modeled through the placement of user-defined nonlinear link elements. The following nonlinear link elements were defined and placed within the grillage model.

4.4.1 Column Plastic Hinges

Since the column was designed to form a plastic hinge at both the top and bottom of the column, it was necessary to include a nonlinear link element, which represented the hinges, at the top and bottom of the column, as shown in Figure 4.5. A moment-curvature

analysis of both the top and bottom of the column was performed using a program developed at Iowa State University, known as VSAT (Levings, 2009). The data from the moment-curvature analysis was then converted to a moment-rotation response using Equation 4.3, which accounts for rotation due to both strain penetration and plastic deformation within the hinge. It should be noted that the rotation due to elastic deformation was taken into account via the elastic frame element used to model the column. The term L'_{sp} represents the length that the elastic effects of strain penetration extend into either the cap or the footing, depending on the location of the hinge being analyzed. The term L_p represents the plastic hinge length and includes the length of the plastic effects of strain penetration as well as the length representing the plastic region of the column, as the maximum curvature over this region was assumed to be constant. The terms Φ_e and Φ_p represent the elastic and plastic curvature components, respectively. The terms f_y, d_b, and L represent the yield stress of the longitudinal reinforcement, the bar diameter of the longitudinal reinforcement, and the total length of the column, respectively.

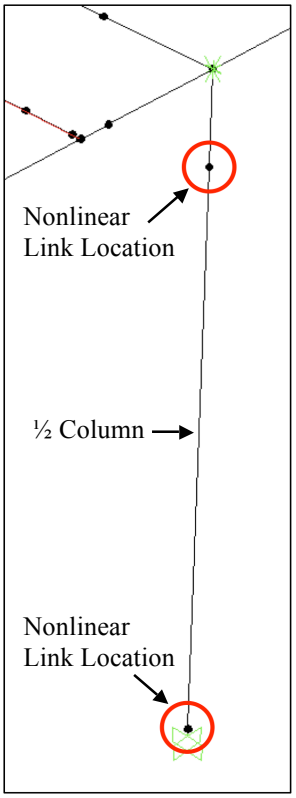

Figure 4.5: Grillage Model Column Nonlinear Link Locations

Therefore, per (Priestley, Seible, & Calvi, 1996), the total rotation within the column plastic hinge region, θ, was defined as:

$$\theta = L'_{sp}\,\phi_e + L_p\phi_p \tag{4.3}$$

$$L'_{sp} = \frac{2}{3}(0.15) f_y d_b \tag{4.4}$$

$$L_p = 0.08L + 0.15 f_y d_b \not\leq 0.3 f_y d_b \tag{4.5}$$

The moment-rotation response input was then directly input into the properties for the nonlinear link element and placed at the top and bottom of the column. The moment-rotation properties that were input into SAP for the nonlinear link elements representing the plastic hinges are shown below in Figures 4.6 and 4.7. It is important to note that the moment values obtained from the moment-curvature analysis were halved before being input into SAP, as only half of the column was modeled due to symmetry. Also, the responses for both the top and bottom plastic hinges were essentially the same, with the bottom hinge being a little stiffer due to a slightly higher axial load from the self-weight of the column.

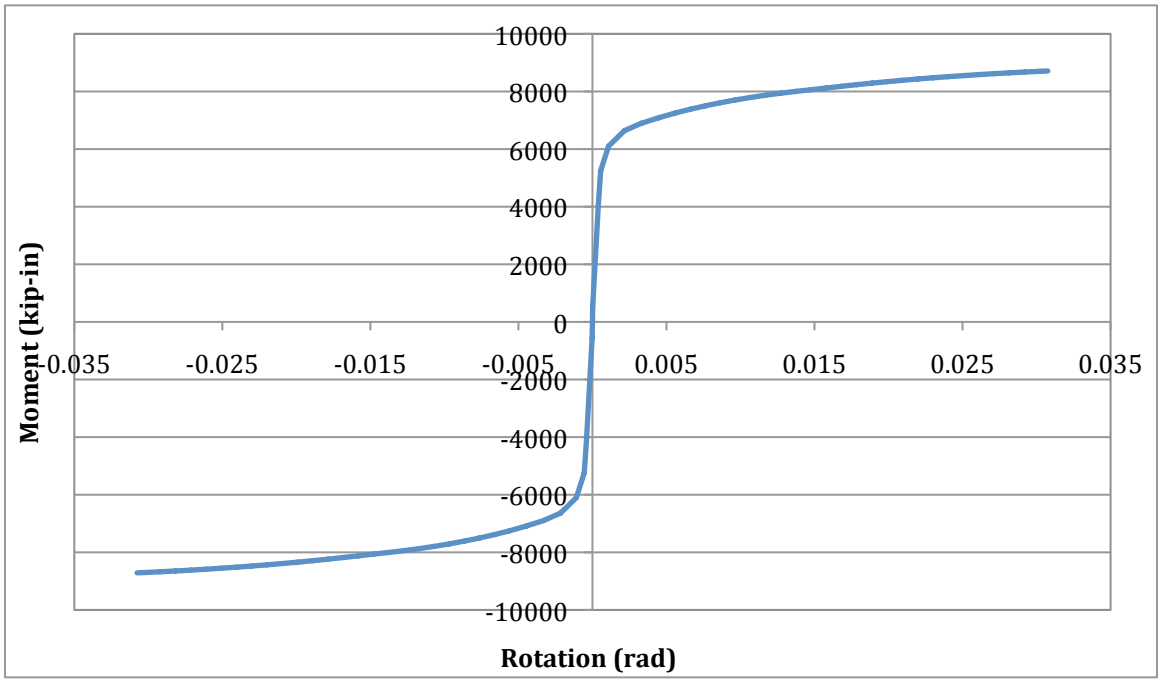

Figure 4.6: Predicted Top of Column Plastic Hinge Moment vs. Rotation Monotonic Response

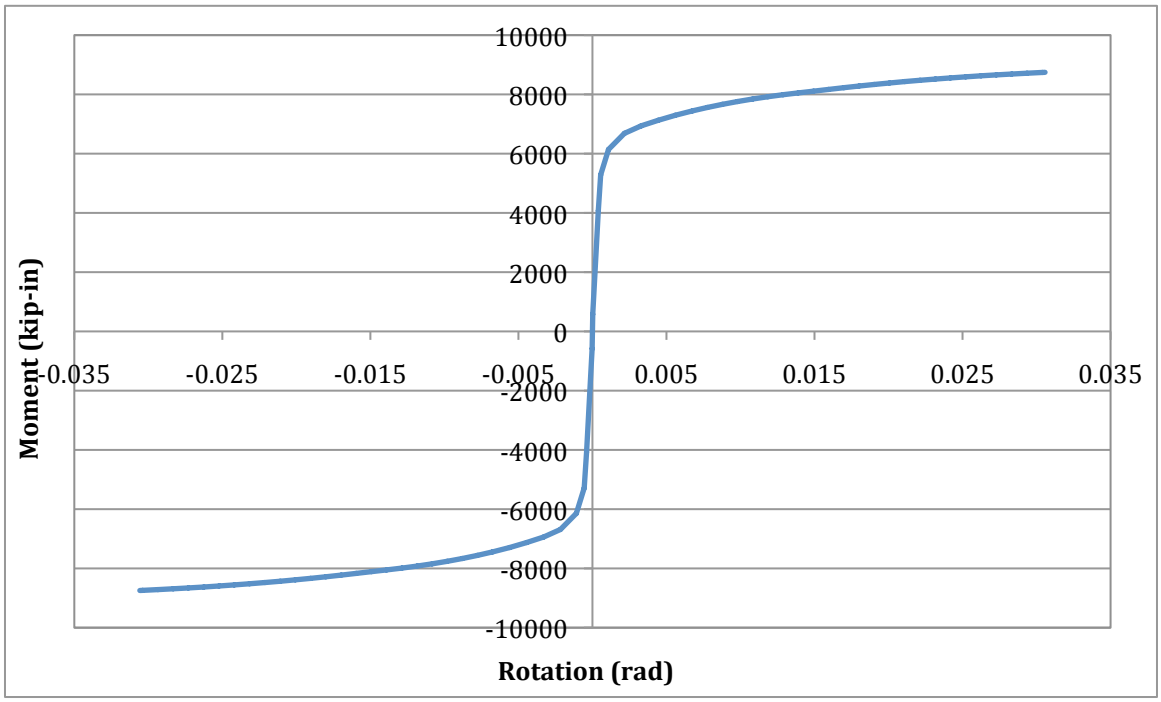

Figure 4.7: Predicted Bottom of Column Plastic Hinge Moment vs. Rotation Monotonic Response

Hysteretic rules were also defined for the nonlinear link element within SAP2000, which provided three possible built-in hysteretic models: Kinematic, Takeda, and Pivot. Since the Takeda and Pivot models are the most widely used for reinforced concrete columns, they were selected as the two primary models of consideration. In order to decide between the Takeda and Pivot models, a comparative analysis was performed based on the results of various column tests provided by the University of Washington column database (University of Washington, 2004). Based on the results of said comparison, specifically column Vu NH3, it was shown that the Pivot model was able to most accurately model the overall hysteretic behavior of the comparison column, as shown in Figure 4.8. Furthermore, the Takeda model defined within SAP2000 did not allow the user to modify its rules, whereas the user was able to define more of the rules when using the Pivot model, providing a more specific set of rules applicable to the column being analyzed. Therefore, the Pivot model was selected to define the hysteretic behavior of the column nonlinear link elements.

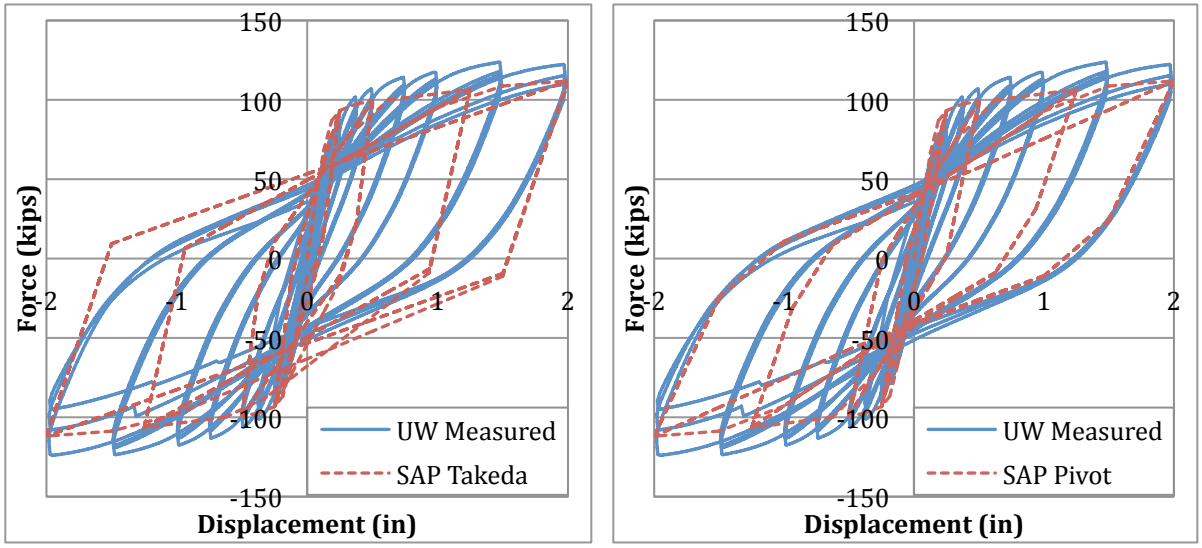

(a) Takeda Hysteresis (b) Pivot Hysteresis

Figure 4.8: Force-Displacement Hysteresis Comparison

In order to define the Pivot model for both the top and bottom nonlinear link elements, the values for α_1, α_2, β_1, β_2, and η had to be defined and input into the SAP2000 hysteretic model. The values α_1 and α_2 were used to define the location of the pivot point used to determine the unloading stiffness when removing the load from a positive and negative moment value, respectively. For the sake of comparison, it was arbitrarily assumed that these values would be approximately the same. The values β_1 and β_2 were used to define the pinching points that the moment-rotation response would pass through when reversing the moment toward the positive and negative direction, respectively. Again, it was arbitrarily assumed that these values would be approximately equal. It is important to note however, that when defining the moment-rotation response within SAP2000, both the first positive and negative moment-rotation values should correspond to the yield condition. This was done because SAP2000 defines the pinching points at a moment value corresponding to βF_y, in which the program assumed that the first point entered after the origin was used to define yield. The value η was used to define the amount of elastic, or initial, strength degradation experienced after any plastic deformation (Computers and Structures, Inc., 2008), (Dowell, Seible, & Wilson, 1998). The values for α and βwere defined using the charts shown in

Figure 4.9 (a) and (b) respectively, which were based on the longitudinal reinforcement ratio and the axial load ratio experienced by the given column (Dowell, Seible, & Wilson, 1998). The longitudinal reinforcement ratio, ρ_l, and the axial load ratio, ALR, were calculated using Equation 4.6 and 4.7, respectively, where A_{sl} represents the area of longitudinal steel, A_g represents the gross area of the column, and f'_c represents the concrete compressive strength. The value for η was taken as 8 in order to reflect an arbitrarily assumed amount of elastic strength degradation, to be used solely as a basis for comparison.

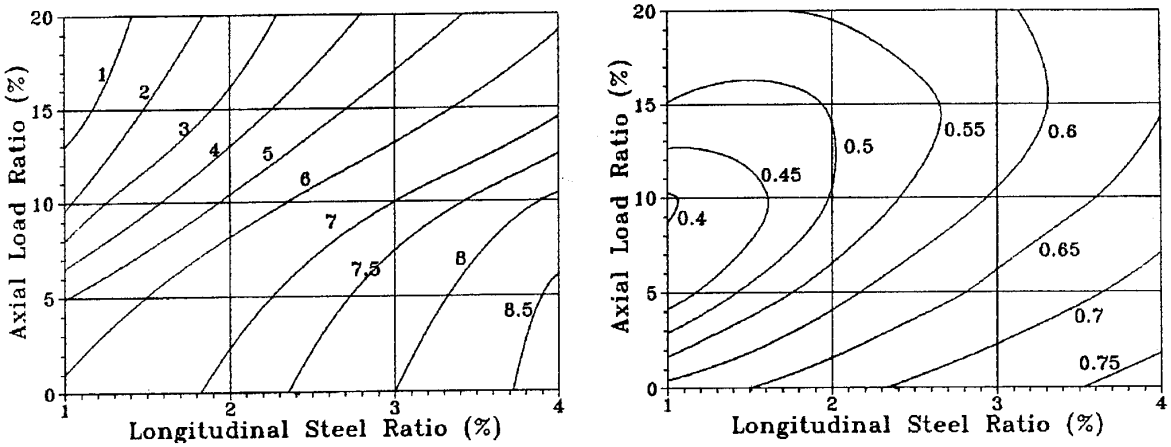

(a) α Parameter Contour (b) β Parameter Contour

Figure 4.9: Pivot Hysteresis Parameters

$$\rho_l = \frac{A_{sl}}{A_g} \tag{4.6}$$

$$ALR = \frac{P}{f'_c A_g} \tag{4.7}$$

4.4.2 Cap Torsion

Though relatively little is still known regarding the prediction of the torsional behavior of reinforced concrete, it was important to at least consider the effects of torsion on the cap beam in the analysis. The overall capacity of the cap beam was initially checked using a friction model (Priestley, Seible, & Calvi, 1996) in order to ensure that no additional

reinforcement or prestressing needed to be added to the cap beam. This was accomplished using Equations 2.12-2.15 and by assuming that the cap beam acted as a composite section with the deck and diaphragm and that a less conservative yield stress was required for friction to develop after any dowel action. The friction model indicated that the cap beam would have a torsional capacity that was greater than the demand as indicated by PBS&J in their design calculations.

Once it was determined that the cap beam had an adequate capacity, it was then necessary to predict whether any cracking would develop during the testing. Since the majority of a section's resistance to torsion lies along its exterior surface, a hollow tube analogy may be adopted in order to calculate the cracking torque, T_{cr}, for the given section (Rahal K. N., 2000). Again, assuming that the cap beam acted as a composite section with the surrounding deck and diaphragm, Equation 2.1was used to calculate the cracking torque of the section. Accordingly, a cracking torque, T_{cr}, equal to 559 k-ft was predicted. Based on both a preliminary SAP2000 analysis and the ABAQUS analysis (Thiemann, 2009), it was observed that the torsion within the cap beam would likely exceed the calculated T_{cr} value. Therefore, it was necessary to develop a nonlinear link element to more accurately model the behavior of the inverted-T cap beam.

As previously stated, there is relatively little information regarding the torsion behavior of reinforced concrete members. As a result, it was decided that a bi-linear response curve, based on parameters for which there is a substantial amount of behavioral information, would be adequate in predicting a generalized behavior. An iterative procedure, as outlined in Chapter 2 and based on Equations 2.2-2.11, was used to calculate the angle of twist given the cracking torque, as well as the angle of twist and torque expected at the ultimate condition (Collins & Mitchell, 1991). The amount of rotation was calculated by multiplying the angle of twist by the length of the cap beam between nonlinear link elements, L, as shown in Equation 4.8. Given the expected torsional behavior at the cracking and ultimate limit states, the following bi-linear torque-twist response curve was developed, as shown in Figure 4.10.

$$\theta = \psi L \tag{4.8}$$

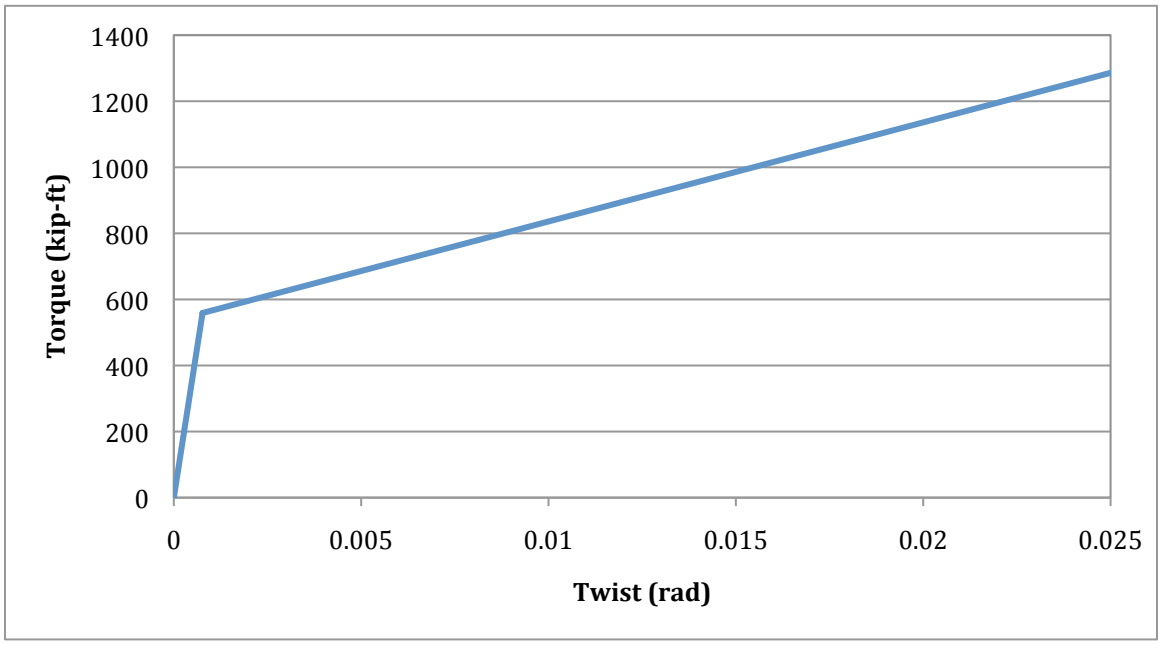

Figure 4.10: Predicted Inverted-T Cap Beam Torque-Twist Response

One nonlinear link element was placed at the midpoint along the cap beam between each girder, as shown in Figure 4.11. It is also important to note that the elastic torsional stiffness of the cap beam was made rigid in order to prevent the elastic portion of the response from being accounted twice within the analysis, thereby resulting in an increased amount of twist for a given torque.

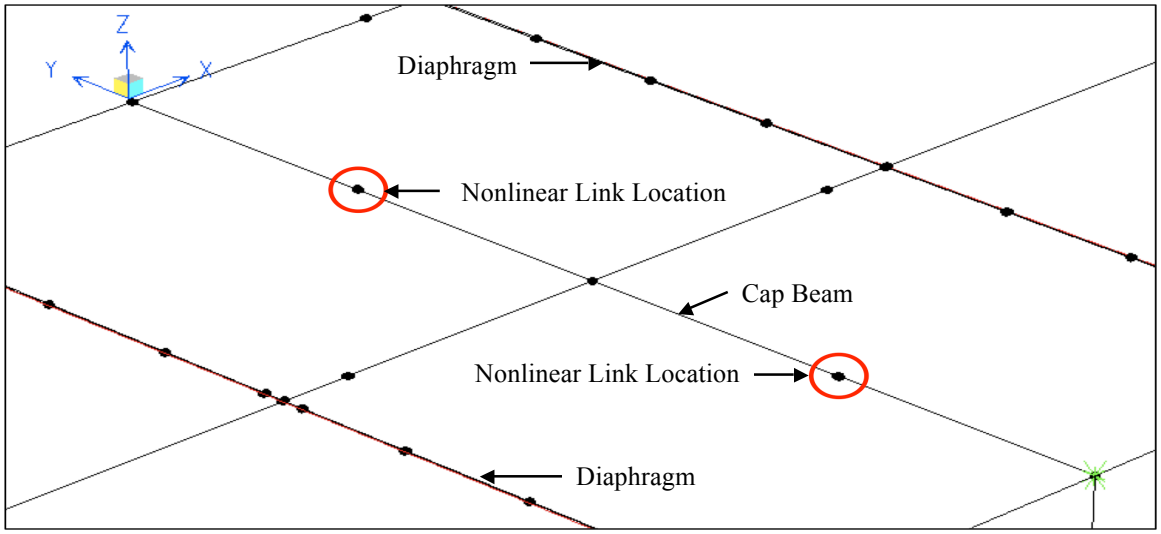

Figure 4.11: Grillage Model Cap Torsion Nonlinear Link Element Locations

4.4.3 Girder-to-Cap Connection

The girder-to-cap connection was one of the most important areas of the model as it was the focus of the research. The procedure that was used in the development of the nonlinear link element that was used for the connection was presented in "3-D finite element analysis of the girder-to-cap beam connection of an inverted-T cap beam designed for seismic loadings" (Thiemann, 2009). This procedure was used, in combination with the results from the ABAQUS finite element analysis of the connection, to develop a moment vs. rotation response for each girder within the connection region, as shown in Figure 4.12. The response took into account the shear-friction interaction between the girder and diaphragm, the dowel action between the girder and the diaphragm, and the resistance of the hooked reinforcement that extended from the cap into the diaphragm, as shown in Figure 3.5. The properties that were derived based on the aforementioned procedure were input into SAP and a link was placed at the location of the connection along each girder element and was connected to the closest diaphragm element, as shown in Figure 4.13. It is important to note that the defined moment values were halved when defining the links that were used on both the exterior and center girders. This was done because these locations only had half the amount of dowels between the girder and diaphragm as well as half the number of hooks between the cap and diaphragm. It should further be noted that this was only true for the center girder as half of it was modeled due to symmetry; had the entire structure been modeled, the moment values for the center girder would not have been halved. For more information regarding the development of the nonlinear girder-to-cap connection properties, refer to (Thiemann, 2009).

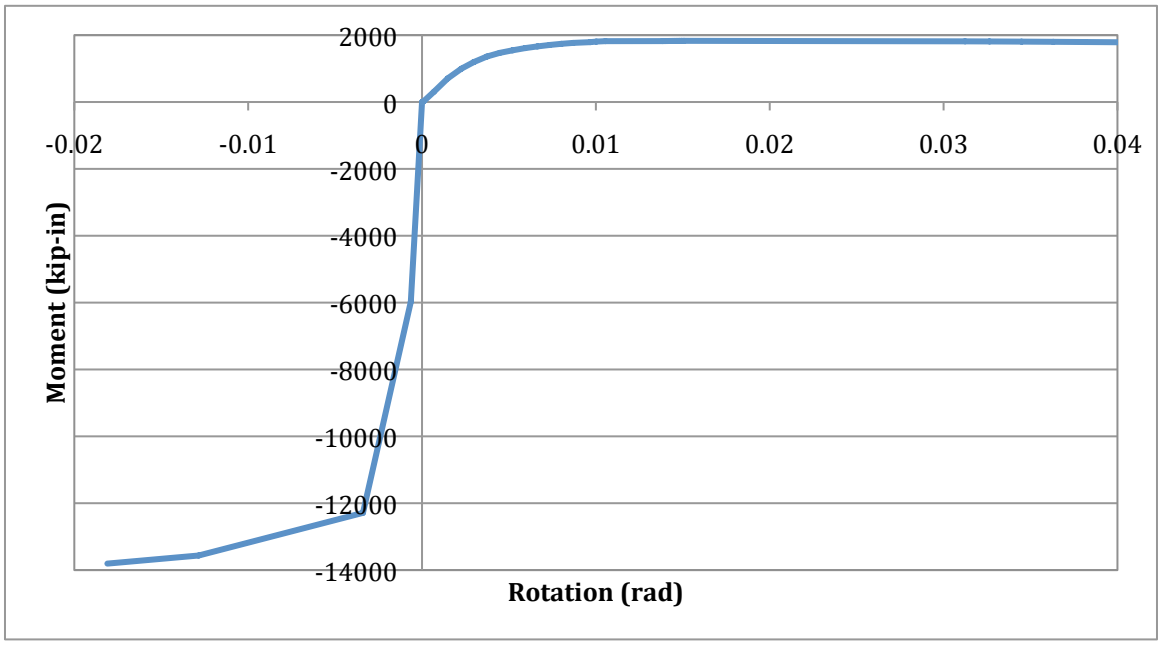

Figure 4.12: Girder-to-Cap Connection Intermediate Girder Moment-Rotation Response

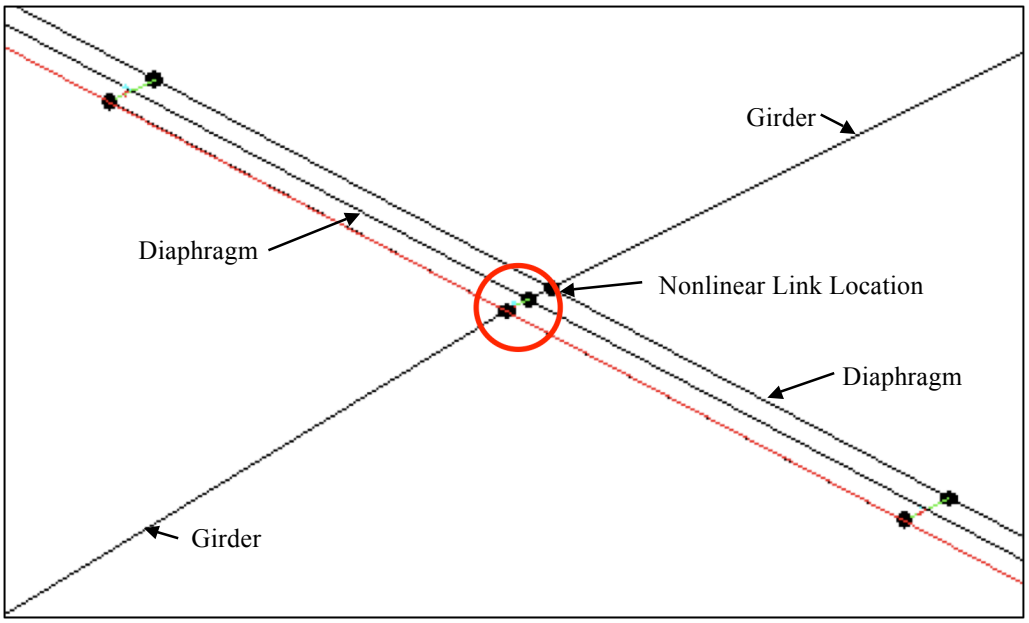

Figure 4.13: Grillage Model Girder-to-Cap Nonlinear Link Location

4.4.4 Cap-to-Diaphragm Reinforcement

Though the contribution of the hooked reinforcement between the cap and diaphragm was taken into account in the girder-to-cap connection nonlinear link element, the strain-

penetration and resulting slip behavior had to be considered in order to achieve a more accurate response. Therefore, a bi-linear moment vs. rotation response curve was developed using Equation 2.16 for the stress-slip behavior of reinforcement embedded in concrete at yield using recommendations from Zhao and Sritharan (Zhao & Sritharan, 2007).

The amount of slip experienced at the ultimate limit state was assumed to be approximately equal to 35 times the value of the slip at yield (Zhao & Sritharan, 2007). It is important to note that the calculated slip values were doubled, as the reinforcement would be expected to slip on both sides of the cap-to-diaphragm interface, through both the diaphragm and the cap beam due to anchorage on either side of the diaphragm-to-cap interface. Once the slip values were obtained, the angle of rotation was calculated using simple trigonometry and by assuming that any cracking in the connection would occur in a linear manner to an estimated neutral axis depth, $y_{N.A.}$, that was obtained from the ABAQUS finite element analysis (Thiemann, 2009), as shown in Equation 4.9. Since this nonlinear link element was in series with the nonlinear link element representing the girder-to-cap connection, it was necessary to define the corresponding moment values in the cap-to-diaphragm link based on the moment experienced in the girder-to-cap link so as not to over- or under-estimate the amount of additional rotation experienced in the connection due to slip. In other words, the moment at the yield condition was defined based on the overall moment observed within connection, per the ABAQUS finite element analysis (Thiemann, 2009). It was assumed that the steel reinforcement within the connection would all yield at approximately the same time. Therefore, the idealized yield moment was defined as the moment at which the majority of the reinforcement within the connection had yielded, as shown in Figure 4.14. Since the ABAQUS finite element analysis was not continued to a true representation of the ultimate condition within the connection, an increase of 30% over the yield moment was used to approximate the ultimate moment within the connection. Since no slip should be expected when the connection experienced a negative moment, it was necessary to define the negative response as a rigid behavior. This allowed all of the negative moment from the girder-to-cap link to be transferred across the connection without influencing its rotation. Figure 4.15 depicts the bi-linear curve that was input into SAP2000.

$$\theta = \tan^{-1}\left(\frac{slip}{y_{N.A.}}\right) \tag{4.9}$$

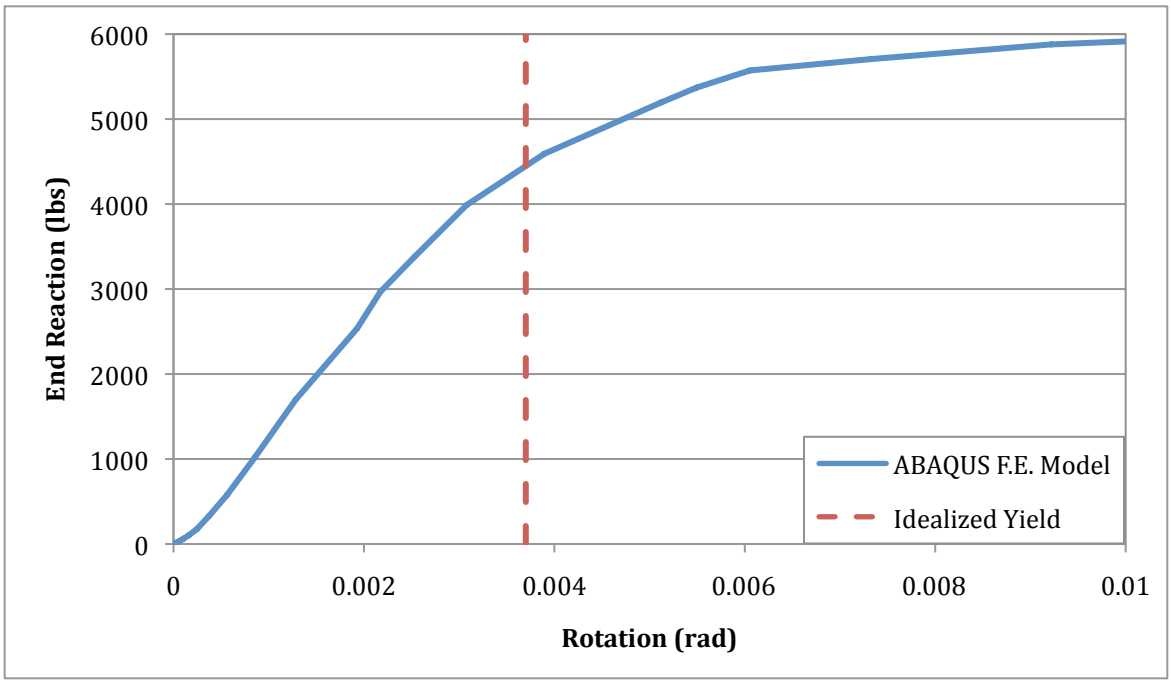

Figure 4.14: Idealized Yield Moment Derivation

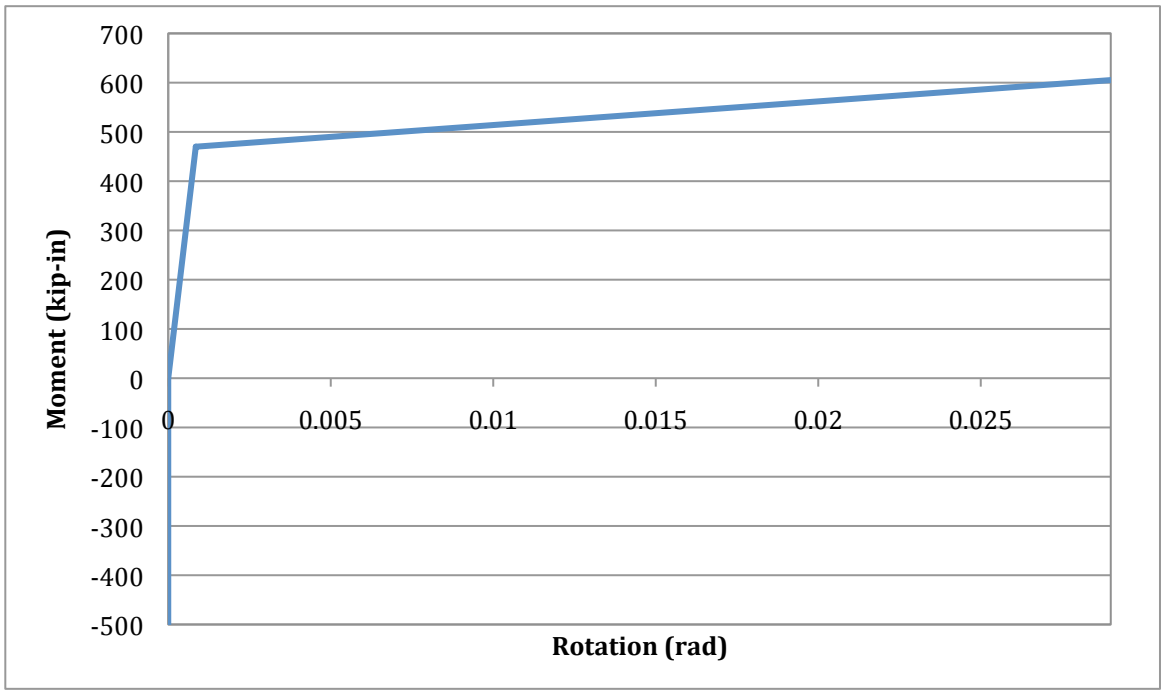

Figure 4.15: Moment vs. Rotation Slip Response of the Cap-to-Diaphragm Reinforcement

The effect that the slip had on the cap-to-diaphragm reinforcement was to increase the amount of rotation experienced at a given moment value. Therefore, as stated earlier, in order to increase the rotation experienced in the model, without affecting the moment capacity of the connection region, the slip link elements were placed in series with the aforementioned girder-to-cap link element, as shown in Figure 4.16.

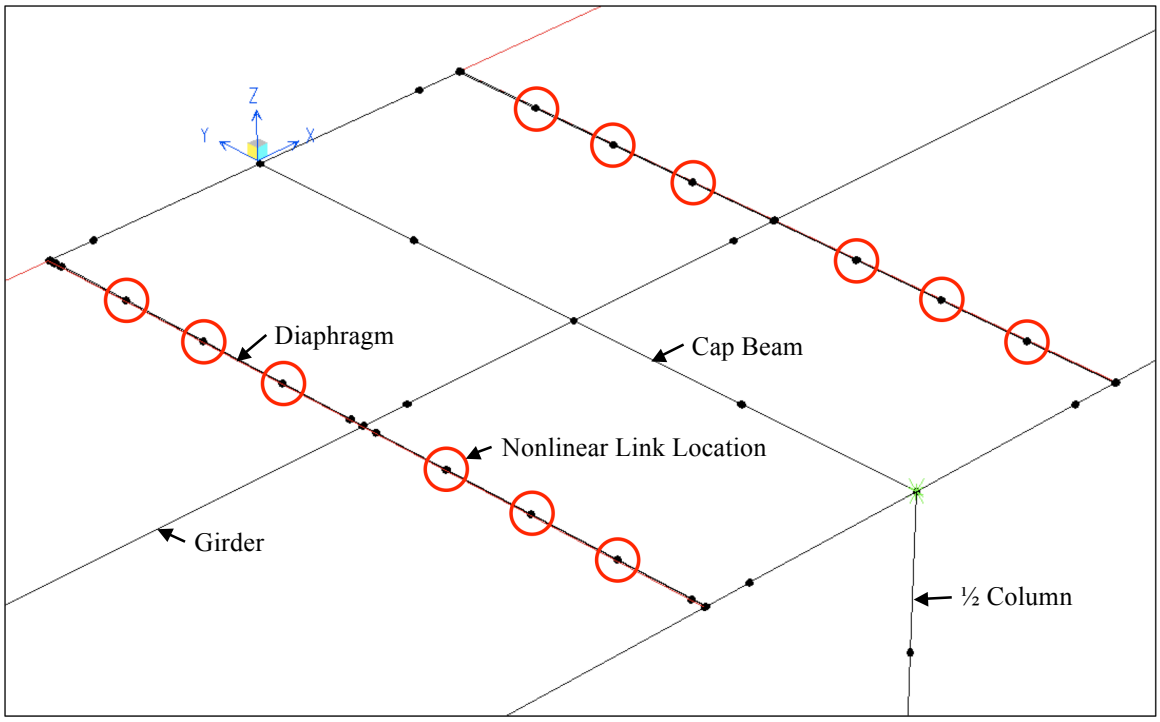

Figure 4.16: Locations of Grillage Model Nonlinear Link Elements Used to Model Cap-to-Diaphragm Reinforcement

4.4.5 Improved Connection

The proposed improvement to the positive moment connection, which consisted of unstressed strands grouted in place between the girders and inverted-T cap beam, also had to be included as a source of nonlinearity within the model. The behavior of this connection was developed using a similar procedure to that of the slip experienced by the cap-to-diaphragm reinforcement as outlined in Section 4.4.4. The moment values at the yield and ultimate stress in the unstressed strands were calculated based on the equivalent stress block procedure, using a neutral axis depth that was assumed to be constant and was obtained from

the ABAQUS finite element analysis. However, since reinforcement embedded in concrete has different bond characteristics than prestressing strands embedded in a duct filled with grout, an alternate procedure was developed in order to derive the expected slip behavior within the proposed connection. Additionally, little experimental data was available regarding the bond-slip behavior of standard sized strands embedded in grout over a length greater than the required embedment or development length, which meant the results of the available experimental data were deemed too unreliable to be used to define globalized response, as they predicted more of a localized behavior for the strand, rather than the cumulative behavior over the entire length of the strand. Therefore, a procedure for determining the bond-slip behavior of reinforcement grouted in ducts was adopted in order to achieve an estimation of the bond-slip behavior of a strand grouted in a duct. Equation 2.17 provided an approximation of the debonded length over which the slip would occur (Raynor, Lehman, & Stanton, 2002). This equation was based on the assumption that a constant bond stress acted along the length of the reinforcement and was derived via a parametric study.

In order to develop a response profile for the bond-slip behavior of the strand, the value for the debonded length was assumed to be constant for all strain values. In order to calculate the slip experienced at a given level of moment within the connection, the strain experienced by the strand at the given amount of moment was multiplied by the debonded length. As before, the slip was then used to calculate the angle of rotation experienced by the connection using Equation 4.9. The following figure, Figure 4.17, shows the moment vs. rotation response that was assumed for the improved connection detail and input into SAP2000.

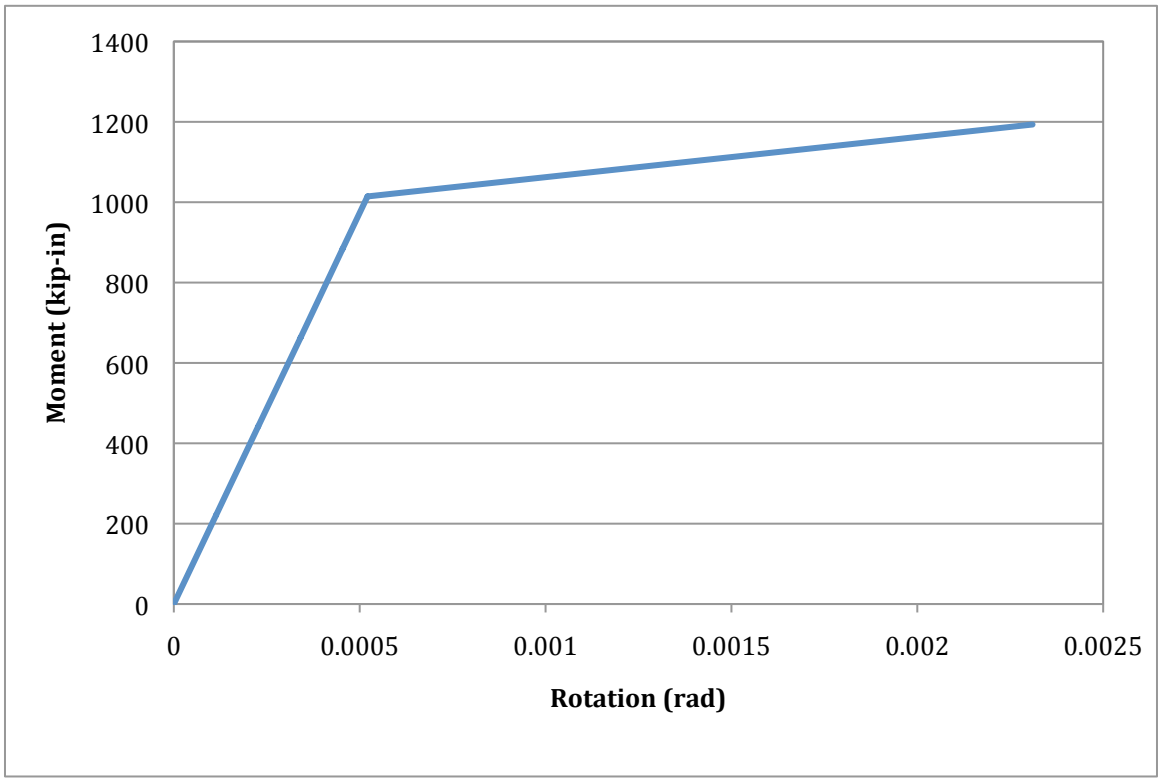

Figure 4.17: Improved Connection Predicted Moment vs. Rotation Response

The nonlinear link element that represented the improved connection detail was placed in parallel with both the girder-to-cap connection and cap-to-diaphragm nonlinear link elements, as shown in Figure 4.18. This was done so that the improved connection could influence both the moment and rotation behavior of both the girder-to-cap and cap-to-diaphragm nonlinear link elements simultaneously. However, since the improved connection had no influence when the connection was subjected to a negative moment, it was necessary to define the negative rotation response of the nonlinear link element as a pinned behavior.

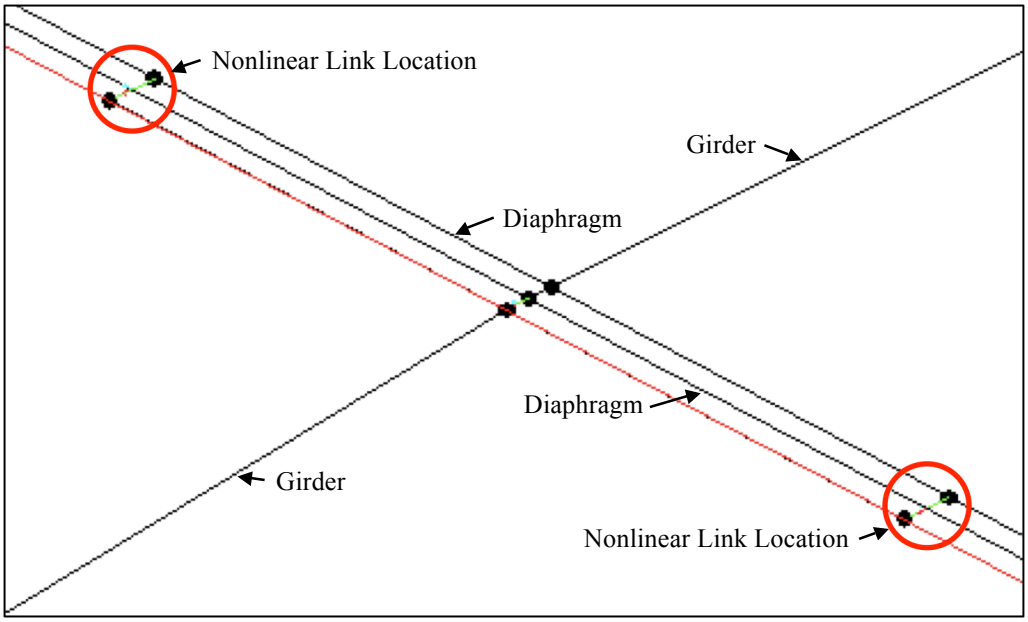

Figure 4.18: Grillage Model Improved Connection Nonlinear Link Location

4.5 Staged Construction

Since the test unit was built and loaded in phases, it was necessary to reflect those phases in the model in order to achieve the correct force conditions along the length of the girders as well as at the critical interface between the girders, diaphragm, and bent cap. Fortunately, this was accomplished in SAP2000 through the use of a "Staged Construction" feature that allowed the user to construct and load the model in stages within a given analysis. Through the use of this feature, the model was assembled in two stages. The first stage was the placement of the girders on the cap beam and abutment. During this stage, the girders were simply supported and the stage one hold-down force was applied to the girders. This was accomplished by connecting the girders and deck to the diaphragm element using a link element that behaved as a pinned connection, as shown in Figure 4.19. The second stage changed the boundary conditions on the girders from simply supported to continuous, in order to reflect the fact that the girders, deck, and diaphragm were all acting as a continuous superstructure at this stage. This was achieved by removing the simply supported link element and adding the various nonlinear connection link elements, as their effects were only realized after all of the concrete had cured. Once those boundary conditions were changed, an additional hold-down force was applied, which represented the barriers and other loads

that were placed on the prototype structure, but not the test unit. Additionally, a distributed load was applied along the length of each girder that represented the stay-in-place formwork and the thickened overhang portion of the deck. It was assumed that both of the aforementioned loads were evenly distributed between girders.

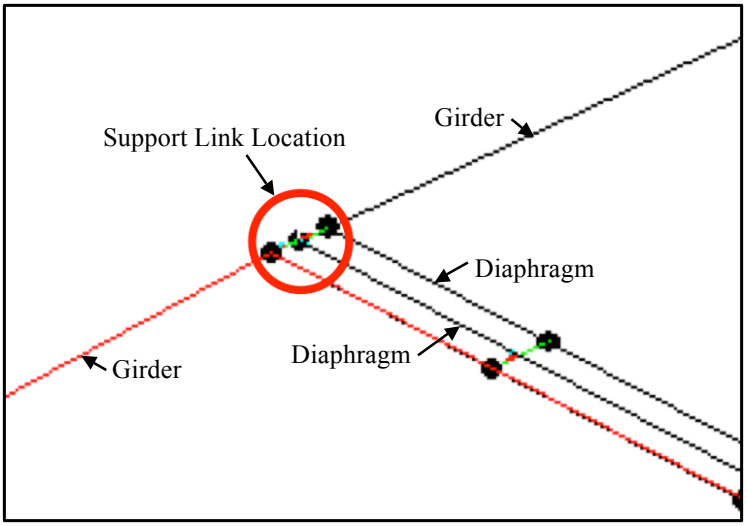

Figure 4.19: Grillage Model Temporary Support Condition Link Element Locations

4.6 Loading Conditions

Aside from including the dead load within each analysis, hold-down forces were also applied during each phase of the stage construction in the same manner as they were in the lab. Each of the hold-down forces were applied at nodes that were placed 16ft away from the centerline of the cap beam, as shown in Figure 4.20. More information regarding the hold-down forces is presented in Section 6.1.3. As mentioned previously, an additional distributed load of 0.00416 k/in was placed along each girder in order to reflect stay-in-place formwork and thickened portion of the deck. It should be noted that this value was halved for the center girder as only half of it was modeled.

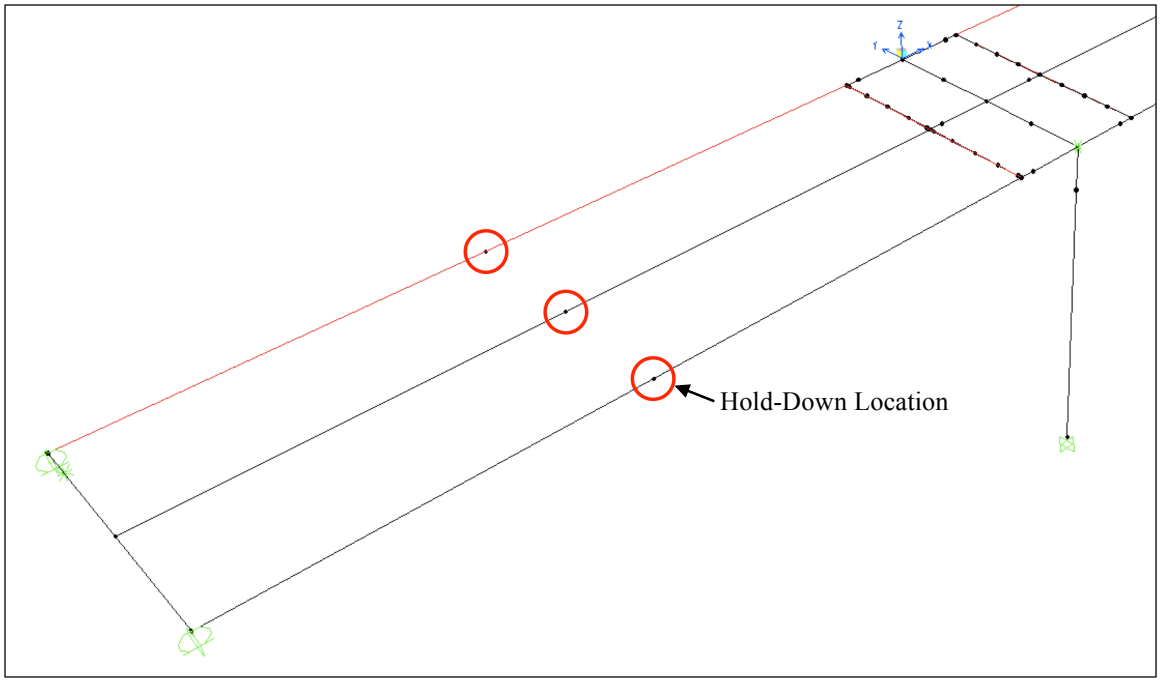

Figure 4.20: Grillage Model Hold-Down Node Locations

4.7 Modifications Made for Phase 2 Model

The same model, described above, was used to make predictions for the second phase of the testing; however, a few minor adjustments were made to the model in order to reflect the changes in boundary conditions and loading that were experienced during Phase 2. First, the loading aspect of the staged construction portion of the analysis was altered. The stage 2 hold-down force was not applied, while the stage 1 hold-down force was removed once the superstructure was made continuous. Second, the superstructure support conditions were altered so that the structure was supported on rollers at the former hold-down location, instead of at the abutment, as it was for the beginning of the analysis. Finally, the vertical displacements were applied at the former location of the hold-down, in order to remain consistent with the actual test setup. The Phase 2 model also did not include any of the degradation that was experienced during Phase 1 of testing; however, cracking of the girders, deck, and column was included using the same respective effective stiffness values that were used for Phase 1.

Chapter 5. ANALYSIS

5.1 Background

The primary analysis that was performed using the grillage model of the test unit, described in Chapter 4, was a push over analysis. This was achieved by initially completing the staged construction analysis in order to obtain the results due to the gravity loads on the structure. A monotonically increasing lateral displacement was then applied to the top of the column and a nonlinear analysis was performed, which used the results of the staged construction analysis as its initial condition.

It should again be noted that a finite element analysis, for a complicated structure such as the test unit, is only able to provide an approximate solution. This is due to the fact that a finite element analysis is a numerical model, thus a closed form solution is highly unlikely. However, when predicting the general, global behavior of the test unit, it was demonstrated, through validations and comparisons, that the grillage model achieved a satisfactory solution.

5.2 Preliminary Analysis and Validation

Before accepting the results of any finite element model, they must be externally validated by an alternate form of analysis. Therefore, in order to validate the preliminary results of the finite element grillage model, before the availability of any test results, a few simpler models were created and compared to the results of hand calculations and other finite element models that were created for both the test unit and prototype structures. Once the actual test data was obtained, the grillage model was then compared to those results and was further modified when needed in order to improve its capabilities such that the improved model could be used in the analysis of future inverted-T bridges.

5.2.1 Preliminary Comparison

Prior to running any of the push over analyses, it was necessary to validate that all of the member properties, the self-weight, and the hold-down forces were adequately modeled within the SAP2000 grillage model. Therefore, the moment profiles along the center,

intermediate, and exterior girders on the North side of the model were compared to both the moment profiles presented in the design documents provided by PBS&J and simple hand calculations, at each stage of the analysis. Since the profiles provided by PBS&J as well as the simple hand calculations were fairly idealistic and did not include the effects of the membrane action within the deck or the additional force transfer via torsion within the abutment, those effects were removed from the initial analysis for comparison. Figures 5.1, 5.2, and 5.3 demonstrate that a satisfactory agreement was obtained at each stage of the analysis and thus, all member properties and preliminary loads applied to the structure were appropriately modeled. Additionally, this resulted in a greater understanding and validated the use of the staged construction feature available within SAP2000.

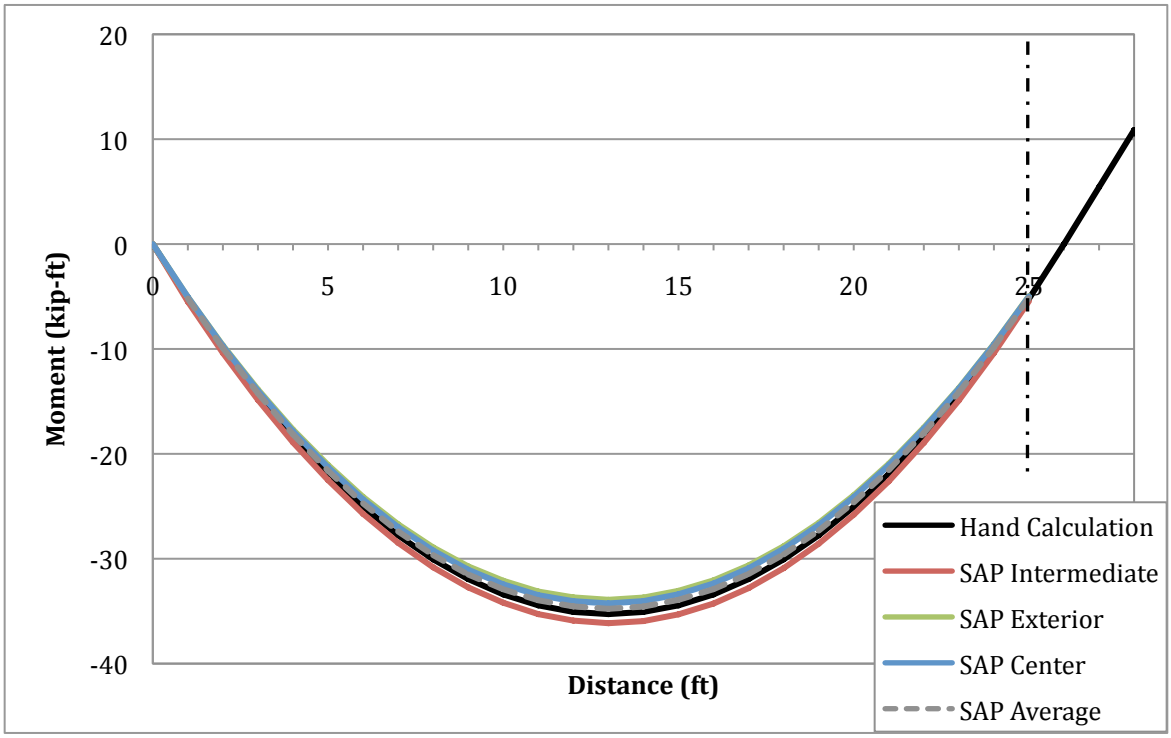

Figure 5.1: Comparison of Moment Profile Obtained for Stage 1 Loading

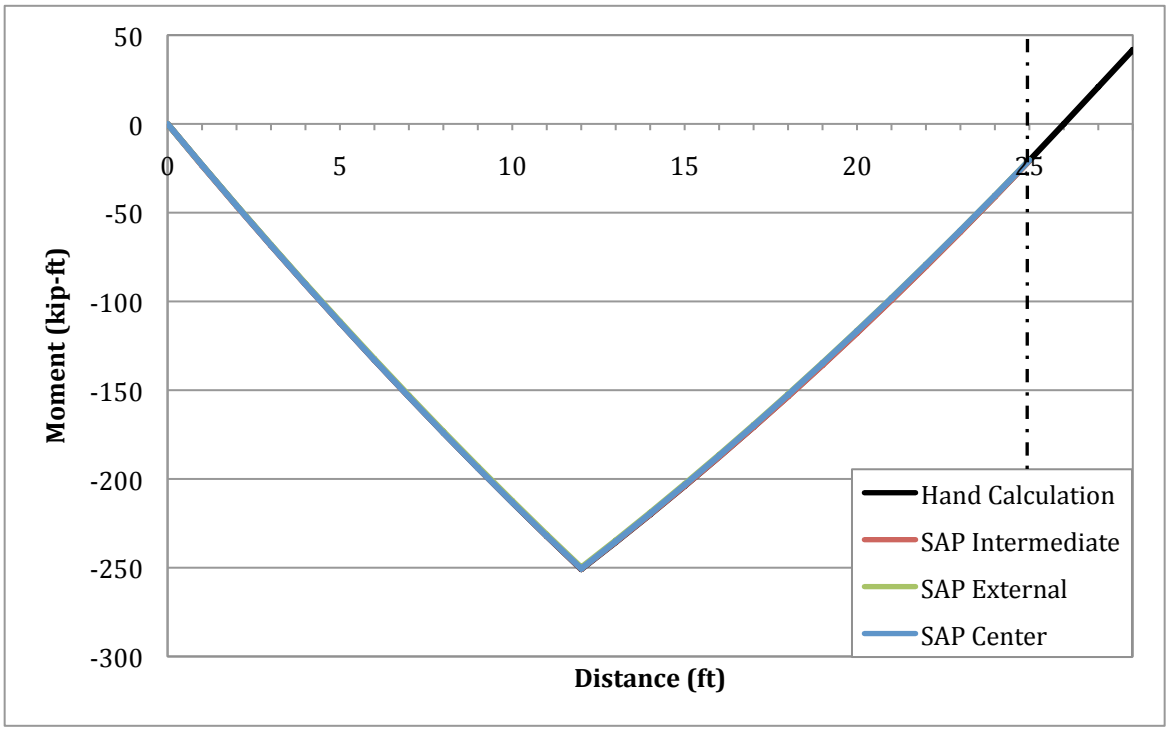

Figure 5.2: Comparison of Moment Profile with Hold-Down Forces for Stage 1 Loading

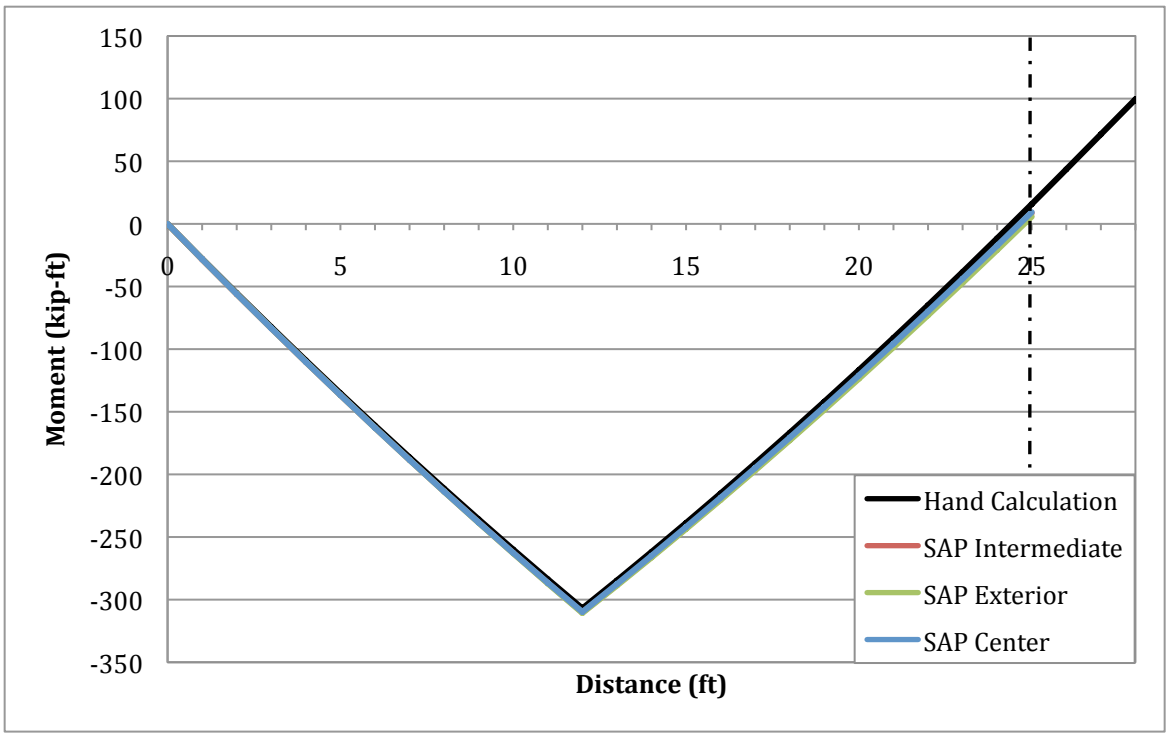

Figure 5.3: Comparison of Moment Profile for Stage 2 Loading

However, the results from the aforementioned analysis were not realistic when considering what was likely to be experienced in the test unit, as they assumed each girder acted independently from one the rest. As a result, an additional analysis was performed, which included the effects of membrane action expected from the deck and the torsional force transfer through the abutments. The consequences of these effects on the moment profiles along the girders are shown in Figures 5.4, 5.5, and 5.6. It should be noted that the membrane action within the deck had the greatest impact on the force redistribution between each of the girders. Though the profiles no longer match as closely to the idealized hand calculations, it was decided that, because the results were more realistic, a satisfactory response had been achieved. Furthermore, it was decided that the discrepancies in the more realistic analysis did not warrant an alteration to the location and magnitude of the hold-down forces applied to the test unit, as a more detailed hand calculation of the prototype, i.e. one that included the various force transfer mechanisms, would likely experience the same relative difference. Additionally, a satisfactory agreement within the connection region was still achieved.

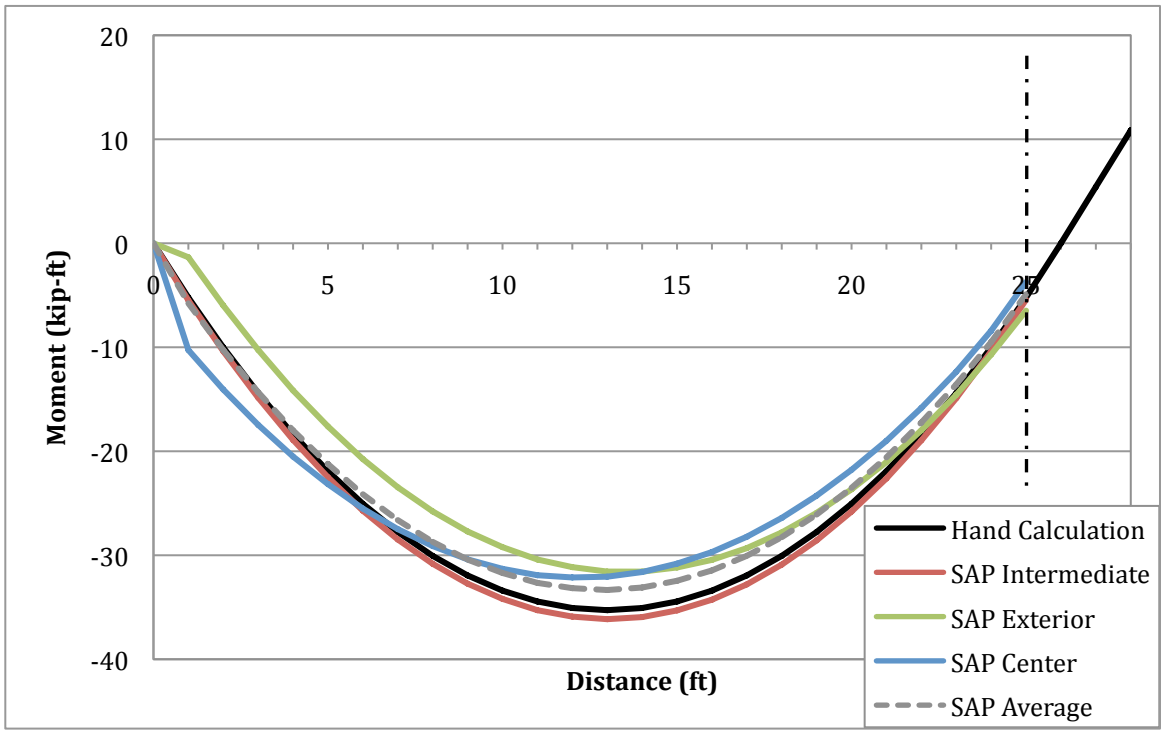

Figure 5.4: Realistic Comparison of Stage 1 Moment Profile

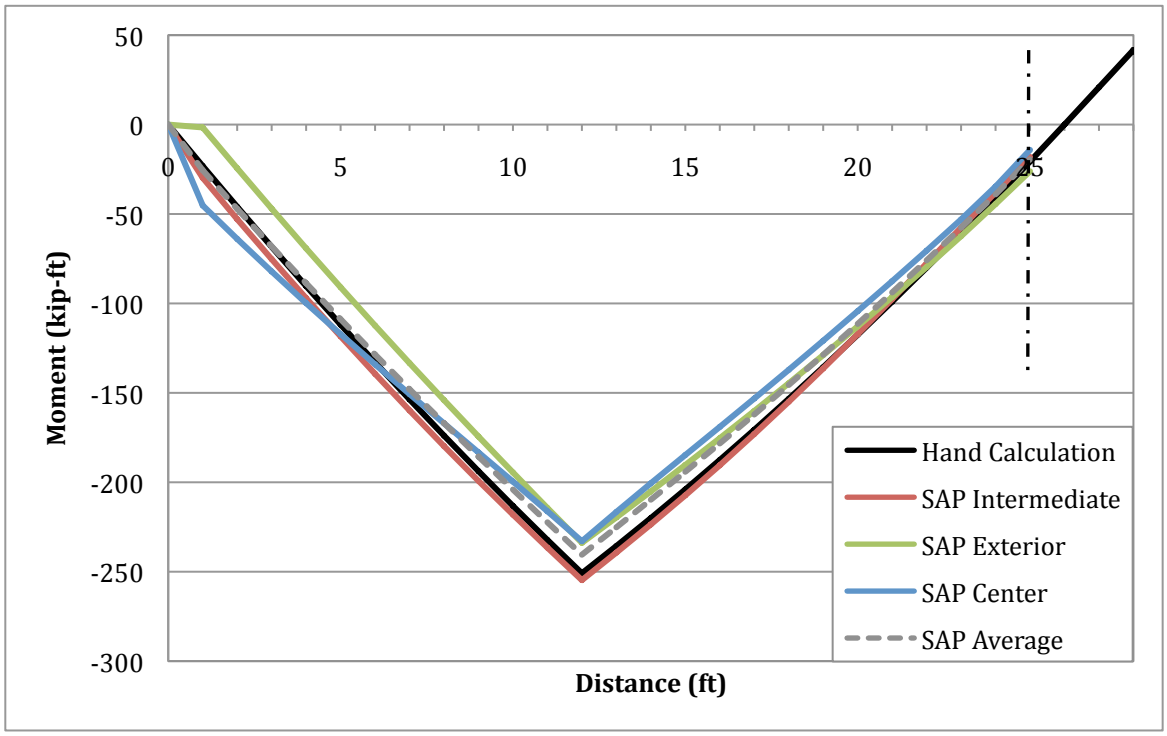

Figure 5.5: Realistic Comparison of Stage 1 Moment Profile with Hold-Down Forces

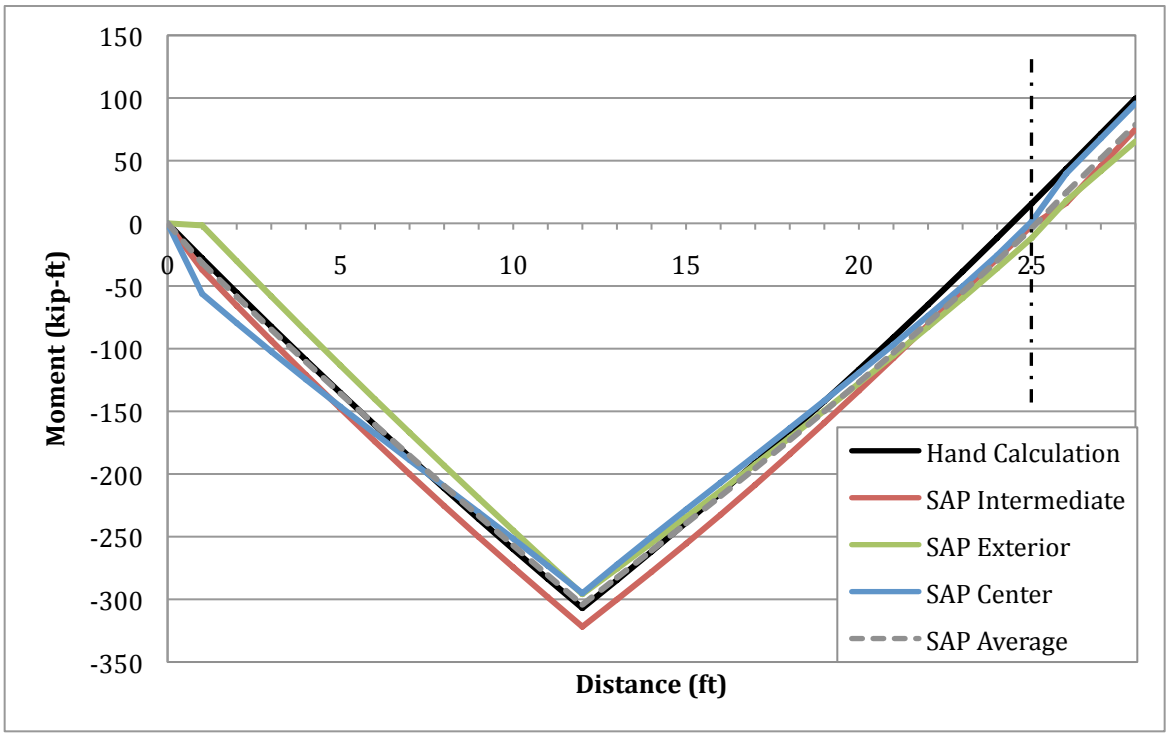

Figure 5.6: Stage 2 Realistic Moment Profile

5.2.2 Comparison with ABAQUS Finite Element Results

The grillage model was also validated against several of the 3-D finite element ABAQUS models of portions of the test unit that were created (Thiemann, 2009). Various single girder grillage models of just the superstructure were created, which represented models that were created in ABAQUS by Thiemann. The majority of the models focused on the validation of the connection details and nonlinear springs that were developed for use in the grillage model, as outlined in Chapter 4.

The first, and primary, model that was validated investigated the nonlinear link properties that were developed based on the results from ABAQUS for use in the grillage model to represent the behavior of the connection between the I-girder and inverted-T bent cap. Both the ABAQUS and grillage models consisted of a single girder and a portion of half of the inverted-T cap beam. The inverted-T cap beam was given pinned boundary conditions at each end, as well as at its midpoint, while the free end of the girder was placed on a roller, as shown in Figure 5.7.

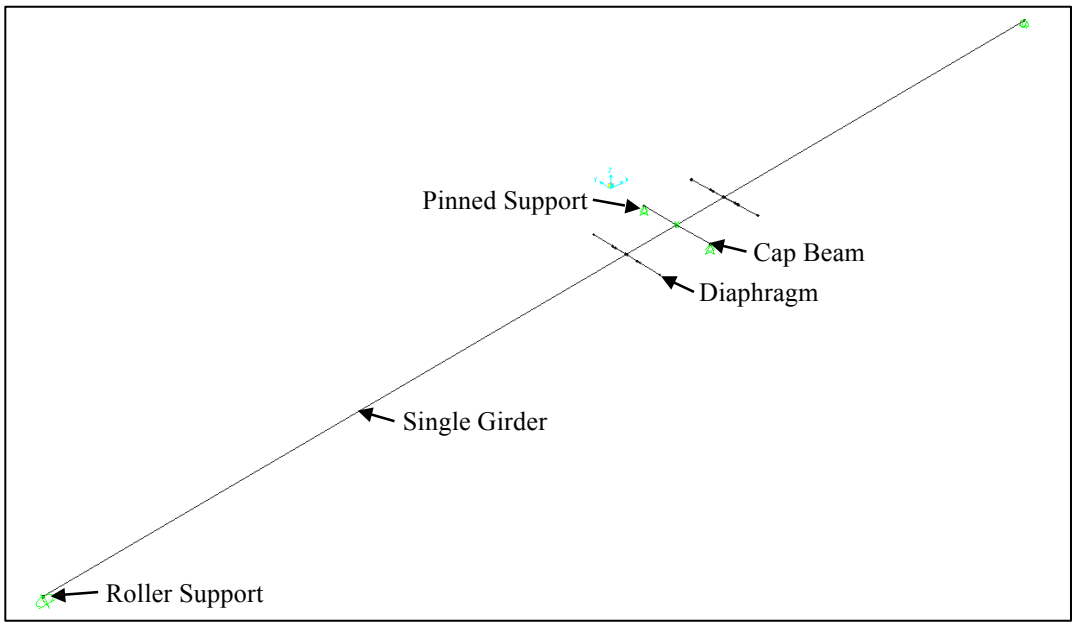

Figure 5.7: Single Girder Grillage Model Used for Comparison

For comparison purposes, plots of the vertical end reaction at the non-connection end of the girder versus the rotation of the center of the cap beam were made. Per Figure 5.8, it

was demonstrated that the nonlinear link elements that were developed for the girder-to-cap connection provided a satisfactory agreement between models. The discrepancies in the initial slope between the ABAQUS and grillage models were due to the initial stiffness values that were used in the grillage model for the girders. One benefit of the ABAQUS model was that it could reflect progressive stiffness degradation as the concrete began to crack and the section displayed nonlinear behavior. Conversely, the grillage model was not as advanced in that manner. Instead, an initial stiffness value was selected, which represented an effective stiffness value for the nonlinear post-cracking behavior of the girder. As demonstrated by the figure below, changing that initial stiffness value made certain phases of the response agree more closely based on the amount of cracking expected to occur within the girder.

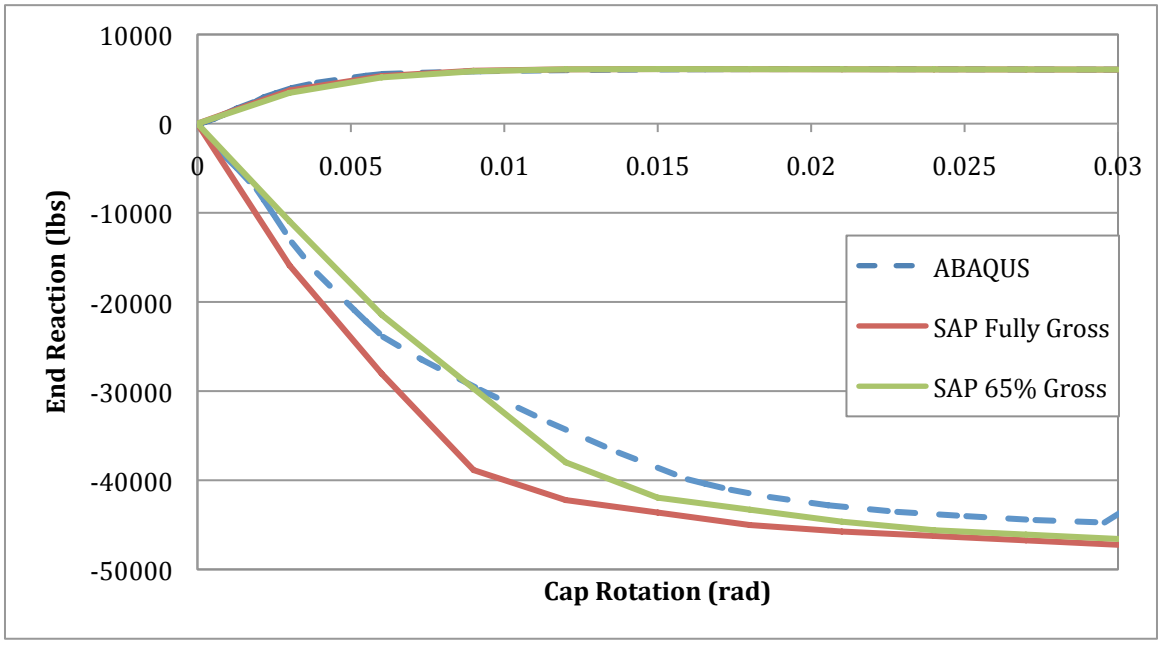

Figure 5.8: Single Girder Model Validation of I-girder-to-Inverted-T Connection Nonlinear Link

The second validation that was performed between the grillage model and ABAQUS single model was in regard to the nonlinear link element that was developed in order to account for the slip behavior of the reinforcement that connected the diaphragm and the inverted-T cap beam between the girders. Using the aforementioned single girder models, the results of the grillage model were compared to two different versions of the ABAQUS

model - one that included the reinforcement without slip and one without any contribution of the reinforcement. Since it was expected that the slipping of the reinforcement would result in larger cap rotations for a given moment, or girder end reaction, the profile for the grillage model should have fallen between the two ABAQUS models. Therefore, as shown in Figure 5.9, it may be concluded that the slip properties that were developed for the reinforcement were adequately validated. Similar to the validation of the connection nonlinear link element, it may be noted that the differences in initial stiffness between the ABAQUS and grillage model were due to the effective stiffness value that was input for the girders.

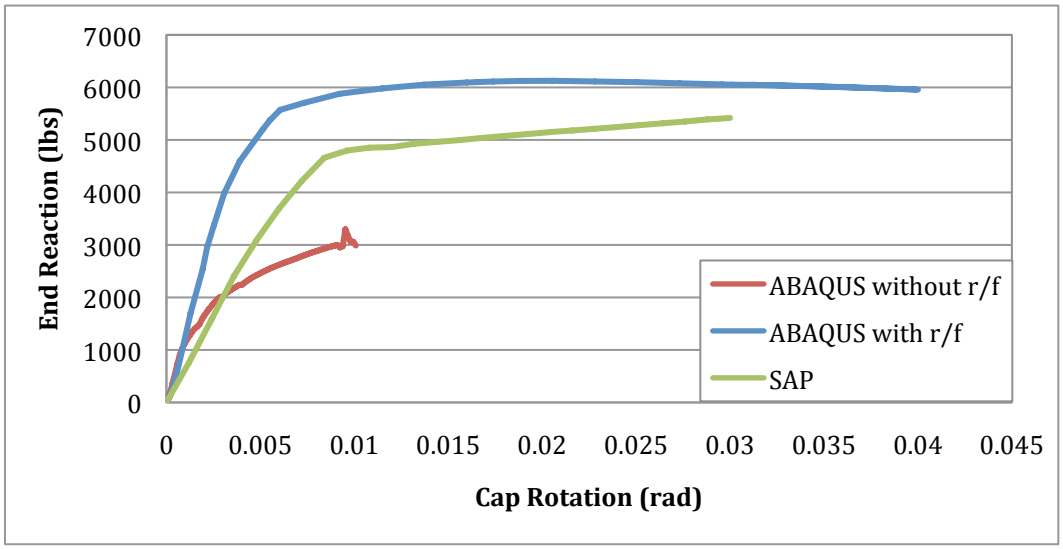

Figure 5.9: Single Girder Model Validation of Inverted-T Cap Beam-to-Diaphragm Slip Nonlinear Link

The third validation that was performed was in regard to the torsion nonlinear link elements that were developed for the inverted-T cap beam. A simple model of the inverted-T cap beam was developed using both ABAQUS and a grillage model in SAP2000. The cap beam was modeled as a cantilever and a torque was applied to the free end. The response provided by ABAQUS was then compared to that of the grillage model. Given the fact that relatively little is still known regarding the torsional behavior of concrete and the uncertainty involved in assuming a modulus of rupture for the concrete under torsion, the results shown in Figure 5.10 provided a sufficient agreement for use in modeling the rest of the test unit. This was especially true given the fact that very small amounts of twist and cracking were

expected in the inverted-T cap beam based on previous research of a similar test unit (Holombo, Priestley, & Seible, 1998) as well as the results of the 3D finite element model of the test unit (Thiemann, 2009).

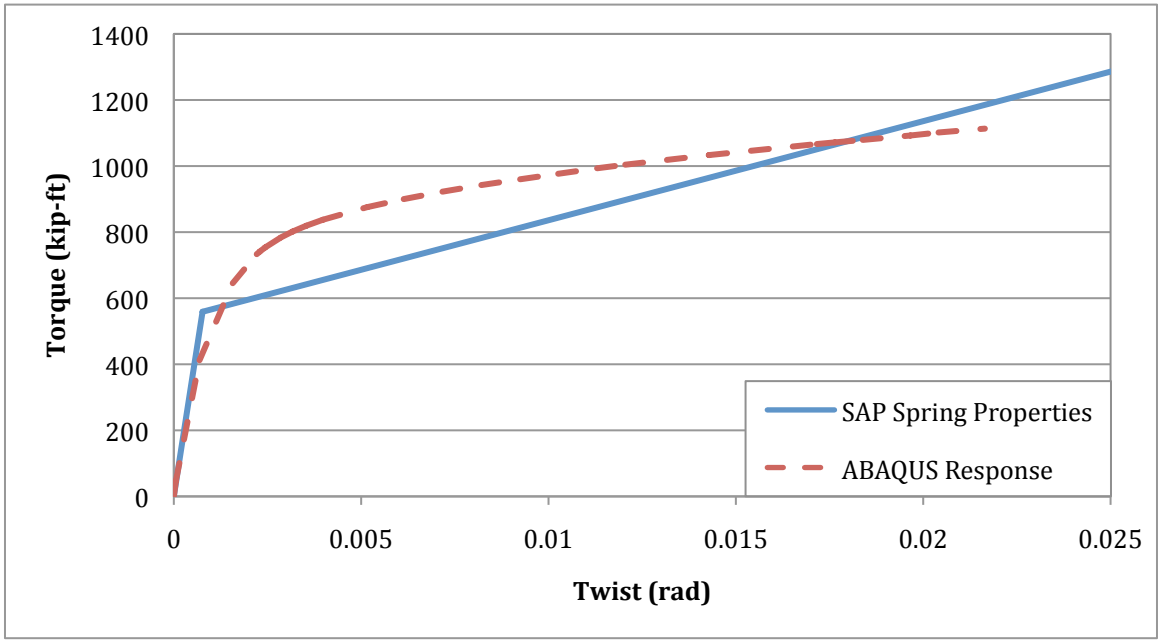

Figure 5.10: Inverted-T Cap Beam Torsion Response Validation

The final validation that was performed between ABAQUS and the SAP2000 grillage model was that of the nonlinear link elements that were used to model the behavior of the improved connection detail. The single girder model that was used in some of the other validations was again used to validate the improved connection link elements. The same boundary and loading conditions that were used to validate the connection spring were used and the behavior was compared in Figure 5.11. Satisfactory agreement was achieved. However, it may be noted that some of the small discrepancies in the comparison were due to the inclusion of slip in the response that was developed for the grillage model as well as the effective stiffness value that was used for the girder.

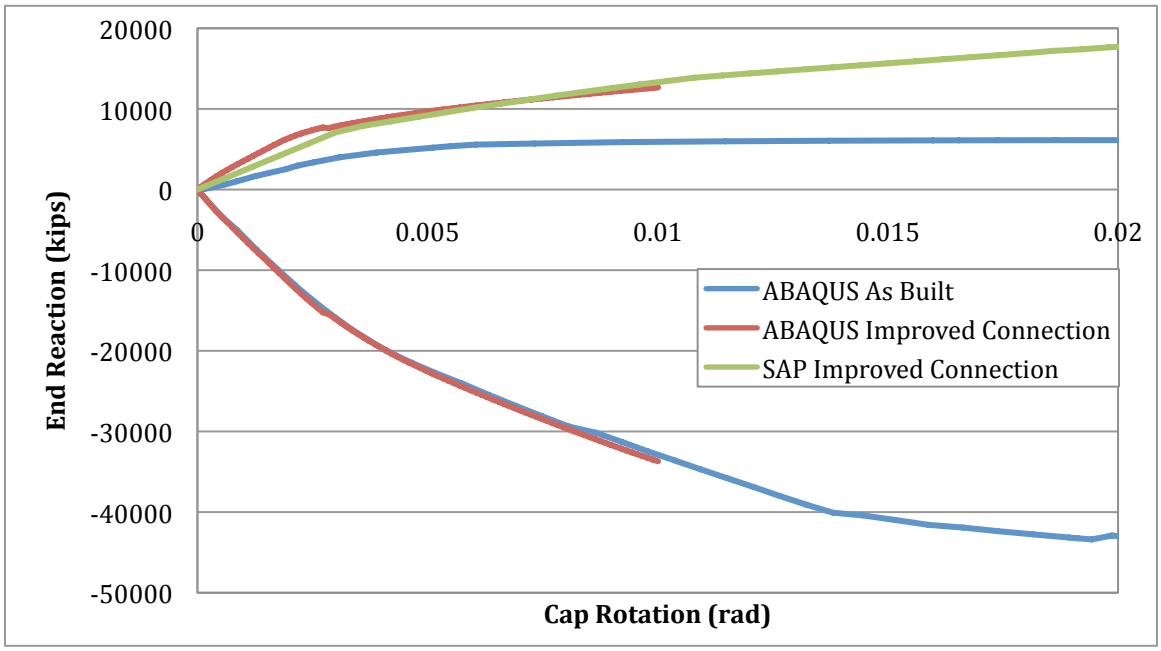

Figure 5.11: Single Girder Model Validation of the Improved Connection Detail Nonlinear Link

5.2.3 Preliminary Test Unit Comparison

During the final stages of construction, prior to the actual start of testing, the string potentiometers that were planned to be mounted below the center, intermediate, and exterior girders on the West side of the specimen, shown in Figures 3.46 and 3.47, were placed and data was collected during the application of the Stage 1 hold-down force, as well as the remainder of the construction; the string potentiometers were removed after the application of the Stage 1 hold-down force in order to remove the deck formwork, but were reinstalled prior to the application of the Stage 2 hold-down and the subsequent testing. Therefore, a preliminary comparison of the data collected from the test unit to the predictions made by the SAP2000 grillage model, in regard to the vertical displacement of the girders during the application of the Stage 1 hold-down force, was performed. In order to make a comparison to the grillage model, it was necessary to make a few minor modifications to some of the member properties to reflect their condition at the time at which the data was collected. Therefore, the girders were given gross stiffness properties, while the dominant bending and membrane stiffness were removed from the deck elements in order to reflect the liquid state of the deck. The vertical displacements were then compared at the location of each of the linear potentiometers along the length of the girders and were connected with a straight line

between points. As shown in Figure 5.12, a very good agreement was observed between the recorded data from the test unit and grillage model analysis results, further validating the suitability of the model. It should be noted that each of the plots of the grillage model analysis results are almost identical due to the removal of the membrane action and stiffness of the deck, which would have otherwise distributed the forces and thus displacements differently between each girder.

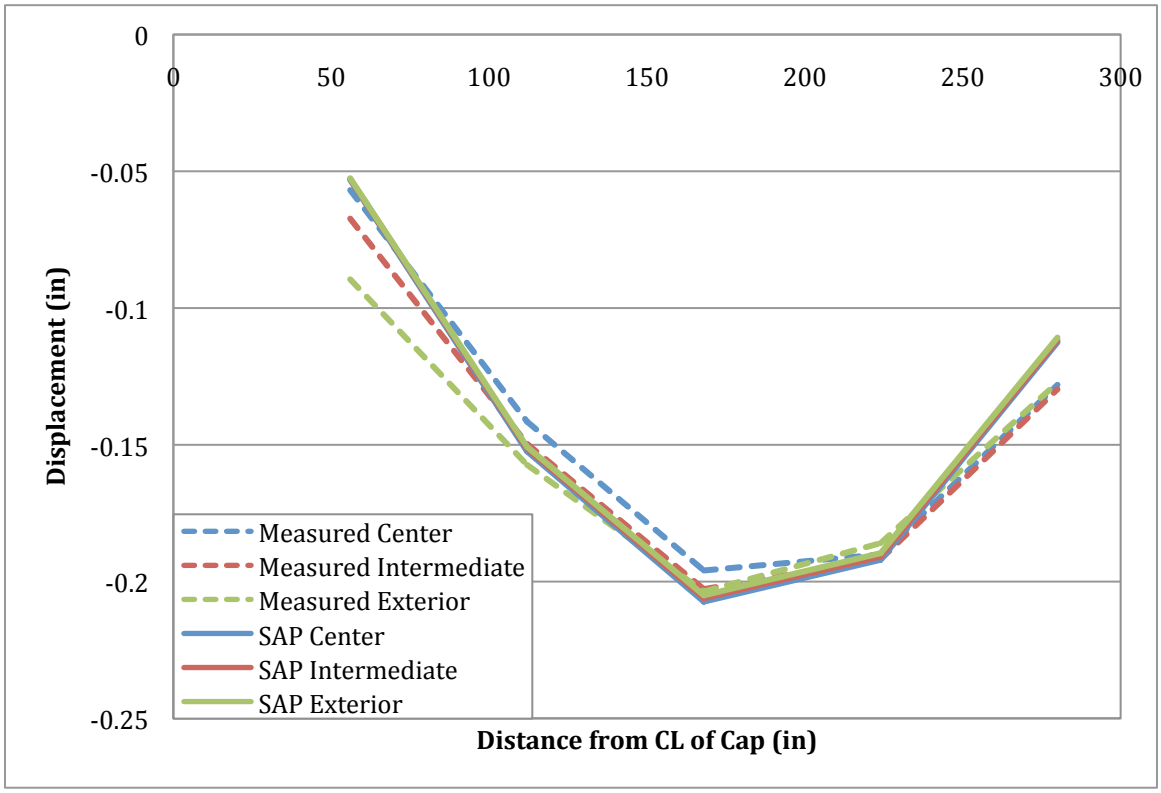

Figure 5.12: Stage 1 Vertical Girder Displacement Comparison

5.2.4 Expected Test Unit Response

5.2.4.1 Phase 1 Prediction

In order to assist in the understanding of the behavior of the test unit during each phase of testing, a few predictions regarding various aspects of its behavior were made based on the results of the pushover analyses performed on the SAP2000 grillage model. The two most critical and informative predictions that were made were the force vs. displacement

response and the observed moment demands within the connection between the girders and the face of the bent cap. The force vs. displacement response of the entire superstructure provided a more global representation of the behavior of the test unit, while the moment demands within the girder-to-cap connection provided a more localized representation of the behavior in the area of most interest, the connection.

The force vs. displacement plot depicts the shear force in the column, which is equivalent to the total force in the horizontal actuators, plotted against the displacement expected at the location of the horizontal actuators, as shown in Figure 5.13. The grillage model was first pushed towards the South, in order to subject the as-built connection detail to a positive moment. A separate analysis was then performed, in which the applied displacement was reversed and the structure was pulled in order to subject the improved connection detail to a positive moment. For the sake of comparison, the sign of the displacement was ignored and only the magnitude was used when plotting Figure 5.13. Both force vs. displacement profiles seemed appropriate based on simple hand calculations, which were used to assist in validating the model. Furthermore, the 3-D finite element analysis demonstrated that the combined positive and negative capacity of the as-built connection should have been enough to produce a plastic hinge at both the top and bottom of the column. However, this alone was deemed unsatisfactory, as the connection would likely sustain significant damage on the positive moment side of the connection as a result (Thiemann, 2009). Therefore, it was decided that the influence of the connection on the force vs. displacement responses might not be as apparent as one might expect. It may be noted that both profiles diverged slightly at around 1 in. of horizontal displacement due to the as-built connection yielding and experiencing a larger amount of rotation over the shown range of horizontal displacement. Examining the specific behavior of the nonlinear link elements within the connection further corroborated this expected behavior. Based on the results of the analysis, it was predicted that the maximum horizontal displacement of the test unit would be approximately 5 in., at which point the plastic hinges within the column would have fully developed and reached their ultimate capacity. However, based on past experiences with similar structures, it was assumed that the structure could achieve approximately 6 in. of horizontal displacement, as shown in Figure 5.14.

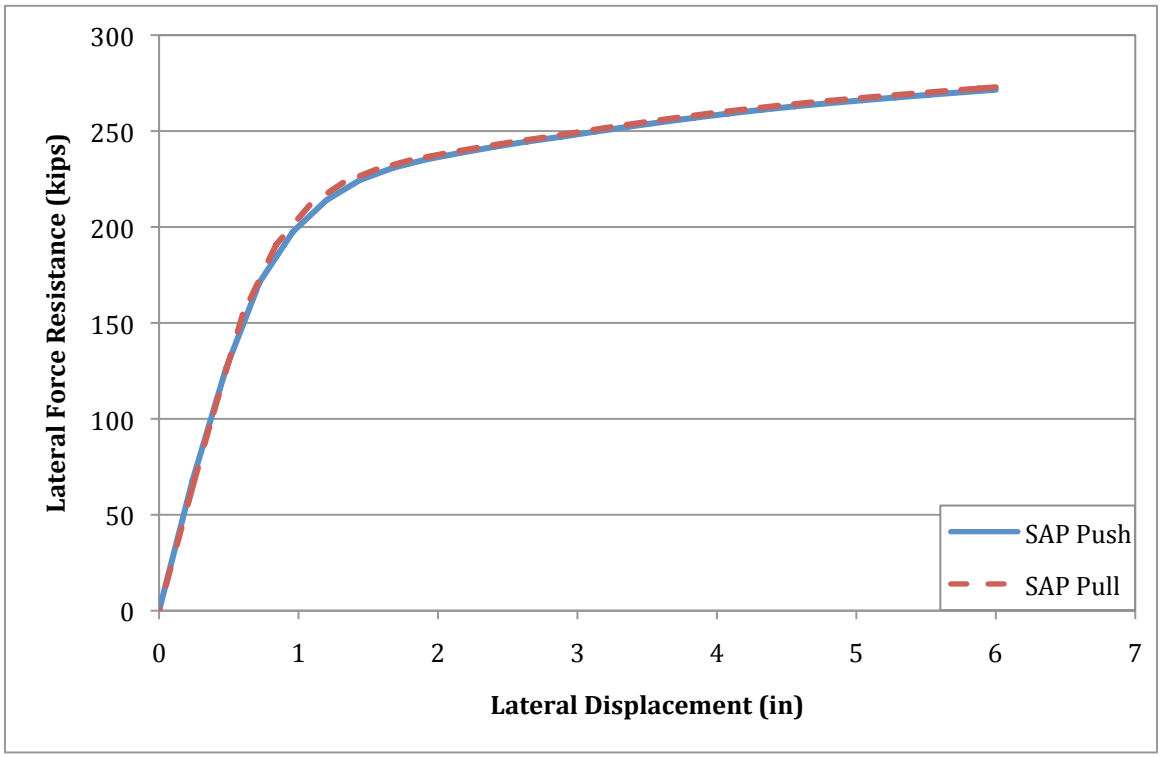

Figure 5.13: Analysis Force vs. Horizontal Displacement Comparison during Phase 1

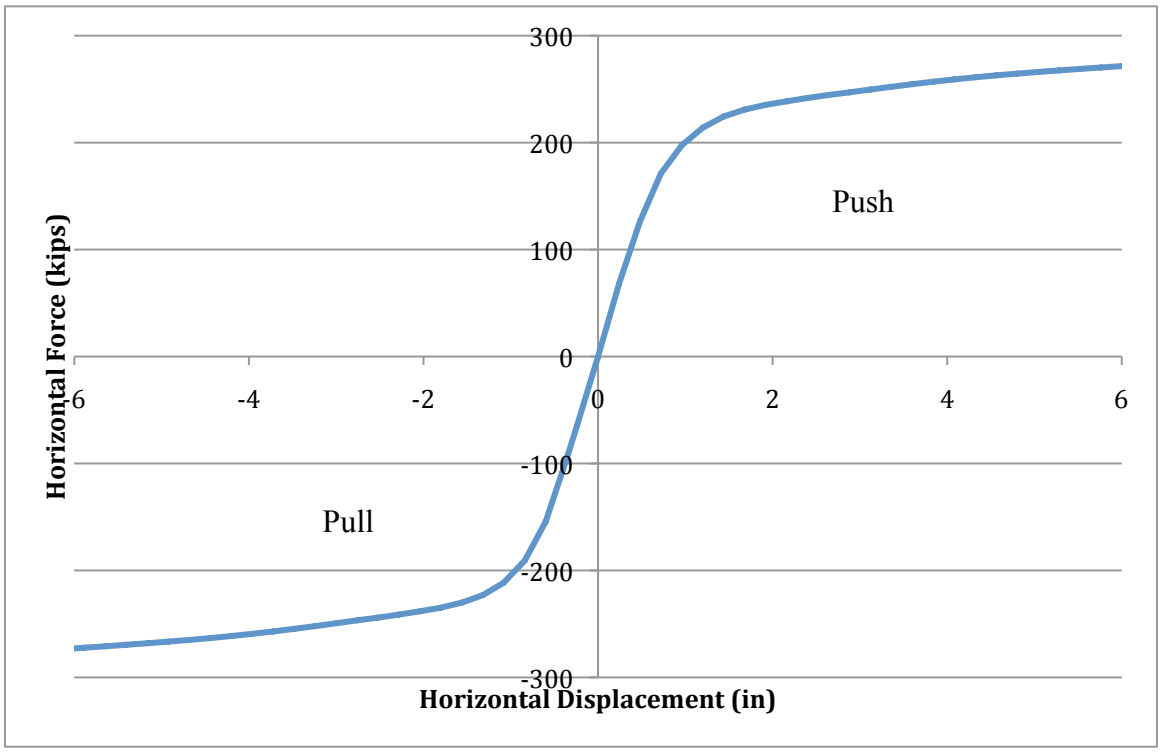

Figure 5.14: Predicted Phase 1 Force vs. Displacement Response

Examining the predicted moment distribution within the connection, as shown in Figure 5.15, demonstrated the impact that the improved connection detail had on the localized behavior of the connection, when compared to the as-built connection detail. First, it may be observed that the connection at the center girder had the greatest moment demand (25% of the total moment on the as-built side and 22.8% on the improved side), followed by the connections at the intermediate (24.6% of the total moment on the as-built side and 21.2% on the improved side) and exterior (12.8% of the total moment on the as-built side and 17.4% on the improved side) girders respectively, which was partially due to the membrane action in the deck. Second, and most importantly, the figure below illustrates that the improved connection detail increased the overall positive moment capacity of the connection by almost twofold. This meant that the connection should easily allow for the formation of a plastic hinge at both the top and bottom of the column, without sustaining significant localized inelastic damage at the girder-to-cap interface, when compared to the performance as-built connection detail, which was expected to experience a significant amount of inelastic damage at the girder-to-cap interface.

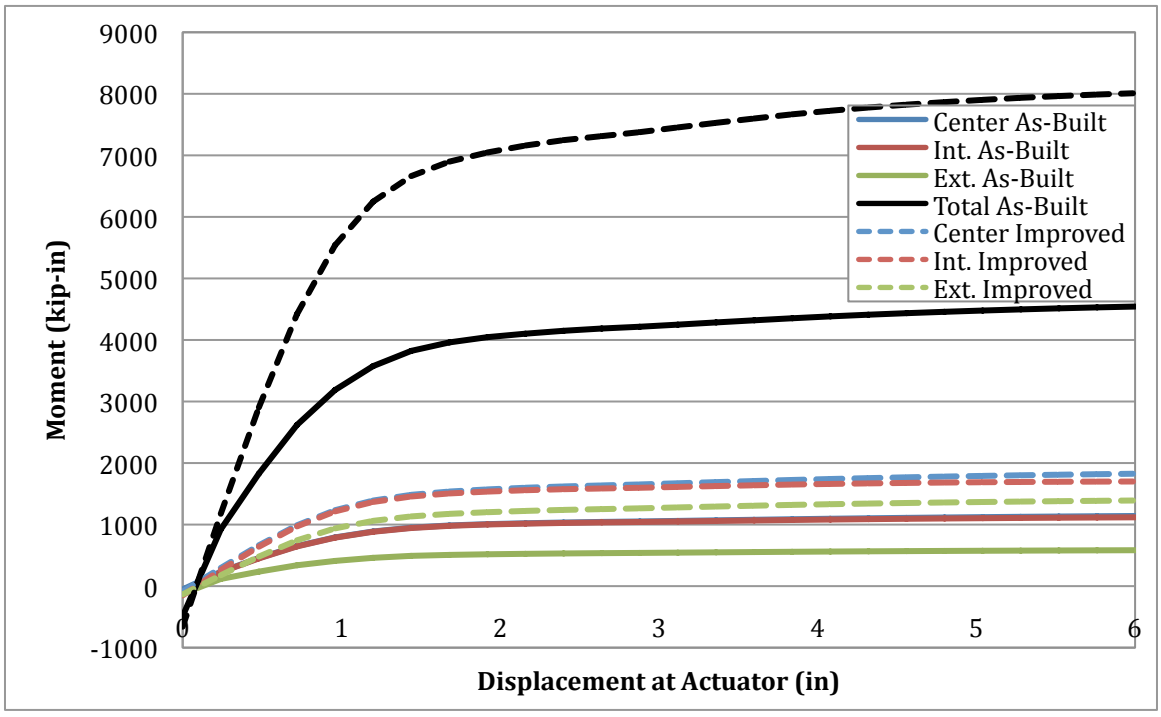

Figure 5.15: Predicted Moment Distribution at the Critical Girder Interface within the Connection during Phase 1

5.2.4.2 Phase 2 Prediction

Similar to Phase 1, a few predictions were made using the grillage model in order to better understand the response of the test specimen during Phase 2 of testing. Again, the force vs. displacement profiles were used to gain a feeling for the globalized behavior, while plots of the moment distributions within the girder-to-cap connection were used to predict the localized behavior of the test unit within the connection region. The sign convention used in the lab was as follows: Pushing the superstructure up corresponded to a positive displacement, while a negative displacement was defined as pulling the superstructure down.

As shown in Figure 5.16, the improved connection detail had a significant effect on the force vs. displacement response when the connection was subjected to a positive moment. As mentioned previously, it is likely that the influence of the improved connection would be more noticeable during Phase 2 compared to Phase 1, as the improved connection controls more of the localized behavior of the connection. Additionally, as expected, the improved connection detail had no influence on the behavior of the connection when subjected to a negative moment. It may also be noted that the response does not intersect the origin, as an initial load in the actuators was required in order to support the superstructure of the test unit. Based on the observed behavior in the individual girder-to-cap connection link elements, it was determined that the predicted maximum positive displacement was approximately 1.25 in. for the as-built connection side of the bent cap and 1.75 in. for the improved connection side, while the maximum negative displacement on both sides was approximately 6.5 in.

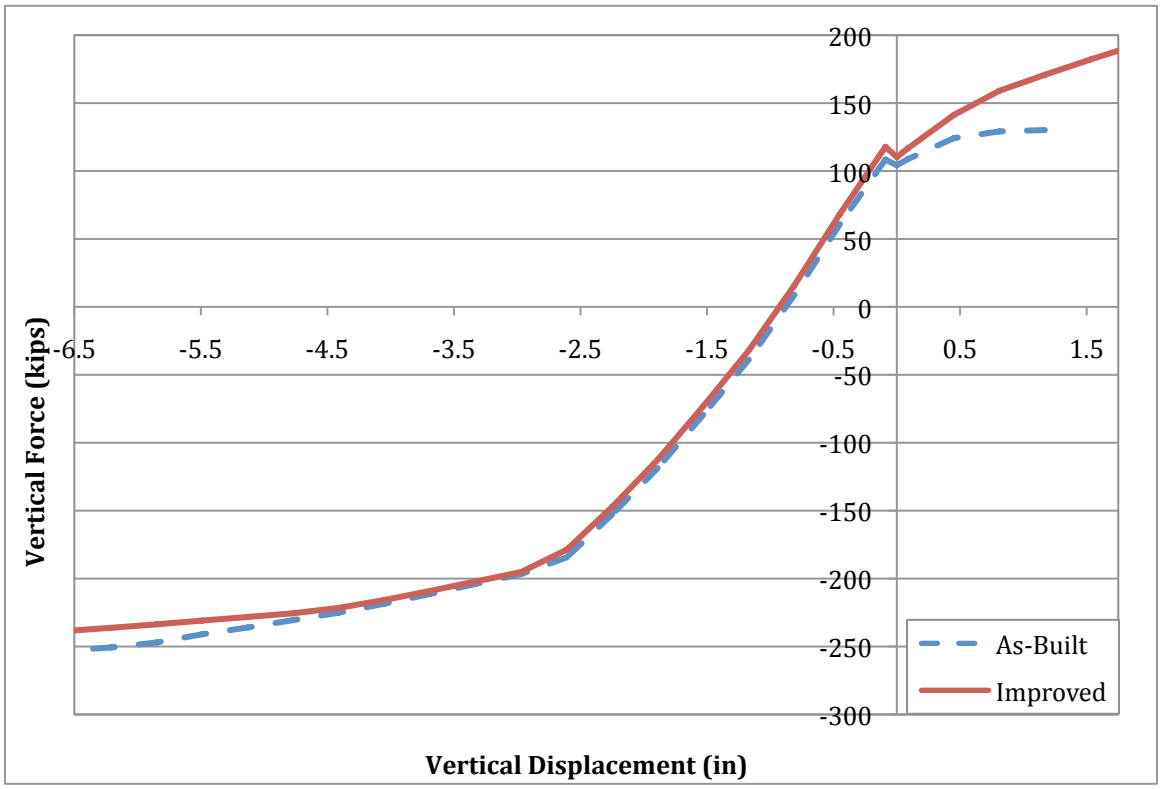

Figure 5.16: Predicted Force vs. Displacement during Phase 2

The second set of Phase 2 predictions were in regard to the moment distribution within the connection region of the test unit. As shown in Figure 5.17, the improved connection detail also had a significant effect on the moment distribution within the connection when subjected to a positive moment. Similar to what was shown in the prediction for the Phase 1 moment distribution between girders within the connection, the connection center and intermediate girders had the greatest moment demand, followed by the exterior girder. Furthermore, it may be observed that the predicted total maximum moment within the connection was over two times greater at the ultimate displacement with the addition of the improved connection detail when compared to the as-built connection detail. Finally, it should be noted that the magnitude of the moment within each girder-to-cap connection was greater during Phase 2, as the total moment demand in each connection was not dictated by the moment demand within the column plastic hinges, as it was during Phase 1. The predicted moment distribution within the connection when subjected to a negative

moment is shown in Figure 5.18. Again, as expected, the improved connection detail had no effect on the connection when compared to the as-built detail.

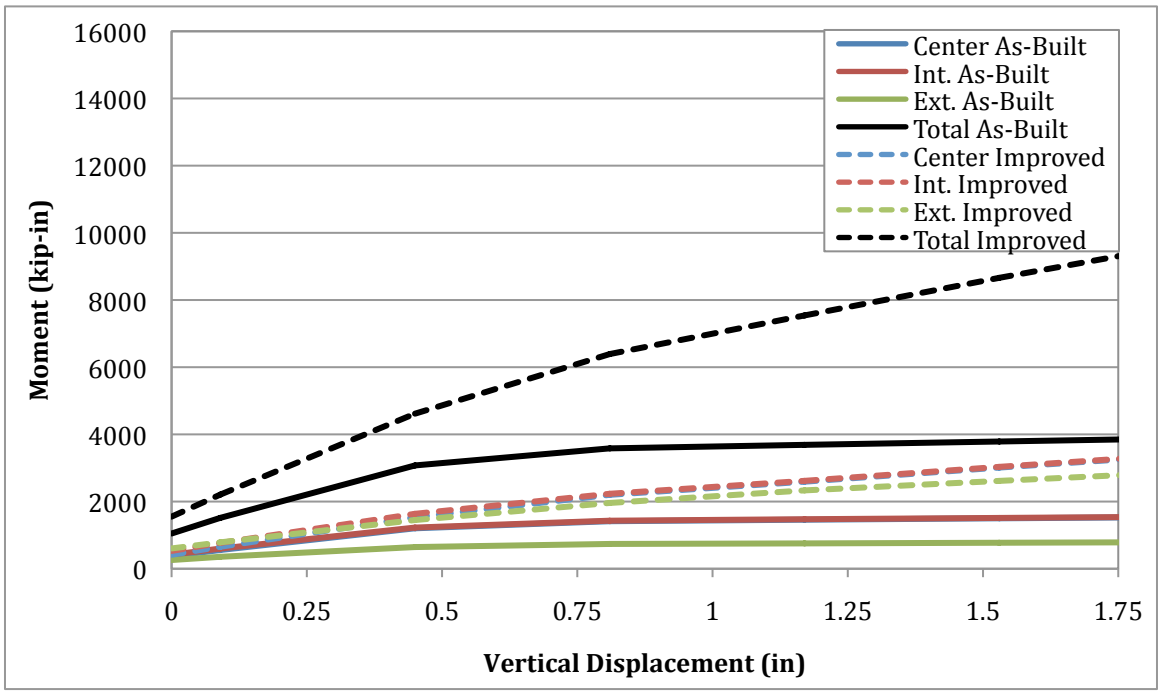

Figure 5.17: Predicted Moment Distribution at the Girder-to-Cap Interface due to Vertical Upward Displacements during Phase 2

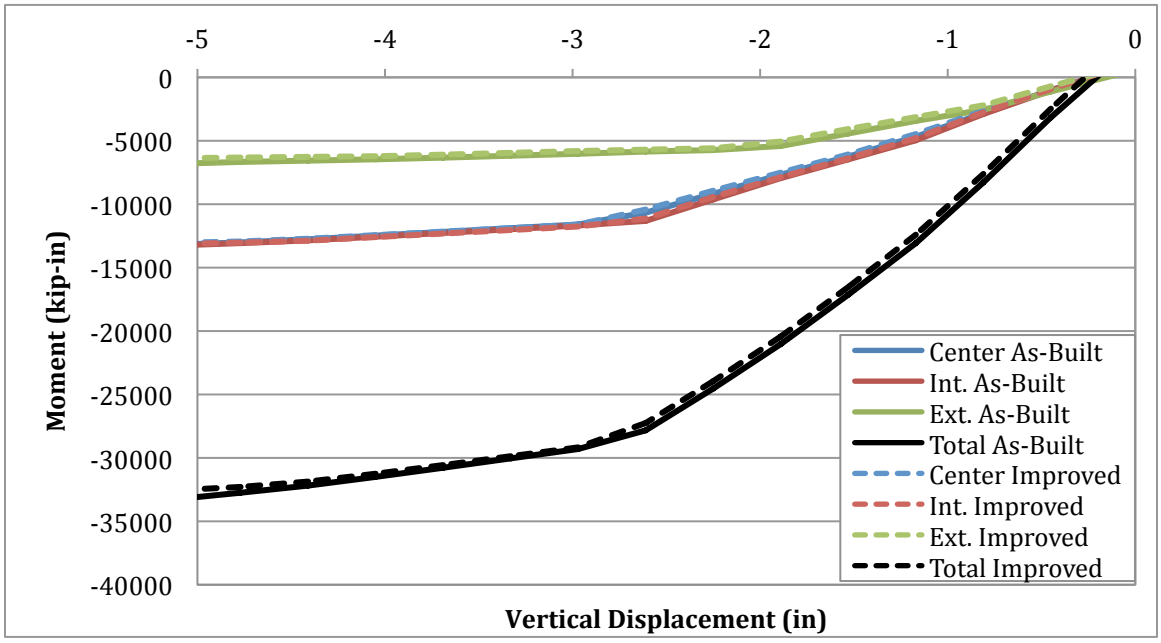

Figure 5.18: Predicted Moment Distribution during Phase 2 Pull

Chapter 6. SEISMIC TESTING

6.1 Phase 1 Test

As mentioned previously, Phase 1 of the testing involved a quasi-static, cyclic test of the 50% scale test specimen. The goal of the testing was to quantify the overall structural behavior of the unit when subjected to seismic loading conditions. Both the as-built and improved girder-to-cap connections were tested simultaneously during this phase.

6.1.1 Actuator Setup

The actuator setup for the Phase 1 test consisted of a total of eight actuators. Two horizontal and two vertical actuators were placed at each abutment. The horizontal actuators were placed in a "V" configuration in order to provide more stability against rotation of the superstructure about its vertical axis, when testing the effects of seismic loading by displacing the superstructure horizontally, as shown in Figure 6.1. The vertical actuators provided structural stability, imposed the correct gravity load effects in the test unit, and ensured that the abutment maintained a constant height relative to the top of the column. Maintaining a constant height relative to the top of the column was important in order to prevent the growth of the column, as the plastic hinges developed, from introducing extraneous loads into the system.

Figure 6.1: Horizontal Actuator Configuration Used During Phase 1 Testing at Each Abutment

6.1.2 Loading Protocol

6.1.2.1 Application of Stage 1 Hold-Down

In order to prevent possible cracking of the column, the following loading protocol was followed when applying the Stage 1 hold-down force: 30% of the total load was applied to the North span; 70% of the total load was applied to the South span; 100% of the total load was then applied to the North span; and finally, 100% of the total load was applied to the South span.

6.1.2.2 Application of Stage 2 Hold-Down

Though cracking of the column was not as great of a concern during the application of the Stage 2 hold-down force, as the increase in moment was less than that which was needed to cause flexural cracking within the column, the following load protocol was followed simply out of precaution: 50% of the total load was applied to the North span; 100% of the total load was applied to the South span; and 100% of the total load was finally applied to the North span.

6.1.2.3 Horizontal Actuator Protocol

As mentioned previously, the test unit was cycled though a number of progressively increasing displacement targets during Phase 1 of testing. Initially, the test unit was subjected to low-level elastic displacements, during which the specimen was cycled through a force of positive and negative $0.25F'_y$, $0.5F'_y$, and $0.75F'_y$, where F'_y corresponded to the condition at which the reinforcement within the plastic hinge region of the column was expected to yield first. Following the aforementioned preliminary cycles, the test unit was cycled through the following levels of displacement ductility, μ_Δ, within the column plastic hinges: ±1, ±1.5, ±2, ±3, ±4, and ±6. In order to more accurately capture the cyclic behavior of the structure, including any possible strength degradation, each level of displacement ductility was subjected to three cycles. Since the maximum expected displacement ductility was approximately 5.4, the actual condition of the specimen at a displacement ductility level of 6 was not well known. It is likely that the plastic hinges within the column could achieve a ductility level higher than what was predicted, given the various assumptions that were made for material properties, especially the confined concrete behavior, which were used in

obtaining the expected maximum ductility. Therefore, provided that the column were not near the point of failure at a ductility level of 6, an additional three cycles at a ductility level of 7.5 was planned. Table 6.1 provides the expected displacements and the corresponding lateral force resistance, as obtained from the SAP2000 grillage model, at each force and ductility level during testing.

Table 6.1: Preliminary Horizontal Testing Protocol Established for Phase 1 Testing

Cycle Level	Expected	
	$\Delta_{absolute}$ (in)	Absolute Actuator Force (kips)
$0.25F'_y$	0.14	40
$0.5F'_y$	0.30	80
$0.75F'_y$	0.46	120
$\mu_\Delta = \pm 1$	0.94	198
$\mu_\Delta = \pm 1.5$	1.41	225
$\mu_\Delta = \pm 2$	1.89	235
$\mu_\Delta = \pm 3$	2.83	247
$\mu_\Delta = \pm 4$	3.77	257
$\mu_\Delta = \pm 6$	5.66	270
$\mu_\Delta = \pm 7.5$	7.07	278

6.1.2.4 Vertical Actuator Protocol

In order to ensure that the vertical actuators maintained stability in the system, without introducing any extraneous loads into the column, it was important to program the vertical actuators to accommodate any growth within the column. Therefore, at various horizontal displacement levels, the column growth was approximated per the procedure outlined in (Holombo, Priestley, & Seible, 1998).

The column was divided into three sections as shown in Figure 6.2, consisting of two inelastic sections, defined by the respective plastic hinge lengths at the top and bottom of the column, and the elastic portion of the column, located between the plastic hinges. Within the plastic hinge regions, the curvature was assumed to be constant, while it varied linearly over the elastic region of the column. The corresponding axial strains within each section were obtained by using the curvature, ϕ, to calculate the strain at the centerline of the column, ε_{cl},

per Equation 6.1, where D and $y_{N.A.}$ corresponded to the column diameter and neutral axis depth of the column cross-section, respectively.

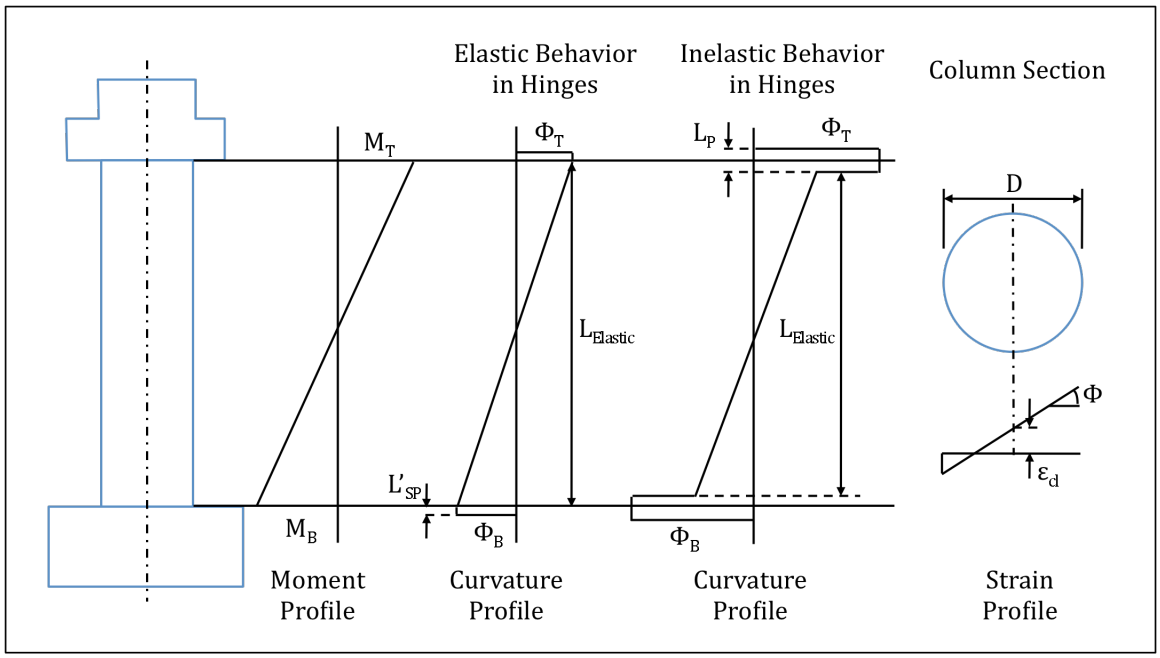

Figure 6.2: Estimating Column Growth in the Vertical Direction

$$\varepsilon_{cl} = \phi\left(\frac{D}{2} - y_{N.A.}\right) \qquad (6.1)$$

The curvature and neutral axis depths were obtained via the moment curvature analysis of the column section within each plastic hinge region. However, for the elastic portion of the column, an average curvature was calculated via Equation 6.2, where I_{cr} represented the cracked moment of inertia of the column at first yield and an average absolute moment along the length of the column, M_{ave}, was computed per Equation 6.3.As stated, both the moment and curvature was assumed to vary linearly along the elastic portion of the column; therefore, an average moment and curvature was used to calculate the growth of the elastic portion of the column, which simplified the integration of growth over the region. The values M_T and M_B in Equation 6.3 represent the moments in the top and bottom column hinges, respectively and were obtained via the SAP2000 grillage analysis at the corresponding level of horizontal displacement. Additionally, the value for the neutral axis depth over the elastic portion of the column was approximated as a value of D/4.

$$\phi_{ave} = \frac{M_{ave}}{EI_{cr}} \tag{6.2}$$

$$M_{ave} = \frac{M_T{}^2 + M_B{}^2}{2(M_T + M_B)} \tag{6.3}$$

Once the strain at the centerline of the column was obtained for each section, it was multiplied by the length of the respective section, L_T, L_B, and $L_{Elastic}$, in order to obtain the column growth for the section, per Equation 6.4. The values for L_T and L_B were calculated per Equation 4.5. The sum of the growth over each section was then taken as the overall growth of the column.

$$\Delta_{Growth} = \varepsilon_{cl} L \tag{6.4}$$

It should be noted however, that Equation 6.4 is only valid in the inelastic regions after the hinges have experienced inelastic behavior, as the equation for the plastic hinge length accounted for both elastic and plastic strain penetration into the column-to-cap and column-to-footing joint regions. Therefore, for displacement levels less than the expected first yield condition, the value of L'_{sp} was used for the length of each hinge, as it only accounted for the elastic penetration effects into the joint region, per Equation 4.4.

Since the superstructure flexibility varied between the as-built and improved connection sides, it was appropriate to calculate a horizontal displacement vs. column growth curve for each displacement direction, pushing to the South to active the as-built positive moment connection or pulling to the North to active the improved positive moment connection detail. The resulting horizontal displacement vs. column growth curves are shown below in Figure 6.3. It should be noted that when one positive moment connection was tested in a given loading direction, the other side's negative moment connection was also tested. For example, both the positive moment connection on the as-built side and the negative moment connection on the improved side were tested simultaneously when the superstructure was pushed to the South.

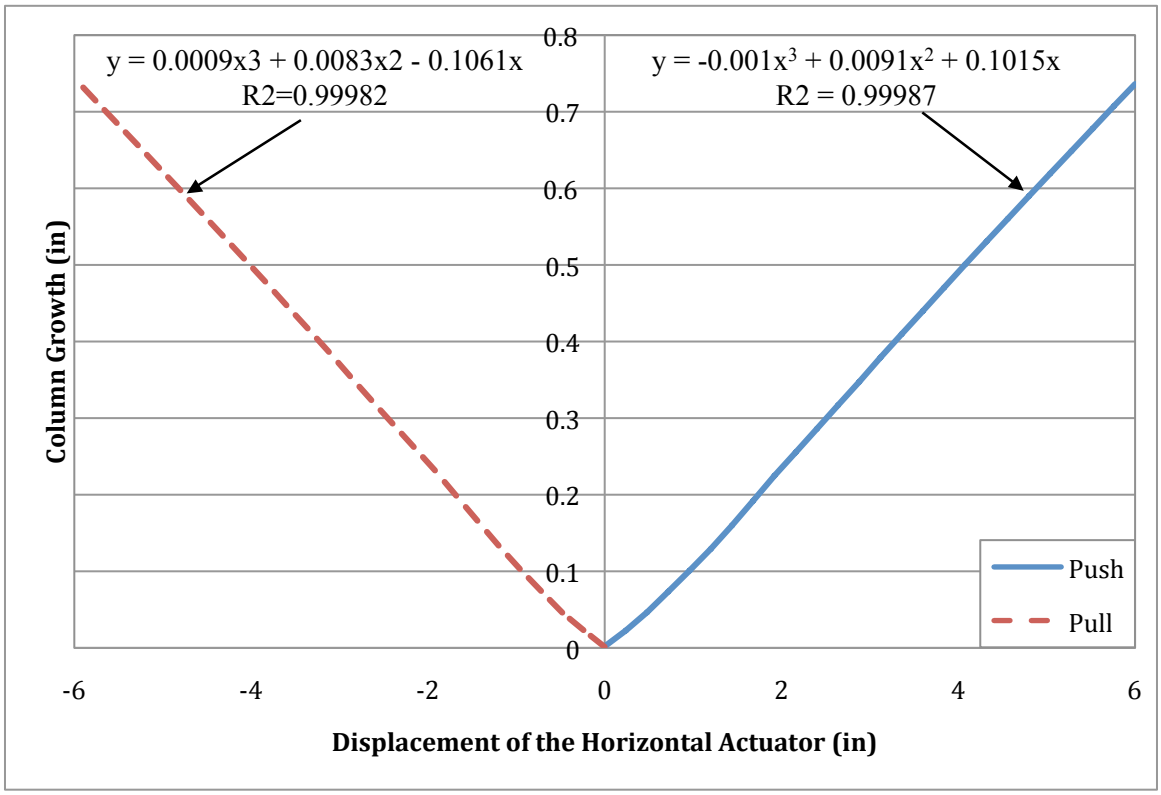

Figure 6.3: Horizontal Actuator Displacement vs. Column Growth

The aforementioned growth curves were used to program the vertical actuators using the best fit equations included in Figure 6.3, in conjunction with active feed back from the external instrumentation, in order to maintain vertical stability within the system.

6.1.3 Hold-Down Forces

In order to accurately subject the Test Unit to the same type of loading that would be experienced by the Prototype, it was necessary to apply a vertical hold-down force on each side of the bent cap. The discrepancy between the forces experienced in the Test Unit and Prototype was due to the fact that the Test Unit consisted of a half span on each side of the cap and that the dimensional scaling applied to the test unit did not result in a correctly scaled gravity load effects. Additionally, loads that were applied to the prototype bridge, such as the future wearing surface and barriers, were not modeled in the test unit. Therefore, without compensating for these dissimilarities, the forces and behavior experienced by the test unit would not adequately compare to the prototype structure, as seen in Figures 6.4 and 6.5. It is

important to note that the moment and shear profiles shown in these figures have been scaled to the test unit and were based on a preliminary structural analysis of the center girder. The dashed lines represent the location at which girder bears on the bearing pad under its dapped end and on the corbel of the inverted-T cap beam.

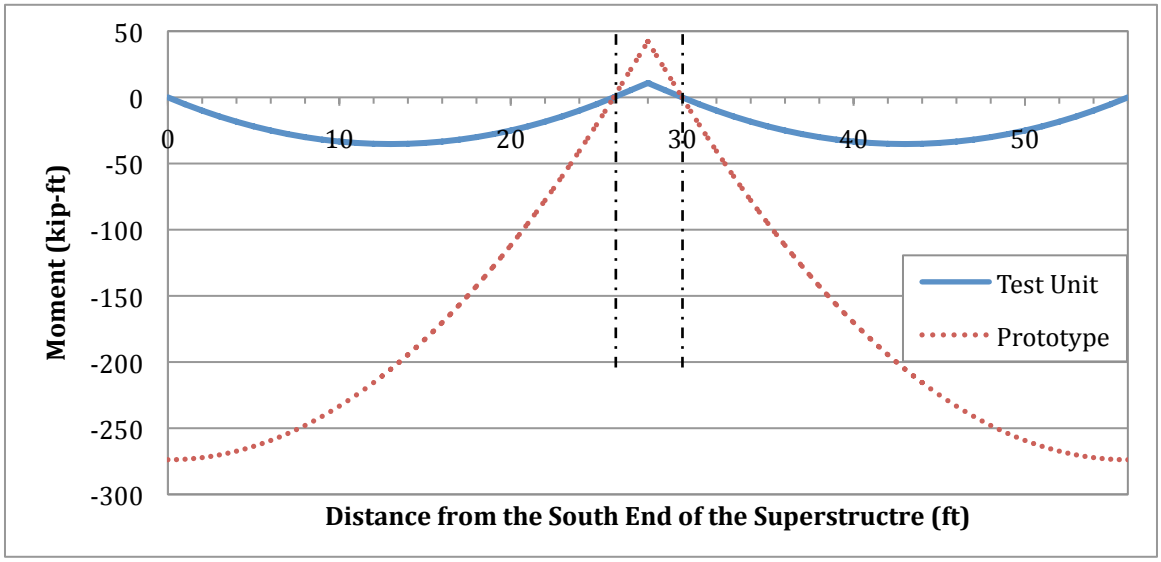

Figure 6.4: Stage 1 Prototype-to-Test Unit Moment Profile Comparison along the Length of the Superstructure without Scaling Compensation

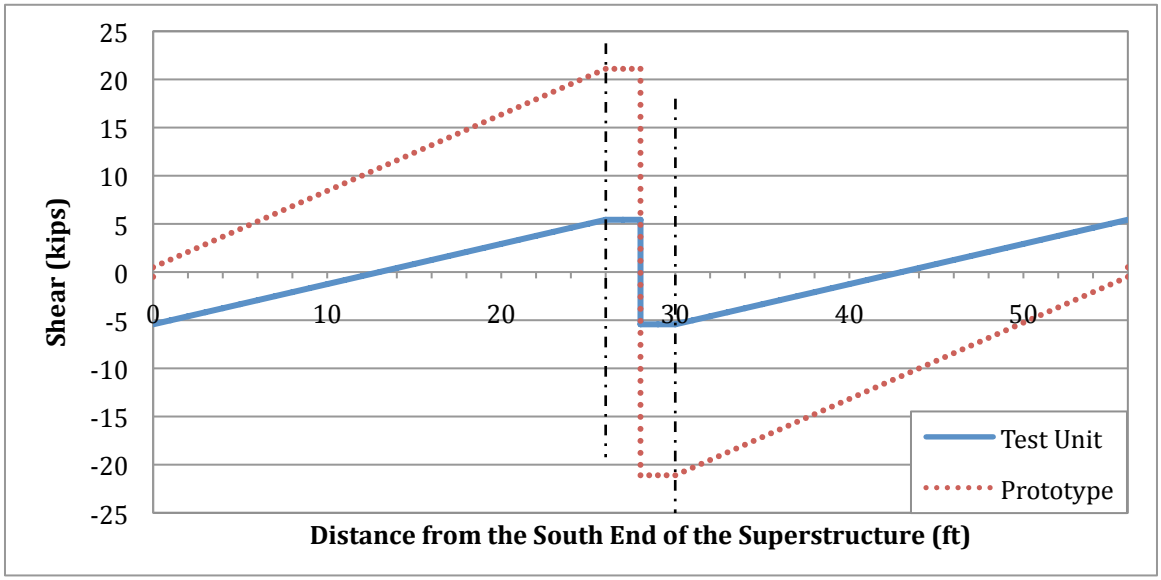

Figure 6.5: Stage 1 Prototype-to-Test Unit Shear Profile Comparison along the Length of the Superstructure without Scaling Compensation

As a result, a whiffle tree arrangement was placed on each side of the column at a distance of 16 ft from the center of the column along the span in order to apply and distribute a hold-down force across the width of the deck and into each girder, as seen in Figure 3.1. This distance was selected based primarily on the anchor-hole layout on the floor of the lab at UCSD as well as the fact that it provided good agreement between the shear and moment profiles within the connection region when the hold-down force was applied. A more detailed description of the whiffle tree is provided in the proceeding section.

A structural analysis of the superstructure indicated that, in order to provide shear and moment agreement within the connection, a hold-down force of 33.4 kips per girder (167 kips total on each span) had to be applied during the construction condition in which the girders were simply supported, which was referred to as "Stage 1." As shown below, this hold-down force was used to correct the self-weight of the girders. The adjusted moment and shear profiles for Stage 1, after the application of the hold-down force, are presented in Figures 6.6 and 6.7.

Once the superstructure was made continuous, known as "Stage 2," through the hardening of the deck, an additional hold-down force of 11.8 kips per girder (59 kips total on each span) was applied in order to provide a final agreement between the shear and moments experienced between the Test Unit and Prototype structures. This hold-down force was also critical in achieving moment agreement within the connection region, which was of primary concern. It should also be noted that the Stage 2 hold-down force represented the additional loads due to the weight of the barriers and other objects that would be experienced by the prototype structure, but were not present on the test unit. Figures 6.8 and 6.9 show the comparison of the moment and shear diagrams after the Stage 2 hold-down. The final adjusted moment and shear diagrams, with the inclusion of the expected seismic inertia forces, which compensate for scaling and the absence of loads observed in the prototype structure are presented below in Figures 6.10 and 6.11.

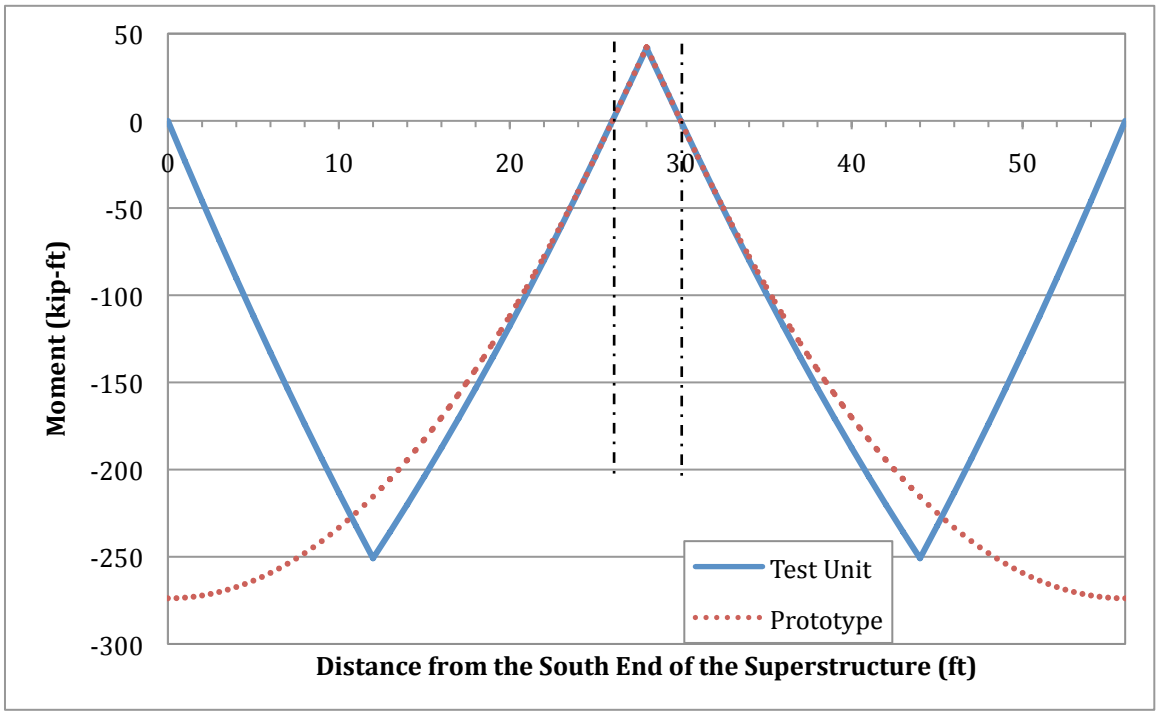

Figure 6.6:Stage 1 Prototype-to-Test Unit Moment Profile Comparison along the Length of the Superstructure After Applying Stage 1 Hold-Down Force

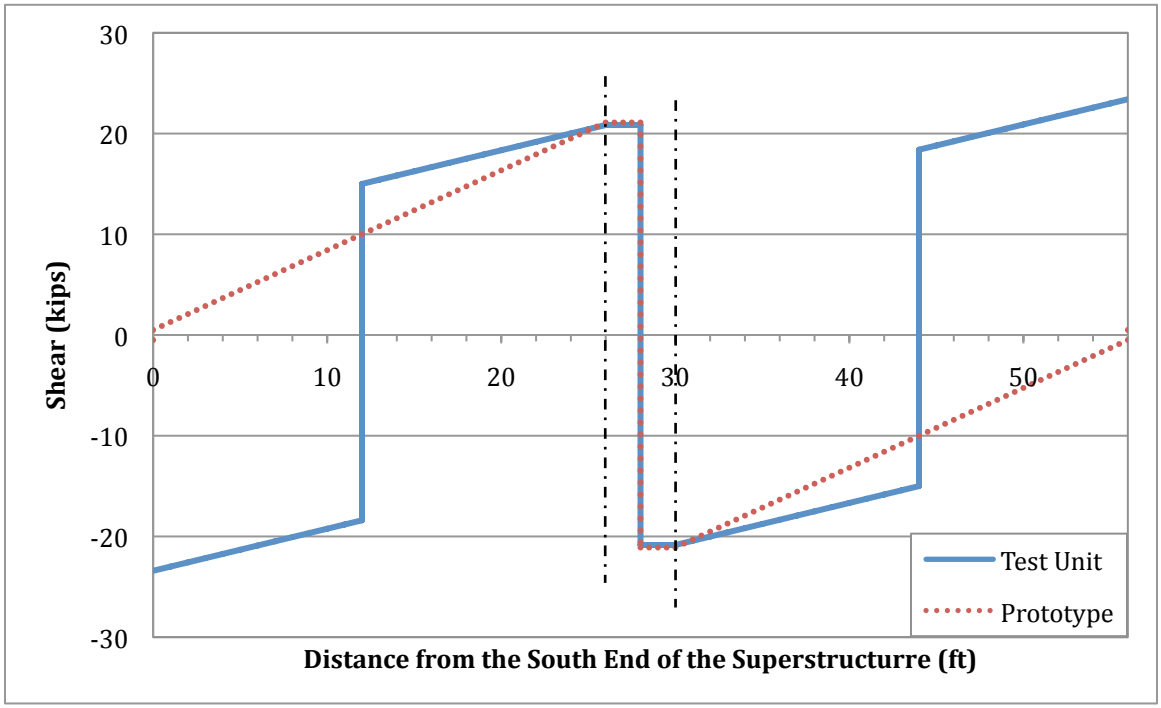

Figure 6.7:Stage 1 Prototype-to-Test Unit Shear Profile Comparison along the Length of the Superstructure After Applying Stage 1 Hold-Down Force

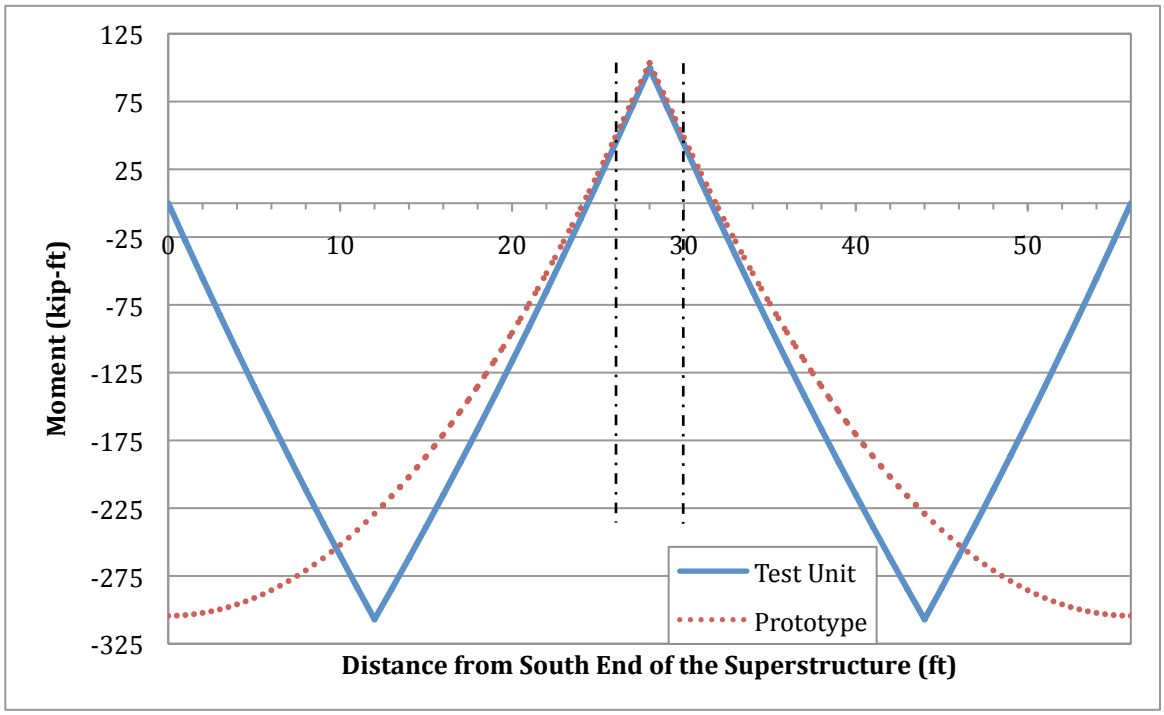

Figure 6.8:Stage 2 Prototype-to-Test Unit Moment Profile Comparison along the Length of the Superstructure After Applying Additional Stage 2 Hold-Down Force

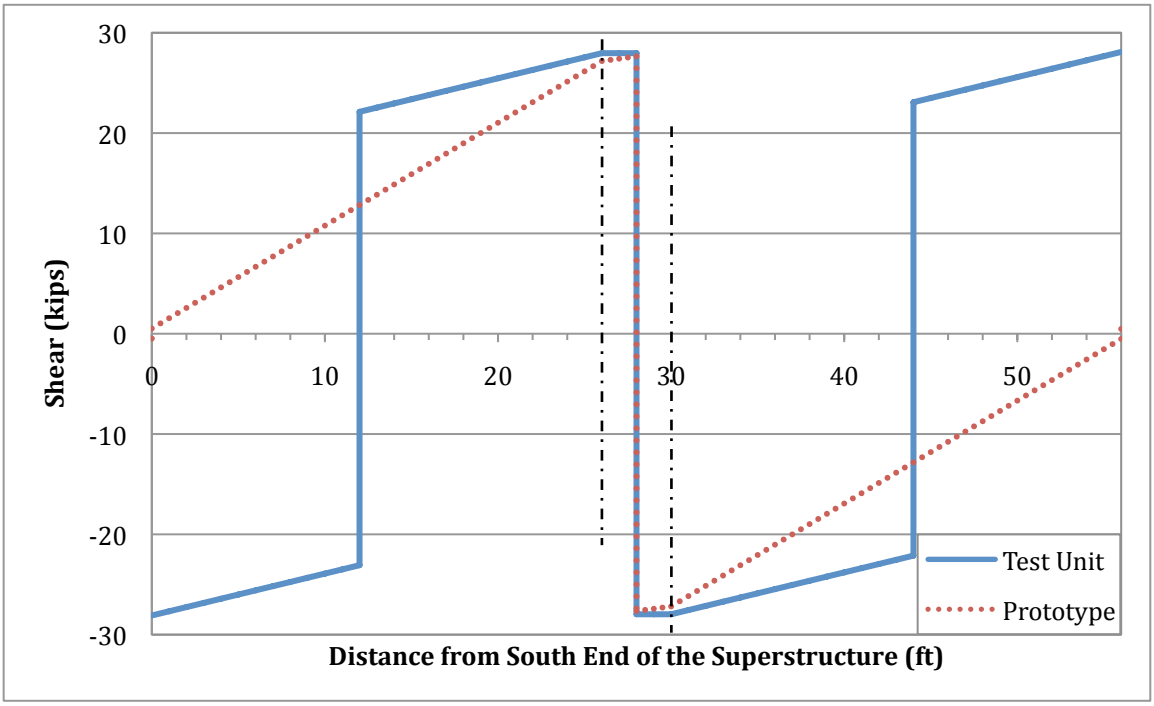

Figure 6.9: Stage 2 Prototype-to-Test Unit Shear Profile Comparison along the Length of the Superstructure After Applying Additional Stage 2 Hold-Down Force

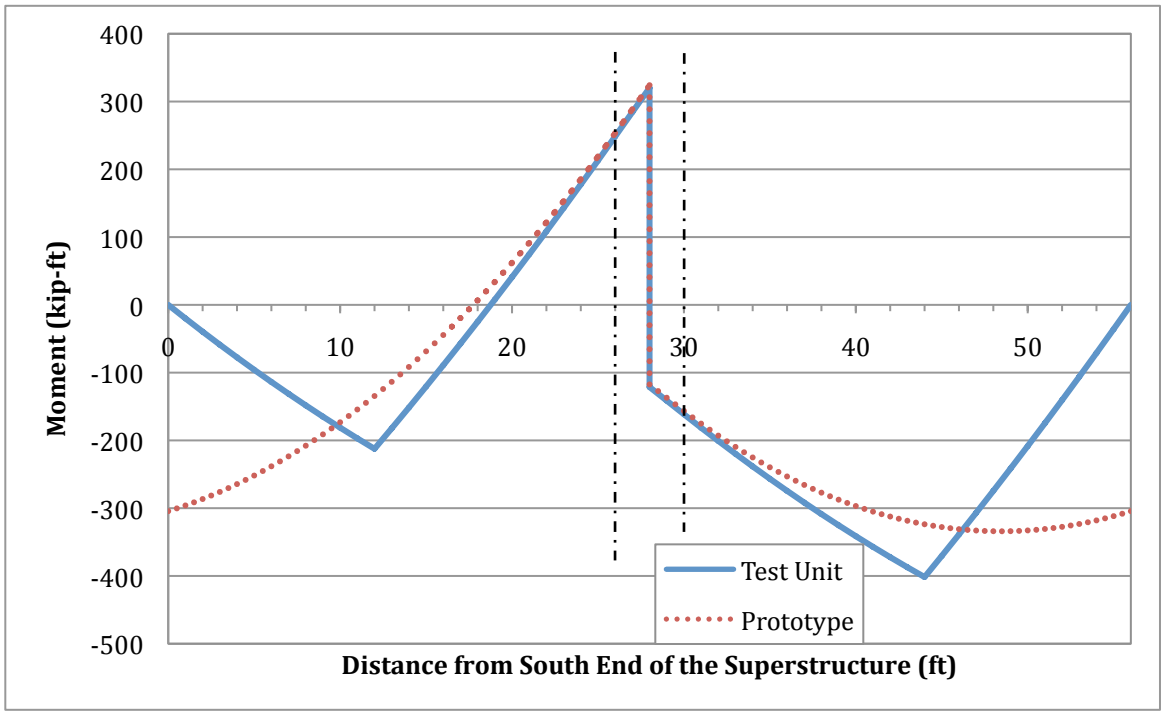

Figure 6.10: Final Prototype-to-Test Unit Moment Profile Comparison along the Length of the Superstructure after Applying Hold-Down Forces and Seismic Effects

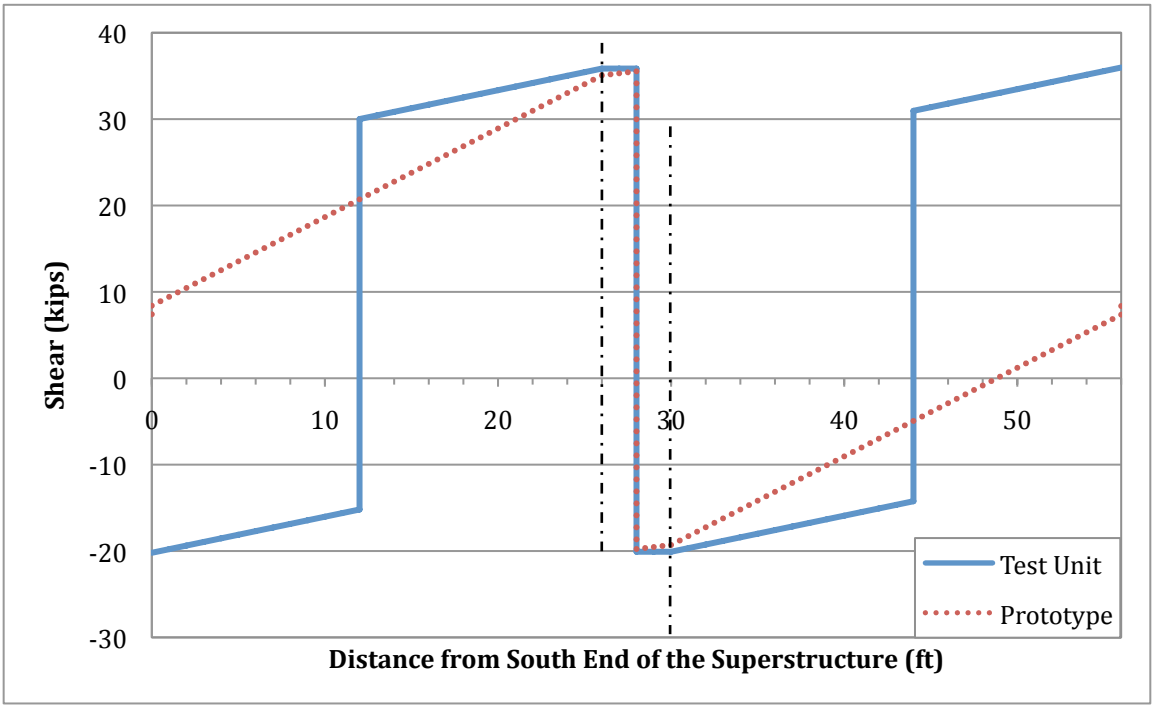

Figure 6.11. Final Prototype-to-Test Unit Shear Profile Comparison along the Length of the Superstructure after Applying Hold-Down Forces and Seismic Effects

It is important to note that the goal of the hold-down force was not to achieve complete shear and moment agreement over the entire span. Instead, the intent was only to provide agreement within the area surrounding regions of focus, which for the purposes of the testing were the girder-to-cap connection regions. Furthermore, it may be noted that some of the profiles for the test unit after applying the hold-down forces were greater than those for the prototype. This was deemed acceptable, as the subsequent response of the test unit would be a conservative representation of what would otherwise be expected. Therefore, the results and conclusions could be applied to a full-scale prototype structure with a high degree of confidence.

6.1.3.1 Whiffle Tree

The purpose of the whiffle tree was to evenly distribute two applied jacking forces to each of the five girders in a given span of the test unit to simulate the gravity load effects of the prototype structure as accurately as possible. The whiffle tree was designed as a series of built-up HSS sections, which were placed next to each other and connected via welded plates in order to accommodate the series of rods that connected each beam, as shown in Figure 6.12. A structural analysis was performed in order to determine the location of the rods within the tree arrangement required to achieve an equal load in all five of the girders in a given span. A jacking force was applied to each of the rods that passed through the floor in order to achieve the appropriate hold-down force as mentioned above; that force was then distributed to the bridge superstructure through the whiffle tree.

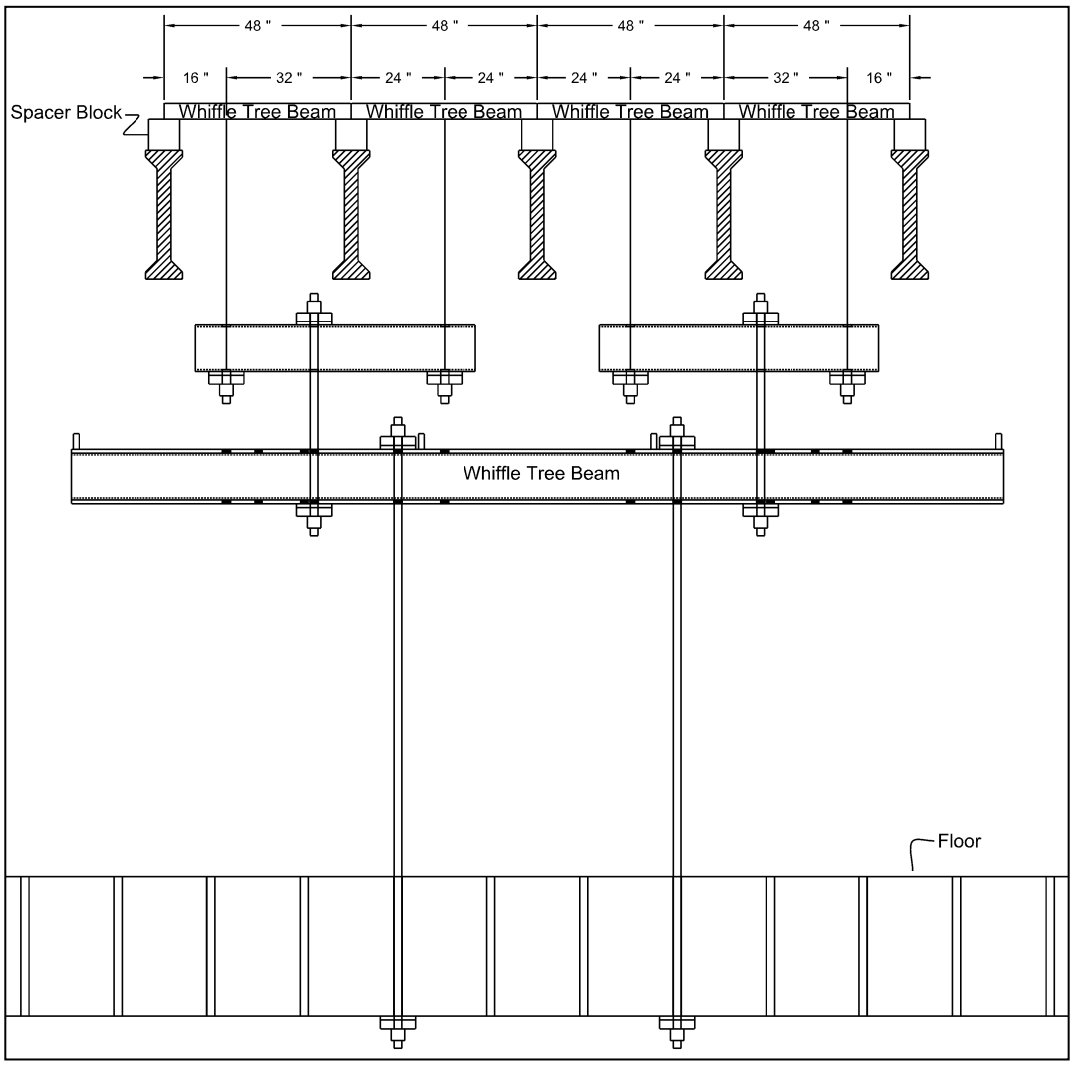

Figure 6.12: Whiffle Tree Arrangement Used to Impose Additional Vertical Loads to the Test Unit During Phase 1 Testing

Holes were placed in the deck in order to accommodate the rods that passed through the superstructure and tied into the beams that were placed on the topside of the girders. Spacer blocks were also included in order to provide a bearing surface for the aforementioned beams and to elevate them above the height of the deck, as shown in Figure 6.13. The spacer blocks were constructed by placing a small 8 in. tall HSS section on top of each girder, centered at a distance of 16 ft from the centerline of the cap beam. The steel beam sections were placed on spacers, approximately ¼ in. thick, and were filled with hydrostone. Each spacer block was leveled and shimmed such that they were all at the same

elevation on each girder. This provided an even bearing surface both at the interface between the steel HSS section and the girder as well as on the topside of the HSS section and the whiffle tree top beam. Additionally, the stirrups protruding out of the top of the girders, that were located within the HSS spacer section, were left straight and were surrounded by hydrostone in order to provide an additional bond between the spacer block and the girder. It should be noted that the large beam at the bottom of the whiffle tree was also designed so that it could be placed directly beneath the girders and used to mount the vertical actuators, while tying the superstructure together during Phase 2 of the testing.

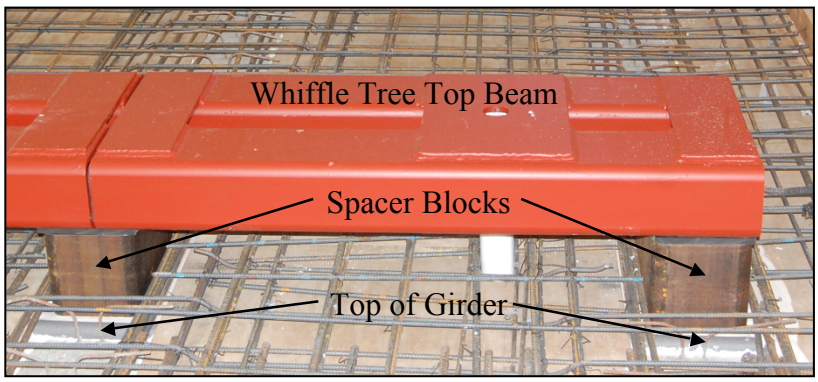

Figure 6.13: Details of Whiffle Tree Spacer Blocks and Top Beams

6.1.4 Phase 1 Test Observations

During the lateral load testing, the extreme column longitudinal bars in the column began yielding at an average lateral displacement of 0.46 in., which was established based on the measured strains in the extreme column longitudinal reinforcement in the push and pull direction of loading during testing at $\pm 1.0F'_y$. By combining this information with the theoretical first yield and idealized yield lateral force resistance, the idealized yield displacement for the test unit was defined as 0.7 in. Consequently, the displacement at each ductility level was obtained as a factor of 0.7 in. Table 6.2 outlines the updated loading protocol during Phase 1 testing.

Table 6.2: Updated Horizontal Test Protocol for Phase 1 Testing

Cycle Target	Δ (in)	Average Absolute Measured Actuator Force (kips)	Number of Cycles
±0.07 F'_y	± 0.05	40	1
±0.17 F'_y	± 0.12	80	1
±0.36 F'_y	± 0.25	120	1
±0.6 F'_y	± 0.42	160	1
μ_Δ = ±1	± 0.7	210	3
μ_Δ= ±1.5	± 1.05	224	3
μ_Δ= ±2	± 1.4	233	3
μ_Δ= ±3	± 2.1	247	3
μ_Δ= ±4	± 2.8	247	3
μ_Δ= ±6	± 4.2	253	3
μ_Δ= ±8	± 5.6	245	2
μ_Δ= ±10	± 7.0	221	1

Under positive moments, cracking between the diaphragm and cap interface did not develop on the underside of the superstructure until a displacement ductility of 1.5 was reached. These cracks were observed in each bay between two girders on the positive moment side and were primarily concentrated near the girders. However, none of the cracks extended along the entire length of the cap. Additionally, cracking was observed at the interface between the bottom flange of each of the girders and the underside of the bent cap under positive moments. On the as-built connection side of the bent cap, the aforementioned girder to cap interface cracks had a width of 0.4 mm at the center girder. Similar cracks were noticed on the improved connection side, when subjected to a positive moment, at a ductility level of 1.5; however, the crack width was only about 0.2 mm at the center girder. At this ductility level, vertical flexural cracking was also noticed along the interface between the web of the girders and the diaphragm on both the improved and as-built connection sides, when each connection was subjected to a positive moment, and extended roughly half way up to the underside of the deck. Finally, significant cracking was observed on the topside of the deck, primarily outside the edge of the diaphragm on the negative moment side of the bent cap. A significant number of the flexural cracks in the deck, which had developed

during earlier cycles due to negative moment, had also connected and spread across the entire length of the deck, indicating the engagement of all five girders in resisting the column moment on each side of the bent cap.

At a displacement ductility level of 2, the previously mentioned flexural cracks between the bottom flange of the center girder and the bent cap on the as-built connection side had widened to 0.5 mm, while the same gap on the improved connection side remained at 0.2 mm. The vertical cracks between the webs of the girders and the diaphragm on both sides of the connection extended almost all the way to the underside of the deck. Cracking on top of the deck continued to develop further away from the bent cap and extended across the entire width of the deck. The first signs of crushing and spalling of the concrete at the top and bottom of the column were also noticed.

Between displacement ductility 3 and 8, the majority of the significant changes to the test unit occurred within the column and the deck near the column. A few new cracks developed in the column; however, the primary observation was that the old cracks began to extend and increase in width. The cover concrete at both the top and bottom column ends also began to crush and spall within the plastic hinge regions as the cycles progressed. Incipient buckling to one of the exposed longitudinal column reinforcement bars was observed in the bottom plastic hinge at a ductility level of 8, on the South side of the column. The number of cracks in the deck increased in an evenly distributed manner and spread across the entire width of the superstructure, the majority of which were located between the diaphragm and vertical tie-down locations on each side of the bent cap. No significant changes were observed in either the as-built or the improved connection regions on the underside of the superstructure. Instead, the cracks remained essentially unchanged in regard to both their extension and width.

By the time the test unit had reached a displacement ductility of 10, or a horizontal displacement of 7 in., it was apparent that the column had reached its ultimate capacity. A significant amount of concrete had crushed and spalled off of the column within the top and bottom plastic hinge regions, as shown in Figure 6.14. Several spirals and longitudinal bars were visible and concrete within the column core had crushed. The majority of the longitudinal column bars within the hinge regions had also begun to buckle across the spirals.

However, no significant further cracking was observed within the connection region between the girders and the cap or diaphragm, as shown in Figure 6.15. Furthermore, no joint cracking between the column and inverted-T bent cap was observed during the entire test. More flexural cracks along the top of the deck had developed between the diaphragm and hold-down locations, while only a few cracks were observed within the cap region. Some of the cracking in the deck, near the stem on the inverted-T also extended all the way through the deck.

Figure 6.14: A Close-Up View of the Column Performance at +7.0 in. of Lateral Displacement (μ_Δ=+10)

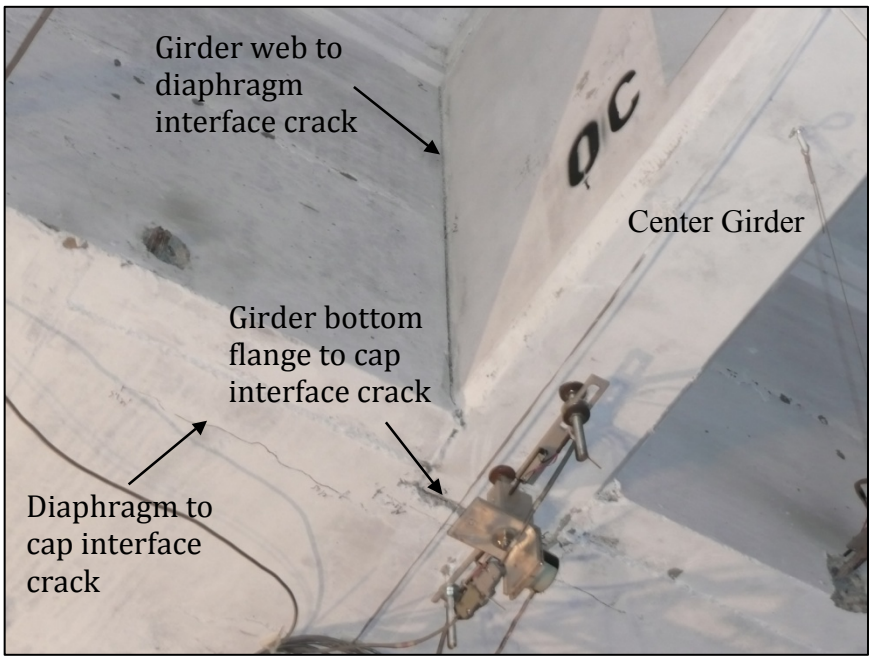

Figure 6.15: Condition of As-Built Center Girder-to-Cap Connection at μ_{Δ}=+8

6.1.5 Phase 1 Test Results

The structure achieved a displacement ductility of 10, corresponding to 7 in. of total horizontal displacement, before buckling of several column longitudinal reinforcement bars was observed, as well as the beginning of a confinement failure, as shown in Figure 6.16. Both the improved and as-built connection between the precast I-girders and cap beam behaved as a fully continuous connection and did not show signs of significant damage or degradation throughout the course of the testing. No joint cracking was observed between the top of the column and the underside of the bent cap at any point during the test. Fairly extensive flexural cracking was observed across the width of the deck, indicating that the diaphragm action of the deck had engaged all of the girders, as shown in Figure 6.17.

Figure 6.16: Buckling in the Top Column Hinge on the North Side at μ_Δ=10

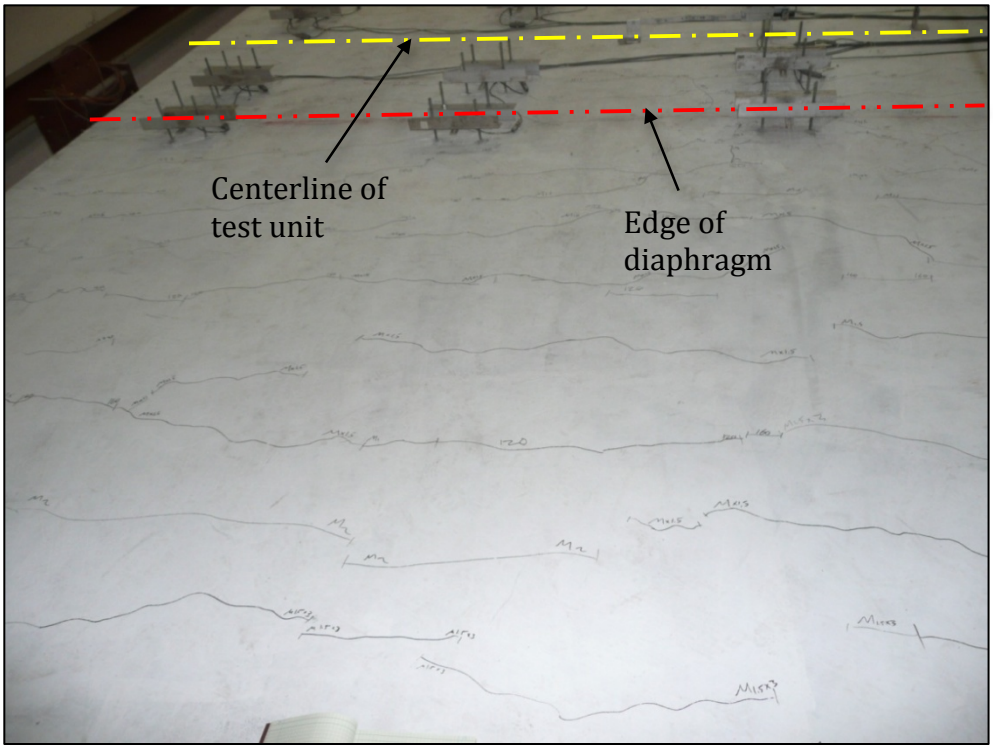

Figure 6.17: Distribution of Flexural Cracking on the Top Side of the Deck at μ_Δ=+10

A comparison of some of the data collected during the test to the predictions based on the SAP2000 grillage model showed generally good results. The horizontal force vs. lateral displacement of the superstructure is shown in Figure 6.18, which showed slight disagreement at small displacements as the grillage model used a cracked effective stiffness for both the column and superstructure sections, rather than the actual gross values for the elastic region of the test. However, the results began to converge at higher levels of displacement as more of the structure began to soften due to the development of cracks and yielding of reinforcement. The plot of horizontal displacement vs. positive as-built connection rotation is shown in Figure 6.19. A satisfactory correlation between the recorded predicted stiffness for the connection is seen, but the connection of the test unit exhibited a relatively small rotation compared to what was predicted. This discrepancy could easily have been caused by the increased strength in the concrete at the time of testing, which was further examined during Phase 2.

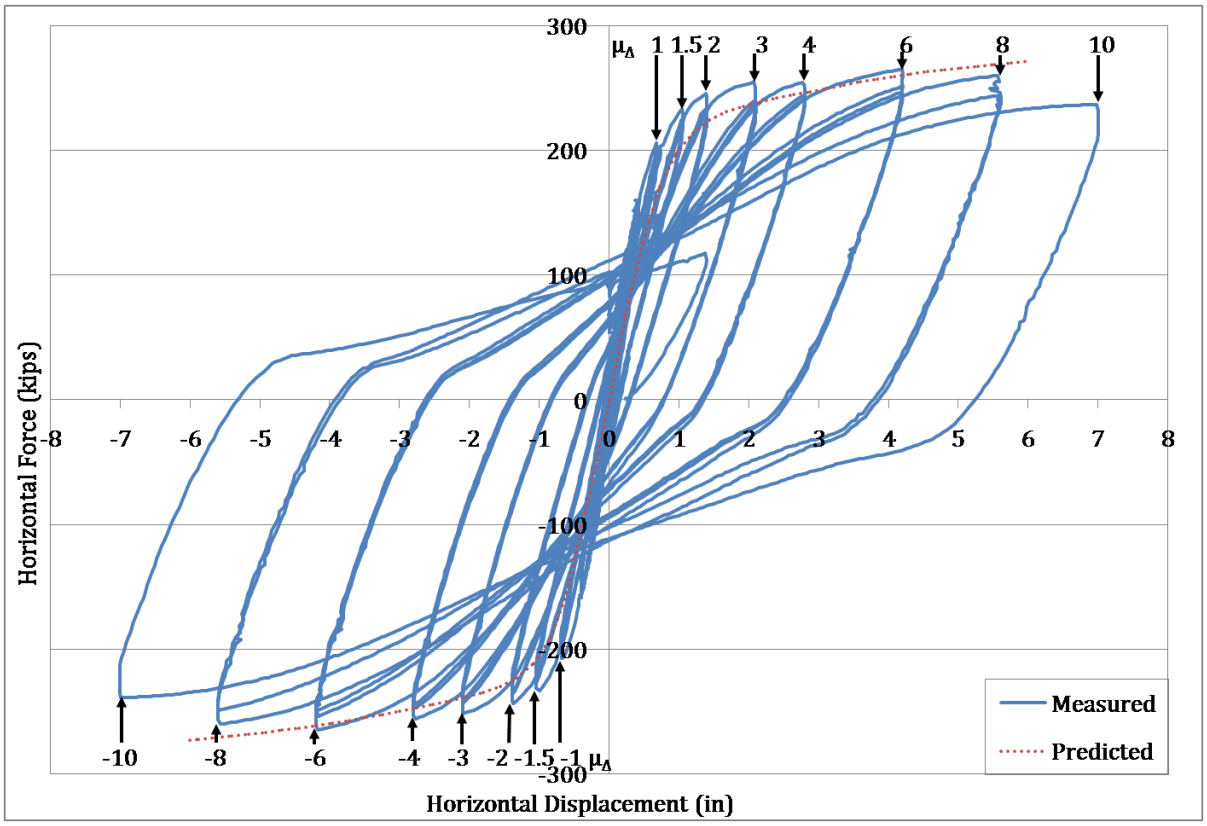

Figure 6.18: Force vs. Displacement Response of Test Unit during Phase 1 Testing

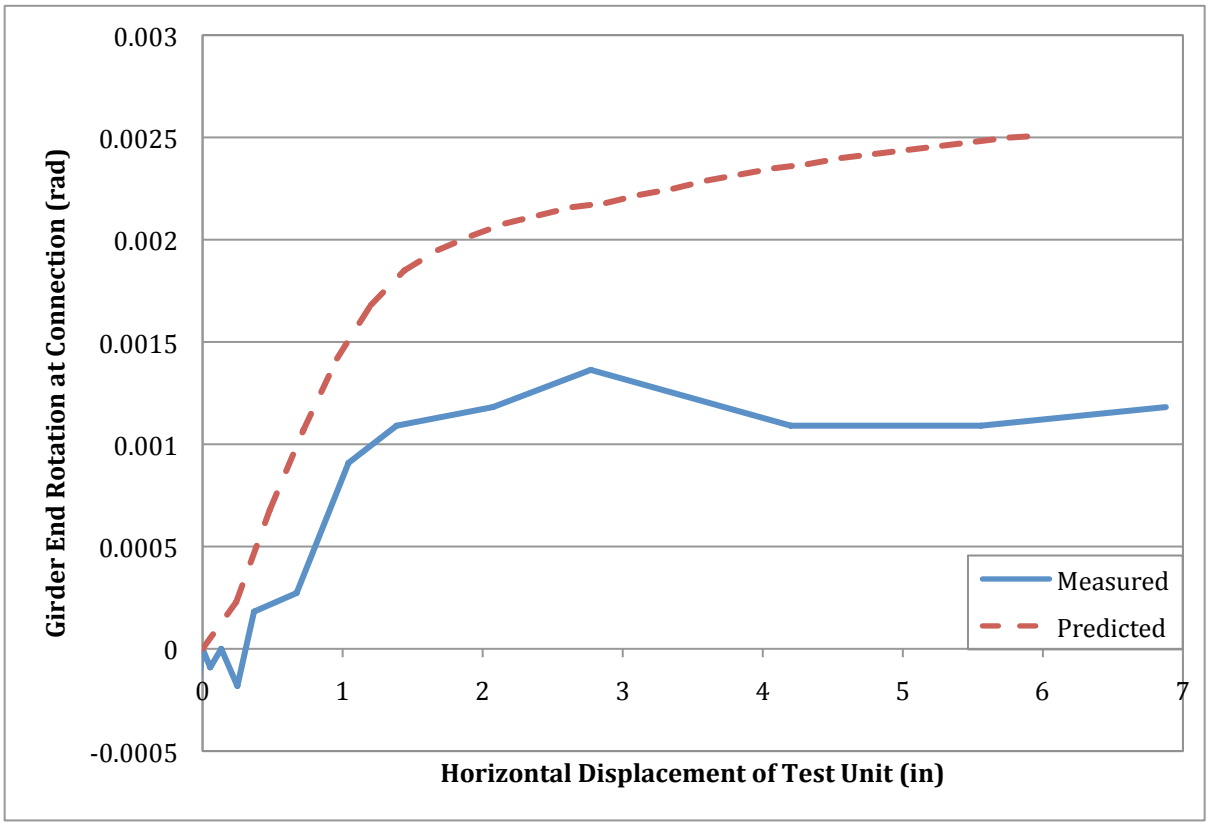

Figure 6.19: Center Girder End Rotation within Girder-to-Cap Connection vs. Horizontal Displacement during Phase 1 Testing

In order to better understand the effectiveness of the grillage model in predicting the behavior of the test unit, as well as any discrepancies between the measured and predicted responses, the response of various localized components were inspected. Since the majority of the overall force vs. displacement response of the structure was largely dependent on the behavior of the column, it was used as a starting point in investigating the localized behavior of the structure. The response of the column was broken into two main components: the primary displacement of the column and the effect that the flexibility of the superstructure had on the rotation at the top of the column, which would in turn influence the overall displacement observed at the top of the column. Investigating the behavior of each of the aforementioned components was crucial in identifying any discrepancies between the predicted and measured local behaviors, which could have influenced the global response. As shown in Figure 6.20, an outstanding agreement was observed between the predicted and

measured response for each of the displacement components of interest, as well as the overall, combined response of the column. This indicates that the column was modeled very well and that the effects of any discrepancies observed within the system might have been cancelled out once their effects reached the column. Since the horizontal displacement component that was used in the global force vs. displacement plot was recorded at the location of the actuator, it is likely that the observed discrepancies were due an inaccurate estimation of either the superstructure or connection stiffnesses. As a result, the displacements due to both stiffnesses were investigated further.

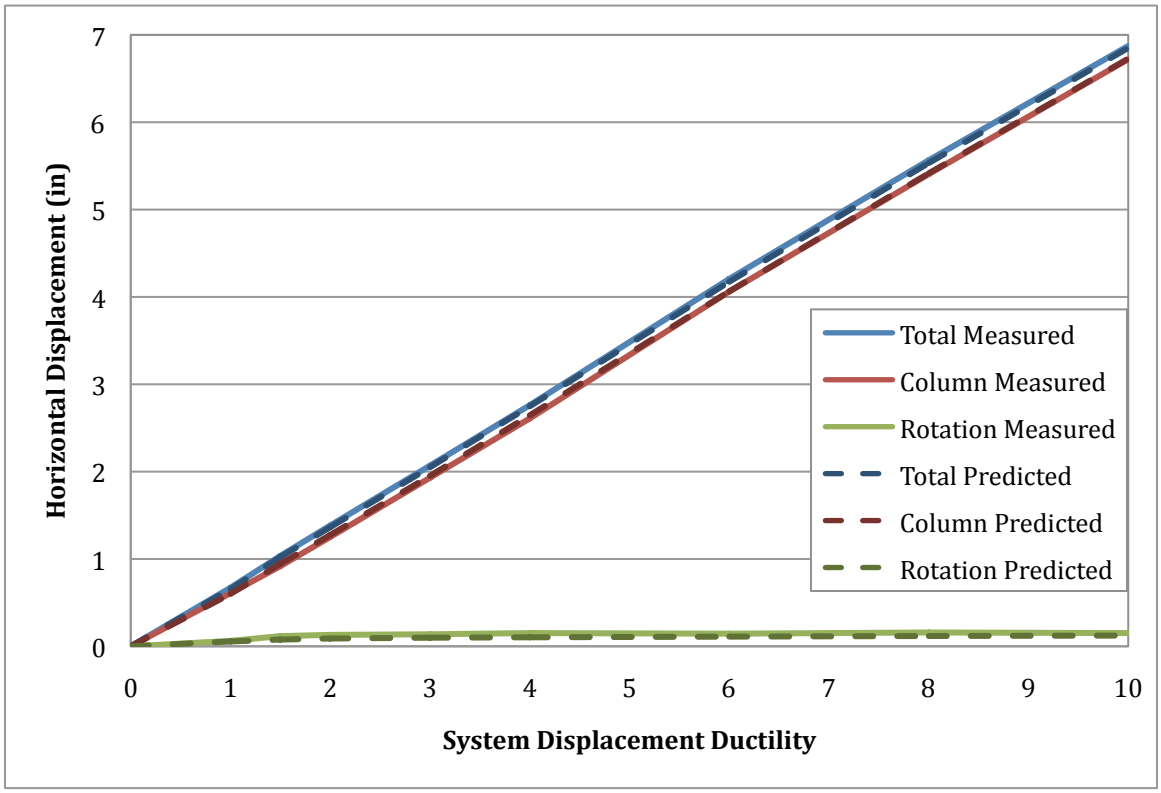

Figure 6.20: Comparison of Column Horizontal Displacement Components

The second localized component for investigation was the overall stiffness of the superstructure. Since an effective stiffness value was used for the composite superstructure section, as outlined in Chapter 4, it was understood that the initial stiffness would not match and that the stiffness would not provide a high degree of precision over the course of the entire test, as the test unit experienced varying degrees of stiffness degradation. Therefore, in

order to investigate this localized response, the vertical displacement at each potentiometer location was plotted along the length of the structure, for the center girder, at a displacement ductility level of 3 and 8. As expected, the measured and predicted stiffnesses do not agree perfectly at each ductility level. It may be observed that the effective superstructure stiffness used in the grillage model over-predicted mid-span displacements at ductility 3 and somewhat under-predicted the same displacements at ductility 8. However, over the entire length of the superstructure, the difference in stiffness is still considered satisfactory, as the displacements were very small relative to the overall girder length. It should be noted that a distance of zero, along the superstructure, was defined as the location of the cap and that the as-built connection detail was located on the negative side of the horizontal axis in Figures 6.21, 6.22, 6.23, and 6.24.

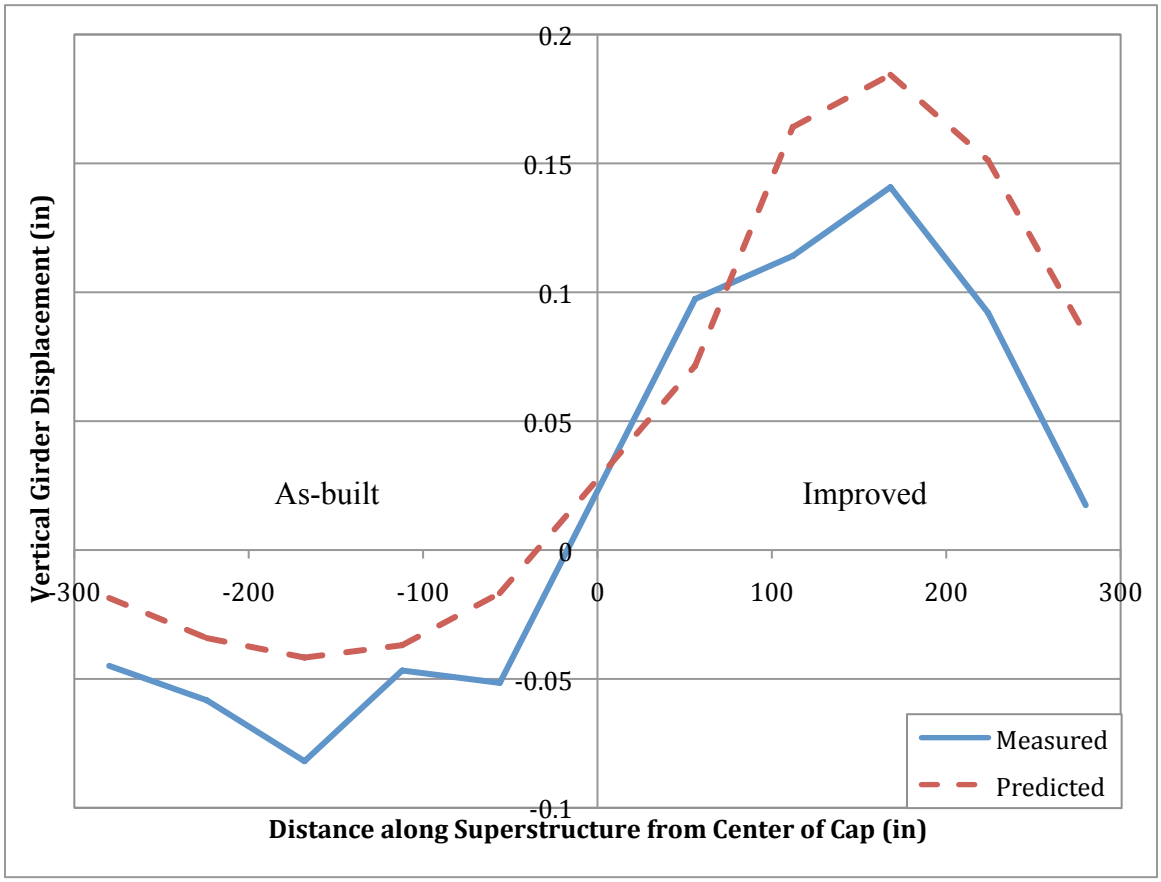

Figure 6.21: Center Girder Vertical Displacements at $\mu_\Delta = +3$

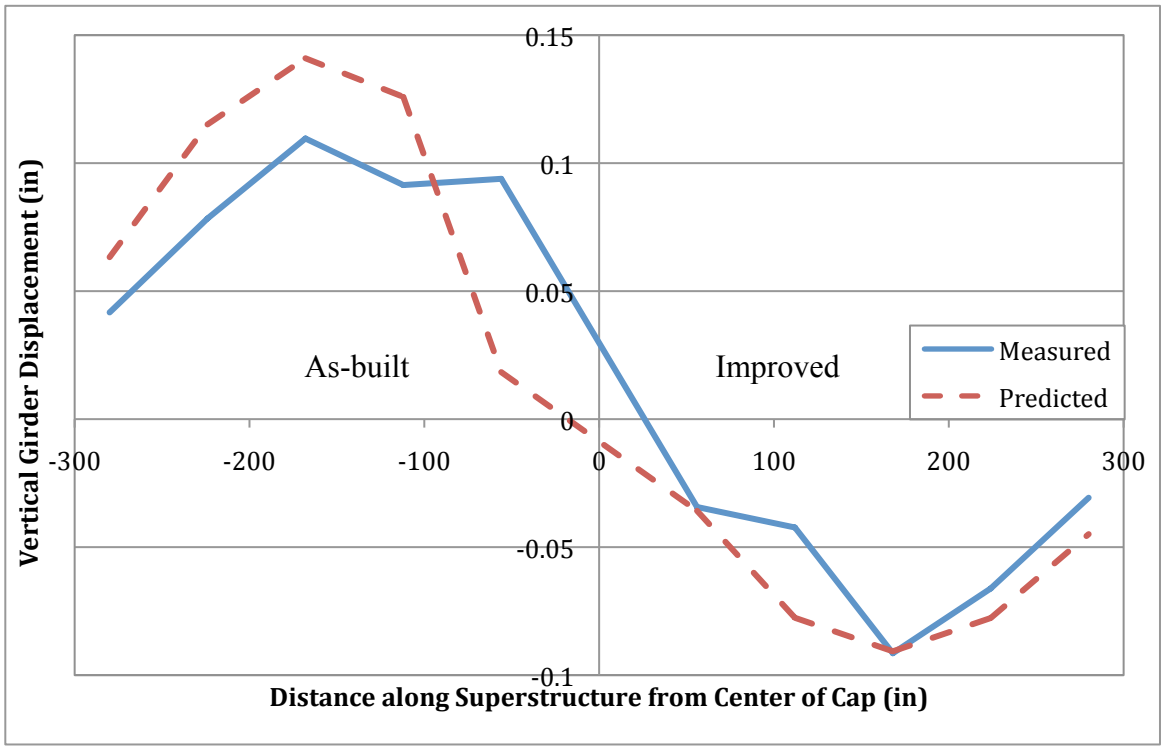

Figure 6.22: Center Girder Vertical Displacements at $\mu_\Delta = -3$

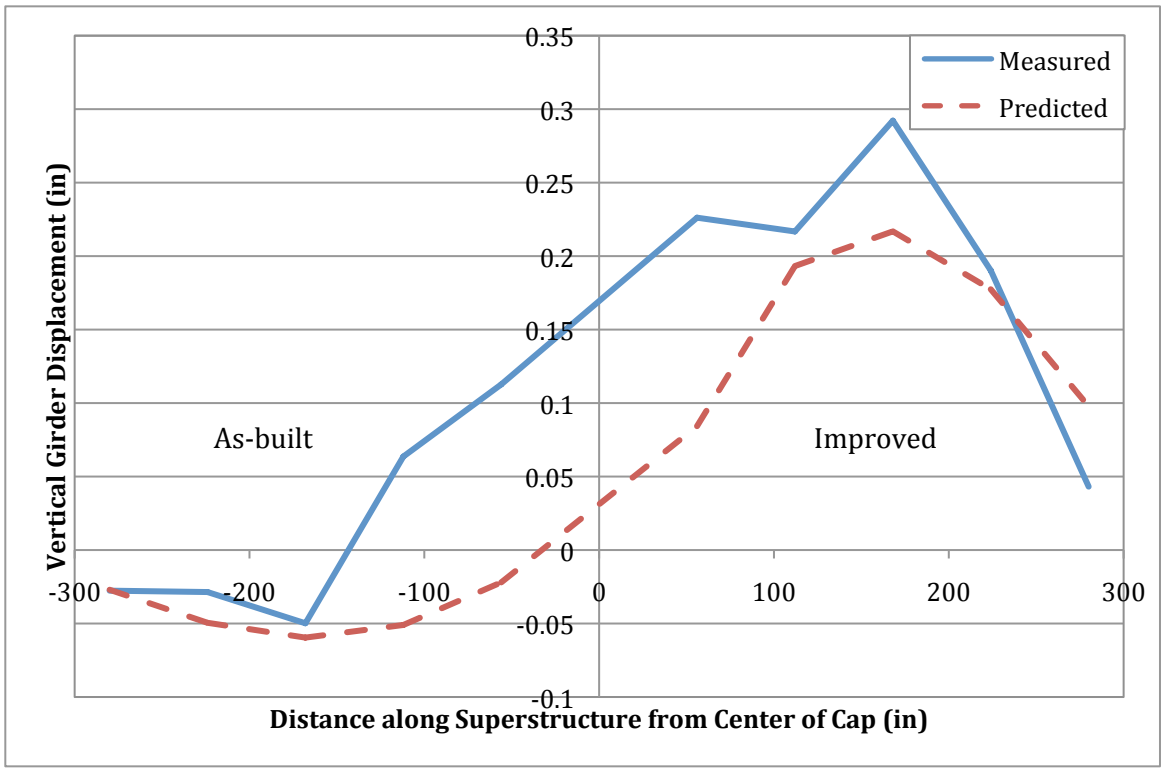

Figure 6.23: Center Girder Vertical Displacements at $\mu_\Delta = +8$

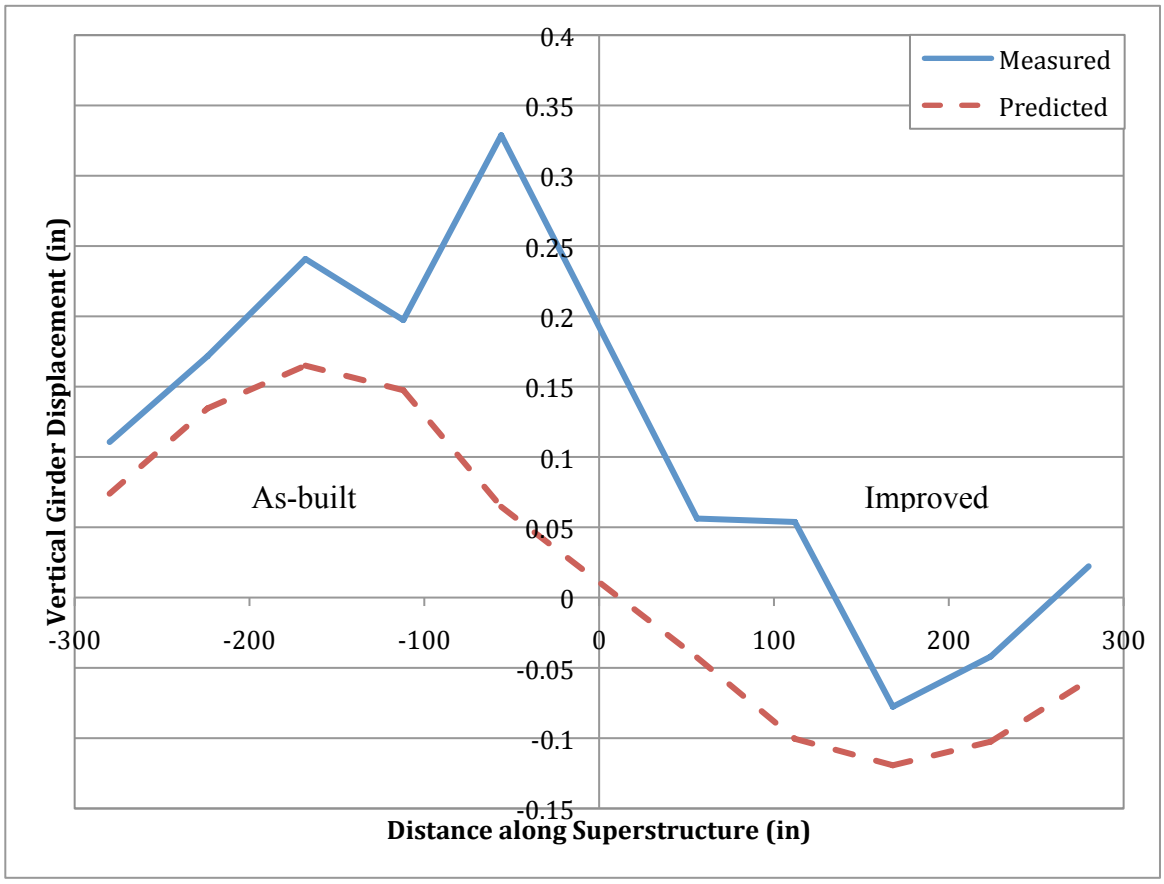

Figure 6.24: Center Girder Vertical Displacements at $\mu_\Delta = -8$

The final component was the remaining girder rotation responses for both connection details at the center girder. As shown below in Figure 6.25, when the underside of the girder was rotating away from the cap, thereby opening a gap on the underside of the girder-to-cap connection, for the improved connection detail, the predicted and measured responses matched reasonably well. The initial measured stiffness for the test unit was slightly higher than the predicted, but overall, the measured response indicated that the connection was more flexible than what was initially predicted. Furthermore, the response of the improved connection rotation, when subjected to a negative moment, which also corresponded to the aforementioned gap closing, also indicated that the connection was slightly more flexible than predicted; however, the initial stiffness showed a better correlation, as shown in Figure 6.26. The reasons behind these discrepancies were still somewhat unknown after Phase 1 of testing and, as a result, were further investigated during Phase 2 of testing (Section 6.2.4).

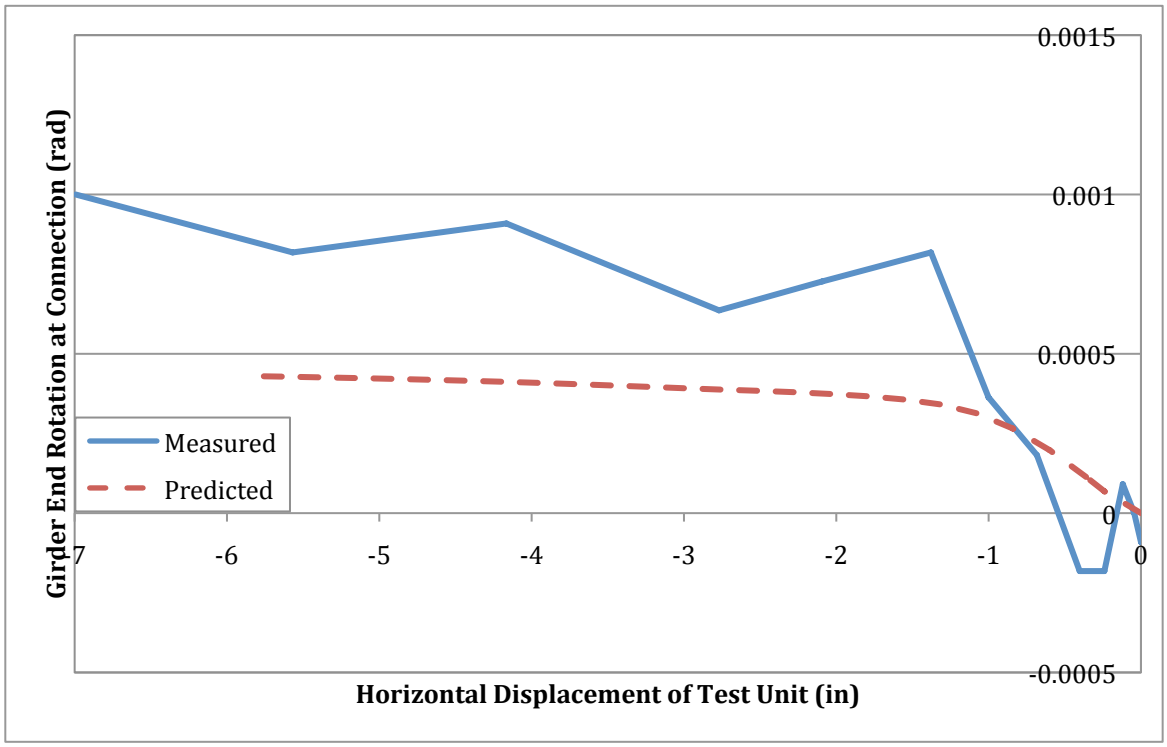

Figure 6.25: Center Girder Improved Connection Girder Rotation/Gap Opening

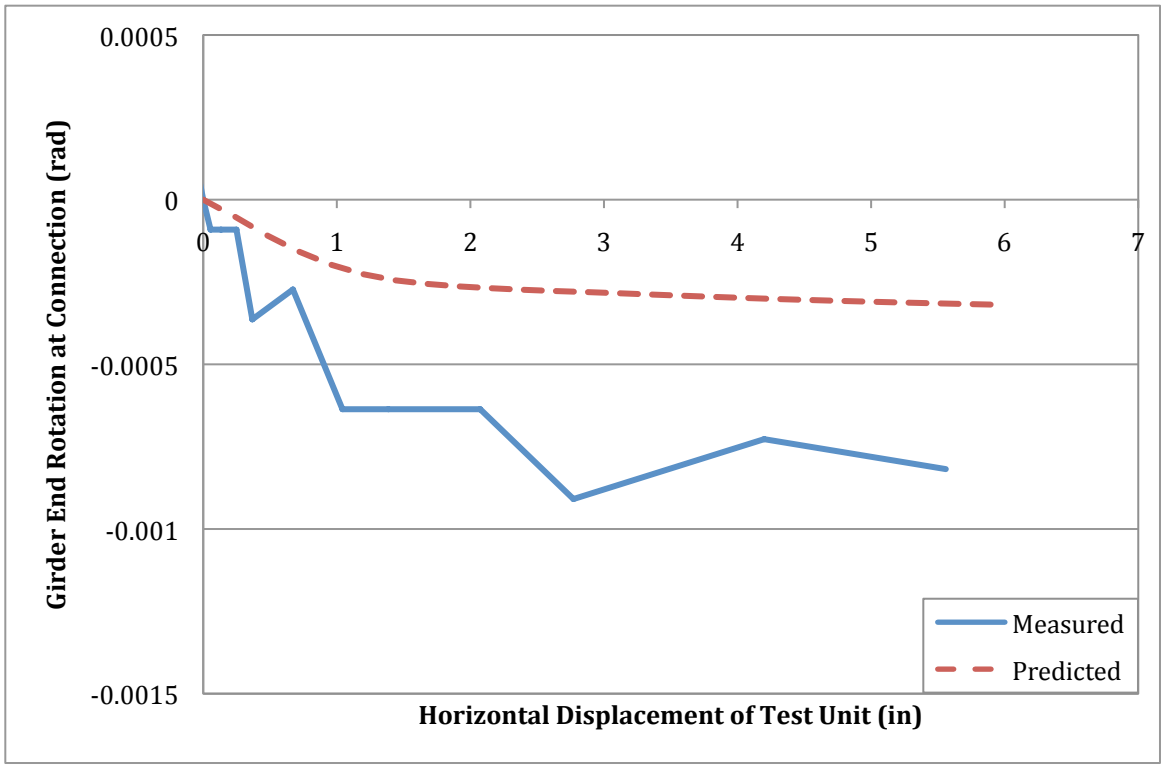

Figure 6.26: Center Girder Improved Connection Girder Rotation/Gap Closing

Overall, the seismic performance of the connections, and the test unit as a whole, was extremely good. The as-built girder-to-cap connections behaved as a fully continuous connection instead of a pinned connection, contrary to current assumptions presented in the Caltrans' Seismic Design Criteria regarding precast girder connections to an inverted-T bent cap. This observation suggests that minimal retrofit measures would be required in order to ensure a satisfactory performance of I-girder to inverted-T bridges in the field. Furthermore, it was established that a satisfactory agreement was achieved between the predicted response of the grillage model and the measured response of the test unit.

6.2 Phase 2 Test

As stated previously, Phase 2 of the testing involved a cyclic vertical push and pull test of each span simultaneously. This phase of the testing focused primarily on the localized behavior of each connection to assess its capacity.

6.2.1 Actuator Setup

Once Phase 1 of the testing was completed, the horizontal actuators on the South end of the superstructure were removed, while the horizontal actuators on the North end remained in place in case there was a need for additional stability within the system. The hold-down forces and whiffle tree were removed from the specimen and both sets of vertical actuators at the ends of the specimen were moved in to the location that the whiffle tree previously occupied. As mentioned earlier, the main beam of the whiffle tree was designed such that it could accommodate the mounting of the vertical actuators.

6.2.2 Loading Protocol

Both the removal of the hold-down forces and the change in boundary conditions, between Phase 1 and 2 due to the placement of the actuators, caused residual moments to develop within the connections, resulting in an unrealistic moment value within the connections. Therefore, in order to correct for the aforementioned effects, the total load in both the North and South sets of actuators was increased slightly to approximately 90 kips of upward force before the start of testing. This was done based on analytical results, which indicated that 90 kips of vertical load was required in each span in order to achieve the same

moment that was at the girder-to-cap interface at the end of construction, with all of the hold-down forces applied, which was defined as the unstressed state for the test unit.

Once the required actuator load was applied to each span, the superstructure was displaced through the following displacement levels, listed in the order in which they were performed: -0.25 in., -0.5 in., -0.75 in., -1 in., -1.5 in., +0.25 in., +0.5 in., +0.75 in. (the negative sign refers to a vertical downward deflections while the positive sign corresponds to a vertical upward deflection). This was done in order to capture the initial stiffness and elastic behavior of the system, so that an appropriate displacement increment and magnitude could be selected for the cyclic displacement levels. Following the initial low-level displacement increments, both superstructure spans were then cycled simultaneously through the following positive and negative displacement cycles: +1/-2 in., +1.5/-3 in., +2/-4 in., and +3/-6 in. Each of the aforementioned cycles consisted of three cycles to the given positive and negative displacements, with the exception of the final cycle. Since significant degradation of the as-built connection was observed at the final displacement level, only one half-cycle was used at +3 in. while two half-cycles were performed at -6 in. It should be noted that the positive and negative displacement magnitudes were not the same, as both connection details had a higher capacity for negative moments than for positive moments.

6.2.3 Phase 2 Observations

During the preliminary, low-level displacement half-cycles, only insignificant damage to the test unit was observed. Under negative displacements, the main observations were extensions of the cracks on the top of the deck that had formed during the horizontal testing phase. By the time the superstructure had been displaced by -0.25 in., it had already subjected the connection, on both sides of the bent cap, to a moment approximately 13% greater than the maximum moment that was achieved during the horizontal load test phase. It wasn't until a displacement of -1 and -1.5 in. that the majority of the reinforcement in the deck had begun to yield, as shown in Figure 6.27, which depicts the strain data for the deck reinforcement that was located at the stem of the inverted-T and above the center, and West intermediate and exterior girders, on the as-built side of the bent cap.

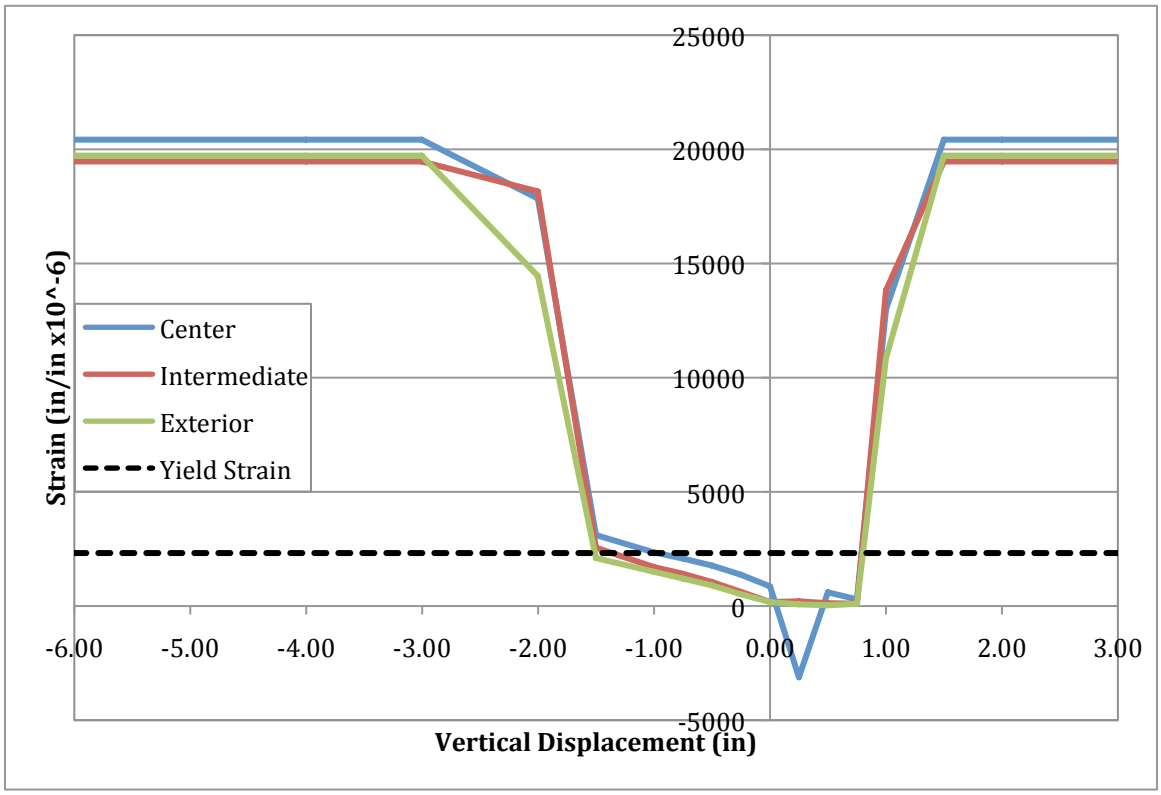

Figure 6.27: Vertical Displacement vs. Deck Reinforcement Strain Above the Inverted-T Stem on the As-built Connection Side of the Cap Beam at Each Girder

At -1.5 in., the majority of the new cracks that had formed on the top of the deck were within the cap region, some of which had become irregular, extending longitudinally along the length of the deck, which was believed to be due to debonding between the deck reinforcement and the concrete as a result of the high strain demand as witnessed in Figure 6.27. It was also observed at this stage that a significant number of the cracks in the deck, which had developed under negative moments on both sides of the bent cap, had extended and penetrated the full depth of the deck, cracking the top flanges of the girders closer to the cap beam. Some of these cracks had also begun to extend into the web of the girders as inclined shear cracks, as can be seen in Figure 6.28.

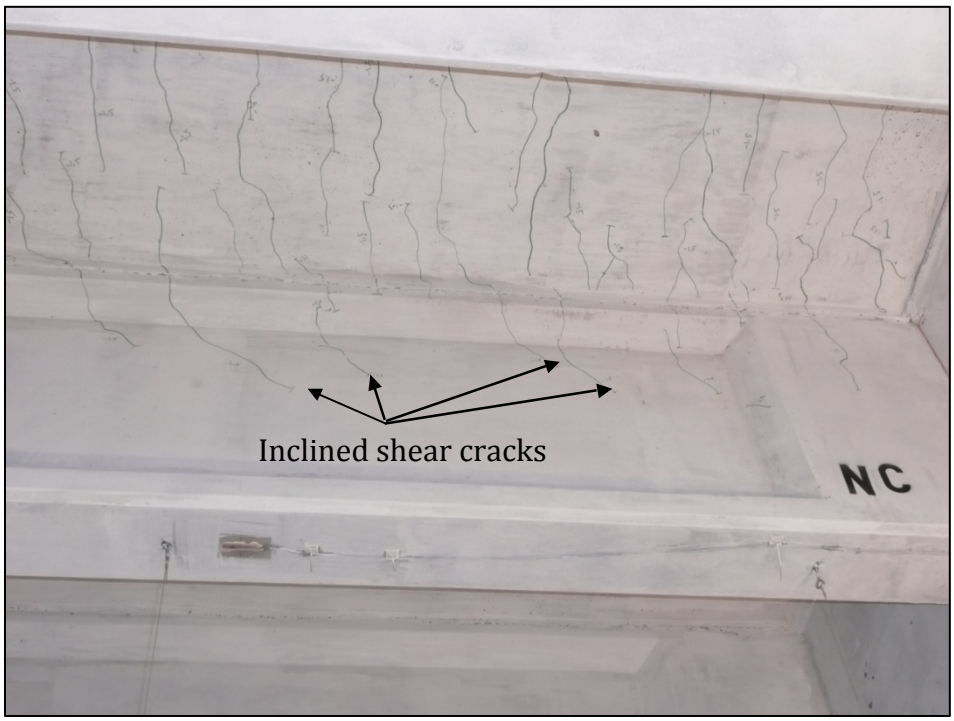

Figure 6.28: Inclined Shear Cracking Observed on the Center Girder on the Improved Connection Side at -1.5 in. Vertical Displacement

Under the positive low-level displacements, the main observation was also extensions of cracks that were formed during the horizontal testing phase. At a displacement of +0.25 in., the minor cracking that was observed during the horizontal load test, along the bottom surface of the cap-to-diaphragm interface, had extended all the way along the length of the cap beam. Some longitudinal cracks had also formed at the edges of the bottom flanges of the girders within the diaphragm, which indicated that the girders were attempting to pull out of the diaphragm and away from the cap beam. The aforementioned cracking was observed on both the as-built and improved connection sides of the cap. Once the superstructure had been displaced by +0.5 in., the as-built connection was subjected to a moment approximately 27% greater than the maximum moment achieved during the horizontal load test phase. At a displacement of +0.75 in., the improved connection side of the cap remained essentially unchanged and experienced no new damage from what was observed during the previous cycles of loads. However, the as-built side was beginning to experience some significant degradation. The gap between the bottom flanges of both the interior and exterior girders

and the cap beam had widened to a width of 0.2 in. The 1-in. thick grout along the bottom interface between the exterior girders and cap had also begun to separate and fall off of the connection, leaving a gap of approximately 1 in., as shown in Figure 6.29. Penetration cracks were also observed on the face of the diaphragm, in a circular manner, around each girder (Figure 6.30). This was likely due to the girders, together with the dowels, attempting to pull out of the concrete in the diaphragm.

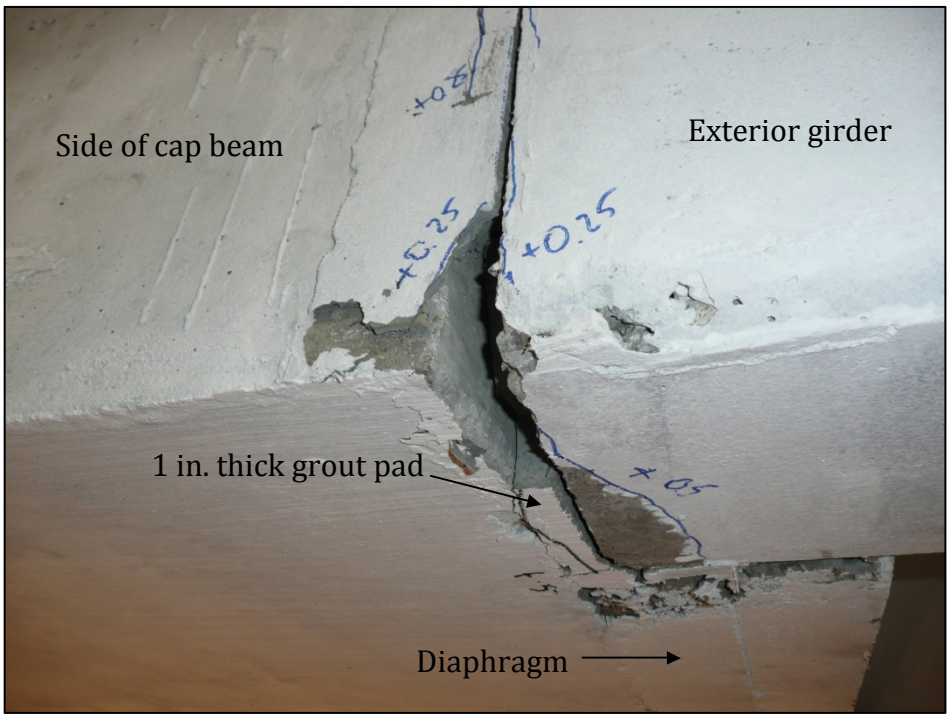

Figure 6.29: Partially Spalled Grout Pad at Girder-to-Cap Interface on the As-built Connection Side at +0.75 in. Displacement

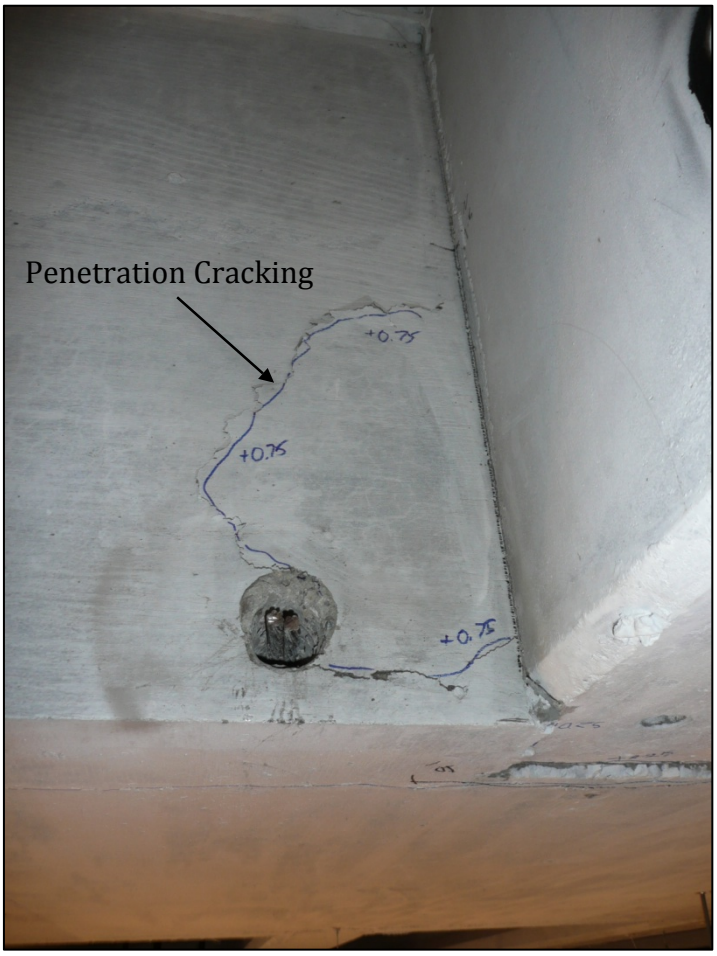

Figure 6.30: Penetration Cracks on the Face of the Diaphragm on the As-built Connection Side at +0.75 in. Displacement

During the first cycle, at a displacement of -2 in., a few new cracks had formed in the deck, while the majority of the existing cracks, on both connection sides, continued to extend and widen across the width of the deck. The most predominant cracks were located at the stem of the inverted-T and at the face of the diaphragm. The cracks at the stem of the inverted-T had a width of approximately 0.075 in., while the crack at the face of the diaphragm had an approximate width of 0.02 in. on the improved side of the connection and 0.025 in. on the as-built side, as shown in Figure 6.31. The observation of the cracks extending across the entire width of the deck indicated that all of the girders were being engaged in resisting the moment imposed upon the girder-to-cap connection. The gap

between the bottom flanges of the girders and the cap, due to the spalling of the grout along the interface, also appeared to have closed at this displacement level.

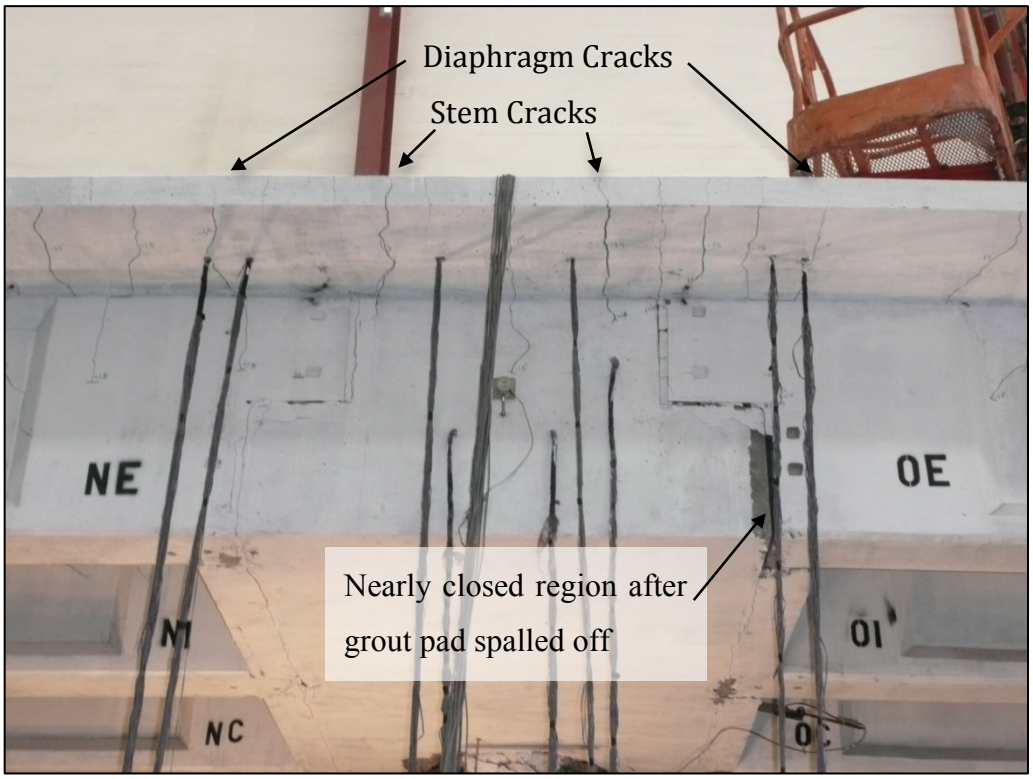

Figure 6.31: Deck Cracking Seen Near the Cap Beam at -2 in. Displacement

On the other end of the aforementioned cycle level, at an upward displacement of +1 in., the grout along the bottom of the interface between the girder and the cap continued to spall, likely due partially to crushing as well as a lack of a direct form of attachment to the cap beam, resulting in a significant loss of grout along the girder-to-cap interface on the as-built side. The penetration cracks on the face of the diaphragm were also much more pronounced on the as-built connection side of the cap beam. Significant crack opening and pull out was observed between the bottom flanges of all of the girders and the cap on the as-built connection side as well. The separation between the bottom flange and the cap was measured at approximately 0.4 in. for each girder. Furthermore, a significant crack, which signaled a separation, between the underside of the deck and the top of the diaphragm was

observed in all of the bays on the as-built connection side, which measured 0.075 in. in the exterior bay and 0.035 in. in the intermediate bay (Figure 6.32). The improved connection side remained essentially unchanged as no new cracking or spalling of the grout pad was observed. Finally, no concrete crushing was observed on top of the deck and no cracking was observed in the bottom flanges of the girders on either side of the cap beam.

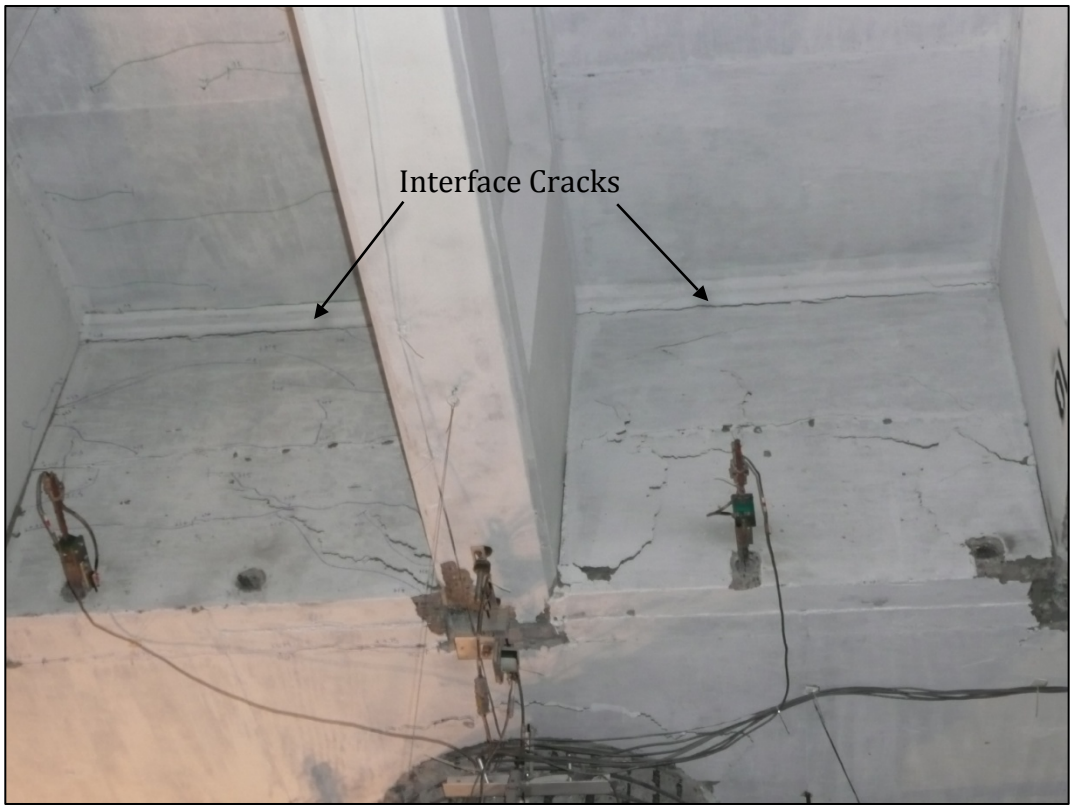

Figure 6.32: Deck-to-Diaphragm Interface Cracking at +1 in. Displacement

At a displacement of -3 in., the gap between the exterior girder and cap beam on the as-built connection side had completely closed. A significant number of crack extensions were observed on top of the deck. The crack along the stem of the inverted-T increased in width to 0.12 in. on the as-built side and 0.1 in. on the improved side, while the crack at the edge of the diaphragm increased to 0.075 in. on the as-built side and 0.04 in. on the improved side. Both of the aforementioned cracks extended all the way through the deck on the as-built

connection side. Some diagonal cracking was also noticed in the Southwest quadrant of the deck, near the location of the actuator.

When the superstructure was displaced to a level of +1.5 in., a significant gap opening was observed between the bottom flanges of the girders and the cap, on the as-built connection side of the cap beam. As the connection on the as-built side opened following the previous negative displacement cycle, concrete spalled off of the bottom flanges of the girders. The penetration cracks on the face of the diaphragm opened and increased in length significantly. A few new penetration cracks were also observed within each bay on the as-built side. At this point, the majority of the grout along the bottom of the interface between the girders and the cap had fallen out of the connection. The improved connection side of the cap beam, however, experienced no significant damage. All of the grout along the interface between the girders and the cap was still present, no penetration cracks were observed on the face of the diaphragm, and the deck did not appear to have separated from the top of the diaphragm on this side. For all practical purposes, the improved connection side appeared undamaged.

No significantly new observations were made on either side of the cap beam when the girders were subjected to -4 in. of displacement. As the as-built connection closed, following the previous positive displacement cycle, concrete spalled off of the diaphragm, exposing some of the reinforcement between the cap and the diaphragm. On top of the deck, increased diagonal cracking was observed throughout and a fairly considerable amount of new flexural cracking was observed over the cap region.

At a displacement of +2 in., very large gap openings were observed on the as-built connection side, between the bottom flanges of the girders and the cap. Significant damage was observed within the diaphragm, as the penetration cracks increased significantly and the diaphragm itself began to break away from the cap beam, as shown in Figure 6.33. No new damage was observed on the improved connection side of the cap beam. However, based on the force-displacement plots and the fact that the crack in the deck at the top of the stem of the inverted-T and the cap was larger than the crack between the bottom flange of the cap and the girder, it was clear that the cap was rotating about the plastic hinge in the top of the column, which had formed during the first testing phase, and the hinge that had formed on

the as-built connection side of the cap as the connection degraded. As a result, it was not possible to develop the required moment or rotation to exercise the improved girder-to-cap connection to its full capacity, which explained the lack of degradation of this connection region. This was further verified when the protocol was changed so that the South actuators were held at zero displacement, while the North side was displaced by +2 in. The cap beam continued to rotate about the column plastic hinge and the as-built connection, which dictated the response on the improved connection side by limiting the moments and rotations generated and again prevented the improved connection from being isolated and exercised. However, the improved connection during the test was subjected to a 10% higher maximum positive moment than that applied to the as-built connection at the same displacement level of +1 in.

Figure 6.33: Damage to As-built Connection Exterior Girder at +2 in. Displacement

The final portion of the test was completed using the original load protocol that was developed. Both sides were displaced by -6 in., followed by +3 in., and a final cycle to -6 in, shown in Figures 6.34 and 6.35. Based on the force-displacement plots for the structure at -6 in. during the test, it appeared as though both connection details still had some additional negative moment capacity, as a significant drop in strength was not noted. However, when the structure was cycled to +3 in., a 42% drop in strength was noticed, which indicated that the as-built connection detail had already reached its ultimate capacity. Therefore, the ultimate displacement for the positive as-built connection was defined as the point at which the strength had decreased by 20% from the maximum force that was applied, which corresponded to a displacement of approximately 1.5 in. This was also apparent by observing the significant amount of damage and pull out of the girders that was observed at a displacement of 1.5 in., as well as the subsequent displacement cycles. Therefore, it was decided that the behavior of the as-built connection had been adequately captured and the test was stopped.

Figure 6.34: Displaced Test Unit at -6 in. of Displacement

Figure 6.35: Overall Response of Test Unit at +3 in. of Vertical Displacement

6.2.4 Phase 2 Test Results

The structure achieved a maximum positive displacement of 3 in. and a maximum negative displacement of 6 in. Both the positive and negative responses were as good, if not better than expected. In fact, the force vs. displacement plot indicated that the structure still had additional negative moment capacity when the test was terminated, as a significant drop in strength was not noticed. Therefore, it is likely that a displacement greater than negative 6 in. could have been achieved. However, extensive and significant cracking was noticed in the deck at the end of the test, with the largest cracks corresponding to the stem of the inverted-T and the outer edge of the diaphragm. Since the cracks spanned the entire width of the structure, it was demonstrated that all of the girders were actively engaged in resisting the applied moment. Finally, as noted earlier, the response of each connection detail was not adequately isolated and thus, the improved connection detail was not fully tested. As the as-built connection yielded, the entire cap beam began to rotate about the column plastic hinge and the as-built connection, thereby limiting the forces and rotations experienced within the improved connection detail.

A comparison of the data collected against the predictions based on the SAP2000 grillage model for the total force applied to the superstructure on the as-built connection side of the bent cap vs. the relative girder displacement, established by subtracting the

displacement of the string potentiometer located closest to the center of the cap beam and the actuator displacement, is shown in Figure 6.36. A relative girder displacement, rather than the displacement of the actuator, was plotted against the force applied to the superstructure in order to remove some of the errors in the measured displacements due to the rotation of the cap beam about the as-built connection and top column plastic hinge. Although the predicted responses captured the general trend adequately, there were some discrepancies observed. For example, the connection actually achieved a greater moment resistance than what was predicted under positive moments while a lower than predicted resistance was seen under negative moments. The increased positive moment resistance was likely due to the increased concrete strengths that were achieved at the time of testing, thereby increasing the stiffness of the members, but not included in the model. However, it is seen that the effective superstructure stiffness values that were input into the grillage model appeared satisfactory for predicting the stiffness of the system.

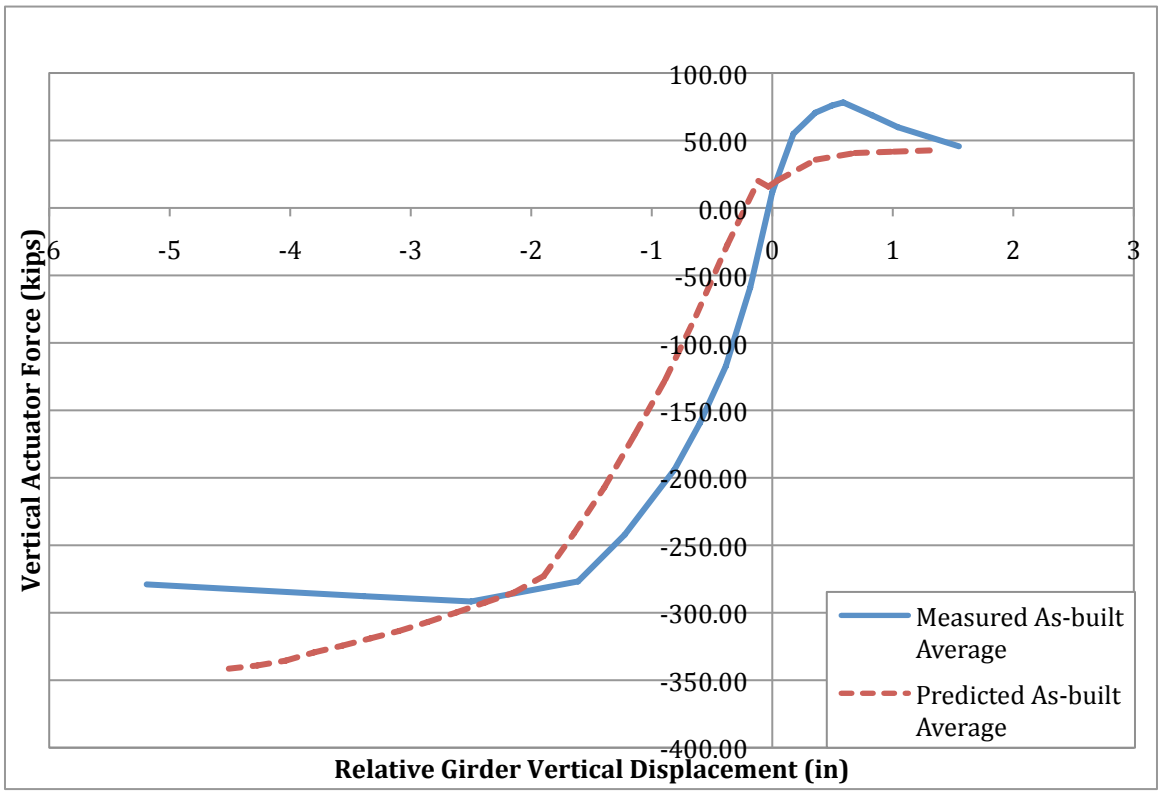

Figure 6.36: Predicted vs. Measured Total Force vs. Relative Displacement for As-built Connection

The connection also achieved larger rotations than were initially predicted, as shown in Figures 6.37 and 6.38. At the end of the testing, it was apparent that the dowel bars within the girders had punched out of the diaphragm, especially at the exterior girders, rather than being fully embedded in the diaphragm and contributing to a fully effective dowel bar action, as shown in Figure 6.39. This was further demonstrated by examining the strains along the bottom, most extreme row of dowels (Figure 6.40), which showed that the strains within the dowels didn't gradually increase and surpass the expected yield strain, as required for a fully effective dowel bar action to develop, until the connection had already reached its ultimate displacement. Additionally, the shear friction mechanism that was expected to take place between the girder and the diaphragm was not as dominant as expected, as the concrete around the girder and within the entire diaphragm, cracked and spalled due to the punching of the dowels. The lack of these primary mechanisms occurring within the connection is the likely explanation for the increased displacement for the girders that was somewhat observed, due to an increase in rotation within the connection. Also, the lower negative moment resistance that was observed within the connection was most likely due to the spalling of the grout pad along the girder-to-cap interface. The loss of this pad increased the rotations experienced within the connection and also effectively decreased the lever arm for the actuator forces about the connection during lower displacement levels, before the girder and the cap came back into full contact with one another.

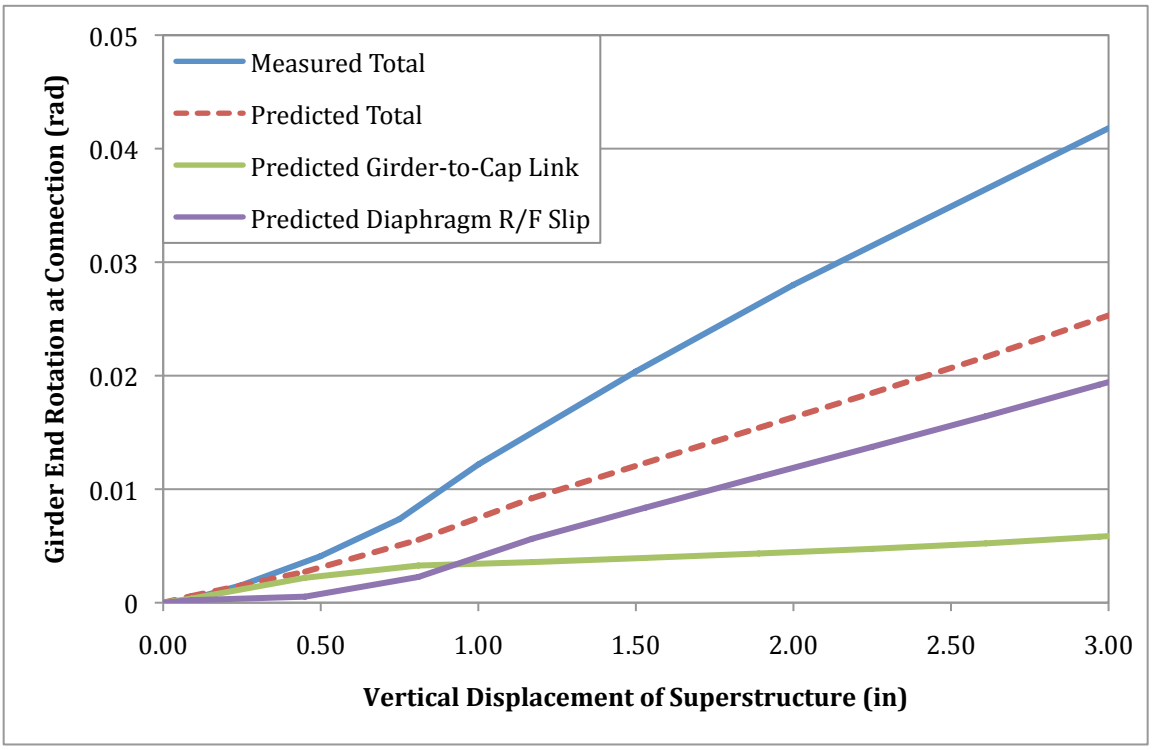

Figure 6.37: Positive Vertical Displacement vs. Center As-built Girder Rotation

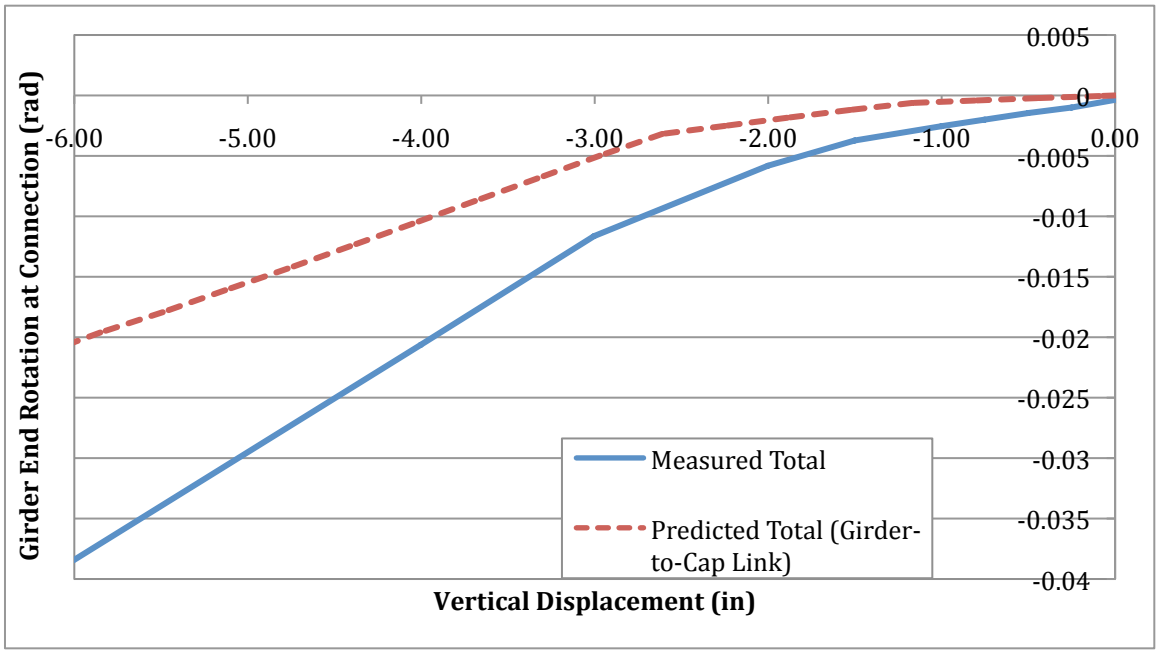

Figure 6.38: Negative Vertical Displacement vs. Center As-built Girder Rotation

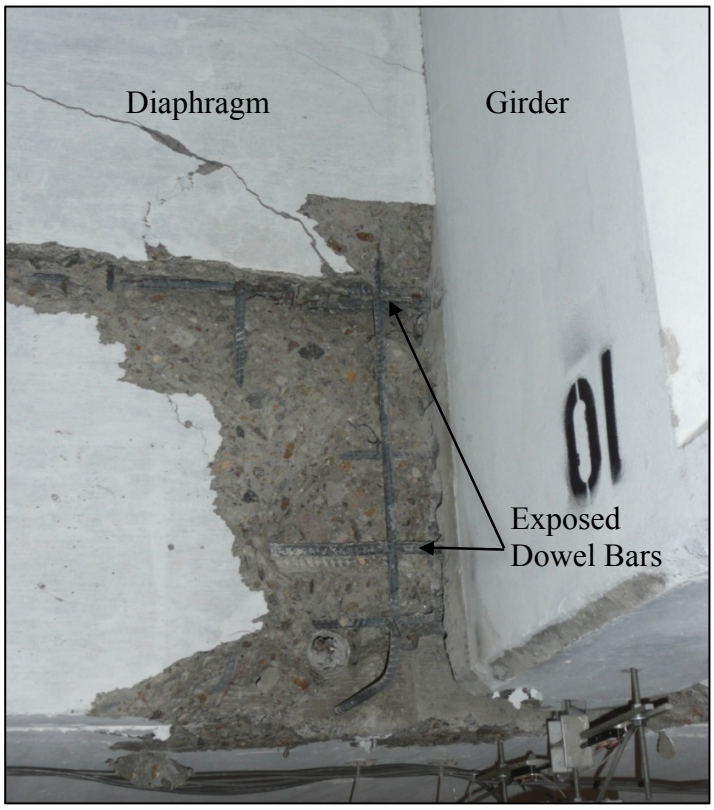

Figure 6.39: Damage Surrounding the Interior Girder in the As-built Connection Region

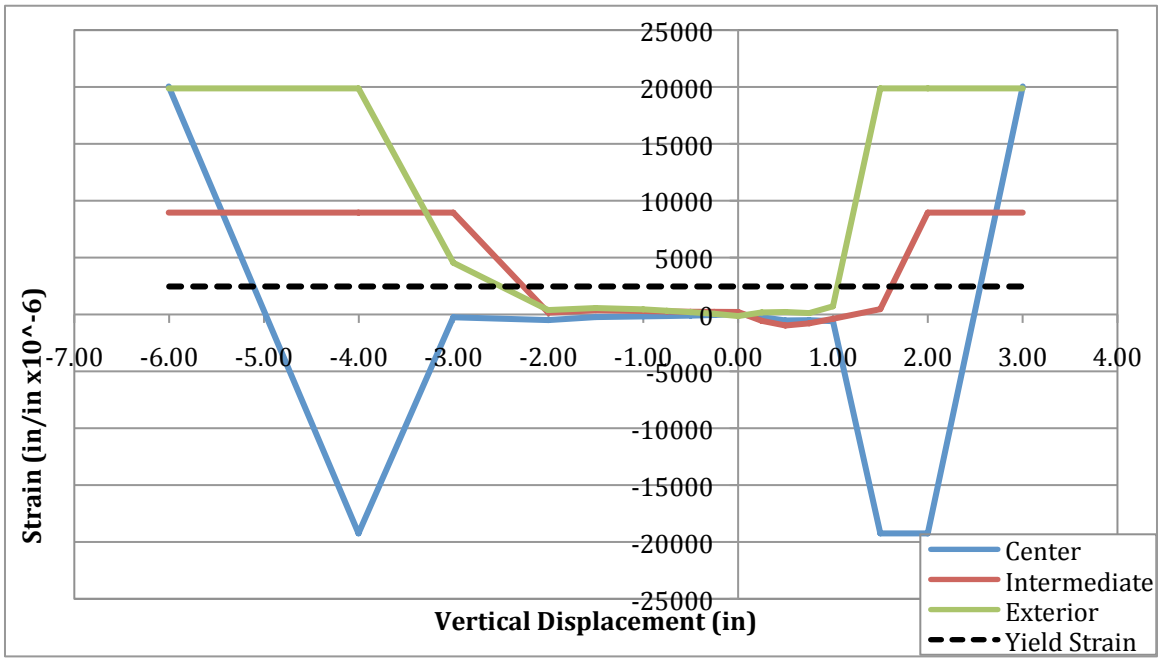

Figure 6.40: Vertical Displacement vs. Bottom Row Dowel Bar Strain on the As-Built Connection Side of the Cap Beam

The participation of these mechanisms was further investigated within the grillage model by breaking the total predicted rotation into its individual link element components. This was done in order to get identify which component was the most significant cause of the discrepancies. Both Figures 6.37 and 6.38 indicate that the girder-to-cap link element was the primary source behind the difference between the measured and predicted responses. As shown in the aforementioned figures, the defined properties for the girder-to-cap link element were too stiff and underestimated the rotations experienced within the connection. As discussed, this was due to the lack of a fully developed dowel bar action, shear-friction mechanism, and the loss of the grout pad along the girder-to-cap interface. Unfortunately, the 3-D finite element model that was used to derive the girder-to-cap link element properties did not adequately account for the degradation of the diaphragm, which in turn resulted in an over-prediction in regard to the contribution of each mechanism and the overall strength and stiffness of the connection. In order to improve the accuracy of the grillage model predictions, it is recommended that the 3-D finite element model be revised to more accurately reflect the measured behavior of the test unit, thus improving the derived input response used in the grillage model.

In general, the as-built connection detail performed much better than expected and confirmed that it can act as a fully continuous connection, for both positive and negative moment and shear, until the column hinge is fully developed under combined gravity and seismic loads. It was clear that the connection had a significant moment resistance beyond what is currently assumed in design practice and did not exhibit significant damage until the superstructure was displaced vertically by -3 and +1 in., at which point the moment in the connection was approximately 4.9 and 1.4 times greater than the maximum moment applied during the horizontal load test phase, respectively. In contrast, it is suggested in Caltrans' Seismic Design Criteria that these positive moment connections be assumed to act as pinned connections.

Chapter 7. CONCLUSIONS

7.1 Overview

The goal of the research presented herein was to gain a better understanding of the seismic behavior, as well as the overall moment resistance and shear transfer capability, of a precast I-girder to inverted-T bent cap bridge connection using analytical and experimental investigations. An improved connection detail was also requested by Caltrans in order to ensure the development of a fully continuous moment connection between the superstructure and bent cap. Though additional work was performed for this project (Thiemann, 2009), the summation of which will be presented in a report to Caltrans, the focus of this thesis was on the development of a finite element grillage model of the test unit as well as the construction and testing of a 50% scale test unit.

Currently, Caltrans engineers design bridges that incorporate an inverted-T bent cap and precast girders with no confinement requirement at the top of the column. This is because the current, as-built design of the precast girder-to-cap connection region is conservatively assumed to be a pin connection, based on recommendations from Caltrans' Seismic Design Criteria (Caltrans, 2006) regarding the use of precast components, which results in a very inefficient and expensive design for these structures. However, it is very likely that these as-built conditions have considerable positive and negative moment resistances, which have the potential for significant cost savings and improved design efficiency. Furthermore, given the extensive structural damage that occurred to bridges during the Loma Prieta earthquake, Caltrans has made it a priority to investigate and ensure that all bridge structures will perform adequately during a future seismic event (Housner & Thiel, 1990).

Therefore, a prototype I-girder to inverted-T bent cap bridge was designed by PBS&J and used to develop a 50% scale test unit. The test unit was then modeled using finite element and the physical structure was constructed and tested. Using information obtained from previous studies regarding moment continuity between girder-to-cap connections, as outlined in the literature review presented in Chapter 2, an improved connection detail was

proposed in order to provide a dependable fully continuous moment connection. As outlined in Section 3.3, the improved connection was established by grouting untensioned prestressing strands along the length of the girders and through the girder-to-cap connection into the inverted-T bent cap.

As discussed in Chapter 4, a finite element grillage model of the test unit was created using SAP2000, a finite element software, and was used to better analyze and predict the behavior of the test unit during both phases of testing. The properties and definitions used to define specific components of the test unit were first validated against an alternate, 3-D finite element model of the test unit (Thiemann, 2009), as well as preliminary data collected from the test unit. It was then possible to use the grillage model to make predictions, and identify areas of interest, regarding the behavior of the test unit. Finally, comparisons between the measured response of the test unit and the preliminary predictions were performed in order to verify the sufficiency of the model and identify any possible modifications that could have been made in order to achieve more accurate results. A monotonic pushover analysis of the grillage model found that the as-built connection detail would have a significant moment capacity and would adequately allow for the formation of a plastic hinge at both the top and bottom of the column in a seismic event. However, it was expected that the connection would sustain damage as a result. Additionally, it was concluded that the improved connection detail would provide a fully continuous moment connection between the superstructure and inverted-T bent cap.

Based on the conclusions drawn from the grillage model, the test unit was constructed and subjected to two phases of testing at the Powell Laboratory of UCSD in order to validate the results of the finite element grillage model and provide more information regarding the performance of the inverted-T bent cap connection. The test unit consisted of a single, circular column, an inverted-T bent cap, and two half spans consisting of five I-girders on either side of the bent cap. One span incorporated Caltrans' current, or as-built, connection detail between the I-girders and the inverted-T bent cap, whereas the other span incorporated the improved connection detail. During the testing, it was expected that the connections between the I-girders and inverted-T cap, in the test unit, would behave as fully continuous

connections and thus the top end of the column was designed with adequate amounts of confinement reinforcement.

The first phase of testing simulated the combined effects of gravity and seismic loading on the inverted-T test unit. The gravity load effects on the test unit were simulated using two sets of vertical tie-downs and four actuators positioned in the vertical direction. In addition, two horizontal actuators placed at each end of the superstructure simulated the horizontal seismic load effects. As part of the horizontal load test, the test unit was subjected to the following positive and negative horizontal force and displacement ductility levels: $\pm 0.25F'_y$, $\pm 0.5F'_y$, $\pm 0.75F'_y$, $\pm 1.0F'_y$, $\pm\mu_\Delta 1$ x3, $\pm\mu_\Delta 1.5$ x3, $\pm\mu_\Delta 2$ x3, $\pm\mu_\Delta 3$ x3, $\pm\mu_\Delta 4$ x3, $\pm\mu_\Delta 6$ x3, $\pm\mu_\Delta 8$ x2, $\pm\mu_\Delta 10$ x1, where F'_y and μ_Δ correspond, respectively to, the first yield force and displacement ductility of the test unit. Each of the force-controlled levels, denoted as a multiplication of F'_y, consisted of one cycle to the corresponding positive and negative force. Similarly, each of the displacement-controlled levels were cycled to the corresponding positive and negative displacement at the given ductility level; however, three cycles were performed at each level, with the exception of $\mu_\Delta 8$ and $\mu_\Delta 10$, in order to capture any effects due to degradation of the structure. Since initial predictions did not expect the structure to achieve $\mu_\Delta 10$, and the column needed to be somewhat preserved for the vertical load testing phase, the testing at $\mu_\Delta 8$ was limited to two cycles while testing at $\mu_\Delta 10$ was terminated after one cycle.

The second phase of testing expanded upon the results and observations made from the horizontal seismic load test, by subjecting the girder-to-cap connections to a larger moment demand and attempting to quantify the ultimate moment capacity of each connection type. This was achieved by mounting two vertical actuators, on both the North and South spans, at what was the location of the hold-down force during the horizontal testing phase. Accordingly, the actuators were mounted at a distance of 16 ft from the center of the cap beam, on both sides. The superstructure was then subjected to the following positive and negative horizontal displacement levels: -0.25 in., -0.5 in., -0.75 in., -1 in., -1.5 in., +0.25 in., +0.5 in., +0.75 in., +1 in./-2 in. x3, +1.5 in./-3 in. x3, +2 in./-4 in. x3, +3 in. x1/-6 in. x2.

7.2 Summary of Test Results

7.2.1 Phase 1

Overall, the performance of the test unit was extremely good in resisting the simulated combined gravity and horizontal seismic load. The as-built girder-to-cap connections behaved as a fully continuous connection instead of a pinned connection. Contrary to what was expected as a result of the aforementioned grillage and 3-D finite element analysis, as well as the current assumptions in Caltrans' Seismic Design Criteria regarding precast connection details, degradation of the positive as-built connection was not observed, which could have been due to limited flexural cracks developing in the girder-to-cap regions. Additionally, the improved girder-to-cap connection detail performed as expected, as a fully continuous connection, and did not experience any significant damage or degradation throughout the testing. Therefore, as intended, plastic hinges developed at the top and bottom column ends and a maximum horizontal displacement of 7 in., corresponding to a displacement ductility of 10, was achieved. Buckling of several column longitudinal bars, as well as the beginning of a confinement failure, was observed in the plastic hinge region as the test unit neared its ultimate displacement capacity.

7.2.2 Phase 2

The second phase of testing was very successful in that it adequately exercised the as-built connections, established the required moment capacities, and ensured a satisfactory shear transfer through the as-built connection. It was clear that the as-built connection detail had a significant capacity for both positive and negative moments. The as-built connection reached its ultimate capacity at a displacement of +1.5 in. and seemed to still have a reserve capacity at -6 in. even though the test was terminated. Unfortunately, due to the progressive failure of the as-built connection during this test, and the damage to the column ends that was sustained during the horizontal seismic load test, the improved connection was not tested to its full capacity. However, the superior performance of the improved connection over the old connection was clearly demonstrated by the test. Since the as-built connection detail degraded before the improved connection, reaching its capacity, it is apparent that the presence of the grouted, untensioned strands improved the performance of the connection

detail to the extent that useful design recommendations can be formulated for inverted-T bridge bents used to support precast I-girders.

7.3 Conclusions

Based on the observations made during both phases of testing, as well as the results of the finite element grillage model, the follow conclusions can be drawn:

- Both the as-built and improved girder-to-cap connection details performed essentially as a fully continuous connection and showed little to no degradation during the horizontal load testing (Phase 1). The positive and negative moment capacities of each connection detail were more than adequate to fully develop a plastic hinge at both the top and bottom of column. Finally, both connection details successfully transferred shear forces from the superstructure into the cap beam.
- The as-built connection detail, though it did experience significant degradation, performed adequately during the vertical load testing (Phase 2). The as-built connection did not experience significant degradation until the positive and negative moment within the connection was approximately 4.9 and 1.4 times greater than that of the maximum moment applied during the horizontal load test. However, the contribution of the dowel action of the embedded dowels between the girder and diaphragm, as well as the shear-friction between the girders and the diaphragm, was not as significant as what was predicted. The improved connection detail seemed to perform better than the as-built detail during the vertical load testing; however, the full moment capacity of the connection was not established, as noted in Chapter 6.
- Based on both Phase 1 and 2 test results and observations, it was concluded that only the top of the column required retrofitting in order to accommodate the formation of a plastic hinge and achieve a satisfactory seismic response. However, it should be noted that doing so will increase the column shear demand, as well as other demands within the system, which should be examined to ensure that the bridge can handle the new force demands. If the top of the column were retrofitted, a maximum horizontal displacement ductility of 10, corresponding to 14 in. of displacement, could be expected for the prototype bridge structure.

- Overall, the grillage model force vs. displacement and girder end rotation at the face of the cap vs. displacement predictions compared very well to the measured response of the test unit for both phases of testing. This proved that the grillage model is an adequate means of predicting the behavior of both current and future inverted-T bridge structures.
- The results of the grillage model could be improved by updating the concrete properties to reflect the compressive strengths recorded at the time of testing, recalculating the column plastic hinge link properties to reflect the increased concrete strengths, and improving the girder-to-cap link element properties by revising the 3-D finite element model that was used in their derivation in order to more accurately reflect the observed behavior of the test unit.
- When using a grillage model to predict the behavior of an I-girder to inverted-T bent cap bridge, subjected to a typical gravity and seismic load combination, it is recommended that Caltrans designers model the connection by simply elastically connecting the members at their joints, thus coupling their effective stiffnesses and degrees of freedom at common nodes. As shown in Figure 7.1, removing the complicated nonlinear link elements within the connection region of the grillage model that were discussed in Chapter 4, and instead elastically connecting the girder elements directly to the cap beam, produced essentially the same result for the predicted force vs. displacement response during the horizontal load testing.

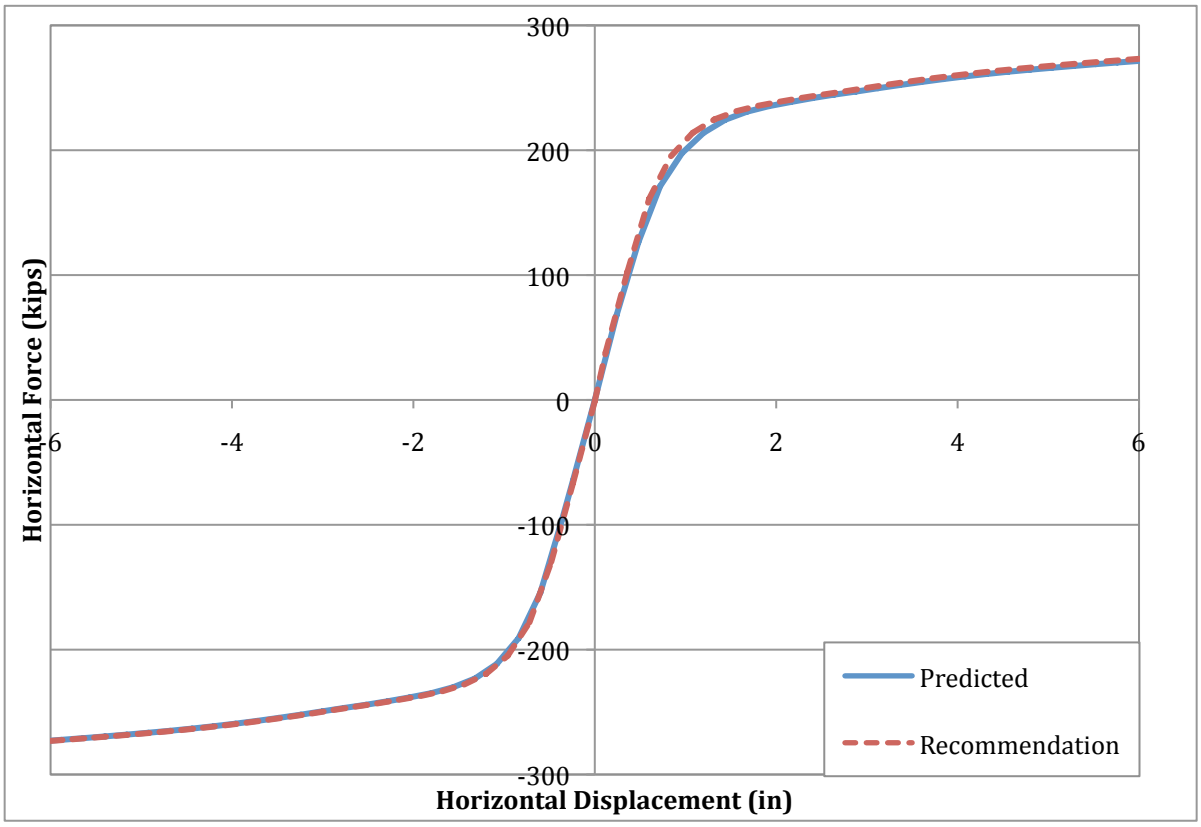

Figure 7.1: Recommended Girder-to-Cap Connection Grillage Modeling Force vs. Displacement Response

7.4 Recommendations for Future Work

The observations made during both Phase 1 and Phase 2 of the test suggest that minimal retrofit measures are required in order to ensure a satisfactory performance of I-girder to inverted-T bent cap bridges in the field. If it can be shown that vertical accelerations would not cause any significant damage to the as-built positive moment connections, seismic retrofit for the existing inverted-T bridges is required only at the column top so that the girder moments can be resisted and a plastic hinge could be developed at this location, which will result in significant cost savings. Though it was observed, at low displacement levels, that the improved connection detail increased the capacity of the connection and prevented the same damage from occurring that was observed within the as-built connection region, the true behavior and ultimate capacity of the improved connection detail was not obtained. Therefore, it is recommended that future research be conducted in

order to better investigate the behavior and capacity of the improved connection detail. In order to better understand and provide a higher degree of confidence in the performance of the prototype I-girder to inverted-T bent cap bridge, it is recommended that the findings and analysis techniques presented in this thesis be used to create a grillage model of the prototype. Finally, it is noted that the good performance of the test unit not only encourages precast construction but also provides new opportunities for cost-effective accelerated bridge construction in high seismic regions. As a result, it would be useful to investigate the connection performance for other types of girders as well.

REFERENCES

Almer, K., & Sanders, D. (2007 йил November). *23rd US-Japan Bridge Engineering Workshop.* Retrieved 2009 йил January from Public Works Research Institute: http://www.pwri.go.jp/eng/ujnr/tc/g/pdf/23/23-8-2sanders.pdf

California Department of Transportation. (2007). *Maintaining California's Bridges*. Retrieved 2009 from California Department of Transportation: http://www.dot.ca.gov/hq/structur/strmaint/

Caltrans. (2006). *Seismic Design Criteria.* California Department of Transportation, Sacramento.

Collins, M. P., & Mitchell, D. (1991). *Prestressed Concrete Structures.* New Jersey: Prentice Hall.

Computers and Structures, Inc. (2008). *CSI Analysis Reference Manual.* Berkeley: Computers and Structures, Inc.

Deng, L., Ghosn, M., Znidaric, A., & Casas, J. R. (2001). Nonlinear Flexural Behavior of Prestressed Concrete Girder Bridges. *Journal of Bridge Engineering* , 276-284.

Dowell, R. K., Seible, F., & Wilson, E. L. (1998). Pivot Hysteresis Model for Reinforced Concrete Members. *ACI Structural Journal* , 607-617.

Freyermuth. (1969). Design of Continuous Highway Bridges with Precast, Prestressed Concrete Girders. *PCI Journal* , 14-39.

Gordon, S. R., & May, I. M. (2004). Observations on the Grillage Analysis of Slabs. *The Structural Engineer* , 35-38.

Hambly, E. (1990). *Bridge Deck Behaviour.* Taylor & Francis.

Hastak, M., Mirmiran, A., Miller, R., Shah, R., & Castrodale, R. (2003). State of Practice for Positive Moment Connections in Prestressed Concrete Girders Made Continuous. *Journal of Bridge Engineering* , 267-272.

Holombo, J., Priestley, M. N., & Seible, F. (1998). *Longitudinal Seismic Response of Precast Spliced-Girder Bridges.* San Diego: University of California, San Diegoq.

Housner, G. W., & Thiel, C. C. (1990). *Competing Against Time: Report of the Governor's Board of Inquiry on the 1989 Loma Prieta Earthquake.* Earthquake Spectra.

Jaeger, L. G., & Bakht, B. (1982). The Grillage Analogy in Bridge Anaylsis. *Canadian Journal of Civil Engineering* , 224-235.

Keogh, D., & O'Brien, E. (1996). Recommendations on the Use of a 3-D Grillage Model for Bridge Deck Analysis. *Structural Engineering Review* , 357-366.

Kostem, C. N., & Ragazzo, S. C. (1993). Grillage Analogy for Multigirder Bridges. *Computing in Civil and Building Engineering* (pp. 188-192). American Society of Civil Engineers.

Levings, J. C. (2009). *Development of a Versatile Section Analysis Tool (VSAT) for use in structural design with a seismic emphasis.* Ames: Iowa State University.

Miller, R., Castrodale, R., Mirmiran, A., & Hastak, M. (2004). *Connection of Simple-Span Precast Concrete Girders for Continuity.* Washington, D.C.: National Cooperative Highway Research Program.

Patty, J., Seible, F., & Uang, C. (2002). *Seismic Response of Integral Bridge Connections.* University of California, San Diego, Structural Engineering. San Diego: University of California, San Diego.

PEER. (2005). *Northridge Earthquake*. (R. o. California, Producer) Retrieved 2009 from Pacific Earthquake Engineering Research Center: http://nisee.berkeley.edu/northridge/

Priestley, M. N., Seible, F., & Uang, C. (1994). *The Northridge Earthquake of January 17, 1994.* La Jolla: The University of California.

Priestley, M., Seible, F., & Calvi, G. (1996). *Seismic Design and Retrofit of Bridges.* New York: John Wiley & Sons, Inc.

Rahal. (2000). *Canadian Jounal of Civil Engineering* .

Rahal, K. N. (2000). Torsional Strength of Reinforced Concrete Beams. *Canadian Journal of Civil Engineering* , 445-453.

Raynor, D. J., Lehman, D. E., & Stanton, J. F. (2002). Bond-Slip Response of Reinforcing Bars Grouted in Ducts. *ACI Structural Journal* , 568-576.

Salmons, J., & McCrate, T. (1977). Bond Characteristics of Untensioned Prestressing Strand. *Journal of Prestressed Concrete Institute , 22* (1), 52-65.

Srinivas, V., Ramanjaneyulu, K., Sukhesh, K., Sasmal, S., & Gopalakrishnan, S. (2004). Automated Grillage Analysis of Continuous Span I- and T- Girder Bridges. *Journal of Structural Engineering* , 101-110.

Sritharan, S., Vander Werff, J., Abendroth, R., Wassef, W., & Greimann, L. (2005). Seismic Behavior of a Concrete/Steel Integral Bridge Pier System. *Journal of Structural Engineering* , 1083-1094.

Staudt, R. H. (2002). *Load Distribution for Steel Girder-Single Concrete Column, Integral-Pier Bridges.* Ames: Iowa State University.

Tadros, M., Ficence, J., Einea, A., & Holdsworth, S. (1993). A New Technique to Create Continuity in Prestressed Concrete Members. *PCI Journal* , 30-37.

Takeda, T., Sozen, M. A., & Nielsen, N. N. (1970). Reinforced Concrete Response to Simulated Earthquakes. *Journal of the Structural Division Proceedings of the American Society of Civil Engineers* , 2557-2573.

Thiemann, Z. (2009). *3-D finite element analysis of the girder-to-cap beam connection of an inverted-tee cap beam designed for seismic loadings.* Iowa State University.

University of Washington. (2004). *PEER Structural Performance Database*. From University of Washington Civil and Environmental Engineering: www.ce.washington.edu/~peera1

Wight, J. K., & MacGregor, J. G. (2008). *Reinforced Concrete Mechanics and Design.* Prentice Hall.

Zhao, J., & Sritharan, S. (2007). Modeling of Strain Penetration Effects in Fiber-Based Analysis of Reinforced Concrete Structures. *ACI Structural Journal* , 133-141.

ACKNOWLEDGMENTS

Thank you to the following individuals for their support and assistance in the completion of the research presented in this thesis. Without their kindness, much of this research would not have been possible:

- Caltrans and Charlie Sikorsky for sponsoring this research project
- Dr. Sri Sritharan for his knowledge and guidance in completing all of the items presented
- Jay Holombo and Sami Megally of PBS&J for their expertise and guidance in the design and construction of the test unit
- Zach Thiemann and Justin Vander Werff for their collaboration and contributions towards the overall project goals
- The staff at UCSD, including Andrew Gunthardt, Paul Greco, Noah Aldrich, Matt Stone, Christopher Latham, Bob Parks, John Ward, Bob Peters, Dan McAuliffe, Tim McAuliffe, Josh Nickerson, Michael Germeraad, Chris Horiuchi, Habib Charbel, and Taylor Gugino, for all of their hard work, assistance, and expertise in the construction and testing of the test unit. Your hospitality was greatly appreciated.
- Matthew Roling and Sriram Aaleti for their assistance and willingness to act as a sounding board for ideas
- My family and friends for their love and support during this process